University of Glasgow

Fang, Juan (2013) *Computer modelling and experimental design of a gait orthosis for early rehabilitation of walking.* PhD thesis.

http://theses.gla.ac.uk/3841/

Copyright and moral rights for this thesis are retained by the author

A copy can be downloaded for personal non-commercial research or study, without prior permission or charge

This thesis cannot be reproduced or quoted extensively from without first obtaining permission in writing from the Author

The content must not be changed in any way or sold commercially in any format or medium without the formal permission of the Author

When referring to this work, full bibliographic details including the author, title, awarding institution and date of the thesis must be given

Glasgow Theses Service
http://theses.gla.ac.uk/
theses@gla.ac.uk

Computer Modelling and Experimental Design of a Gait Orthosis for Early Rehabilitation of Walking

Juan Fang

Submitted in fulfillment of the requirements for the

Degree of Doctor of Philosophy

School of Engineering

College of Science and Engineering

University of Glasgow

January, 2013

Abstract

Walking is a fundamental human activity [1]. Rehabilitation of walking is one of the essential goals for patients with spinal cord injury (SCI) or other neurological impairments [2, 3]. Early rehabilitation is desirable to maximise the beneficial effects, so training programmes should be initiated even when patients are still on bed rest. In order to promote early rehabilitation of patients with incomplete spinal cord injury who cannot maintain an upright posture, a Gait Orthosis for Early Rehabilitation (GOER) of walking was designed [2] and evaluated in this PhD work.

This research started with a gait analysis experiment, through which the kinematics and kinetics of overground walking were investigated. Based on experimental walking data from able-bodied subjects, a least squares algorithm was developed to approximate the foot trajectories with circles. The determination of the best-fit circle for the toe trajectory over the whole gait cycle provided the basis for inducing toe movement by a rigid bar. Therefore a model of a two-bar mechanism was developed in Matlab/SimMechanics to simulate supine stepping. The simulated kinematics, including the angles of the hip, knee and ankle joints, showed comparable ranges of motion (ROMs) to the experimental walking performance in able-bodied subjects. This two-bar model provided the basis for the development of the GOER system.

The intersegmental kinetics of the lower limb motion during supine stepping were investigated through computer simulation. A model of a leg linkage was firstly developed to simulate upright walking. After the model was validated by successful simulation of dynamic performance similar to experimental overground walking, the model was rotated by 90^{o} to simulate stepping movement in a supine posture. It was

found that the dynamics of the hip joint were significantly influenced by the position change from upright to supine, which highlighted the importance of a leg-weight support during supine stepping. In contrast, the kinetics of the ankle joint were much influenced by the forces applied on the foot sole which mimicked the ground reaction occurring during overground walking. Therefore a suitable force pattern was required on the foot sole in order to train the ankle joint during supine stepping.

The simulated kinematic and kinetic results provided the basis for the design process of the GOER system. A GOER prototype with mechanisms for one leg was manufactured, which included a bar linkage to move the leg frame upwards and downwards and a cam-roller mechanism to rotate the shoe platform. The bar-cam GOER prototype achieved coordinated movements in the leg frame through constant rotation of an electric motor. Preliminary tests were carried out in three able-bodied subjects who followed the movements produced by the GOER prototype. The subjects felt walking-like stepping movement in the lower limb. Synchronised motion in the hip, knee and ankle joints was obtained, with the ROMs in the physiological ranges of motion during overground walking. The experimentally obtained joint profiles during supine stepping matched the simulated supine stepping and were close to the profiles during overground walking.

Apart from inducing proprioceptive feedback from the lower limb joints, the GOER system required dynamic stimulation from the shoe platform to mimic load occurring during the stance phase of overground walking. Activated by pneumatic components, the shoe platform managed to apply forces on the foot sole with adjustable amplitudes. The pneumatic shoe platform was evaluated in ten able-bodied subjects and managed to induce walking-like pressure sensation on the foot sole with physiological

responses from the leg muscles.

In summary, this thesis developed and evaluated a new gait training robotic system targeting supine stepping for patients who are still restricted to a lying position. The conceptual design process was developed through computer modelling and it was implemented as a prototype. Evaluation tests on able-bodied subjects proved the technical feasibility of the robotic system for supine stepping and led to recommendations for further development.

Contents

Abstract 2
Contents 5
List of Tables 10
List of Figures 12
Acknowledgements 20
Author's Declaration 23
Thesis Outline 24
Contributions 27
Publications 29
Abbreviations 30
Chapter 1. Introduction 33
1.1. Nervous System 33
1.1.1. Neurones and nerve fibre classification 34
1.1.2. The brain 36
1.1.3. Spinal cord 40
1.2. Somatic System 45
1.2.1. Somatic sensory system 45
1.2.2. Somatic motor system 47
1.2.3. Muscle 49
1.3. Spinal Reflex 51
1.3.1. Monosynaptic reflex 52
1.3.2. Polysynaptic reflex 53
1.4. Spinal Cord Injury 54
1.4.1. Epidemiology of SCI 55
1.4.2. Causes of SCI 55
1.4.3. Lesion types 56
1.4.4. Lesion level 57
1.4.5. Neurological classification 57
1.4.6. Incomplete SCI syndromes 59
1.5. Health Degeneration after SCI 60
1.5.1. Cardiovascular disorders 60
1.5.2. Pressure ulcers 61
1.5.3. Musculoskeletal deterioration 61
1.5.4. Bone fracture 62
1.5.5. Neurological development after SCI 63
1.6. Conclusions 64

Chapter 2. Literature Review....65
2.1. Rehabilitation after SCI....65
2.1.1. Spontaneous recovery....66
2.1.2. Activity-dependent spinal cord plasticity....68
2.2. Theories for Rehabilitation of Walking....70
2.2.1. Central pattern generator (CPG) in animals....71
2.2.2. CPG in humans....73
2.3. Rehabilitation of Walking....75
2.3.1. Conventional gait training....76
2.3.2. Lower limb orthoses....77
2.3.3. Therapist-assisted BWSTT....80
2.3.4. FES....84
2.3.5. FES orthoses....87
2.3.6. Robotic gait orthoses....89
2.4. Early Rehabilitation Systems....98
2.5. Aims and Objectives of the PhD Research....101
Chapter 3. Gait Analysis Experiment....104
3.1. Normal Walking....104
3.2. Experiment Description....107
3.2.1. Equipments and subjects....108
3.2.2. Experimental procedures....109
3.2.3. Data analysis....110
3.3. Results....113
3.3.1. Kinematic performance....114
3.3.2. Ground reaction forces....121
3.3.3. Internal moments....127
3.4. Discussion....134
3.5. Conclusions....135
Chapter 4. Model Development....137
4.1. Circle Fit Approximation of the Ankle, Heel and Toe Trajectories....137
4.1.1. Introduction....137
4.1.2. Methods....139
4.1.3. Results....144
4.1.4. Discussion....152
4.1.5. Conclusions....155
4.2. Kinematic Modelling of the GOER System....155
4.2.1. Introduction....156
4.2.2. Methods....157
4.2.3. Results....164

4.2.4. Discussion 172
4.2.5. Conclusions 174
4.3. Kinetic Analysis of Stepping in a Supine Position 174
4.3.1. Introduction 175
4.3.2. Methods 175
4.3.3. Results 180
4.3.4. Discussion 189
4.3.5. Conclusions 191
Chapter 5. Prototype Design of the GOER System 192
5.1. Actuation Configuration 192
5.1.1. Power requirements from the two-bar GOER model 192
5.1.2. Concept development of Actuation 1 197
5.1.3. Design of Actuation 1: a four-bar linkage 199
5.1.5. Design of Actuation 2: a cam mechanism 209
5.1.6. Power requirements from the bar-cam GOER model 218
5.1.7. Material selection 220
5.1.8. Electric motor selection 223
5.1.9. Conclusions 226
5.2. Shoe Platform Design 226
5.2.1. Functional shoe requirements 226
5.2.2. Shoe platform components 231
5.3. Prototype Presentation 234
5.4. Conclusions 236
Chapter 6. Experimental Evaluation of the GOER Prototype: the Bar-cam System 238
6.1. Introduction 238
6.2. Methods 239
6.2.1. The GOER system description 239
6.2.2. Experimental procedures 243
6.3. Results 248
6.3.1. Preliminary test 248
6.3.2. Test on subjects 251
6.4. Discussion 255
6.5. Conclusions 259
Chapter 7. Experimental Evaluation of the GOER Prototype: the Shoe Platform 260
7.1. Introduction 261
7.2. Methods 262
7.2.1. Equipment description 262
7.2.2. Subjects and measurement devices 264

7.2.3. Test procedures 266
7.2.4. Data analysis 269
7.3. Results 272
7.3.1. Single-stimulus sub-test 272
7.3.2. Cyclic-stimulation sub-test 282
7.4. Discussion 285
7.5. Conclusions 291
Chapter 8. Discussion 292
8.1. Gait Data Requirements and Recording Process 292
8.2. Computer Design of the GOER System 294
8.2.1. Circle approximation of the toe trajectory 294
8.2.2. Kinematic simulation of supine stepping 296
8.2.3. Kinetic analysis of supine stepping 297
8.2.4. Simulation of the bar-cam GOER system 298
8.3. Evaluation of the GOER Prototype 299
8.3.1. Joint angles induced by the bar-cam system 299
8.3.2. Foot sole stimulation induced by the shoe platform 300
8.4. Overall Evaluation of the GOER System 301
Chapter 9. Conclusions 303
Chapter 10. Future Work 305
10.1. Gait Analysis Experiment 305
10.2. The Bar-cam GOER Prototype for the Other Leg 307
10.3. Investigation of New Actuation Concepts 308
10.4. Electrical Stimulation for Sensory Feedback 309
10.5. Improvement of the Dynamic Shoe Platform 310
10.6. Conclusions 311
Appendices 312
Appendix 1: Model of a two-bar system 313
Appendix 2: Model of a leg linkage 315
Appendix 3: The two-bar model for power analysis 317
Appendix 4: The cam-roller assembly 319
Appendix 5: The model of the bar-cam GOER system 320
Appendix 6: The CAD drawings of the driven bar and leg frame 323
Appendix 7: The model of the bar-cam GOER system with a counterweight 327
Appendix 8: The CAD presentation of the motor and gearbox 331
Appendix 9: The CAD drawings for the shoe elements 334
Appendix 10: The controller electronics 340
Appendix 11: Failure mode analysis 341
Appendix 12: Question sheet 342

Appendix 13: Feedback from the subjects.....343
Appendix 14: Question sheet.....346
Appendix 15: Feedback from the subjects.....347
List of References.....357

List of Tables

Table 1.1: Classification of nerve fibres (taken from [9]. M: motor fibres; S: sensory fibres). 35

Table 3.1: Functions and contralateral leg positions of different sub-phases in the gait cycle [235]. 106
Table 3.2: Subject information. 109
Table 3.3: Normalised mass and length of lower limb segments (taken from [1]). 112
Table 3.4: Walking speeds for subjects (NC: normal cadence). 114

Table 4.1: Relative error of four methods with respect to the leg length (%) for the ankle, heel and toe trajectories in three subjects walking at 100% of NC. 147
Table 4.2: The X coordinates of the circle centres x_c and radii r of best-fit circles with respect to the leg length (%) for the ankle, heel and toe trajectories in three subjects walking at various speeds. 152
Table 4.3: The difference (Mean ±SD) of the phase shift (%) and ROM error (%) between the model and experimental data of all three subjects. 171

Table 5.1: Target performance of the rocker in the four-bar linkage for stepping at three speeds. 201
Table 5.2: Configuration of bar linkages for leg motion at all three cadences. . 208
Table 5.3: The mass and lengths of body segments for 5% to 95% of the population (taken from [275]). 221
Table 5.4: Anthropometric data and target maximal force requirements of the shoe platform [281]. 231

Table 6.1: Subject information (all male). 246

Table 7.1: Subject information. 266
Table 7.2: Force amplitudes at various pressures (manufacturer's data). 267
Table 7.3: RMS during MVC and at rest (μV). 272
Table 7.4: Mean RMS at stimulation of 3.5 bar with a long rise time ($\%MVC_{RMS}$). 276
Table 7.5: The ankle angle change (degrees) induced by the upward movement of the pressure plate during mechanical stimulation. 276
Table 7.6: Mean RMS for stimulation by a short rise time ($\%MVC_{RMS}$). 280
Table 7.7: Reflex latencies (ms) for stimulation by the pressure plate with a short rise time. NA means no reflex was observed. 281

Table. A 1: Motor specifications (Maxon EC 45). 332
Table. A 2: Gearbox specifications (Maxon planetary gearhead GP 62). 333
Table. A 3: Failure mode analysis. 341

List of Figures

Figure 1.1: Lateral view of the brain: the division of the four lobes (taken from [5])....36
Figure 1.2: Functional classification of the sensorimotor cortex (taken from [5]). 38
Figure 1.3: Motor homunculus (taken from [11]).....39
Figure 1.4: Sensory homunculus (taken from [11]).....39
Figure 1.5: Spinal nerve classification (taken from [13]).....41
Figure 1.6: The key sensory points of the human body (taken from [14]). 42
Figure 1.7: Dermatome maps (taken from [13]).....42
Figure 1.8: Structure of the spinal cord (taken from [5]).....44
Figure 1.9: Descending and ascending spinal tracts (taken from [15]). 46
Figure 1.10: The ascending tracts (taken from [13]). 46
Figure 1.11: Lateral corticospinal tract (modified based on a picture from [16]). 48
Figure 1.12: Muscle fibre structure and neurone innervation (from [18]).....51
Figure 1.13: Stretch reflex (from [22]). 52
Figure 1.14: Flexor reflex (from [29]). 54
Figure 1.15: Standard neurological classification of spinal cord injury (from [14])....59

Figure 2.1: Therapist-assisted BWSTT (from [155])....82
Figure 2.2: The prototype of LOPES (from [194]).....90
Figure 2.3: The Lokomat. 94
Figure 2.4: The Lokohelp system. 96
Figure 2.5: The Erigo.....100

Figure 3.1: Timing of gait phases (modified from [234] and [235]). 105
Figure 3.2: Marker placement. Subfigure (a) shows markers mainly for the left leg (from [238]) and subfigure (b) shows markers mainly for the right leg (from [235]). 108
Figure 3.3: Free body diagram of the leg segments.....111
Figure 3.4: Joint angles for three subjects walking at 100% of NC. 116
Figure 3.5: Joint angles for three subjects walking at 75% of NC. 119
Figure 3.6: Joint angles for three subjects walking at 50% of NC. 120
Figure 3.7: Normalised ground reaction forces for three subjects walking at 100% of NC.....123
Figure 3.8: Normalised ground reaction forces for three subjects walking at 75%

of NC.....125
Figure 3.9: Normalised ground reaction forces for three subjects walking at 50% of NC.....126
Figure 3.10: Normalised internal joint moments for subjects walking at 100% of NC.....129
Figure 3.11: Normalised internal joint moments for three subjects walking at 75% of NC.....131
Figure 3.12: Normalised internal joint moments for three subjects walking at 50% of NC.....133

Figure 4.1: Leg position in the new reference system. The X-Y reference centre (0, 0) is at the hip joint axis. Black dots at the lateral malleolus, calcaneus and second metatarsal head indicate the ankle, heel and toe, respectively. The distances from the hip centre to the ankle, heel and toe are represented respectively by dashed lines as l_A, l_H and l_T. A dash-dot line L represents the vertical distance from the hip to the ground. 140
Figure 4.2: Circle fit approximation of the foot trajectories of S1 walking at 100% of NC. Circles in solid, dashed, dotted and dash-dot lines are fit circles from Methods 1 to 4 (marked as M_1, M_2, M_3 and M_4), respectively. The centres are marked with stars, dots, crosses and plus signs, respectively. The foot trajectories (relative to the hip) considered for circle approximation are shown as thick solid lines, while those not involved in the approximation (the ankle and heel trajectories during swing) are thick dotted lines.....146
Figure 4.3: Circle fit approximation (Method 1) of the ankle (upper) and heel (lower) trajectories (relative to the hip) in the stance phase of S1 walking at 100% of NC. The best-fit circles are shown as dash-dot lines, with the radius represented as an arrow. The ankle and heel trajectories in the stance phase are shown as solid lines, while those in the swing phase are dotted lines.....148
Figure 4.4: Circle fit approximation (Method 1) of the toe trajectory (relative to the hip) in the whole gait cycle of S1 walking at 100% of NC (upper). The best-fit circle is represented by a dash-dot line, with the radius shown as an arrow. The toe trajectories (both the stance and the swing phases) are shown as solid lines. A zoomed view is presented in the lower subfigure.....149
Figure 4.5: Ankle trajectories and the best-fit circles in S1 walking at 100% (solid line), 75% (dashed line) and 50% (dotted line) of NC. 150
Figure 4.6: Mean errors from the best-fit circle approximation (Method 1) error of three subjects walking at three speeds. Bars in black, grey and white refer to 100%, 75% and 50% of NC, respectively. All errors are normalised to their respective leg length. 151

Figure 4.7: Development of the two-bar model. 159
Figure 4.8: Schematic diagram of the model. 161
Figure 4.9: Two actuators profiles to simulate S1 walking at 100%, 75% and 50% of NC. 164
Figure 4.10: A sequence of eight positions over one gait cycle, showing every 12.5% of the gait cycle. The leg is shown as solid lines while dashed lines represent Bar 1. Bar 2 coincides with the foot sole. T is the duration of the whole gait cycle. 165
Figure 4.11: Kinematics in S1 walking at different speeds. Dashed lines represent the simulated angles while solid lines with shaded areas represent experimental mean angles ±SD. 167
Figure 4.12: Kinematics in S2 walking at different speeds. Dashed lines represent the simulated angles while solid lines with shaded areas represent experimental mean angles ±SD. 169
Figure 4.13: Kinematics in S3 walking at different speeds. Dashed lines represent the simulated angles while solid lines with shaded areas represent experimental mean angles ±SD. 170
Figure 4.14: Free body diagram of the leg segments in an upright position. 176
Figure 4.15: Free body diagram of the leg segments in a supine position. 177
Figure 4.16: Trajectory of the centre of pressure from the heel to the toe in S1 walking at 100% of NC. The foot length of S1 is 0.25 m. 181
Figure 4.17: Internal joint moments in three subjects walking at 100% of NC: solid, dashed, dotted and dash-dot lines are respectively the moments during experimental overground walking, simulated upright walking, simulated supine stepping with full ground forces and simulated supine stepping with 30% of upward ground force. 183
Figure 4.18: Internal joint moments in three subjects walking at 75% of NC: solid, dashed, dotted and dash-dot lines are respectively the moments during experimental overground walking, simulated upright walking, simulated supine stepping with full ground forces and simulated supine stepping with 30% of upward ground force. 185
Figure 4.19: Internal joint moments in three subjects walking at 50% of NC: solid, dashed, dotted and dash-dot lines are respectively the moments during experimental overground walking, simulated upright walking, simulated supine stepping with full ground forces and simulated supine stepping with 30% of upward ground force. 187

Figure 5.1: Torque requirements. 196
Figure 5.2: Power requirements. 196
Figure 5.3: Three options for Actuation 1. 197

Figure 5.4: A bar linkage ABCD. Bar AB is the crank and Bar CD is the rocker. The trajectory of the rocker tip is shown as a dash-dot curve. Three typical positions ABCD, AB_1C_1D and AB_2C_2D are presented. γ_1: $\angle$CDH; γ_2: $\angle BAB_1$; γ_3: $\angle C_1DH$; γ_4: reflex angle $\angle B_1AB$; γ_5: $\angle CAC_1$; γ_6: $\angle B_2C_2D$. 200
Figure 5.5: Four-bar linkage design. The rocker is lengthened at the other end, with triangles showing the points of foot attachment. 202
Figure 5.6: Bar lengths as a function of γ_7, which describes the position of the crank base A. 205
Figure 5.7: The transmission angle as a function of γ_7, which describes the position of the crank base A. 206
Figure 5.8: The setup of the bar linkage to move the driven bar (ABCD achieves the lowest position of the driven bar for toe off, while AB_1C_1D produces the upmost position of the driven bar for heel strike). 206
Figure 5.9: The driven bar performance induced by the bar linkage and the target model.....208
Figure 5.10: The cam-follower mechanism. The solid curve represents a cam, which rotates at the point *B*. The solid straight line represents the follower, pivoting at the point *A*. The follower contacts the cam initially at the point *C*. If an arbitrary point D_1 is to contact with the follower, the cam should rotate from the point D_1 to *D*, so that the follower contacts with the cam at the point *D*, with the position of the follower as the straight dashed line AD. The thick dash-dot circle *A* is the trajectory of the follower, while the thin dash-dot circle *B* is the trajectory of the point D_1 during rotation of the cam. 210
Figure 5.11: The cam and four representative positions of the followers (AB, A_1B_1, A_2B_2 and A_3B_3): the thick solid curve is the cam profile. Circle *O* (thick dash-dot curve) is the potential trajectory of the pivot of the follower. Circle B_1 (thin solid curve) is the potential trajectory of the tip of the follower for contact of the point B_1. The straight lines BD, B_1D_1, B_2D_2 and B_3D_3 represent the common nominal lines. The arrow lines BC, B_1C_1, B_2C_2 and B_3C_3 show the directions of the followers, which are normal to the corresponding lines AB, A_1B_1, A_2B_2 and A_3B_3. Four pressure angles, $\angle$CBD, $\angle C_1B_1D_1$, $\angle C_2B_2D_2$ and $\angle C_3B_3D_3$ are shown as θ, θ_1, θ_2, and θ_3. 213
Figure 5.12: The maximal pressure angle according to various follower lengths. 215
Figure 5.13: The cam for walking at 100% of NC (R_b = 0.08 m, L_f = 0.05 m). 216
Figure 5.14: Cams for slower walking. 217

Figure 5.15: The cam-bar linkage setup of the GOER system. The segment ABCD is the bar linkage. The cam is mounted at the point E. The leg segment is represented by EFGH. 219
Figure 5.16: The simulated torque and power of the bar-cam GOER system stepping at 100% of NC. 220
Figure 5.17: The simulated power for the bar-cam GOER system with the leg frame in three different conditions. 223
Figure 5.18: Ground reaction force during the stance phase (COP: centre of pressure). 227
Figure 5.19: The simplified upward force profile on the foot sole to simulate walking at 100% of NC: the dashed line is the force for the heel (HL) while the solid line is for the forefoot (FF). The left Y axis shows the amplitude of the force taking place during overground walking, while the right Y axis shows the target amplitude for the shoe platform (30% of ground reaction force). 228
Figure 5.20: The simplified upward force profile on the foot sole to simulate walking at 75% and 50% of NC: the dashed line is the force for the heel (HL) while the solid line is for the forefoot (FF). The left Y axis shows the amplitude of the force taking place during overground walking, while the right Y axis shows the target amplitude for the shoe platform (30% of ground reaction force). 230
Figure 5.21: Pneumatic shoe platform. 232
Figure 5.22: The GOER prototype. The user places the leg in the leg frame (1) and the foot on the shoe platform (2). The leg is moved by a driven bar (3), which is moved via a bar linkage (4). The foot is rotated by a cam (5). The electric DC motor (6) rotates the bar-linkage and transmits rotation to the cam via a chain (7). 235
Figure 5.23: The shoe platform. 235
Figure 5.24: The prototype performance. 236

Figure 6.1: The GOER prototype. The user places the leg in the leg frame (1) and the foot on the shoe platform (2). The leg is moved by a driven bar (3), which is actuated by a rotary bar linkage (4). The foot is rotated by a cam (5). The DC motor (6) rotates the bar-linkage and transmits rotation to the cam via a chain (7). The trajectories of the leg frame (including the joints of the hip (A), knee (B) and ankle (C)) and the driven bar (including the tip (D) and the pivot point (E)) are recorded to investigate the motion induced by the GOER prototype. 240
Figure 6.2: FCIV motor controller platform. 241
Figure 6.3: The controller panel. 242

Figure 6.4: The control loop. 242
Figure 6.5: The test setup with a subject. 247
Figure 6.6: The motor speed with an empty leg model (leg frame). The downward and upward arrows show the time when the disturbance was added and removed from the leg frame. The stars mark the observed jittering. 249
Figure 6.7: The performance (mean ± SD) of the driven bar. The solid line is the performance from the test while the dashed line shows the model simulation of the bar-cam system as described in Figure 5.9. 249
Figure 6.8: The joint performance of the leg frame. The solid lines show experimental mean values while the shaded areas are standard deviations. The dashed lines are model simulation results. 250
Figure 6.9: The leg performance of S1. The solid lines show experimental mean values while the shaded areas are standard deviations. The dashed lines are model simulation results. 252
Figure 6.10: Stick diagram of movement in S1. 253
Figure 6.11: The leg performance of S2 and S3. The solid lines show experimental mean values while the shaded areas are standard deviations. The dashed lines are model simulation results. 255

Figure 7.1: The shoe platform structure. 263
Figure 7.2: The pneumatic system for mechanical force stimulation. 264
Figure 7.3: Force profile for walking simulation. 269
Figure 7.4: Heel stimulation at 2 bar in S3 with a long rise time. The dashed lines show the mechanical stimulation periods with the amplitudes as the reflex thresholds. 273
Figure 7.5: Heel stimulation at 3.5 bar in S3 with a long rise time. The dashed lines show the mechanical stimulation periods with the amplitudes as the reflex thresholds. 274
Figure 7.6: Forefoot stimulation at 3.5 bar in S3 with a long rise time. The dashed lines show the mechanical stimulation periods with the amplitudes as the reflex thresholds 274
Figure 7.7: Heel stimulation in S3 with a short rise time. The dashed arrow shows reflex-induced ankle perturbation. The dashed lines show the mechanical stimulation periods with the amplitudes as the reflex thresholds. 278
Figure 7.8: Heel stimulation in S6 with a short rise time. The dashed arrow shows reflex-induced ankle perturbation. The dashed lines show the mechanical stimulation periods with the amplitudes as the reflex thresholds. 279

Figure 7.9: Forefoot stimulation in S6 with a short rise time. The dashed lines show the mechanical stimulation periods with the amplitudes as the reflex thresholds. 279
Figure 7.10: Heel stimulation in S7 with a short rise time. The dashed arrow shows reflex-induced ankle perturbation. The dashed lines show the mechanical stimulation periods with the amplitudes as the reflex thresholds. 280
Figure 7.11: Walking simulation responses of S7. The dashed lines show the mechanical stimulation periods with the amplitudes as the reflex thresholds. 283
Figure 7.12: Zoomed version of Figure 7.11. The upward and downward arrows show the start and end times of stimulation on the foot sole. The solid arrows represent the heel pressure plate and the dashed arrows indicate the forefoot pressure plate. The dashed lines show the mechanical stimulation periods with the amplitudes as the reflex thresholds. 283
Figure 7.13: RMS values (relative to resting state) during walking simulation tests. 284

Figure A. 1: Model of a two-bar system. 313
Figure A. 2: Model of a leg linkage. 315
Figure A. 3: The model for torque and power simulation. 317
Figure A. 4: The cam-roller mechanism. 319
Figure A. 5: The model of the bar-cam GOER system. 320
Figure A. 6: The inner tube of the driven bar. 323
Figure A. 7: The outer tube of the driven bar. 323
Figure A. 8: The inner tube of the thigh frame. 324
Figure A. 9: The outer tube of the thigh frame. 324
Figure A. 10: The inner tube of the shank frame. 325
Figure A. 11: The outer tube of the shank frame. 325
Figure A. 12: The thigh support. 326
Figure A. 13: The calf support. 326
Figure A. 14: Model of the bar-cam GOER system with a counterweight. 327
Figure A. 15: CAD presentation of the Maxon motor EC 45. 331
Figure A. 16: CAD presentation of the Maxon planetary gearhead GP 62. 331
Figure A. 17: Foot plate for the heel. 334
Figure A. 18: Foot plate for the forefoot. 335
Figure A. 19: Pressure plate for the heel. 336
Figure A. 20: Pressure plate for the forefoot 337
Figure A. 21: Foot stop. 338

Figure A. 22: Toe connection. 338
Figure A. 23: Ankle connection. 339
Figure A. 24: The controller electronics. 340

Acknowledgements

I would like to express my sincere thankfulness to Professor Kenneth J. Hunt for this exciting PhD work. I am much inspired by his knowledge and achievements in the field of mechanical design and system control. His suggestion and encouragement have helped me to start the research efficiently. I am very grateful for his suggestion on the thesis writing. I would like to thank Dr. Aleksandra Vuckovic for her support in this research. She is always ready to give me help when I need it. This work would not be finished if I had not been helped by Dr. Henrik Gollee. He taught me how to choose the actuator for my project and design the test. Many special thanks also go to Professor Bernard Conway: your support is precious. You advised me to attend biomechanics courses in the University of Strathclyde, which opened the research opportunity for my project. You advised me to carry out the gait analysis experiment in your advanced Biomehanics gait lab, which provided me with valuable experiment data. Many thanks to Dr. Sujay Galen, who is always ready to solve gait related problems for me. You helped me to carry out the gait experiment, from which I knew how to use the Vicon motion system, and more importantly, I knew the features of normal gait. Without your help I would not be able to finalise the target requirements of the robotic system described in this thesis. Sincere thanks go to the electronics specialist Mr. Calum Cossar from Scottish Power Electronics and Electric Drives Consortium. You lent me the power system and the controller for the electric motor, which allowed me to carry on the tests. I cannot imagine how far I could go without your help.

My thanks go to all of my other colleagues in the Centre for Rehabilitation Engineering. Special thanks go to Colm Craven. You taught me how to use our lab facilities, showed

me how to record EMG signals and advised me how to analyse EMG data. Angus Mclachlan and Euan Mccaughey helped me with my experiments by developing Matlab model for data recording. Andrew Dunne gave me the chance to walk with the Lokomat, through which I knew how a rehabilitation device works. Thanks Dr. Sylvie Coupaud and Admanntia Mamma for sparing time talking with me to relieve stress. A special thank goes to my officemate Muhammad Abul Hasan who spent much time in my test, providing useful EMG data.

My thanks go to the people at the Queen Elizabeth National Spinal Injuries Unit at the Southern General Hospital. Sincere thanks go to Mr. David Allan who allowed us to join in the Unit for my research and contributed to this work with helpful advice. A special thank goes to Jon Hasler for his physiological suggestion of training methods and the desirable features of the rehabilitation system from a physiotherapist view.

Many thanks to Elaine McNamara, who helped me a lot to apply for this PhD research. Sincere thanks go to all the staff from the mechanical workshop who manufactured the GOER prototype for me. Mr. Brian Robb helped me choose the suitable structures and materials for the prototype. George Sylvie suggested me with the cam-chain concept, which enabled the prototype moved by a simple electric motor. Of course, the prototype would have been useless if no subjects had tried it. Thanks to all the subjects who participated in this research. Thank you for your patience during the test.

I would like to acknowledge the China Scholarship Council for the financial support for this study and GU68 Engineer Trust for the funding of the motor purchase.

Last but not least, I would like to thank my family for the support all the four years. Special and sincere thanks go to my husband for his precious suggestion on my PhD and his economical and emotional support over the last few years. I wish to express my greatest gratitude to Mama, Papa and my Granny for their love to me. I would not be able to do this without your encouragement.

Author’s Declaration

I hereby declare that this thesis is my own work and that, to the best of my knowledge and belief, it contains no material previously published or written by another person nor material which to a substantial extent has been accepted for the award of any other degree or diploma of the university or ther institute of higher learning, except where due acknowledgment has been made in the text.

Juan Fang

Glasgow, Scotland, 13 September 2012

Thesis Outline

Chapter 1. This chapter describes the anatomy and physiology of the brain and the spinal cord. Functional impairments and neurological adaptations after spinal cord injury (SCI) are discussed. The pathophysiological consequences of SCI highlight the importance of rehabilitation strategies to alleviate health deterioration.

Chapter 2: In this chapter theories for rehabilitation of walking after SCI are discussed, followed by an overview of rehabilitation programmes, including traditional physiotherapy and newly-developed robotics-assisted training. After a critical examination of the literature related to devices for early rehabilitation of walking, this chapter outlines the aims and objectives of the PhD work.

Chapter 3: This chapter describes a gait analysis experiment to record the performance of overground walking in three able-bodied subjects. The general methodologies employed in the experiment are detailed. The kinematics and kinetics of overground walking at various speeds are presented.

Chapter 4: This chapter describes modelling and simulation of supine stepping. Based on the results of gait analysis, a circle-fit algorithm was derived to approximate the foot trajectories. Then a model of a two-bar system was developed to simulate the kinematics of supine stepping at various speeds. Furthermore, the kinetics of supine stepping were analysed through a model of a leg linkage. These simulation results provided the basis for the conceptual development of the GOER system.

Chapter 5: This chapter describes structural development of the GOER system,

including analysis of various actuation setups, design of a bar-cam mechanism and selection of materials for each component. This chapter concludes with a GOER prototype, which includes a bar-cam system for passive leg movement and a dynamic shoe platform for walking-like mechanical force stimulation on the foot sole.

Chapter 6: This chapter evaluates stepping performance produced by the GOER prototype. The kinematics of supine stepping were investigated through a preliminary test of the GOER prototype with an empty leg frame, followed by an evaluation test on three able-bodied subjects whose legs were moved by the GOER prototype. The angles of the hip, knee and ankle joints during supine stepping were measured and compared with the results from model simulation and experimental overground walking. The bar-cam GOER prototype produced lower limb motion which was comparable to the physiological motion of overground walking.

Chapter 7: This chapter evaluates the performance of the shoe platform in ten able-bodied subjects. The platform firstly produced single stimuli on the foot sole, to allow determination of the optimal force patterns based on EMG analysis. Then the platform implemented cyclic stimulation on the foot sole to simulate the ground reaction forces occurring during overground walking. Subjects experienced physiological responses from the tibialis anterior and soleus muscles and felt cyclic pressure from the platform which was reported to be similar to the ground reaction forces occurring during overground walking.

Chapter 8: This chapter describes future work that has been identified in design and evaluation of the GOER prototype.

Chapter 9: This chapter summarises the main conclusions of this thesis.

Contributions

1. Foot trajectories relative to the hip joint at various walking speeds were revealed to be curved, with the best-fit circles obtained using a least squares algorithm. It is confirmed that the ankle and heel move in circular paths in the stance phase. The toe is found to follow a circular trajectory in the whole gait cycle. This observation improved knowledge about normal gait, and provided a novel methodology for the design of lower limb orthoses.

2. A model of a two-bar mechanical system was developed which succeeded in simulating supine stepping at various speeds with the movement of the lower limb joints similar to overground walking. The model provided the conceptual basis for the design of the robotic GOER system which produces stepping in users who are restricted to a supine position.

3. A model of a leg linkage was developed to simulate the kinetics of upright walking and supine stepping, which was a useful testbed to investigate the dynamics of the lower limb during supine stepping in the GOER system. The computer modelling provided information for the mechanical design of the GOER system.

4. The GOER prototype was manufactured and the control strategies of the GOER system were investigated, followed by preliminary tests of the GOER system on able-bodied subjects. The GOER prototype successfully produced lower limb motion similar to the physiological motion of overground walking. The manufacture and evaluation of the GOER prototype provided insights for further

development of a GOER system for early rehabilitation of walking.

5. A shoe platform was designed and manufactured to apply dynamic forces on the foot sole for walking simulation. It produced walking-like sensation as well as physiological responses from the leg muscles in able-bodied subjects. The shoe platform can be incorporated in the GOER system to achieve dynamic simulation of supine stepping. It is also an important tool for investigation of the effect of mechanical stimulation on the foot sole.

Publications

[1] Fang, J., H. Gollee, S. Galen, B. Conway and A. Vuckovic, *Preliminary modelling of a robotic gait through ankle actuation* in *XXIII Sandbjerg Symposium on Neuroplasticity and Neurorehabilitation, Danish Society for Neuroscience*. May, 2009.

[2] Fang, J., H. Gollee, S. Galen, B. Conway and A. Vuckovic, *Modelling of a gait robotic device for early rehabilitation of walking* in *17th Congress of the European Society of Biomechanics*, Edinburgh. July, 2010.

[3] Fang, J., H. Gollee, S. Galen, B. Conway, D. Allan and A. Vuckovic, *Kinematic modelling of a robotic gait device for early rehabilitation of walking.* Proceedings of the Institution of Mechanical Engineers, Part H: Journal of Engineering in Medicine, 2011. **225**(12): p. 1177-1187.

[4] Fang, J. *A gait robotic device for early rehabilitation of walking.* in *SET for Britain*, UK Parliament, House of Commons, London, 14th March 2011.

[5] Fang, J. and A. Vuckovic, *Design of a shoe platform to simulate ground reaction force* in *6th UK and RI Postgraduate Conference in Biomedical Engineering and Medical Physics*, 14th - 16th, August, Glasgow.

Abbreviations

AFO = Ankle-Foot Orthosis

ALEX = Active Leg Exoskeleton

ARTHuR = Ambulation-assisting Robotic Tool for Human Rehabilitation

ASIA = American Spinal Injury Association

BA = Brodmann areas

BWS = body weight support

BWSTT = body weight support treadmill training

CNS = central nervous system

COP = centre of pressure

CPG = central pattern generator

DOF = degree of freedom

FA = feet adjacent

FCIV = flexible controller in the fourth generation

FES = functional electrical stimulation

FF = forefoot

GC = gait cycle

GOER = Gait Orthosis for Early Rehabilitation

HGO = Hip Guidance Orthosis

HKAFO = Hip-Knee-Ankle-Foot Orthosis

HL= heel

HR = heel rise

IC = initial contact

iSCI = incomplete spinal cord injury

KAFO = Knee-Ankle-Foot Orthosis

LOPES = Lower Extremity Powered Exoskeleton

MVC = maximal voluntary contraction

MVC_{RMS} = the root mean square value during maximal voluntary contraction

NC = normal cadence

OH = orthostatic hypotension

OI = opposite initial contact

OT = opposite toe off

PAM/POGO = Pelvic Assist Manipulator and the Pneumatically Operated Gait Orthosis

PNS = peripheral nervous system

RGO = Reciprocating Gait Orthosis

RMS = root mean square

ROM = range of motion

SCI = spinal cord injury

SD = standard deviation

SOL = soleus

TA = tibialis anterior

TO = toe off

TV = tibia vertical

VCM = Vicon Clinical Manager

Chapter 1. Introduction

Summary: All movements and consciousness about movements of the different parts of the human body are coordinated by the central nervous system (CNS): the brain and the spinal cord [4]. The somatic system transmits sensory and motor information to and from the CNS through different pathways. The muscles and the innervated axons provide the basis for voluntary movement control as well as involuntary spinal reflexes. Damage to or disease of the spinal cord may result in loss of motor, sensory and autonomic function below the level of the lesion [5]. Functional impairments from spinal cord injury (SCI), combined with secondary complications, severely reduce quality of life [6]. Neurological adaptations after SCI, such as spasticity and muscle atrophy, reduce mobility and further deteriorate the daily life of people with SCI. The pathophysiological consequences of SCI highlight the importance of rehabilitation strategies to prevent muscle atrophy and to alleviate health deterioration [7].

1.1. Nervous System

The nervous system is a network of neurones, which processes and transmits information by electrical and chemical signals. The human nervous system consists of the central and peripheral nervous systems. The central nervous system (CNS) refers to the neural network that is encapsulated within the bone: the brain and the spinal cord [5]. The remaining part of the nervous system outside the CNS is the peripheral nervous system (PNS). The PNS includes the visceral PNS and the somatic PNS. The visceral PNS, also called the autonomic nervous system, consists of the neurones that innervate the internal organs, blood vessels, and glands. In contrast, the somatic PNS, which includes nerves that innervate the skin, joints, and muscles, is under voluntary control

[5]. The PNS and the CNS communicate mainly through the spinal cord.

1.1.1. Neurones and nerve fibre classification

The basic functional unit of the nervous system is a neurone (also called a nerve cell). A typical neurone has a cell body (or soma), dendrites, and an axon [8]. Dendrites are thin structures that arise from the cell body, often extending and branching to form a complex 'dendritic tree'. An axon, which is a long, slender extension of a neurone, conducts electrical impulses away from the cell body so as to transmit those impulses to other neurones through synaptic processes. A neurone can have many dendrites, but it normally has only one axon. Neurones have different sizes and structures, resulting in different conduction velocities of the action potential [8].

Neurones are functionally classified into sensory neurones, motor neurones and interneurones [5]. Sensory neurones are activated by sensory input (such as touch or heat from the external environment) and transmit the sensation into the CNS, while motor neurones convey control commands to induce muscle contraction. Interneurones connect different types of neurones. The pathways for transmitting electrochemical impulses in the CNS are called tracts while those of the PNS are called nerves. Sensory nerves (also called afferent nerves) conduct signals from sensory receptors through ascending tracts to the brain, while motor nerves (efferent nerves) transmit signals from the brain to their target skeletal muscles through descending tracts [5].

Peripheral nerve fibres have two classification systems based on their diameters. Lloyd and Hunt classified sensory neurons into the groups Ia, Ib, II, III and IV [9]. As shown in Table 1.1, the sensory fibres in this classification have a corresponding

group in the other system defined by Erlanger and Gasser, which classifies both sensory and motor neurons as A, B and C [9]. Fibres of the A group have a large diameter and high conduction velocity, compared to groups B and C. B fibres mainly form the autonomic nervous system, while the A and C groups form the somatic nervous system, which is responsible for transmitting sensory information to and motor information from the CNS [5]. Motor fibres include A-α, A-β and A-γ motor neurones, which are involved in muscle contraction. Sensory fibres include A-α (Ia fibre or Ib fibres), A-β (II fibres), (A-σ) (III fibres) and C (IV fibres) fibres, which are responsible for detecting muscle tension and the senses of light touch, pain and temperature [9]. The motor and sensory fibres will be further discussed in Section 1.2.

Table 1.1: Classification of nerve fibres (taken from [9]. M: motor fibres; S: sensory fibres).

Lloyd and Hunt (Sensory)	Erlanger and Gasser (Sensory and Motor)	Diameter (μm)	Velocity (m/s)	Function
Ia	A-α	10-20	50-120	M: motor neurone (extrafusal muscle fibres, both slow and fast)
				S: muscle spindles
Ib	A-α	10-20	50-120	S: Golgi tendon organs, touch, and pressure
II	A-β	4-12	25-70	M: motor neurones to intra/extrafusal muscle fibres
				S: secondary muscle spindle afferents, touch, pressure, vibration
III	A-γ	2-8	10-50	M: small gamma motor neurones to intrafusal muscle fibres
	A-σ	1-5	3-30	S: light touch, pain & temperature (acute)
IV	B, C	< 2	< 2	S: pain & temperature

1.1.2. The brain

The smooth and accurate performance of various motor tasks involves combining information to the somatic sensory system and from the somatic motor systems, with important processes taking place in the high levels of the nervous system: the brain. Located entirely within the skull, the brain consists of three parts: cerebrum, cerebellum, and brain stem [5]. The large convoluted area in Figure 1.1 is the cerebrum. Below the cerebrum is the cerebellum, which is a centre for movement and balance control. The remaining part of the brain is the brain stem, which transfers information between the cerebrum, the cerebellum and the spinal cord.

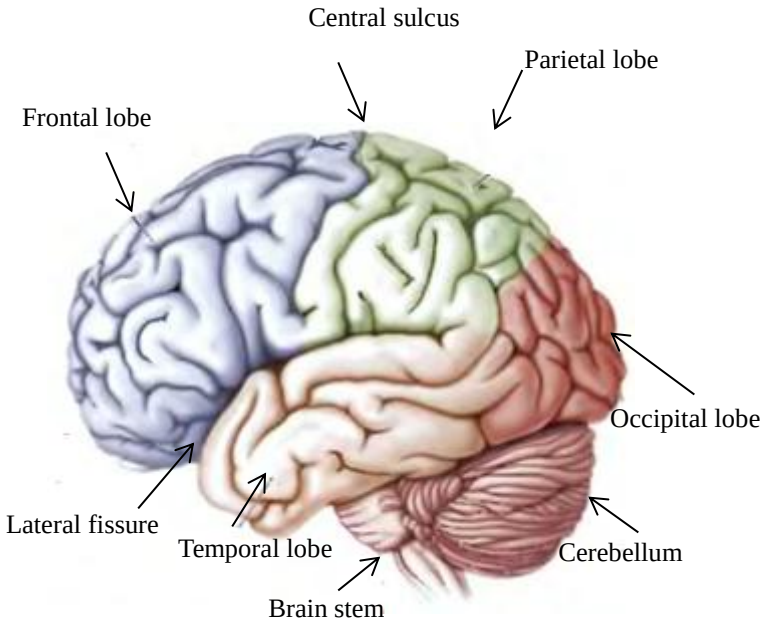

Figure 1.1: Lateral view of the brain: the division of the four lobes (taken from [5]).

There are many convolutions on the surface of the cerebrum. The bumps are called gyri (singular: gyrus), while the grooves are called sulci (singular: sulcus), with especially deep grooves called fissures [5]. Sulci and fissures divide the human cerebrum into several lobes, as shown in Figure 1.1. At the back of the cerebrum lies the occipital lobe,

ventral to the deep lateral fissure is the temporal lobe, while the top areas are the frontal and parietal lobes, which are separated by the central sulcus [5]. Different brain regions take responsibility for different functions. The precentral gyrus controls voluntary movements, such as movement of the hands and legs, while the postcentral gyrus is related to somatic sensation, i.e. information allowing humans to recognize the environment (temperature, pain, etc.) [5].

The brain has a clear mapping for each body segment. Research in the latter 19th century localized specific brain regions which are responsible for specific motor or sensory functions [10]. The surface of the cerebrum (called the cerebral cortex) is divided into motor, sensory and association areas, as shown in Figure 1.2. Based on the concept that anatomical divisions of the brain correspond to functional divisions of the human body, the cortical architecture has been mapped into Brodmann areas (BA) [10]. Various cerebral areas are referred to by different BA numbers according to their function and structure. For example, BA4 is the primary motor cortex while BA 3, 1 and 2 are the sensory areas [5].

The major motor areas are located in the posterior portion of the frontal lobe. The motor cortex includes BA4 (the primary motor cortex, also called M1) and BA6 (the supplementary motor area in the middle and the premotor area laterally). M1 contains large neurones, which control muscles through the spinal cord. The premotor area plans actions and refines movements based upon sensory inputs. The major sensory areas include BA 17, 18 and 19 (visual cortex) in the occipital lobe, BA 41 and 42 (auditory cortex) in the temporal lobe and BA 3, 1 and 2 (somatosensory cortex) in the parietal lobe.

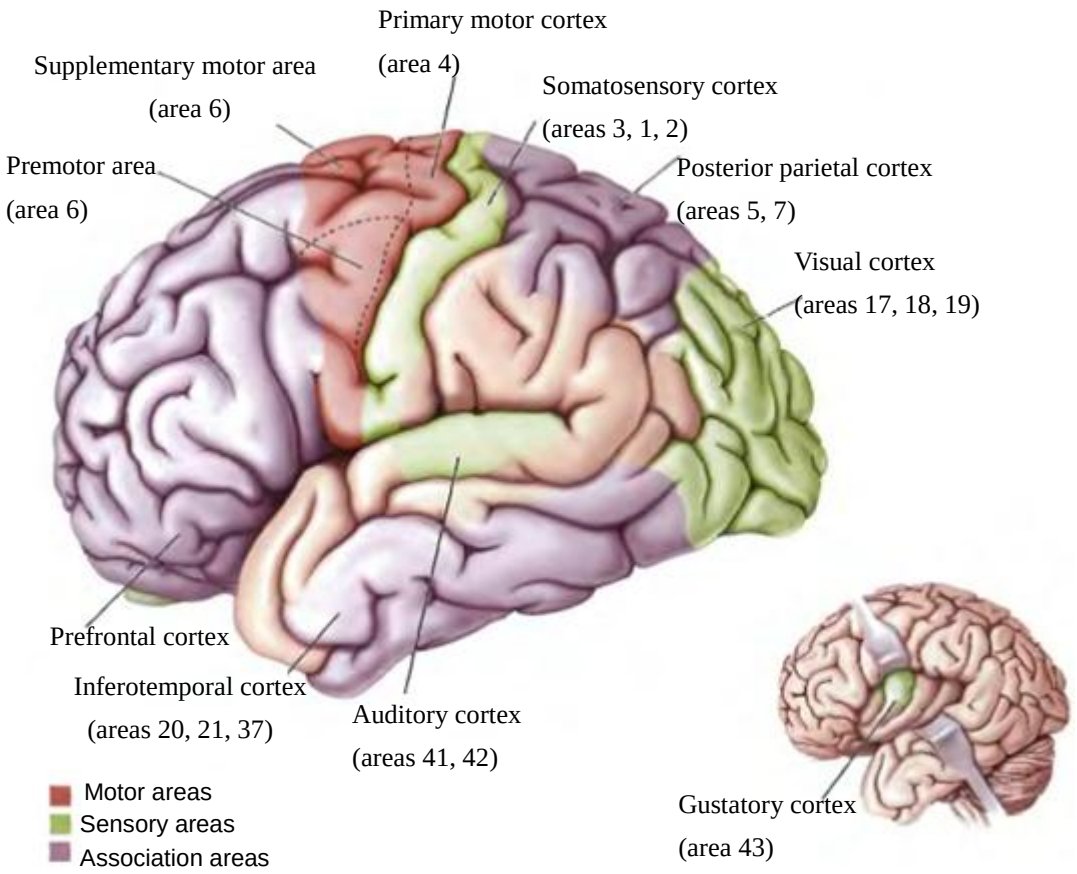

Figure 1.2: Functional classification of the sensorimotor cortex (taken from [5]).

The cerebral cortex has a corresponding somatotopic representation for processing information from each body segment. In the primary motor cortex M1, this somatotopic map is called a motor homunculus (shown in Figure 1.3), which illustrates the location and amount of cortical area associated with movement control of a particular segment. Although it represents each segment in an orderly way, the homunculus map is not scaled to the human body in size. The leg area located around the midline is small compared to the face and mouth areas which are located laterally on the cerebral hemisphere. The amount of cortical surface dedicated to a body segment is related to the degree of the required motor control [11]. Therefore, a large area of M1 is dedicated to moving the dexterous fingers. Due to their relatively large area in the motor cortex, the hands can make accurate and complex movements.

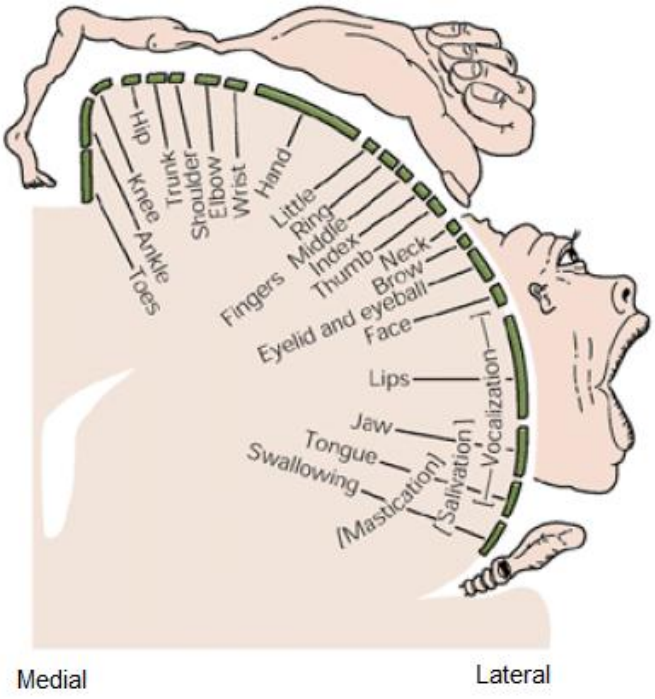

Figure 1.3: Motor homunculus (taken from [11]).

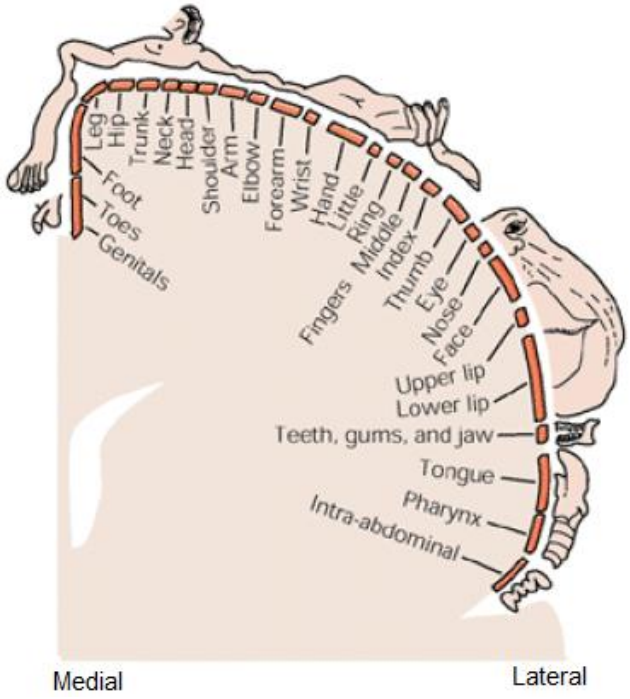

Figure 1.4: Sensory homunculus (taken from [11]).

In contrast to the motor area located in the frontal lobe, the part of the cortex concerned with the somatic sensory system is located in the parietal lobe. Brodmann area 3b, located on the postcentral gyrus, is regarded as the primary somatosensory cortex (called S1) [11]. It is responsive to somatosensory stimuli. Similar to M1, the receptive fields of S1 also produce an orderly map of the body on the cortex, which is called the sensory homunculus, as Figure 1.4 shows. The sensory homunculus illustrates the location and amount of cortical area receiving sensory information from a particular segment. Obviously the sensory homunculus map is not scaled to the human body either. The mouth, tongue, and fingers have the largest area, while the trunk and arm areas are small. The degree of innervation from each segment determines its mapping size on the brain [11]. For example, the sensory receptive field for the hands occupies a larger area than that for the shoulder.

The motor and sensory mapping helps to understand how the brain sends commands to and interprets feedback from each body segment. The brain controls the whole body through three levels [5]. First of all, the forebrain sets the movement patterns and plans strategies of how to achieve the target movements. Then mechanisms such as the motor cortex and cerebellum figure out when and how to contract the muscles smoothly and accurately. The last level of control involves the brain stem and more importantly the spinal cord. They are combined to activate appropriate motor neurones and interneurone pools to achieve target movements and make any necessary adjustments of posture, based on the sensory feedback.

1.1.3. Spinal cord

Located in the bony vertebral column, the spinal cord has spinal nerves which innervate the body. The spinal cord is the vital mechanism which transmits information

between the brain and parts of the body, such as the skin, joints, and muscles [12].

The spinal cord, as shown in Figure 1.5, is a long tubular bundle of nervous tissue that extends from the brain. The longitudinally distributed nervous tissues primarily transmit the signals between the PNS and the brain. Sensory signals enter and motor information exits from the spinal cord via segmental root nerve pairs [13]. The spinal nerve roots are classified based on the vertebrae between which they exist. Within the spinal vertebrae exist 31 spinal nerve pairs associated with four sections [13], as shown in Figure 1.5.

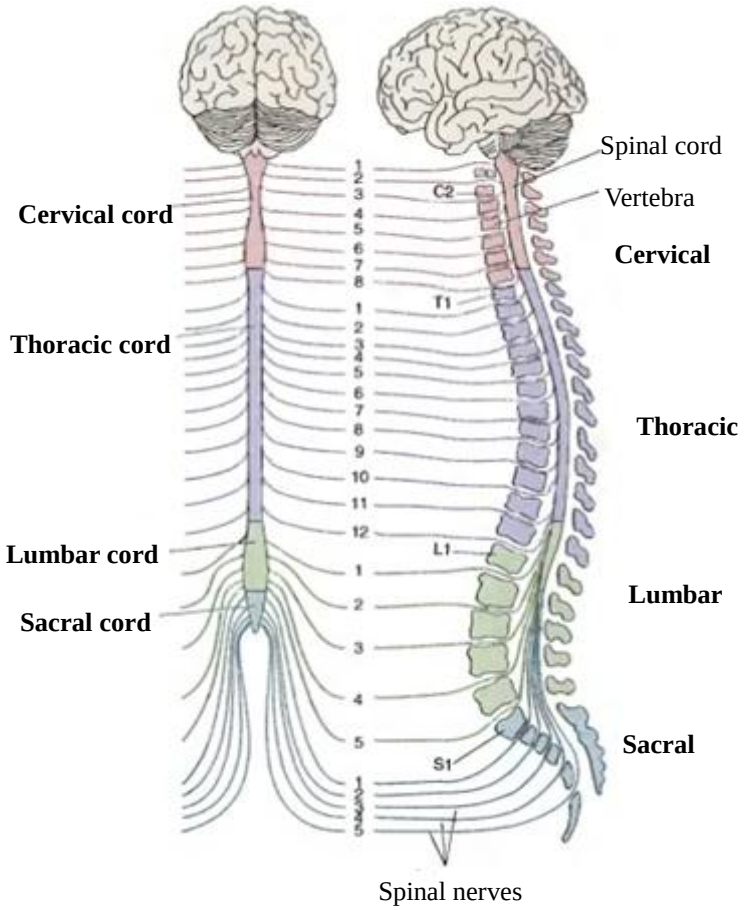

Figure 1.5: Spinal nerve classification (taken from [13]).

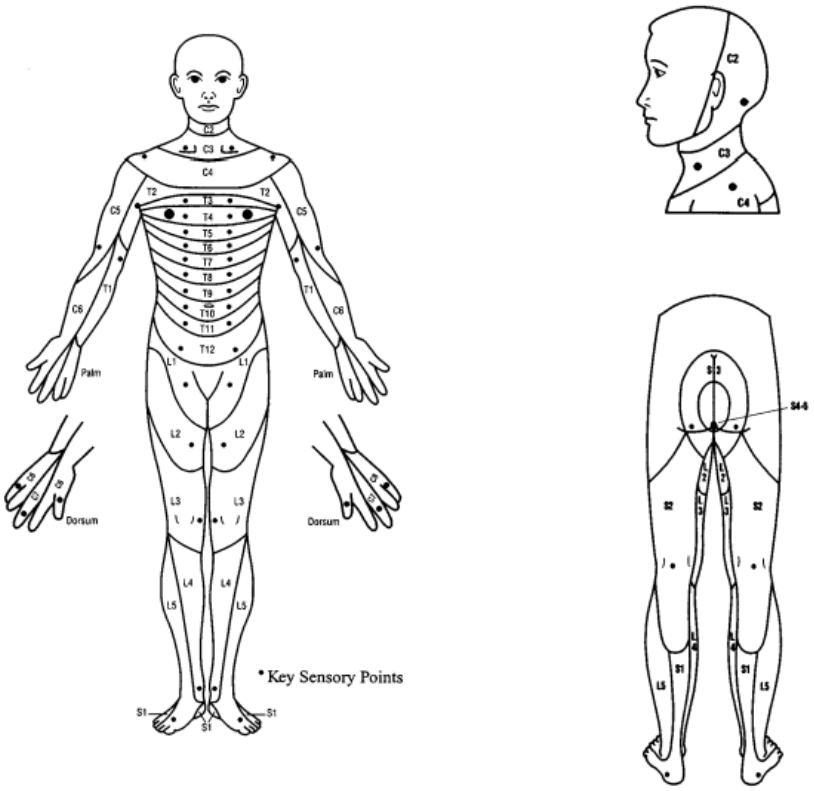

Figure 1.6: The key sensory points of the human body (taken from [14]).

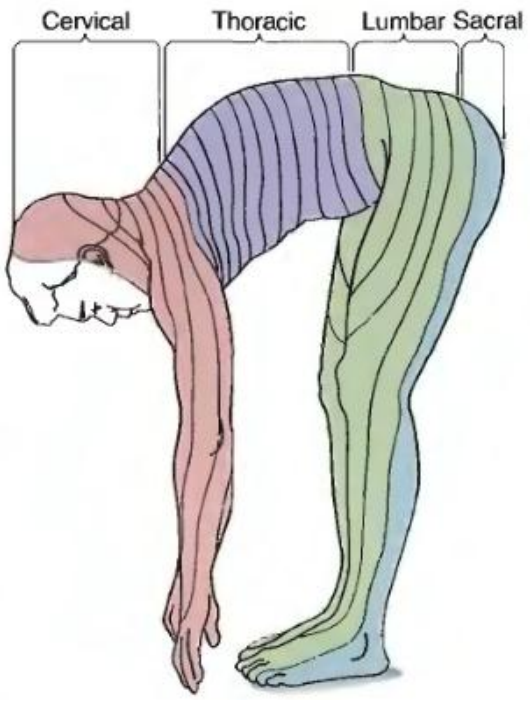

Figure 1.7: Dermatome maps (taken from [13]).

Spinal roots have sensory and motor fibres. A skin area innervated by sensory fibres of a single nerve root is known as a dermatome, while the group of muscles primarily innervated by motor fibres of a single nerve root is defined as a myotome. The distribution patterns of dermatomes and myotomes are relatively consistent from person to person. The dermatomes cover the whole body, with the key sensory points of the human body demonstrated in Figure 1.6 [14]. The organization of the dermatomes and the corresponding body segments for each section can be depicted when one bends over to stand on both hands and feet, as Figure 1.7 shows. Cervical nerve pairs (C1-C8) innervate the muscles and glands of the neck, shoulder and upper limbs; thoracic nerves (T1-T12) innervate the chest and abdominal organs; lumbar nerves (L1-L5) innervate the lower limbs; sacral nerves (S1-S5) take account of the genitals, lower digestive tract and bladder while coccygeal nerve (Co) is distributed to the skin over the tailbone [13].

Spinal nerves enter and exit the spinal column through notches between each vertebra of the vertebral column. As shown in Figure 1.8, each spinal nerve inside the vertebrae attaches to the spinal cord by means of two branches: the ventral root and the dorsal root [13] . The ventral root contains motor axons, which carry information away from the spinal cord, while the dorsal root contains sensory axons, which bring sensory information into the spinal cord. Sensory axons which carry information from the somatic sensory receptors to the spinal cord are called primary afferent axons, such as axons innervating the skin. The primary afferent axons enter the spinal cord through the dorsal roots, with the cell bodies lying in the dorsal root ganglia [13].

The spinal cord is protected by three layers of tissue, with the dura mater in the outermost, the arachnoid mater in the middle and the pia mater in the innermost layer [5]. A cross-section of the spinal cord displayed in Figure 1.8 shows that the central

grey matter is surrounded by the white matter. The butterfly-shaped grey matter contains neuronal cell bodies. Each half of the spinal grey matter is divided into the dorsal, lateral and ventral horns. The lateral horn has visceral neurones that innervate the internal organs, blood vessels, and glands. The ventral horn contains the somatic motor neurones while the dorsal horn has the somatic sensory neurones. In contrast to the dorsal root ganglia which contain primary sensory neurones, the dorsal horn mainly contains second-order sensory neurones, which receive sensory inputs from the primary afferents. The white matter, which is located in the peripheral region of the spinal cord, contains the long axons that run up and down the cord to generate ascending (sensory), descending (motor) and transverse fibre tracts (opposite sides of the cord). The white matter is divided into three columns: the dorsal, lateral and ventral columns, with spatial distribution as shown in Figure 1.8.

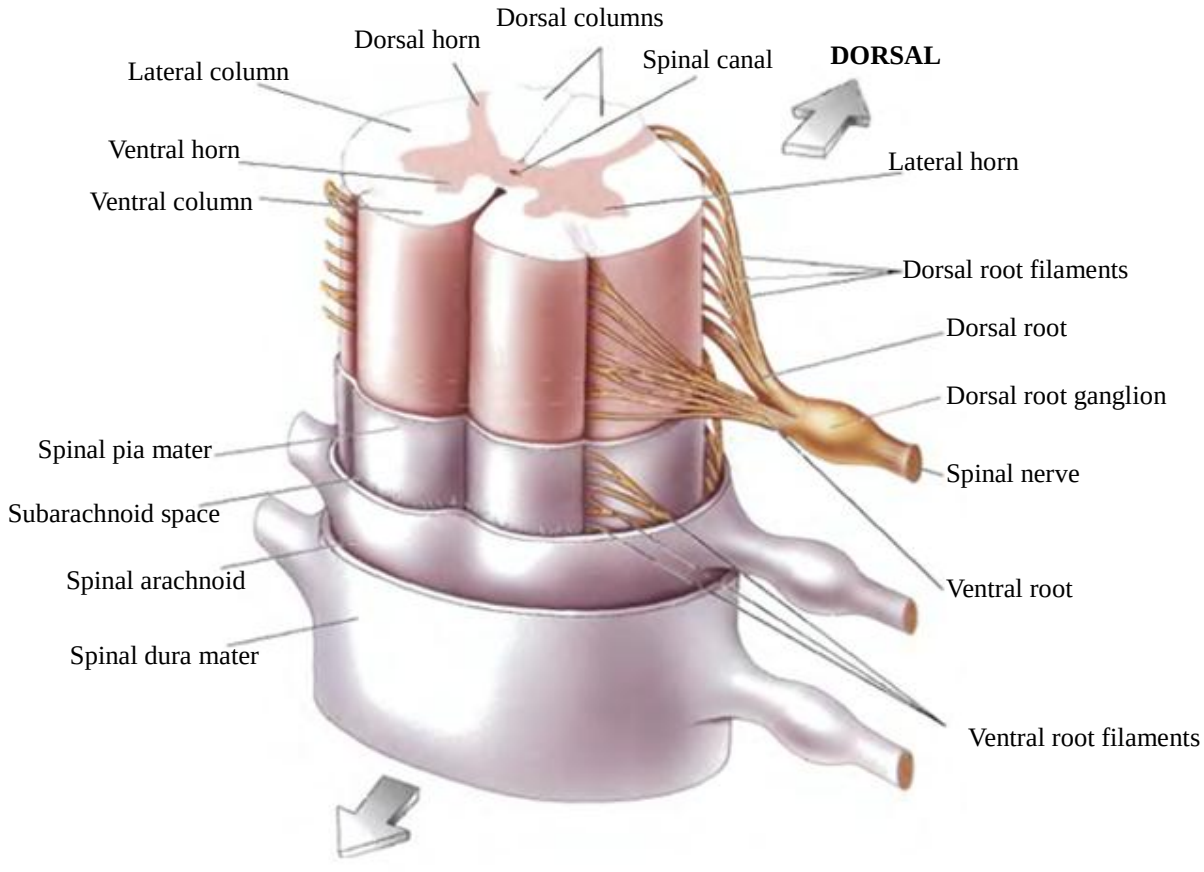

Figure 1.8: Structure of the spinal cord (taken from [5]).

1.2. Somatic System

As described above, the nervous system apart from the brain and spinal cord is the PNS, while the somatic system, as one part of the PNS, has nerves innervating the skin, joints, and skeletal muscles [5]. The somatic system includes sensory and motor systems, which carry sensory and motor information both to and from the CNS. Accurate motor control cannot be achieved without feedback from the somatic sensory system or voluntary control by the somatic motor system. This complicated process involves different pathways for transmission of motor and sensory information.

1.2.1. Somatic sensory system

The somatic sensory system includes all the somatic receptors and the innervated axons. The skin is innervated by many primary afferent axons, which bring stimuli from the somatic sensory receptors to the spinal cord or to the brain [13]. Existing all over the body, somatic receptors detect sensations such as touch, temperature, pain, and body position [13]. Three types of the sensory receptors are the most important in the somatic sensory system [13]. The first type is mechanoreceptors, which are sensitive to mechanical stimuli, such as vibration, touch or pressure. The second type is nociceptors, which transmit the sensations of pain and temperature. They respond to mechanical, thermal and chemical stimuli. The last type of receptor in the body is proprioceptors, which provide information on the position and movements of the body segments.

To ensure accurate and smooth motor control, the brain receives sensory feedback continuously from the spinal cord via many ascending tracts. The cerebellum receives the sensory information for balance control through the ipsilateral spinocerebellar tract,

which can be seen in the cross-section diagram of the spinal cord shown in Figure 1.9 [15]. The cerebral cortex receives various afferent inputs from the limbs and trunk from ascending tracts, as marked blue in Figure 1.9. Such ascending tracts transmit sensory information in two ascending pathways, as shown in Figure 1.10.

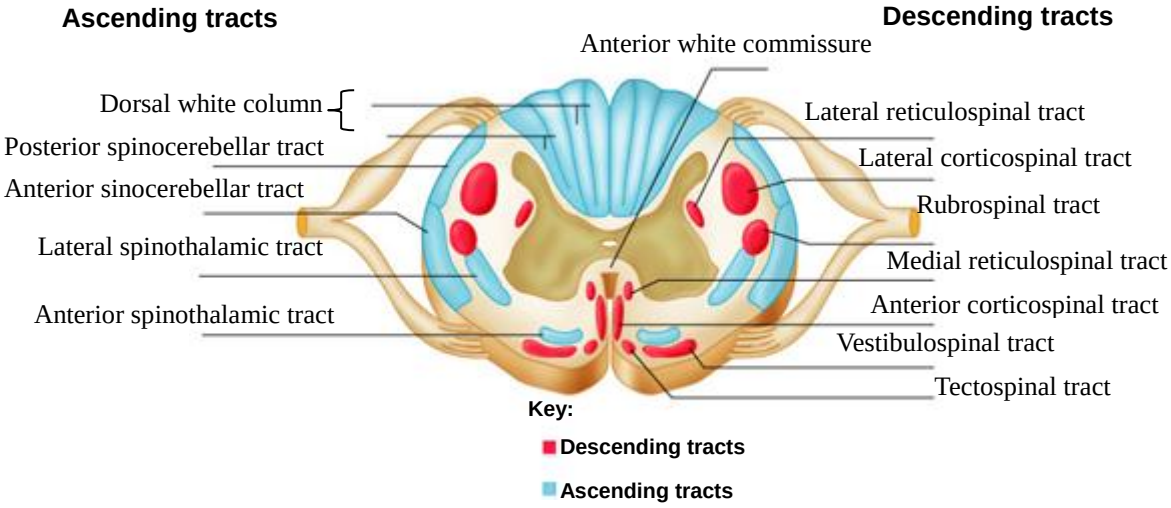

Figure 1.9: Descending and ascending spinal tracts (taken from [15]).

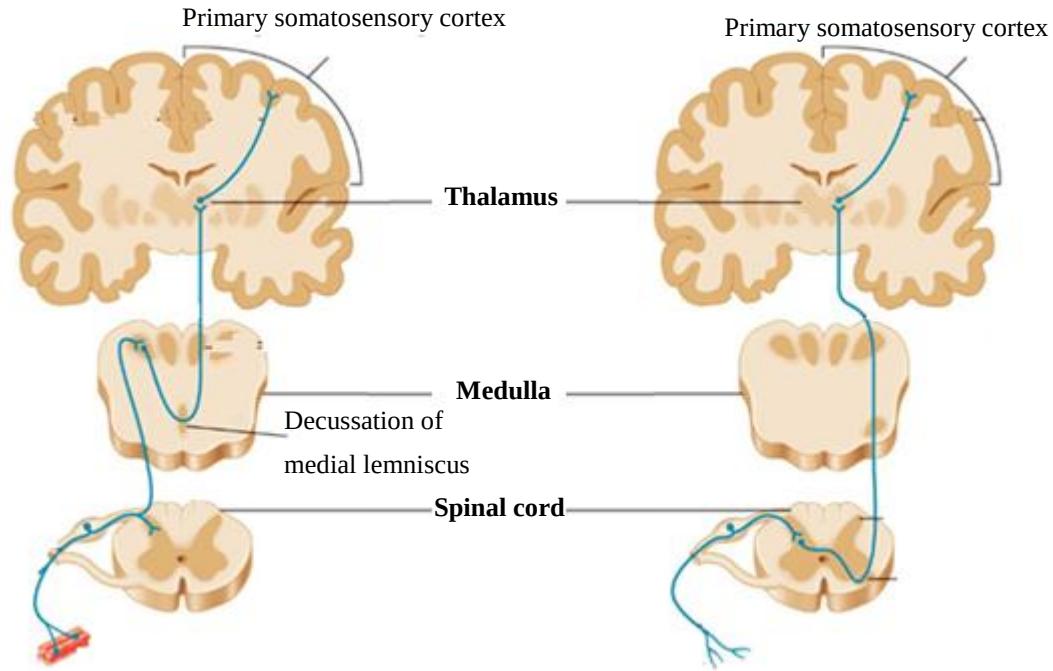

(a) Dorsal column-medial lemniscal pathway. (b) Spinothalamic tract.

Figure 1.10: The ascending tracts (taken from [13]).

The sensations of light touch, pressure and proprioception are transmitted by large-diameter dorsal root ganglion axons. Such large axons ascend in ipsilateral dorsal columns to the junction of the spinal cord and medulla, and then cross (or decussate) to the contralateral side and finally project to specific regions of S1 in the contralateral cerebral hemisphere [13]. This cross-over process is called decussation and this tract is called the dorsal column-medial lemniscal pathway, as shown in Figure 1.10(a). Other types of sensation, such as pain and temperature, are transmitted through second-order neurones in the dorsal horn of the spinal cord. The axons of these neurones cross to the contralateral side immediately after they enter the spinal cord, then ascend through the thalamus and terminate at S1. This forms the spinalthalamic tract (see Figure 1.10(b)) [13]. The existence of two different ascending pathways results in the situation that some sensory information, such as light touch, ascends ipsilaterally, while other afferent input, such as pain and temperature, ascends contralaterally.

1.2.2. Somatic motor system

Similar to the definition of the somatic sensory system, the somatic motor system includes motor neurones and the corresponding innervated skeletal muscles [15]. The somatic motor system receives commands from the brain through many descending tracts, as marked red in Figure 1.9.

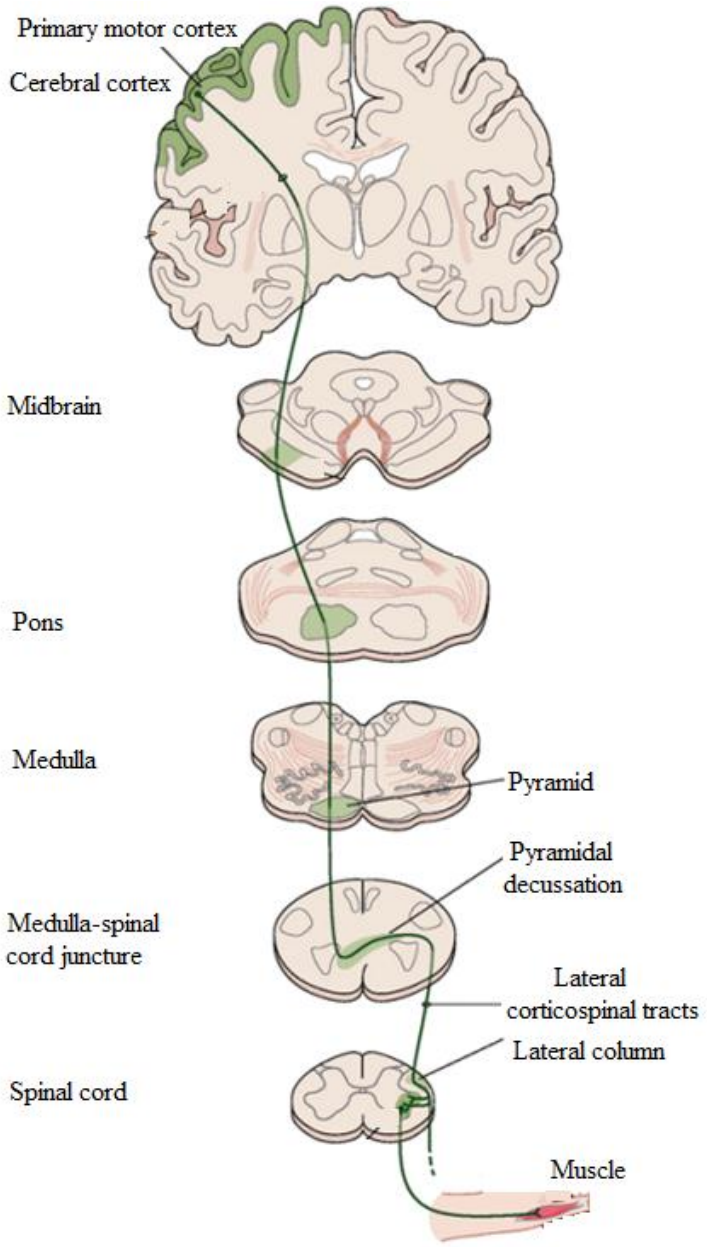

Figure 1.11: Lateral corticospinal tract (modified based on a picture from [16]).

Among the many tracts demonstrated in Figure 1.9, the reticulospinal, vestibulospinal and tectospinal tracts are related to activities of balance-keeping and locomotion, which are under control of the brain stem. The lateral pathways (rubrospinal and corticospinal tracts) are involved in voluntary movement of the distal musculature and are under direct cortical control [17]. As shown in Figure 1.11, the axons originating in the motor cortex travel through the thalamus and form the pyramidal tract at the junction of the

medulla and spinal cord. Then the pyramidal tract crosses at the pyramidal decussation, terminates in the lateral column of the spinal cord and forms the lateral corticospinal tract. The lateral corticospinal tract transmits information from the motor cortex to the ventral horns, and thereby controls the segmental muscles. This results in the situation that the right motor cortex directly commands the movement of the left side of the body, and vice versa [16].

1.2.3. Muscle

As described in Section 1.2.2, one of the most important components in the somatic system is skeletal muscle. Muscle is a contractile tissue within the human body which produces force and movement. The muscles in the body can be generally classified into striated and smooth muscle [18]. Smooth muscle is mainly found in visceral organs, such as the bronchus, the intestine, and blood vessels. Striated muscle has two subcategories: cardiac and skeletal. Innervated by the autonomic nervous system, cardiac muscle is mainly involved in heart contraction [18]. Skeletal muscle, which is mostly connected to bone through tendons, achieves skeletal movements such as locomotion and maintenance of posture [18]. For an average adult, skeletal muscle takes up about 42% of body mass for males and 36% for females [19].

In contrast to involuntary cardiac and smooth muscle, skeletal muscle can be voluntarily controlled. As Figure 1.12 shows, skeletal muscle consists of extrafusal muscle fibres, which are innervated by the lower motor neurones with their cell bodies in the anterior horn of the spinal cord [18]. Motor neurones are classified into upper and lower motor neurones according to their positions. Upper motor neurones refer to the nerve tracts in the neural pathways between the brain and the anterior horn cells of the

spinal cord. The nerve fibres connecting the anterior horn of the spinal cord to the relevant muscle are the lower motor neurones [20]. Extrafusal muscle fibres are innervated by α motor neurones. α motor neurones mainly participate in muscle force generation. One α motor neurone and the muscle fibres it innervates make up a motor unit. Each motor unit is innervated by a single motor axon branch from the CNS. The individual motor unit or the combined action of these motor units induces muscle contraction. The collection of motor neurones that innervates a single muscle is called a motor neurone pool [18].

In parallel with extrafusal muscle fibres are muscle spindles, which encapsulate intrafusal fibres. A muscle spindle is innervated by group Ia and II afferent fibres. Group Ia fibres are capable of detecting changes of muscle length and velocity, whereas group II fibres detect changes in muscle length. As the zoomed area in Figure 1.12 shows, intrafusal fibres are innervated by γ motor neurones, which help to ensure the sensitivity of a muscle spindle [18]. The muscle spindle combined with the innervated sensory axons forms a stretch receptor. If the muscle is stretched, the muscle spindle will be excited and activates both α and γ motor neurones, which results in muscle contraction (stretch reflex).

Stretch receptors are one type of proprioceptors. Another type of proprioceptor are Golgi tendon organs. Innervated by group Ib sensory axons, Golgi tendon organs mainly detect the tension inside the muscle [18]. In contrast to stretch receptors, which are in parallel with muscle fibres, Golgi tendon organs are located in series at the junction of muscle and tendon.

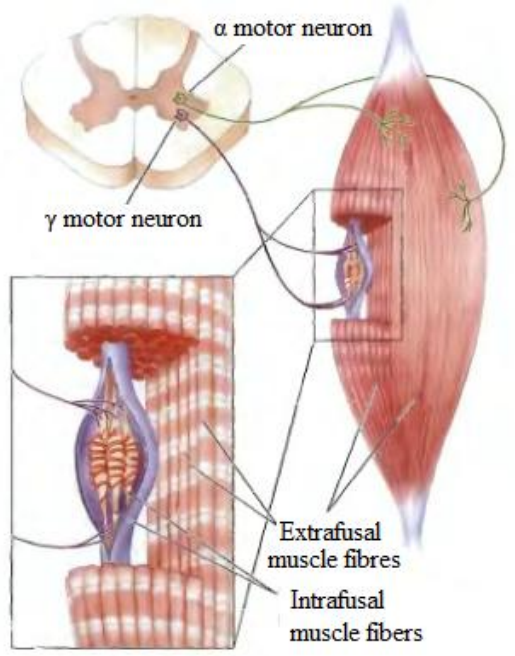

Figure 1.12: Muscle fibre structure and neurone innervation (from [18]).

Muscle spindles and Golgi tendon organs detect body movement and provide feedback for accurate voluntary control of the human body. Apart from muscle control and sensory information processing, the somatic system is involved in reflex activity, which is an involuntary and rapid movement in response to a stimulus [21].

1.3. Spinal Reflex

Involuntary muscle movement without conscious input from the brain is defined as a reflex [21]. The reflex that is mediated by neural circuits entirely confined to the spinal cord is the spinal reflex. The spinal reflex is elicited by the activation of the spinal reflex arc, which includes the muscle as well as the innervated sensory and motor axons passing between the vertebrae at the same spinal level [21]. A spinal reflex is classified into a monosynaptic or polysynaptic spinal reflex [21].

1.3.1. Monosynaptic reflex

A monosynaptic reflex involves direct connections between sensory and motor neurones in the spinal cord. Knee jerk and the stretch reflex are typical examples of monosynaptic reflexes. As shown in Figure 1.13, muscle stretching because of tapping on the patellar tendon or any other mechanical force activates Ia sensory axons in the muscle spindle. Ia afferents then transmit such stretch induced biological signals to their cell bodies in the dorsal root ganglia. Then α motor neurones in the spinal cord are activated and send efferent impulses back to the muscle for contraction. Such muscle contraction in response to the muscle stretch is called the stretch reflex [22]. The muscle contraction involves only one synaptic process in the activation of the Ia sensory and the α motor neurones. Therefore the latency (the time between the stimulus initiation and the reflex response) of the monosynaptic reflex is very short, ranging from 35-50 ms for soleus [23]. As a result, the stretch reflex is a quick reaction to unexpected disturbances, resulting in maintenance of the muscle at a constant length.

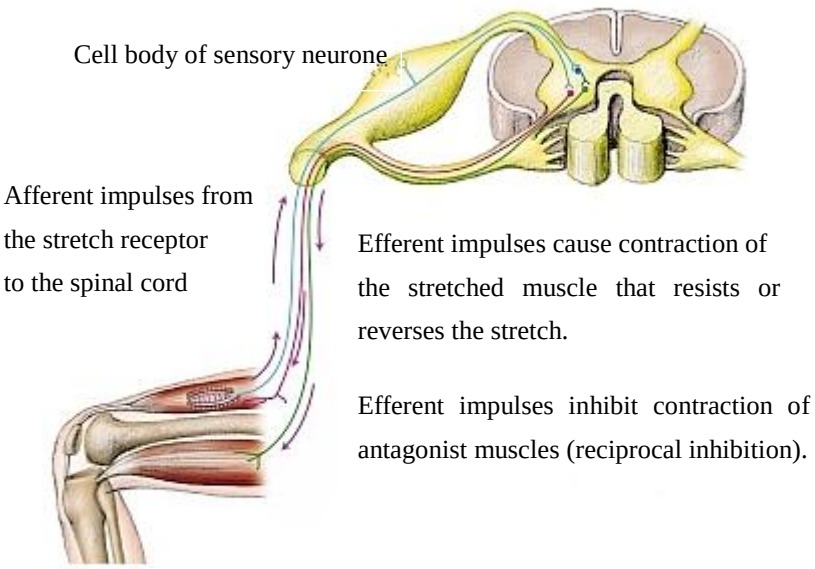

Figure 1.13: Stretch reflex (from [22]).

1.3.2. Polysynaptic reflex

Most other spinal reflexes involve polysynaptic circuits. Compared to the monosynaptic reflex, polysynaptic reflexes respond more slowly to the stimulus, resulting in a longer latency ranging from 50-120 ms for lower leg muscles [24-26]. A cutaneous reflex is a polysynaptic reflex in response to a cutaneous stimulus. Cutaneous receptors such as mechanoreceptors detect such a stimulus as a touch, a scratch or mechanical pressure and induce a cutaneous reflex [21]. A typical example of the cutaneous reflex in the lower limbs is the corrective reaction to stumbling over unexpected objects during walking [27] or running [28].

High stimulation intensity induces a cutaneous flexor reflex with movements such as ipsilateral flexion and/or the concomitant contralateral extension [28]. When a person steps on a sharp tack as shown in Figure 1.14, the nociceptors in the skin detect the noxious information and transmit signals through afferent fibres to the spinal cord, where the information is distributed to interneurones. A branch of the afferent pathway excites interneurones in the lumbar region of the spinal cord, resulting in contraction of the thigh flexor muscle. One branch also continues upward to the L2 segment, exciting the hip flexor muscles. This process finally induces the coordinated activity of two muscle groups to withdraw the whole leg away from the painful stimulus [29].

Cutaneous flexor reflexes work not only at a single joint but coordinate the activity of multiple joints simultaneously. Similar to the stretch reflex, the flexor reflex takes place without conscious intervention of the brain. However, the flexor reflex can be modified by the brain's participation. People can inhibit the withdrawal response by voluntary brain control [30].

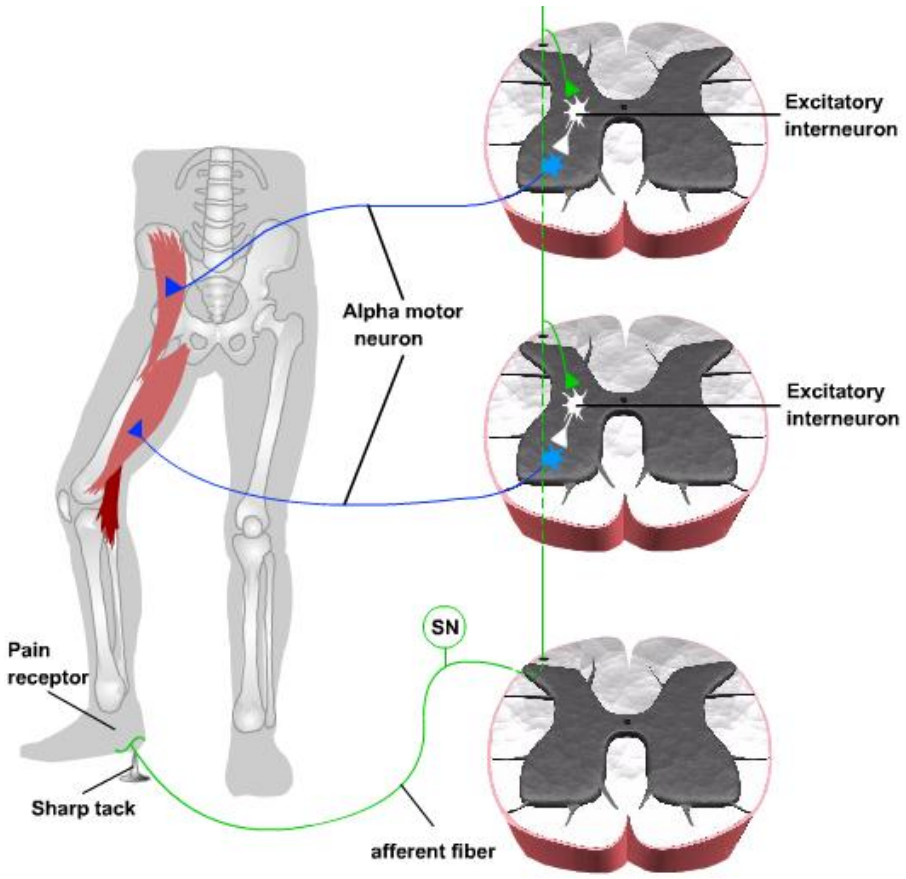

Figure 1.14: Flexor reflex (from [29]).

The spinal reflexes described above interact with human movement. The stretch reflex prevents muscle overstretching and maintains postural balance while the cutaneous flexor reflex produces coordinated patterns of muscle contraction to withdraw from noxious stimuli [11]. Reflexes of various types serve as the basic units for human movements [21].

1.4. Spinal Cord Injury

Damage to or disease of the spinal cord may interrupt the neural pathways between the brain and the muscles. Spinal cord injury (SCI) results in impairment of motor, sensory and autonomic function below the level of the lesion, which brings disability of varying

severity to the patients.

1.4.1. Epidemiology of SCI

SCI is a global phenomenon with annual reported incidences for different countries and regions ranging from 10.4 per million in the Netherlands, to 83 per million in Alaska, USA in the early 1990s [31]. The highest incidence of SCI occurs in North America, followed by Asia. The incidence is estimated to be 40 per million in the United States, with approximately 12,000 new cases each year [32]. The global prevalence of SCI per million inhabitants ranges from 223 in Stockholm and 280 in Helsinki to 681 in Australia and 755 in the USA [31]. The incidence is approximately 10-15 per million in the UK [33]. There were an estimated 40,000 individuals with SCI in the United Kingdom, with 745 new admissions to spinal injuries units in 2001 [34].

1.4.2. Causes of SCI

SCI can result from traumatic and nontraumatic causes. It is estimated that two thirds of all patients with SCI have traumatic injury. Events such as traffic accidents, falls, sports and recreational activities induce fracture or dislocation of vertebral segments and damage of the spinal cord tissue [35, 36]. Combined with haemorrhage, the initial traumatic injury triggers inflammation, which results in further damage to spared white matter located at the site of injury [37, 38]. Young healthy male individuals are more likely to suffer traumatic injury than female individuals [33].

Nontraumatic injury mainly comes from multiple sclerosis [39], vertebral spondylosis, tumorous compression and some congenital diseases [40]. People with nontraumatic

SCI are reported to be significantly older than those with traumatic SCI (55 versus 39 years) [39]. Females have a higher proportion of nontraumatic SCI than traumatic SCI [41].

1.4.3. Lesion types

Damage to the motor and/or sensory neurones results in various degrees of dysfunction of movement control [18] and may cause complete or incomplete paralysis. Paralysis does not mean that the muscles cannot function but that they cannot be controlled by the brain. Any damage to the motor-sensory spinal circuits located in the lower motor neurones destroys signal transmission for the spinal reflex. Therefore lower motor neurone lesions induce flaccid paralysis due to the disruption of the basic movement unit of spinal reflexes. Any damage to the upper motor neurones spares the reflex arc but interrupts the interaction between central control and the spinal reflex. Upper motor neurone lesions result in spastic paralysis with exaggerated and uninhibited sensorimotor reflexes below the lesion level [20].

Spinal cord lesions are generally classified anatomically and clinically. A transection of the spinal cord results in loss of sensation and paralysis of the muscles in parts of the body caudal to the lesion. Such anatomical lesions often occur to experimental animal models through special preparation. Unless penetrated by a sharp object, the spinal cord is rarely hemisected or transected in humans. Lesions often include infarction or mechanical deformation caused by swelling or contusion, which interrupts normal neural transmission [42].

1.4.4. Lesion level

Spinal cord lesions can occur at different levels and induce impairments with varying severity. Injuries are normally classified based on the affected vertebral segments [15].

Cervical SCI is most common in the elderly [43]. Injuries to the cervical regions of the spinal cord are defined as tetraplegia, which normally causes impairment or loss of motor and/or sensory function in all four limbs as well as the trunk and pelvis. Based on the correspondence between the spinal segments and the controlled body areas as depicted in Figure 1.7, lesions at different spinal segments induce function impairments at different locations. A cervical lesion above C4 results in paralysis of all torso muscular systems. Patients with SCI at C3 or above need ventilation assistance to achieve breathing. Lesions between C4 and T1 have various degrees of sensorimotor sparing in the shoulder and/or the arm. Lower injuries in the thoracic, lumbar or sacral regions are called paraplegia, where the trunk, pelvis and lower limbs usually have impaired function and/or sensation [33]. As the most common locations within the spinal cord for tumorous invasion and vertebral spondylosis are in the thoracic and lumbosacral regions, people with nontraumatic SCI are more likely to suffer from paraplegia than from tetraplegia [40].

1.4.5. Neurological classification

Variation in the level and severity of the lesion results in substantial variation in neurological deficits. In order to assess sensorimotor function, the Neurological Standards Committee of the American Spinal Injury Association (ASIA) designed a system to classify the neurological impairment of people with SCI [14].

SCI normally affects transmission of sensory and motor signals across the lesion site. The extent of damage determines the severity of the motor deficit and loss of sensation. By examining the dermatomes and myotomes, the severity of SCI can be classified into five ASIA classes as follows:

A= complete. No motor or sensory function is preserved in the sacral segments S4-S5;
B= incomplete. Sensory but no motor function is preserved below the neurological level and includes the sacral segments S4-S5;
C= incomplete. Motor function is preserved below the neurological level, and more than half of key muscles below the neurological level have a muscle grade less than 3;
D= incomplete. Motor function is preserved below the neurological level, and at least half of key muscles below the neurological level have a muscle grade greater than or equal to 3;
E= Normal. Sensory and motor function is normal.

In the above classification, the muscle grade is a scale for a patient's physical muscle strength. A muscle grade of 3 means the patient can hold the test position against gravity but can tolerate no additional pressure [44].

The neurological classification scales are presented in Figure 1.15. An injury inducing complete loss of sensory and motor function including the sacral segments S4-S5 is defined as clinically complete SCI while any situation with partial preservation of sensory and/or motor function below the neurological level, including the sacral segments S4-S5, is classified as incomplete SCI (iSCI). Incomplete injury is more prevalent than complete, with 91% of nontraumatic injury and 58% of traumatic injury classified as incomplete [40].

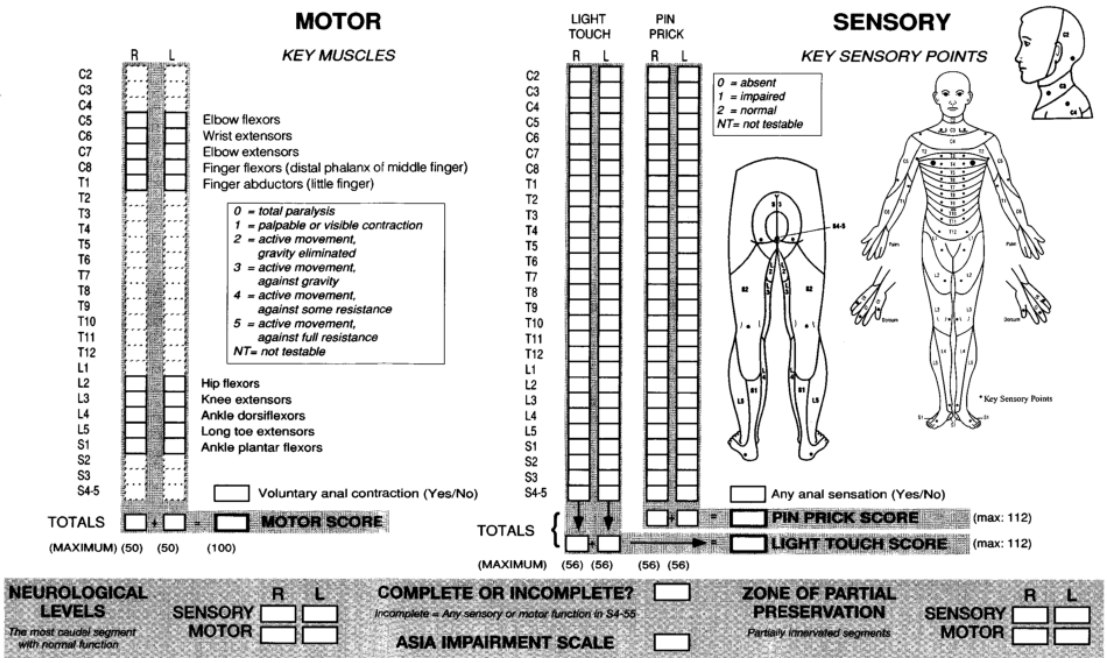

Figure 1.15: Standard neurological classification of spinal cord injury (from [14]).

1.4.6. Incomplete SCI syndromes

Incomplete SCI (iSCI) partially damages the spinal cord with some function spared, which results in various SCI syndromes. Incomplete SCI syndromes can be characterized into central cord syndrome, anterior cord syndrome and Brown-Séquard syndrome. Other syndromes such as conus medullaris syndrome and cauda equina syndrome may also result from incomplete injury [39]. The most common syndrome is central cord syndrome. As the name implies, it refers to an injury at the centre of the spinal cord [15]. Central cord syndrome affects the upper extremities more than the lower extremities [39]. Anterior cord syndrome has a lesion at the anterior two thirds of the spinal cord but the function of the posterior cord is spared [15]. This results in various losses of motor function and sensation to pain, temperature and pinprick, with preservation of proprioception and light touch. Brown-Séquard syndrome constitutes 2-4% of all traumatic SCI [15]. The senses of light touch, deep pressure, and

proprioceptive information are disrupted on the same side as the injury, while the senses of pain and temperature are impaired on the opposite side [39]. Conus medullaris syndrome and cauda equina syndrome result from injury to the sacral cord and lumbar nerve roots within the spinal canal, which usually causes areflexic bladder and bowel as well as flaccid paralysis [15]. Compared to cauda equina syndrome, which has no sacral reflex preserved, conus medullaris syndrome results from lesions localized proximal to the sacral cord, which occasionally shows a sacral reflex [39].

1.5. Health Degeneration after SCI

People with SCI suffer from loss of sensation and/or motor function, and disruption of autonomic function. Apart from the primary effects of the injury, patients suffer further health degeneration as secondary complications, which raise the need for suitable rehabilitation and care strategies.

1.5.1. Cardiovascular disorders

Lesions above T5 generally affect autonomic innervation of the heart and lungs, which results in weakened cardiac control [45]. This is because sympathetic outflow to the heart and lungs comes from levels T1-T5 [46]. Due to lack of venous muscle pump activity, people with SCI commonly suffer orthostatic hypotension (OH), which is a clinical condition defined as a significant decrease in blood pressure during position change, such as head-up tilt from lying, or sitting to upright standing [47]. OH elicits a passive shift of blood away from the thoracic area and toward the distensible veins of the splanchnic region and lower extremities [48]. Patients with SCI have episodes of dizziness, light headedness (pre-syncope) or loss of consciousness if OH occurs.

Approximately 50% of paraplegics and 80% of tetraplegics suffer OH, with the greatest severity occurring in patients with complete tetraplegia [47]. Due to impaired motor function, most individuals with SCI have sedentary life patterns. They are susceptible to cardiopulmonary deconditioning as well as metabolic disturbance [49].

1.5.2. Pressure ulcers

Prolonged compression over a bony prominence combined with decreased tissue perfusion and ischemia induces pressure ulcers. Increased friction between the skin and the support is an additional factor for pressure ulcers [39]. The loss of sensation prevents early detection of such skin problem. Skin care is a critical component of health maintenance for patients with SCI. Pillows and cushions should be employed to create a comfortable soft seat. The patients should be taught how to change position regularly. Close attention should be given to minimizing friction over the skin when patients are to be moved [39].

1.5.3. Musculoskeletal deterioration

Individuals with SCI experience various degrees of musculoskeletal deterioration [50]. The musculoskeletal system retains a remarkable degree of load-dependent plasticity, with structure gradually adapted according to physical demands. Regular physical training increases muscle volume, while reduced activity results in muscle atrophy and weakness. As a result of disuse, patients with SCI demonstrate rapid atrophy of the paralysed muscles, with the lower-limb muscles being 45% smaller six weeks after injury [51].

Apart from muscle weakness, SCI triggers a transformation of muscle composition. Skeletal muscle broadly constitutes two subtypes of muscle fibres: Type I (slow twitch fibres) and Type II (fast twitch fibres) [18]. Red Type I fibres can utilise more oxygen and sustain aerobic activity, resulting in fatigue resistance. Type II is further divided into IIa with high oxidative capacity, and IIb as anaerobic, glycolytic, "white" muscle. Type IIa fibres are red fibres and fatigue resistant while anaerobic Type IIb are white and quicker to fatigue. The healthy population has various types of muscles composed of fast and slow twitch muscle fibres. Spinal cord injury can affect the proportion of the different fibre types present in muscle tissue, with the consequence that muscle fibres change from slow-twitch, fatigue-resistant muscle to fast-twitch, fatiguable muscle [52]. This muscle transformation affects the potential endurance capacity of patients with iSCI who have some motor function [53].

1.5.4. Bone fracture

Similar to the load-dependent plasticity of muscle, bone responds to mechanical stimuli. Paralysis or a long term sedentary lifestyle leads to reduced loading in the skeletal system, which brings an imbalance in bone metabolism. Patients with SCI usually experience bone demineralization after injury. Bone mineral density decreases at a rate of 2–4% a month, and reduces to only half of the normal density in the paralyzed limbs within the first 3 years after SCI [54, 55]. The reduction of strain applied on the bone is thought to be an important contributor to bone demineralization [56]. Due to osteoporosis, fractures may easily occur during daily activities such as bed-wheelchair transfer [57], which further restricts the mobility of patients with SCI and increases the chance of rehospitalisation. The annual incidence of fracture is about 2% in patients with motor complete SCI and the incidence increases over time, with the average time

of first fracture being 9 years after injury [58]. It is thought that there may be some benefit to regular intensive loading activities in the early stage of rehabilitation [59].

1.5.5. Neurological development after SCI

Apart from physiological degeneration, SCI-induced sensorimotor interruption generates neurological adaptations, which are often presented as spinal shock initially followed by spasticity.

The characteristics of spinal reflexes change according to the time after SCI [60]. Within 24 hours after injury, patients experience areflexia/hyporeflexia, where normal spinal reflex responses, such as the stretch and flexor reflexes are absent. The tibial H-reflex (a reflex after electrical stimulation of sensory fibres, which is analogous to the mechanically induced spinal stretch reflex) returns by about 24 hours. The cutaneous reflex becomes stronger during the period between 1 to 3 days after injury. Most tendon reflexes first reappear from approximately 4 days to 1 month after injury [60].

Within one month to one year after injury, patients with upper-motor-neurone SCI suffer from spasticity/hyperreflexia. Cutaneous reflexes and deep tendon reflexes become hyperactive and may respond to minimal stimuli, such as light touch. Spasticity refers to involuntary, uncontrolled muscle spasms and increased tone due to increased spinal reflexes. Spasticity normally presents as spastic hypertonia, which is a motor disorder characterized by a velocity-dependent increase in tonic stretch reflexes (muscle tone) with exaggerated tendon jerks, and increased muscle tone resulting from hyperexcitability of the stretch reflex [61]. Following recovery from spinal shock,

spasticity appears with spasms such as extensor spasms, flexor withdrawal spasms and clonus, in individuals with upper motor neurone lesions, especially in patients with iSCI [62, 63]. In order to prevent any potential injury to the patient, spasm may be reduced through pharmacological interventions targeted at the central or peripheral neuromuscular mechanism [64].

In summary, people with SCI suffer not only from the primary consequences of the injury, such as paralysis or loss of sensation, but also from a number of secondary issues. Complications, including metabolic disorders and musculoskeletal deterioration, tend to reduce mobility and further deteriorate the daily life quality of people with SCI [6].

1.6. Conclusions

In summary, damage to or disease interrupting communication between the brain and the spinal cord may result in impairments of motor, sensory and autonomic functions. As a consequence of the physiological problems associated with SCI, many individuals have neurological impairments and functional deficits. This highlights the importance of suitable rehabilitation programmes, to reverse or to alleviate health degeneration [7]. Rehabilitation technology has been used in an attempt to restore walking function of patients with SCI in clinical settings with encouraging results. The following chapter briefly discusses the basic theory of SCI rehabilitation. The available literature relating to the research and use of various kinds of rehabilitation systems for recovery of walking in people with SCI is then examined and discussed with particular emphasis on early rehabilitation of walking.

Chapter 2. Literature Review

Summary: SCI disrupts signal transmission between the brain and the spinal networks, resulting in varying degrees of function impairment below the injury level. Neural plasticity provides a basis for rehabilitation after SCI. Research on the central pattern generator (CPG) gives evidence for restoration of locomotion. For patients with iSCI where some function is preserved in the lower extremities, intensive task-specific locomotor training has been shown to promote gait restoration [65]. An overview of rehabilitation programmes of walking, including traditional physiotherapy and the newly developed robotic-assisted training, is given, followed by a critical examination of the literature related to early rehabilitation programmes for walking. The aims and objectives of the research described in this thesis are then given based on these findings.

2.1. Rehabilitation after SCI

SCI brings various impairments which severely reduce the quality of life of patients. However, due to neural plasticity, various degrees of recovery can be obtained after injury. Neural plasticity refers the capacity of neurones to rearrange anatomical and functional connectivity according to environmental circumstances, resulting in new or modified features and behaviours [66]. The central nervous system (CNS), based on neural plasticity, is capable of continuous alteration of neural pathways and synapses. Such plasticity exists in both healthy and injured situations, which enables variable degrees of recovery both in the brain and the spinal cord. Recovery occurs both spontaneously after injury and in response to rehabilitative therapies.

2.1.1. Spontaneous recovery

Neurones can spontaneously increase their plasticity after injury and construct new networks, which provides the basis for recovery and compensatory behaviours [67]. Some spontaneous recovery can be observed within a few days after injury [68]. In response to disrupted axonal pathways and/or segmental spinal cord circuits, biological systems renew themselves for functional compensation. Anatomically spontaneous plasticity induced by SCI includes sprouting, axon elongation and synaptic remodelling [69]. Both the damaged and the intact neurones can grow dendrites and/or lengthen axons to project into the damaged area. Research on rats [68] demonstrates that SCI leads to a remodelling of synaptic structures in the motor cortex. Rats with a right cervical overhemisection injury at the C4 level show dendritic spines (small membranous protrusions from a neurone's dendrite that typically receives input from a single synapse of an axon) in the motor cortex with increased diameters. SCI leads to a higher proportion of longer spines [68]. Apart from anatomical modulation of neurones, the cells around the lesion are stimulated by the injury to proliferate spontaneously. The new cells replace some of the damaged cells [38, 70], resulting in novel pathways to re-establish the lost supraspinal control [71].

As injured axons in the mature CNS have relatively limited regeneration capability, spontaneous recovery of motor function is mainly mediated by structural reorganization of the spared motor system. Research on animals demonstrates that substantial brain mapping reorganization occurs spontaneously in response to SCI. Compensatory remodelling mechanisms such as synaptic plasticity, axonal sprouting and cellular proliferation trigger CNS reorganization, which occurs at multiple levels of the neuraxis including the motor cortex, the brainstem, spinal cord centres as well as

descending supraspinal tracts [68].

Research on monkeys suggested that sensorimotor cortex organization could be modified after SCI [72, 73]. After a partial section of the dorsal columns in the cervical region, hand stimulation still activated the hand territory in BA 3b (which can be seen in Figure 1.2) because of the remaining dorsal column afferents. After about one month the area of activation was greatly expanded. After half a year, large reorganization occurred such that the hand territory became responsive to afferent inputs from the face [73]. The capacity for dynamic modulation of representational maps is not limited to the sensory neocortex, but is also evident in the motor maps of the adult primary motor cortex [74, 75].

A large degree of reorganization of sensorimotor cortical maps has been revealed in adult mammals following SCI, and such cortical plasticity is gradually being detected in humans as well. Studies with transcranial magnetic stimulation demonstrated motor cortex plasticity in both chronic and acute patients with SCI [76, 77]. Patients with complete SCI at low thoracic levels showed a larger fraction of the motor neurone pool activated by magnetic stimulation, with motor evoked potentials from a larger number of scalp positions than healthy subjects [76]. An expanded cortical motor map of the preserved segments (such as biceps muscle) was also detected in patients as early as 6 days after SCI [77]. The area of expansion depends upon the degree of intact motor function following SCI at different spinal levels. Paraplegics showed a stronger and more widespread cortical activation compared with tetraplegics [78]. It is suggested that spontaneous reorganization of neuronal activity occurs within these supraspinal sensorimotor centres, most probably as a consequence of reduced and altered afferent input from the spinal cord [78].

Spontaneous cellular, structural, and electrophysiological changes occur in the brain and spinal cord [79]. Some of these spontaneous changes promote recovery, while some appear to be maladaptive, such as inter-limb reflex activity. Stimulation of lower limb nerves or the skin in persons with injury to the cervical spinal cord induces contraction of the distal upper limb, due to new synaptic interconnections between lower limb sensory afferents and motor neurones in the cervical region [80]. Such contacts between ascending afferents and cervical motor neurones do not appear to provide any functional benefit. Rehabilitative strategies could be used to enhance adaptive plasticity and/or mitigate maladaptive plasticity to enhance recovery after SCI.

2.1.2. Activity-dependent spinal cord plasticity

Plasticity occurs in the CNS and it can be shaped by physical activity. The CNS possesses the capacity to acquire new function based on use and activity. The brain's activity-dependent plasticity is commonly seen, for example, in that right-handed people have a more dexterous right hand, but continuous practice and usage of the left hand can make both hands similarly dexterous. The spinal cord, like the brain, shows activity-dependent plasticity [81-84]. Peripheral inputs or central outputs from the brain can cause lasting changes in the spinal cord. Cats with complete spinal cord transection with preserved forelimb function could be trained in standing or stepping, if specific training was carried out. However, step-trained cats could not stand while stand-trained cats could not step [81]. Activity-dependent spinal cord plasticity is important for motor skill learning [85], which is also demonstrated in humans. Numerous clinical studies have clearly demonstrated that rehabilitation can be improved by task-specific training. For example, patients who underwent locomotor

training with adequate sensory input had greater mobility than those without gait training [82-84], while intensive hand training showed significant improvements in hand function [86-88].

The mechanism of activity-dependent plasticity can be explained by cellular and molecular function improvement. Physical training, including active or passive training, increases neurotrophins, a bundle of proteins which promote neuronal survival, differentiation and growth [66]. Brain-derived neurotrophic factor mediates learning and memory, alleviating cognitive decline. Physical exercise regulates the levels of the neurotrophic factor, decreases lesion size and enhances cognitive and motor function [66]. Furthermore, physical activity promotes regenerative sprouting in various tracts after SCI. It was shown that wheel running stimulated fibre growth caudal to the lesion in mice [89], while treadmill training increased axonal regrowth and collateral sprouting proximal to the lesion site [90]. Activity induced cellular change modulates axon connectivity in interneurones, which in turn correlates with functional recovery [91].

Apart from cellular function, activity produces lasting change in the spinal cord via sensory inputs with impact on motor function. The function of spinal circuits can be modulated by physical activity. Sensory input to the spinal cord changes the motor neurone excitability, which is revealed by research on spinal reflexes. For example, afferent input related to C-fibre stimulation can induce habituation and sensitization of flexion withdrawal reflexes [92]. Epidural electrical stimulation in motor-complete patients induced rhythmic lower limb motion. This revealed that the physiological state of spinal networks can be modulated by sensory information into a source of control for movement in the absence of supraspinal input [93, 94]. Assisted stepping with sensory

input activated the motor neurone pool resulting in a reciprocal pattern of activity in the lower limbs of patients with iSCI, with activation of some muscles which could not be recruited during their voluntary contraction of individual joints [95]. Such observations provide evidence that activity dependent plasticity can be manipulated to induce therapeutic effects.

CNS plasticity provides important neurochemical foundations for rehabilitation. Although CNS plasticity remains throughout life, it should be activated in an appropriate manner at an appropriate time. Task-specific rehabilitation should be started as soon as is safely possible [66]. Patients with SCI show a gradually decreased flexor reflex amplitude over time, which might imply a gradual loss of activity from spared neurones following SCI, most probably due to immobility [96]. Early rehabilitation training should be organized to maximize positive neurological adaptations.

2.2. Theories for Rehabilitation of Walking

Neural plasticity theory highlights the importance of a suitable rehabilitation programme. Advances in acute medical management of SCI have improved survival rates. The mean life expectancy of people with SCI ranges from 70% to 92% of the normal population [97]. Given that the mean age of patients sustaining their injury is in the early thirties [31], individuals with SCI live many years with their disability and the associated morbidity. When asked about their priorities during rehabilitation, patients with SCI consider restoration of walking as one of their most important goals [98, 99]. There are some theories and evidence which support rehabilitation of walking after SCI.

2.2.1. Central pattern generator (CPG) in animals

Many animals models have demonstrated that the adult mammalian lumbosacral spinal cord can achieve stepping in the absence of supraspinal input as long as adequate sensory information is provided periodically and balance is secured [100-105]. Such spinal networks for generation of rhythmic patterned locomotion are now called the central pattern generators (CPGs).

There are many reports of locomotion recovery after spinal transection in lower vertebrates and mammals [101, 103, 105]. Without any central control, rhythmic patterned locomotion can be achieved by the CPGs. At the start of the last century, the intrinsic capability of the spinal cord to produce rhythmic movements was discovered from classical experiments on dogs [106]. After various investigations on rodents and other vertebrates including turtles [107], chickens [108] and cats [109], CPGs in animals were found to be comparatively autonomous neural networks located from the lower thoracic (T11 to T13) through the lumbar regions of the spinal cord [110].

In the early 1900s, stepping movement was induced in a spinal cat with a complete lesion [106]. Modern evidence of CPGs came from an experiment on kittens carried out by Forssberg and colleagues [111]. Fourteen kittens had spinal cord transection between T10 and T12. Some muscle tone appeared in the hindlimbs one or two days after the spinal cord transection. When the trunk was held, there was alternating flexion and extension in the hindlimbs. As the kittens got older, they could walk without assistance for several steps. When the hindlimbs were placed on a treadmill, the kittens could adjust to walk at a wide range of speeds. If the speed increased sufficiently, the stepping could switch into a gallop. The shape and duration of EMG bursts from the

flexors and extensors in the lower limbs during treadmill locomotion were quite similar to those from healthy cats [111]. These behaviours were not restricted to the hindlimbs. Similar methods have been utilized successfully to induce stepping or fictive locomotion in the forelimbs [112, 113].

CPG networks provide the essential mechanism of spinal locomotion on the treadmill. However, adequate sensory inputs appear indispensable so as to adapt the spinal locomotion pattern to external conditions [114]. Studies on disturbed locomotion showed that cutaneous inputs played important roles in adapting locomotion to disturbances. For example, if one swinging hindlimb was transiently halted by an object, this limb would rise higher above the object to avoid the disturbance [115]. Afferent input from the skin around the feet contributes to EMG patterns [114]. After various degrees of denervation of cutaneous nerves at the ankle level of the hindlimbs, cats with partial denervation recovered locomotion, while completely denervated cats with no cutaneous inputs never recovered walking, regardless of training [101, 116].

Limb load and hip extension were revealed to be of great importance for locomotion coordination. The load function during locomotion was first proposed by Duysens et al. based on their observations on denervated cats [117]. The ankle flexor activity is inhibited after the ankle extensor is loaded, which results in a delayed swing phase. Limb loading largely influences locomotor activity in the walking cat [117]. Conway et al. further observed that proprioceptive input from the load resets central locomotor rhythm in spinal cats [118]. The importance of hip position in the initiation of flexion was discovered in an experiment in spinal cats walking on a treadmill [119]. When one leg's paw was supported off the treadmill, the contralateral limb continued walking, with rhythmic flexion and extension in the walking leg. It was only when the lift-off

limb was brought to a specific extension position that it initiated the swing phase. The extended hip position had a critical effect while the position of the ankle and knee failed to induce any effect. In conclusion, a certain extended hip position and a consequent small load applied on the limb activates the CPG networks to induce locomotion in animals.

2.2.2. CPG in humans

CPG networks contain adequate neuronal elements to produce rhythmic outputs which are quite close to normal motor patterns [103]. Positive evidence of CPGs in lower mammals has encouraged investigation of CPGs in humans [120]. In marked contrast to the abundance of evidence in animals, firm evidence of CPGs for stepping in the human is not so easy to obtain. One reason is that the healthy human has increased supraspinal control of walking from the mature nervous system [121]. Locomotion control from the developed brain might override the coordination functions from the spinal circuit. Another reason is that intense research in decerebrated or spinal humans so as to investigate direct evidence of CPGs is difficult [122]. There are some individuals falling into these categories, due to accidents or illness. But investigation on such populations is limited because stepping movement is hard to induce due to physical weakness [123]. In spite of many difficulties in CPG research on humans, many clues of the CPG's existence in humans have been captured by scientists.

Firm evidence was obtained from individuals whose brains were not fully developed. Human infants serve as good subjects for the study of generator networks in human walking. This innate stepping movement in infants between the ages of ten days and ten months was investigated by Yang et al. [122, 124]. Most infants displayed

apparent muscle activity of the flexor and extensor muscles when supported to step on a treadmill. By changing activity duration of the extensor muscles, infants achieved stepping at various speeds on the treadmill [122]. Evidence of CPGs in adults was revealed by Bussel et al. based on long-latency, late-flexion reflex responses in paraplegics [24]. Later hints of CPGs were obtained from rhythmic myoclonic movements of the trunk and lower limbs in a patient with clinically complete cervical spinal cord transection [125].

Epidural electrical stimulation in humans offers further evidence of CPG networks. Electrical stimulation on the lumbar spinal cord of a chronic patient with complete SCI induced rhythmic motion in the lower limbs when the subject was in a lying position [93]. Stepping sensory epidural stimulation of a chronic paraplegic with no motor but partial sensory function resulted in locomotor-like patterns in the leg muscles during manually assisted leg movement on a treadmill [94]. The muscle activity displayed a similar pattern to that in healthy subjects, as far as duration was concerned. This observation proved that CPG networks exist in the human spinal cord, and that it can be activated by appropriate sensory stimulation.

Similar to results from animals, CPG networks in humans are largely affected by the hip joint position and the load afferents on the foot sole. When complete paraplegics were supported to walk on a treadmill, the initiation of the complex bilateral leg muscle activity was found to be related to the hip joint angle [126, 127]. Further research suggested that the human spinal cord could modulate motor pool output in response to the load inputs [128]. The muscle activity of the lower limbs was directly related to peak limb load, and the response was similar in all subjects independent of the level of available supraspinal input.

In summary, research on CPG networks in animal models provides promising results for locomotion rehabilitation. Peripheral sensory information is indispensable so as to get an adaptable locomotion [119]. Hip extension is revealed to be of great importance for locomotion coordination while load inputs from the lower limbs guide locomotion for various walking phases and conditions. Increasing evidence of CPG networks in humans provides a further basis for design of rehabilitation strategies. Sensory inputs including appropriate hip joint positions combined with adequate lower-limb loading serve as important requirements for rehabilitation of walking.

2.3. Rehabilitation of Walking

Rehabilitation aims to help patients become as functional as possible, while taking account of disabilities and personal needs. Restoration of the walking ability is considered as the hallmark of a rehabilitation programme [129]. Based on task-orientated neural plasticity, suitable physical training is required for patients with SCI so as to restore walking.

Walking relearning after SCI is challenging, especially for those with a severe injury. Therefore a large multidisciplinary group of rehabilitation specialists, including nurses, physical therapists, physicians, and others, aims to develop effective strategies for ambulation. It has been well established in recent years that task-specific training is needed for function restoration, e.g. for gait training [129]. The most widely adopted approaches for neurological rehabilitation of walking include conventional overground training, training with orthoses, body weight support treadmill training (BWSTT), training with functional electrical stimulation (FES) and robotic orthosis technology [129].

2.3.1. Conventional gait training

Depending on the patient's physical condition, conventional gait training takes place overground with physical assistance provided largely by therapists [129]. Abnormal motor tone and postural reactions are typical phenomena in patients with neurological deficits and are considered as two key reasons for impaired motor function [63]. Therefore the muscle tone is initially addressed by such therapies as passive or active rotation of the patient's leg segments. Conventional rehabilitation strategies for lower limb function enhancement after SCI aim to restore or maintain the normal range of motion of each joint and elicit selective muscle contraction patterns, and thereby help patients control posture and motion.

Conventionally, gait training does not start until a patient has adequate strength and the necessary balance to support and maintain a standing position [129]. When the patient is physically too weak to maintain an upright position, some activities that can be implemented in a lying position are employed, including hip rotation, knee flexion and ankle massage. These passive training methods aim to maintain active joints for potential gait training [129]. Later on the patient is challenged to achieve various body positions, ranging from lying to sitting, and from sitting to standing. Position transfer is managed with physiotherapist assistance or the help of an external device, such as a tilt table for inclined lying. Supported standing training can be implemented with employment of a standing frame that locks the patient's knees in extension.

Conventional training ordinarily proceeds beyond supported standing only if the patient has adequate endurance and stability to stand in parallel bars [130]. Gait training starts with isolated motion within a gait cycle, e.g. weight shifting or limb loading.

Physiotherapists often help to adjust the trunk position and guide the leg movements. As the patient progresses in the single motion learning, physiotherapists introduce more complicated gait-targeted movements, such as heel strike and toe off [63]. By verbal instruction and tactile guidance, the physiotherapists assist the patient in loading the stance leg and mimicking the sense of ground force reactions. The physiotherapists also aim for at least 10 degrees of hip extension at the end of the stance phase and a correct position for heel strike at the initiation of stance [129].

By providing appropriate physiological afferent stimuli to the patients, conventional rehabilitation has been confirmed to promote the functional abilities of patients with SCI, with incomplete patients benefiting the most [130, 131]. More than 90% of ASIA C and all ASIA D patients achieved walking with minimal assistance after a twelve-week conventional gait training period [132]. However, conventional training is labour intensive for the physiotherapists who provide manual assistance for control of the trunk, pelvis, hip, knee, and ankle simultaneously. Therefore, the duration and intensity of rehabilitation is restricted, among other factors, by the physical fitness and ability of the physiotherapists to offer suitable rehabilitation practice.

2.3.2. Lower limb orthoses

The physiotherapist's working load can be partially reduced if some assistive orthoses are adopted. Furthermore, the use of bracing can ensure safe overground walking. Patients with SCI have many common motor deficits, such as a weak ankle joint, flat foot contact, knee collapse and excessive hip flexion. These factors have inspired many researchers to design bracing systems, also called orthoses, to aid foot clearance during the swing phase, to position the foot at the heel contact and to improve stability during

the stance phase [130].

Working in parallel with the lower extremity, a lower-limb orthosis aims to improve leg function by providing additional support. Rigid orthoses are often utilized to immobilize weak segments, while flexible orthoses allow limited mobility in the sagittal plane and constrain motion in the frontal and transverse planes. Orthoses, unless otherwise defined, are normally passive devices without actuators. They should be adjustable to the size and muscle strength of the patient. Physiotherapists normally evaluate the patient's limbs to see whether they are physically strong enough for adoption of orthoses [133]. There are several types of orthoses available to support standing and walking function [134], ranging from single-joint braces to whole-leg braces that extend from the lower back to the ankle.

An Ankle-Foot Orthosis (AFO) is employed to support the ankle-foot complex and control motion of the ankle to assist walking [135]. A traditional AFO has an upright metal brace, while the current AFO is more often made from plastic materials to reduce the weight. Most AFOs control ankle motion with a posterior stop limiting plantarflexion and/or a spring assisting dorsiflexion. During early stance, the upright brace bends backwards slightly. Therefore during the late stance phase, the plastic brace recoils forward to lift the foot automatically for swing phase initiation [136].

Patients with a weak knee joint may need a Knee-Ankle-Foot Orthosis (KAFO, also known as long-leg braces), which has an extra knee joint locking mechanism similar to the AFO [134]. The traditional KAFO fixes the knee and ankle in an appropriate standing position and allows ambulation with crutches. Walking with such a fixed knee joint is tiring, because the hip joint needs rising more than normal walking so as to

achieve ground clearance during the swing phase. This results in gait compensation skills, such as circumduction, hip hiking, and external rotation. To solve these problems, recent KAFOs are normally equipped with a pair of hinges that are locked to support constant extension of the knee during the stance phase, while the hinges are unlocked to allow bending during the swing or sitting phases [137, 138]. Such stance-control KAFOs allow knee flexion in the sagittal plane without medial-lateral rotation and hyperextension.

The patient who requires more hip and trunk stability needs a Hip-Knee-Ankle-Foot Orthosis (HKAFO), which has an extra pelvic band and two hip-joint braces over the KAFO [139]. The simple HKAFO prevents abduction and adduction with limited hip rotation. Two typical HKAFOs are the Hip Guidance Orthosis (HGO) and the Reciprocating Gait Orthosis (RGO). The HGO has flexion and extension stops for walking and a release mechanism that allows 90^{o} flexion for sitting. The RGO allows reciprocal hip motion in the sagittal plane through the reciprocal link so that flexing one hip joint extends the contralateral hip. Depending on the power of the lower limb muscles, use of these gait orthoses typically requires substantial support from the upper limbs [139].

The use of orthoses provides better stabilization of the relevant joints, resulting in improved leg function. More importantly, orthoses reduce the strenuous physical demands on physiotherapists, and some orthosis users even achieve independent walking [129]. Many studies confirm the positive results of using orthoses, such as increased step length and compensated motor control [136, 140, 141]. Orthoses facilitate the ability to stand independently and to achieve some functional ambulation skills, such as stepping up on kerbs or climbing stairs with crutches. Patients with

incomplete SCI increase gait speed and endurance when walking with an AFO, compared to walking without [142]. Further therapeutic effects have been observed, including reductions in the incidence of pressure sores and bone fractures [143].

The successful use of orthoses/braces is, however, largely dependent on individual factors, including the injury level, age, motivation, upper extremity strength, as well as spasticity and contractures [144]. Patients with complete SCI require external assistance to achieve basic stepping without falling. Orthoses are more appropriate for patients who have good postural control and a good level of physical fitness. Although patients with iSCI may benefit from the use of othoses, in many cases the quality of walking is not sufficient for daily life. The speed is relatively slow, with a high energy cost [139, 145-147]. The maximum walking speed achieved with the use of orthoses ranges from 0.15 to 0.45 m/s [145, 148, 149], which is less than half of the optimal speed (1.1 m/s) required for successful daily ambulation.

2.3.3. Therapist-assisted BWSTT

In order to reduce the risk of falling for those who cannot keep balance, Body Weight Support (BWS) has been used to assist gait training [150]. Using an overhead harness, BWS unloads a proportion of body weight to assist patients in an upright position. BWS reduces excessive hip and/or knee flexion during the stance phase. More importantly, BWS provides a more secure environment for training, therefore the patient is confident and more motivated to practise walking. BWS also provides better balance control [151]. The harness provides support to the trunk without generating any compensatory asymmetry or forward trunk flexion. BWS relieves physiotherapists from labour-intensive work. It is challenging for them to simultaneously adjust posture,

balance and stepping, as in conventional therapy. With BWS holding the trunk and securing balance, physiotherapists can fully concentrate on improving the coordination of movement. As the BWS rehabilitation programme progresses, the amount of body weight support can gradually decrease, challenging the patient to support more weight during postural and balance control.

BWS is sometimes used during overground walking [151]. However, those who have weak muscles in the lower limbs cannot create enough friction for overground forward progression if too much of their weight is supported by BWS. Practical rehabilitation of walking with BWS is usually carried out using a treadmill [152]. Initiated in a study by Barbeau et al. [153] in 1987, the training approach called Body Weight Supported Treadmill Training (BWSTT) opened new perspectives for patients with SCI. This gait training strategy was motivated by experiments on spinal animals which restored locomotion after treadmill training [65, 101, 153]. CPG theory implied that locomotion could be achieved by integrated afferent sensory inputs. In order to provide an adequate sensory stimulus for rehabilitation of walking, the gait pattern during locomotor training should be as close as possible to the gait pattern of able-bodied people during overground walking.

BWSTT programmes use a harness to assist the patient in an upright position on a treadmill as shown in Figure 2.1. The moving treadmill belt translates the standing leg backwards, with adequate hip extension at the end of the stance phase. Suitable swing speeds and step lengths are adjusted manually by the physiotherapists. They place one hand above the patient's popliteal fossa and the other hand above the patient's heel to facilitate the swing phase, including foot clearance at toe off and foot stabilization at heel strike. BWSTT is carried out with help from one to three physiotherapists,

depending on the severity of the patient's injury. One or two therapists sit by the side of the patient. One more assistant stands behind with the hands on the patient's hips to facilitate trunk alignment, pelvic rotation, weight shifting, and hip rotation [154]. Furthermore, mirrors are placed in front of and at the side of the patient to provide visual feedback of body position and leg motion. BWSTT is designed to provide as much sensory feedback as possible, similar to that occurring during normal overground walking.

Figure 2.1: Therapist-assisted BWSTT (from [155]).

Therapist-assisted BWSTT is considered as a safe and effective approach to facilitate locomotor rehabilitation after SCI [82]. Numerous studies have investigated the training effects of BWSTT in patients with SCI [82, 83, 156-160]. Patients with complete injury can achieve stepping with coordinated flexion/extension movements and phasic EMG activity during BWSTT [83, 156, 157]. Many patients with iSCI recover walking abilities to various degrees after BWSTT [158-160], with improved symmetry of load capacity and muscle activation patterns from the lower limbs [158, 161]. Regular BWSTT (150-300 minutes per week, 3 to 23 weeks) enabled more than 70% of wheelchair-bound patients to walk independently, and those who could already walk before BWSTT improved walking speed and endurance [82]. BWSTT is at least as efficient as conventional methods of gait restoration. Studies [82, 159] showed that more than 80% of subjects with iSCI who underwent BWSTT achieved improvements in functional ambulation compared to only 50% of the initially non-ambulatory subjects who improved functional ambulation after a conventional rehabilitation programme. The multicentre randomized Spinal Cord Injury Locomotor Trial [132, 162] also reported notable improvements in walking function in patients with iSCI after 12 weeks of BWSTT. Therefore, the efficiency of BWSTT has been affirmed by such extensive clinical trials.

BWSTT, compared to conventional overground training and training with passive orthoses, secures postural stability through BWS and assists smooth forward progression. All three gait training interventions discussed so far involve extensive manual assistance from physiotherapists. The advantage of manual assistance is that the physiotherapist moves the patient’s body segments through direct contact. The experienced physiotherapist can recognize the level of assistance that the patient needs for basic stepping, and provides various amounts of assistance as required within each

step cycle. However, this assistance may be inconsistent, because it is a subjective judgement, resulting in different inputs from different physiotherapists, or variation when the same physiotherapist becomes fatigued as the training progresses [163]. It is labour intensive work for physiotherapists to act as the main source of power to assist training. In order to provide more assistance to patients and reduce the labour intensity of the physiotherapists, it would be beneficial if a training modality can be employed which provides additional energy for walking training. Such additional mechanisms can be "muscle actuators" induced by FES or mechanical actuators, achieved by additional mechanical devices.

2.3.4. FES

FES can be described as an active power system, capable of eliciting motor responses for standing and/or walking apart from a range of other functions. Functional electrical stimulation uses short bursts of electrical pulses to generate muscle contraction. The electrical stimulation intensity determines the muscle contraction level, thereby controlling motion. Stimulation intensity is adjusted by its pulse waveform, amplitude, duration and frequency [164]. By adjusting stimulation intensity, FES can reduce disability and produce functional activation of paralyzed muscles [165]. Electrical stimulation employs surface electrodes or implanted electrodes for better activation and mobility control [166].

FES was initially employed to correct foot drop in stroke patients [167]. It was applied on the peroneal nerve to improve the swing phase by activating the tibialis anterior muscle for ankle dorsiflexion. The stimulation was triggered by hand or by foot switches using either force-sensing resistors or mechanical contacts. The utilization of

FES in patients with SCI has received substantial interest since the 1970s, when muscle contraction and the standing position were achieved in this population [164, 168, 169].

Patients with complete SCI adopt FES as part of an assistive device for permanent use. With stimulation of muscles around the ankle and knee joints, paraplegic individuals with complete SCI regained a simple reciprocal locomotion pattern [169], and achieved basic stepping in parallel bars [170]. Long-term training improved maximal stimulated knee moment with symmetrical muscle responses from both legs [171]. However, in order to improve the walking pattern, extra stimulation channels on hip flexors, extensors and abductors were required for appropriate hip motion, which resulted in a complex multichannel stimulation strategy [172, 173]. Furthermore, the absence of all motor and sensory (in particular proprioception) function reduces the gait restoration efficiency. Without proprioceptive feedback, patients with complete SCI totally rely on visual observation of limb position to relearn walking [174]. Depending on muscle condition, patients with iSCI use different stimulation methods for walking rehabilitation. If the patient has a weak ankle, gait synthesis can be achieved by stimulation of ankle plantarflexors to assist push-off at the end of the stance phase and to enhance initiation of the swing phase. If the patient has an unstable knee joint, the knee extensors are stimulated to stabilize the stance leg. Extra stimulation is applied over the hip extensors for better position [174].

FES-assisted walking systems induce simultaneous hip flexion, knee flexion and ankle dorsiflexion by activation of the withdrawal reflex. As discussed in Chapter 1, patients with SCI often exhibit exaggerated spinal reflexes that have negative effects on gait training [175]. The use of FES to induce complex withdrawal reflex movements is believed to restore normal spinal reflex activity, thereby decreasing the functional

impairments [175]. As expected, most studies showed that patients with iSCI improved their gait parameters (walking speed or distance) when FES was used [174, 176]. FES reduces the effort from the physiotherapist, and assists some patients in independent walking [176]. It is well established that repetitive movement training associated with afferent input facilitates recovery of motor function [177]. An EMG-induced FES system results in better motor control than non-triggered electrical stimulation because the muscle contraction and joint translation are coordinated with the patient's cognitive intention [178].

Walking performance is influenced by how long and how actively the patient regularly practises. Long-term training with FES-assisted walking brings a significant increase in the strength of voluntary contraction [179]. One year's usage of FES increases maximal overground walking speed [180]. The improvements in functional ambulation persist even when the stimulator is turned off (carry over), including increased walking speed, cycle length and frequency as well as stance time when the patients walk on their own [180]. FES modifies joint angular kinematic patterns in walking, but long-term training integrates these changes into functional gains [180]. Benefits of FES exercises are more than just a matter of walking distance or speed. FES produces therapeutic benefits, including reduced spasticity, less muscle atrophy and increased postural stability [179].

In spite of varying degrees of success in patients with different degrees of injury, FES succeeds in activating the weakened or paralyzed muscles for gait rehabilitation. Compared to passive motion guided by physiotherapists, FES-assisted motion is driven by the patient's own muscle. FES has been investigated as an effective tool for muscle activation in gait training, and employed in conjunction with mechanical orthoses or BWSTT training, in the hope of reducing the need for manual assistance.

2.3.5. FES orthoses

FES orthoses have been designed for patients with SCI, based on the high energy expenditure in walking assisted by conventional mechanical orthoses. FES is utilised to elicit a withdrawal reflex of the lower extremity with the goal of improving the gait pattern and reducing manual assistance. Furthermore, combination with orthoses can simplify the FES stimulation system, especially for those patients who do not have adequate balance. Given that mechanical orthoses are effective in stabilizing the lower limbs, the hybrid orthosis achieves mechanical stability from an orthosis with a prototype walking pattern induced by FES. Research has found additional positive effects of FES orthoses compared to FES or mechanical orthoses alone [142, 181-183]. FES hybrid orthoses increased gait speed and endurance, improved the gait pattern and reduced upper extremity exertion [142, 181]. FES may also be combined with bracing to stabilize the trunk and to facilitate forward progression [181-183].

In order to provide a more secure gait training environment for those who are physically weak, FES technology has been combined with BWSTT, reducing the need for manual assistance. The motorized treadmill assists propulsion of the stance limb, which promotes hip extension. The swing phase can be assisted with FES by using the flexion withdrawal response evoked by stimulation of the common peroneal nerve. The activation of reflexes provides further theoretical support for FES combined with BWSTT [99]. FES-assisted BWSTT has been tested with promising clinical results [184]. An overall enhancement of functional ambulation was achieved in patients with ASIA C SCI, demonstrating favourable outcomes when BWSTT was combined with FES [184]. After long term use of FES assisted treadmill training (1.5 hours a day, 3 days a week for 3 months), chronic patients with iSCI who initially had asymmetrical

lower limb function demonstrated improved intra-limb coordination, with increased walking speed and lower extremity muscle strength [185]. Four weeks of BWSTT combined with FES (25 minutes a day, 5 days a week) increases walking endurance more than conventional therapy, resulting in a better effect on overground gait parameters [186].

Although laboratory studies reported the efficacy of FES systems in improving ambulatory function for patients with SCI, the effectiveness of FES technology varies between patients with different degrees of muscle strength and injury levels. Different stimulation parameters, such as pulse width, frequency, and duration need to be adjusted for each individual so as to attain an optimal training stimulus. It was reported that some patients found they could use the FES device easily on a regular basis and that they walked better with FES, while others reported difficulties in finding the best electrode positions and parameters for effective stimulation [187]. As is well established, muscle deconditioning after SCI is characterized by a reduction in the size of individual muscle fibres and changes of muscle fibre type [51]. These alterations result in a loss of strength and/or reduced endurance of muscular contraction. Such functional changes of the muscle indicate a need for FES to reverse muscle degeneration, but at the same time they present obstacles to implementation of FES. Because of muscle structure modification over time, contraction via FES in SCI is not as efficient as in able-bodied subjects. The reduced endurance of muscle contraction results in rapid fatigue, which restricts the general application of FES in people with SCI.

2.3.6. Robotic gait orthoses

In contrast to FES orthoses, dynamic orthoses utilize mechanical actuation to induce motion of the human body. Mechanically actuated orthoses can provide consistent, repetitive and prolonged gait training. Many types of actuators, including electric motors [188, 189], torsion springs [190], and artificial pneumatic muscle [191-193], have been investigated with positive results in movement control. Apart from relatively simple orthoses for one or two segments of the lower limb described in [188-193], various complex robotic orthoses have been developed to guide the training of both lower extremities and to support body balance. Such systems include the Lower Extremity Powered Exoskeleton (LOPES) [194], the Active Leg Exoskeleton (ALEX) [195], the Ambulation-assisting Robotic Tool for Human Rehabilitation (ARTHuR) [196], the Pelvic Assist Manipulator and the Pneumatically Operated Gait Orthosis (PAM /POGO) [197], as well as three commercially available rehabilitation devices: Lokomat [198], Lokohelp [199] and the G-EO robotic gait system [200].

The LOPES device, designed by Asseldonk et al. at the University of Twente, includes an exoskeleton for each leg and a pelvic support, as shown in Figure 2.2 [194]. The pelvic support can translate freely back and forth and from left to right. A parallelogram device with bearings and weight compensation allows upward and downward motion of the trunk. Each leg exoskeleton has three rotational electric motors: two at the hip joint (for flexion/extension and abduction/adduction) and one at the knee (for flexion/extension), providing three degrees of freedom (DOFs). LOPES is designed to operate with a treadmill. The patient is balanced with supports around the pelvis and hip to reduce the skin irritation which may occur when using an overhead harness BWS system.

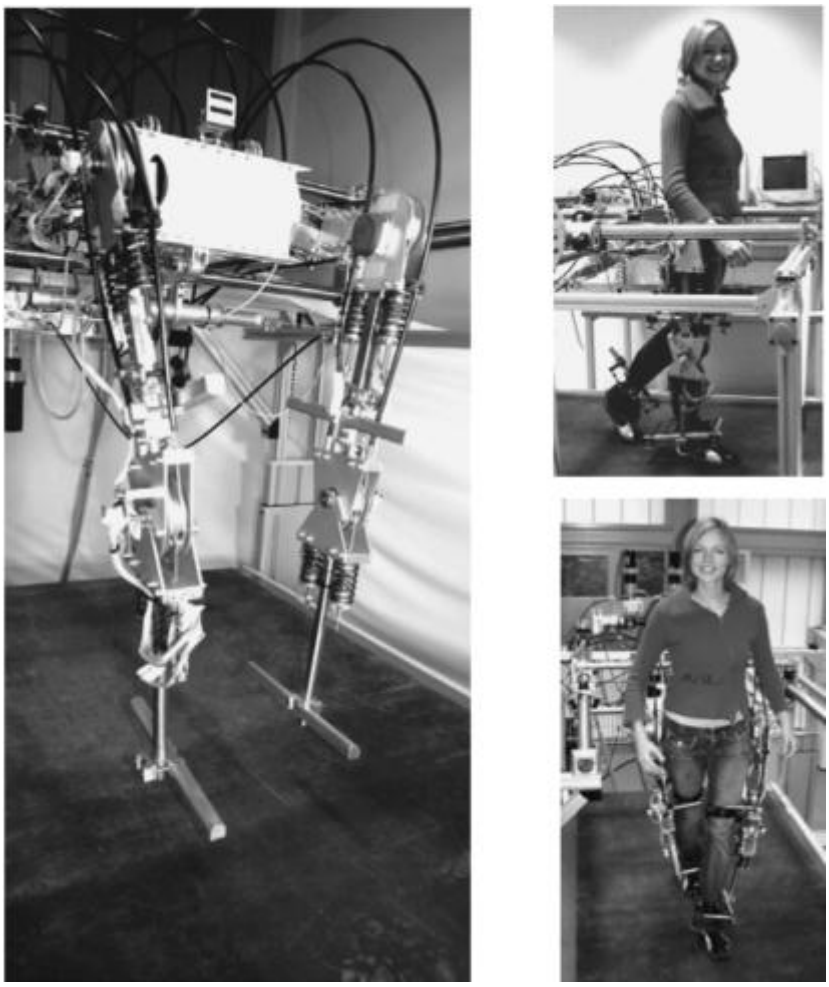

Figure 2.2: The prototype of LOPES (from [194]).

The LOPES system has two modes of operation. The "patient-in-charge" mode allows the user to walk unconstrained by the device, while the "robot-in-charge" mode has the system guide the user to move in predetermined walking patterns. The intended application for most patients with iSCI lies between both modes, known as the "therapist in charge" mode, where appropriate corrective or supportive torques can be applied to the leg joints and the pelvis when patients try to walk with their own effort. The LOPES prototype has been tested on able-bodied persons in the "patient in charge" mode. The walking pattern in LOPES resembles treadmill walking [194]. However, a general clinical evaluation of LOPES on patients with various severities of SCI has to be undertaken. One limitation of the LOPES system is that the lower limb is guided in

the hip and knee joints, while the ankle and foot are left without any support. Patients who have weak ankle joints might have problems in achieving correct ankle rotation in LOPES.

In contrast to LOPES, the ALEX system, which was developed by Scholz et al. at the University of Delaware in 2007, has additional bracing to secure the foot [195]. The foot brace passively holds the foot, but the ankle angle is constantly monitored using an encoder. ALEX has five components: the Walker, the trunk orthosis, and the segments of the thigh, knee and foot. The former two elements combine to support body weight but allow for vertical and lateral translations. The latter three components collaboratively move the lower extremities. The trunk is passively supported by a parallelogram mechanism called a gravity balancing orthosis, which alters the level of gravity load by adjusting the spring parameters. The leg orthoses are driven by linear servo motors at the hip and knee joints. ALEX applies forces on the foot, based on the "assist-as-needed" rule to help the leg move on a desired trajectory. Healthy subjects were found to relearn the newly-defined walking pattern during training with ALEX [195, 201]. Two chronic stroke survivors showed encouraging improvements in their locomotion ability after three five-day training sessions with ALEX. Improvements were reflected in an increase in mean walking speed (from 1.2 to 1.75 m/s) and improved gait patterns [202].

While LOPES and ALEX have passive ankle rotation, the ARTHuR robotic system, developed by the Biomechatronics Lab at the University of California, guides leg motion through direct ankle control [203]. It makes use of a linear motor with two coils and a V-shaped two-bar linkage, which are connected to the subject's ankle through a padded cuff [196]. ARTHuR can generate substantial forces for movements of the

ankle joint in the sagittal plane. Preliminary tests on healthy subjects with various heights demonstrated that the ankle trajectories during training with ARTHuR were very similar to their own normal walking trajectories [196]. A clinical trial on patients with chronic SCI showed ARTHuR could perform subject-specific assisted walking, resulting in reduced manual assistance from the physiotherapists [203]. However, the study investigated only the foot trajectories, while the hip joint motion was not reported.

The robotic system PAM/POGO, also developed by the University of California, is a pneumatically actuated robot that allows a full range of natural motion of the legs and pelvis during treadmill walking [197]. PAM has two 3-DOF robotic segments, which allows free motion of the pelvis during stepping using a BWS system. PAM provides lateral and rotational pelvic movements. POGO, as an attachment to PAM, provides sagittal rotations for the hip and knee joints during the swing phase, and stabilizes the knee joint during the stance phase. Actuated by pneumatic cylinders, the PAM/POGO system is able to produce large forces with relatively lightweight moving parts. Preliminary experiments on five chronic patients (one ASIA C and four ASIA D) demonstrated that PAM/POGO could synchronise pelvic movement with leg motion. Muscle activity during PAM/POGO-assisted training was very similar to that during physiotherapist-assisted training [197]. The clinical efficacy of long-term training with PAM/POGO is yet to be investigated.

In contrast to the robotic gait orthoses discussed above which use a treadmill, the WalkTrainer allows actual overground ambulation [204]. Initiated by the Swiss Foundation of Cyberthosis, the WalkTrainer has two leg exoskeletons, a pelvic orthosis and an active body weight support, which are assembled in a “deambulator” (frame of

the WalkTrainer) [3]. The deambulator is equipped with motorized rolling wheels, allowing overground translation. Each leg orthosis is fully actuated at the hip, knee and ankle joints, with motion of the whole lower limb in the sagittal plane. In order to provide pelvic support as physiotherapists do, the pelvic orthosis has six DOF with six motor-actuated axes. The WalkTrainer can generate natural walking patterns with normal pelvic motion. Another feature of the WalkTrainer is that muscular participation is enabled through closed-loop electrical muscle stimulation. With the combination of mechanical motors and muscle stimulation, the WalkTrainer aims to produce gait training which is as close as possible to natural overground walking, including leg motion, muscle activation, and visual and proprioceptive feedback. The WalkTrainer was used by six paraplegic subjects (ASIA A: 2, ASIA C: 1 and ASIA D: 3). Each training session started with a 10-minute warm-up via leg muscle stimulation (10 Hz) while the subjects stayed still in the WalkTrainer. This was followed by one-hour walking training and finally 10-minute cool-down via leg muscle stimulation (10 Hz). This test demonstrated the feasibility of paraplegics walking in the system [204]. Clinical trials have yet to be undertaken to evaluate the rehabilitation potential.

All the robotic gait rehabilitation systems described above are still under development and evaluation in the lab, although some have already been used to conduct clinical testing. There are some commercially available gait orthoses, such as the Lokomat shown in Figure 2.3. The Lokomat robotic gait-orthosis (Hocoma AG, Volketswil, Switzerland) consists of two lower extremity orthoses and a dynamic BWS system [198]. A parallelogram arrangement combined with a passive spring allows limited upward/downward pelvic motion [205]. The hip and knee joints are actuated in a gait-like pattern by small DC motors and linear ball screw assemblies. Both ankle joints are passively fixed by elastic straps. The dynamic control system can precisely

synchronise the treadmill speed with the speed of the lower extremity orthoses. The kinematic trajectories and training efficiency of the Lokomat have been extensively investigated. In spite of a greater range of motion (ROM) of the hip and ankle joints in the Lokomat, the overall kinematics in the Lokomat are similar to physiotherapist-assisted treadmill walking [205].

Figure 2.3: The Lokomat[1].

[1] Available from: http://www.hocoma.com/produkte/lokomat/. Accessed on 03/11/2011.

So far, the Lokomat, as the most widely used robotic gait orthosis, is the most clinically evaluated system. The efficiency of gait training using the Lokomat was confirmed in patients with iSCI [206]. In order to investigate the function of robot assistance in gait training, two small randomized control trials were started to compare functional ambulation outcomes between four strategies of gait training: BWSTT plus therapist assistance, BWSTT plus robot assistance (Lokomat), BWSTT plus FES, and overground gait training [207, 208]. Analysis of the quality of the gait pattern revealed that all these modes of gait training yielded improvements in overgound walking. Both studies demonstrated that these four modes of gait training gave positive results, with improved walking cadence and step length. Although it is hard to say which training modality is best [209], the observation of improved step symmetry in the therapist-assisted and robot-assisted BWSTT groups further confirms the efficacy of robotic technology in gait training [208].

The LokoHelp system (LokoHelp Group, Germany) shown in Figure 2.4 is also commercially available. The Lokohelp is also operated with the assistance of BWS and a motor-driven treadmill system [199]. However, the treadmill acts as the driver of limb motion. The LokoHelp device is fixed at the central part of the treadmill surface and translates the treadmill movement into a walking-like foot trajectory. Gait is achieved by the fixed trajectory of the footplates positioned on both sides of the device [199]. Clinical trials with patients (two with thoracic ASIA C iSCI, two with traumatic brain injury, one with ischemic stroke and one with intracerebral haemorrhage) showed that six weeks of training on the LokoHelp reduced the external assistance required during walking in all subjects [199]. A randomized controlled cross-over trial was conducted on patients with neurological deficits to compare the training efficacy of the LokoHelp and locomotor training with manual assistance. The results demonstrated that the

LokoHelp system induced similar improvements to the manual locomotion training, but with reduced therapeutic assistance [210].

Figure 2.4: The Lokohelp system[2].

In spite of these promising results, the LokoHelp system has limited ability to vary the gait pattern. Studies on animals suggested that high variability in robotic assistance promoted the recovery of the injured spinal cord compared to low variability training [211]. Although the LokoHelp system can adjust the velocity between 0–2.5 km/h, the step length and foot trajectory are always the same because the track is fixed to the footplate.

The G-EO system, which was initially developed as an improvement of the gait trainer

[2] Lokohelp. Available from: http://www.lokohelp.net/en/products/movies-and-pictures/. Accessed on 13/11/2011.

[212], has been commercially available since 2009. The gait trainer controls the motion of two foot plates directly in a walking-like trajectory using rotary motors [213]. The actuator system for each lower limb consists of a fixed sun gear and a circulating planet gear. Each footplate bar, with one end eccentrically connected to the planet gears and the other end to a crank, follows an ellipsoid-like trajectory. The foot trajectory can be adjusted by selecting different gear sizes and eccentricities. Balance is secured through an overhead harness. The gait trainer controls leg motion directly as an end-effector, without the need of a treadmill.

Tests on able-bodied subjects demonstrated that the foot trajectories induced by the gait trainer were very similar to normal walking during the major parts of stance and swing, although some differences existed in the transition periods, such as pre-swing and loading [98]. Four weeks of clinical research on patients with neurological deficits was carried out in two groups: a test group who received 20 minutes of locomotor training in the gait trainer plus 25 minutes of physiotherapy and a control group who had 45 minutes of physiotherapy. The results showed that the gait trainer system produced locomotor improvement in 41 of 77 patients, which was significantly greater than in the control group (17 of 78 patients) [214]. As the gait trainer has no leg orthoses, electrical muscle stimulation is sometimes employed to stabilize the knee during the stance phase. Regular locomotor training on the gait trainer, combined with electrical stimulation (half an hour each day for 5 weeks) in addition to conventional therapy, resulted in improved walking ability in four patients with iSCI, with doubled gait speed and endurance [215].

Further to relearning walking in the plane, the gait trainer was upgraded with a fully programmable footplate [216, 217], becoming the current G-EO system [200]. The

footplate can be programmed to move in 3-DOF, so that in addition to walking with an individual pattern on a flat surface a patient can also practise stair climbing and descent. Research on eight able-bodied subjects [200] and six hemiplegics [218] confirmed that the G-EO system simulated the kinematics of stair climbing, with similar muscle activity to that during actual stair climbing [218]. Severely injured stroke patients, who cannot stand independently, achieved independent walking and stair climbing after about one month of training in the G-EO system (25-30 min every workday) [218]. The G-EO system appears to produce promising results in gait training. However, further studies are needed to investigate the kinematics of the lower limbs, including angle profiles of the hip, knee and ankle joints.

2.4. Early Rehabilitation Systems

The devices described above focus on upright locomotor training paradigms, many of which have demonstrated promising results. However, it is challenging for some physically weak patients to perform upright training. As discussed in Chapter 1, most patients with SCI suffer from orthostatic hypotension (OH) in the acute phase. Furthermore, some severely injured patients may require a period of bed rest for management of their spinal fracture [33]. In addition, pressure sores, which often develop in patients with SCI, can prevent use of BWS due to pressure over the sitting area. The resultant muscle weakness, complicated by OH, restricts the early adoption of an upright position for robotic walking as delivered via orthotic devices such as the Lokomat. There are alternative approaches for early rehabilitation for those who cannot maintain an upright position.

Tilt table mechanisms have been adopted for early rehabilitation, e.g. the Erigo system

(Hocoma AG, Volketswil, Switzerland) [219]. The Erigo consists of a traditional tilt table with two thigh cuffs and two foot plates (see Figure 2.5). The upper body part of the tilt table can be continuously tilted from supine up to 80 degrees. Each thigh cuff is actuated to flex and extend the lower limb. Each foot is fixed on a foot plate by a strap. A special spring-damper mechanism under the foot plate applies load to the foot sole when the hip and knee joints are extended. The Erigo allows patients in the early post-injury phase to practise simple leg extension and flexion, although the lower limb kinematics are quite different from overground walking.

Another type of rehabilitation intervention which can be used for those who cannot stand is training in a recumbent position, as exemplified in recumbent tricycles [220], the MotionMaker [221] and the MoreGait system [222]. A recumbent tricycle is an adapted tricycle with a tilted back support for patient training. Assisted by electric motors on the pedal crank, the recumbent tricycle induces cyclic leg motion to promote physical fitness [220]. The recumbent lower limb orthosis MotionMaker induces cyclic lower-limb motion as in recumbent cycling. Developed by the Swiss Foundation for Cyberthoses, the MotionMaker system is composed of a recumbent trunk plate and two leg orthoses with the hip, knee and ankle joints actuated by motors [221]. It can generate different patterns of leg extension and flexion with active ankle rotation, including tricycle-like motion. Furthermore, both the recumbent tricycle and the MotionMaker employ electrical muscle stimulation in order to create active and progressive muscle activation during exercise [220, 221]. Multi-channel electrostimulators are adopted and control units are designed to synchronise the electrical stimulation and the motor control.

Figure 2.5: The Erigo[3].

The MoreGait system was designed by the Orthopedic University Hospital (Heidelberg, Germany) for walking rehabilitation with the user in a recumbent position [222]. Driven by pneumatic muscles over the thigh and the shank, the device flexes and extends the lower limbs. Furthermore, stimulative shoes, equipped with pneumatic cylinders, provide walking-like cyclic mechanical stimulation on the foot soles to mimic the ground reaction forces that occur during overground walking [222, 223].

[3] Available from: http://www.hocoma.com/en/products/erigo/. Accessed on 05/12/2011.

MoreGait thus provides important sensory inputs by moving the lower limbs and stimulating the foot soles.

Clinical research confirmed that early rehabilitation systems such as the recumbent tricycle [224], the MotionMaker [221] and Moregait [225] could strengthen the muscles and develop muscle endurance as well as joint mobility for patients with SCI. These devices can prepare patients for gait training, but they do not specifically target gait training. The kinematics of the lower extremities are not similar to walking-like stepping [223, 226]. A system for early rehabilitation of walking is lacking.

2.5. Aims and Objectives of the PhD Research

Motivated by knowledge about activity dependent plasticity, rehabilitation should be carried out with a task-specific programme, i.e. in order to relearn walking, natural gait training should be practised. Based on the CPG theory of locomotion, there are currently many rehabilitation systems to assist walking training. However, a limitation of current gait rehabilitation technology is that patients are trained in an upright position. It is quite common for patients with SCI to require some time on bed rest. Physical weakness combined with OH makes it difficult to achieve standing for patients early after injury, resulting in a postponed initiation of rehabilitation.

The outcome of gait restoration therapy is dependent on the initiation time of the rehabilitation programme [7], which should be early enough to prevent muscle weakness [227]. Most successful recovery of patients with SCI is normally obtained within the first 6 months [228, 229], while only modest improvement in motor function is obtained after this [39]. The rate of recovery is greatest in the first half year

after injury and then it begins to plateau [230, 231]. Research on the course of spinal neuronal activity following SCI emphasizes the need for early rehabilitation [7]. Prolonged immobilization leads to a gradual reduction in spinal activity, and may result in the situation that the spinal neurones can seldom be activated by training [66]. Patients with SCI require early and continued activity-targeted training to maintain normal neural excitability with possible benefits for locomotion as well as reduction of secondary complications.

This literature review on rehabilitation technology has revealed that only few systems are designed for early rehabilitation. Furthermore, these systems are not specifically designed for walking restoration. A system which aims to promote early rehabilitation of walking is lacking. Therefore this PhD research aims to design a system to promote early neurological rehabilitation of walking for patients with iSCI who may still be restricted to a lying position.

The robotic orthosis is emerging as a promising rehabilitation technology, because it reduces the physical effort from physiotherapists and allows more intensive repetitive training for patients. In order to promote early rehabilitation of walking, the research developed and tested a new generation of bar-linkage mechanisms which allow patients to generate natural stepping movements in a supine position. Based on the fundamental guidelines for early training, it was necessary to design a new Gait Orthosis for Early Rehabilitation of walking (GOER) with the following properties:

1. The patient is able to perform stepping in a supine position;
2. The ankle joint is activated to allow coordinated kinematics of the lower limbs;
3. Different speeds can be accommodated to produce different training modalities;
4. Haptic feedback on the foot sole is provided to mimic the ground reaction forces.

In spite of the benefits of FES, the GOER system utilizes mechanical actuators to obtain consistent, repetitive stepping motion and to minimize uncontrollable activation of reflex loops. The GOER is designed to promote early rehabilitation of walking in a lying position, where the required torque for a supine stepping leg is different from the torque during overground walking (see Chapter 3 and Chapter 5 for further information). The employment of FES for ankle rotation in the GOER system might train the muscles in a way that is different from the normal performance during overground walking.

Dynamic modelling and simulation is an important tool for system analysis and an effective starting point for mechanical design, such as for exoskeletons reported in the literature [190, 232]. A starting point for this study was development of a computer model of bar-leg systems which simulate coordinated inter-limb kinematics of walking-like movements in a lying position. The model simulated lower-limb movements at different cadences with variable step lengths. Then a dynamic shoe mechanism was designed using pneumatic actuators and tested in able-bodied subjects. The purpose of the shoe mechanism was to mimic the forces experienced on the foot sole during overgound walking. The research concluded with a prototype of the GOER system and performance evaluation. All of these aspects are described in detail in the following chapters.

The GOER system aims to promote recovery of neurological function by inducing as much sensory feedback as possible from the lower limbs while the legs move in a walking pattern.

Chapter 3. Gait Analysis Experiment

Summary: In order to investigate the representative performance of overground walking, a gait analysis experiment was performed in three able-bodied subjects. The purpose of the experiment was to generate and record joint trajectories of the lower limbs and ground reaction forces, which would be used later in the design of the GOER system.

3.1. Normal Walking

Normal walking is a complicated sensory-motor task that involves synergistic movements of both lower limbs. Gait includes a series of repeated events such as heel strike and toe off. A gait cycle is defined as the time interval between successive instances of initial foot-to-floor contact for the same foot [233]. It includes a stance phase, during which the foot contacts the ground, and a swing phase, when the foot is off the ground. The stance phase starts with the heel striking the ground and ends with toe off. The stance phase lasts about 60% of a gait cycle at a self-selected normal walking speed (see Figure 3.1). The stance phase is normally divided into three sub-phases: initial double limb support, single limb support and later double limb support. The sub-phase of initial double limb support includes the time from initial contact (IC) to opposite toe off (OT). From OT to opposite initial contact (OI) is the sub-phase of the ipsilateral single limb support, when the ipsilateral foot is pivoted on the ground from the foot flat to heel rise (HR) position. The sub-phase of later double limb support starts from OI to ipsilateral toe off (TO). Similarly, the swing phase, which lasts about 40% of a gait cycle, has several typical leg positions, such as feet adjacent (FA) and tibia vertical (TV). The swing phase involves ankle rotation, which

lifts the toe off the ground. When the swing foot is adjacent to the other foot, the toe is at its lowest extent during the swing phase. Toe clearance is a key factor in ensuring normal gait. Therefore the FA position is also sometimes called the toe clearance position [234]. Then the swing leg gets the tibia vertical (TV) position and finally contacts on the ground for the next IC. Therefore the swing phase is also divided into three sub-phases: pre-swing (from TO to FA), mid-swing (FA to TV), and terminal swing (TV to IC). The function of each phase is described in Table 3.1.

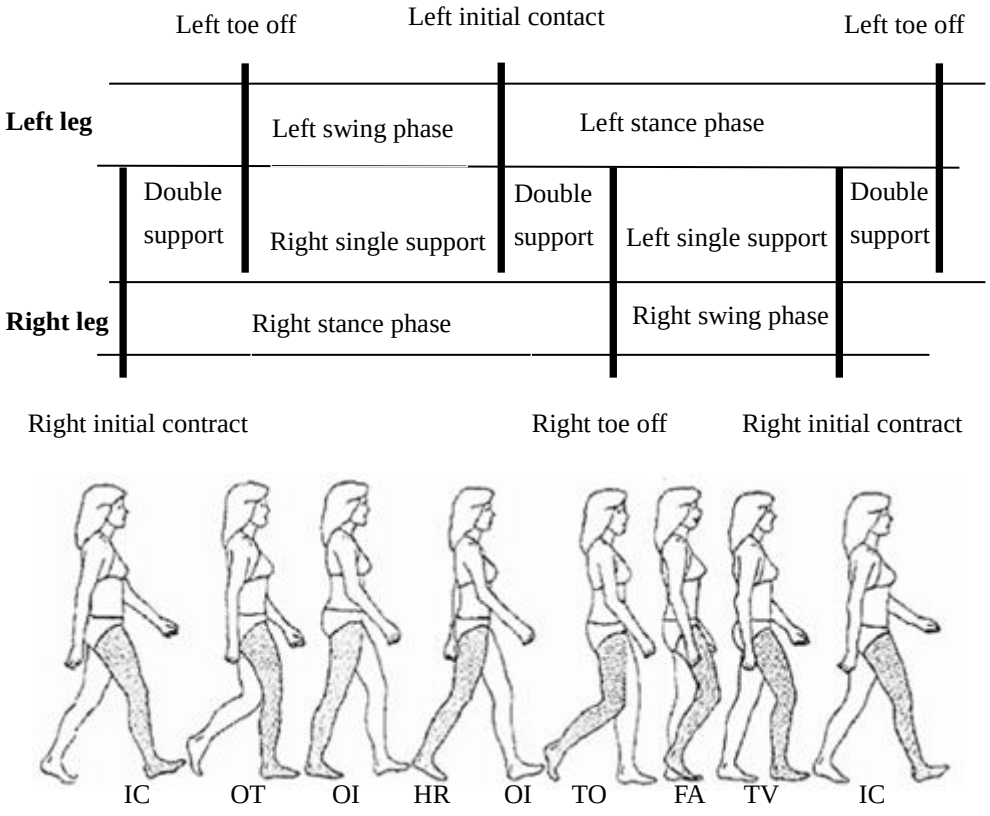

Figure 3.1: Timing of gait phases (modified from [234] and [235]).

Walking events occur in a similar sequence, regardless of the actual walking speed and elapsed time. Therefore gait is often normalised as a percentage of the cycle instead of time, which allows intra- and inter-individual comparison of walking. A gait cycle is described with initial heel strike at 0% and the following ipsilateral heel strike at 100%.

Furthermore, normal subjects have a similar sequence of walking in both legs, with the legs a half cycle out of phase.

Table 3.1: Functions and contralateral leg positions of different sub-phases in the gait cycle [235].

Sub-phase	Period (% cycle)	Function	Position of the contralateral Limb
Initial double limb support	0-10	Loading, weight transfer	Second double limb support
Single limb support	10-50	Support of entire body weight; centre of mass moving forward	Swing
Second double limb support	50-60	Unloading and preparing for swing	Initial double limb support
Pre-swing	60-75	Foot clearance	Single limb support
Mid-swing	75-85	Limb acceleration to the front	Single limb support
Terminal swing	85-100	Limb deceleration, preparation for weight transfer	Single limb support

To describe walking, stride and step lengths are often adopted. Stride length is the linear distance in the plane of progression between two successive points of foot-to-floor contact from the same foot, while a step length is the distance between two successive points of foot-to-floor contact from two feet [233]. One stride equals two steps. Cadence is the number of steps within a given time period. Healthy subjects change their speed by varying both stride length and cadence. Walking speed largely depends on the duration of the swing phase [233]. Therefore, in slow walking, the swing phase is usually shorter than 40% of the gait cycle.

Walking requires a suitable ground support for the standing leg. Various forces on the leg segments at different gait phases result in complicated kinetics of walking. Moments at the hip, knee and ankle joints, which are related to the ground reaction forces, provide the fundamental dynamic basis of locomotion.

In order to design a system for generation of normal walking pattern, a gait experiment was proposed using the Vicon motion analysis system to record the segment trajectories during overground walking. Although there are publications describing normal gait features (such as the hip, knee and ankle angles), walking data of the segment displacement trajectories, which is the key information for model development (to be described in Chapter 4), are not available. Treadmill walking might be possible to provide walking patterns, but overground walking was performed in this project, because: (i) people are most used to overground walking, while subjects generally require some time to learn how to walk normally on a treadmill; (ii) we have a standard gait lab available to record overground walking data of the segment movement and ground force reaction simultaneously, while the treadmill requires an additional force plate to measure the reaction forces during walking, which brings the additional difficulty of synchronising the recording of the movement pattern and the force reaction; (iii) overground walking is what I am trying to model in this project and therefore overground walking was preferred. The Vicon motion analysis system, which is the most widely adopted system for walking pattern investigation [236], was used in this work.

3.2. Experiment Description

In order to record performance of the lower limbs during overground walking at various speeds, a gait experiment was carried out. Ethical approval was obtained from the Bioengineering Departmental Ethics Committee at the University of Strathclyde, Glasgow, UK.

3.2.1. Equipments and subjects

Gait analysis was performed using a Vicon motion analysis system (Oxford Metrics Ltd., Oxford, UK). Eight infrared cameras, with a sampling frequency of 120 Hz, were used to capture the displacement of reflective markers which were placed on various bony segments of the lower limbs. In order to record the motion of both lower limbs during overground walking, the Vicon Clinical Manager (VCM) marker set for lower limb motion recording was adopted [237]. As shown in Figure 3.2, seventeen markers were arranged with one marker at the sacrum (SACR) and the other sixteen markers at eight bony points bilaterally: anterior superior iliac spine (LASI, RASI), greater trochanter (LGTR, RGTR), thigh (LTHI, RTHI), knee (LKNE, RKNE), tibia (LTIB, RTIB), lateral malleolus (LANK, RANK), heel (LHEE, RHEE) and second metatarsal phalangeal joint (LTOE, RTOE).

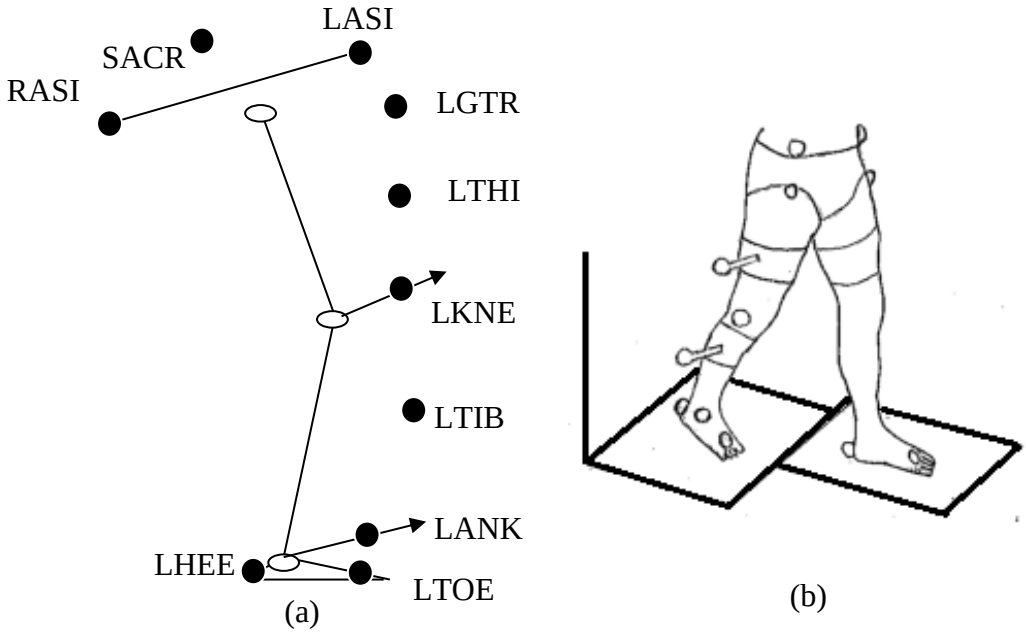

Figure 3.2: Marker placement. Subfigure (a) shows markers mainly for the left leg (from [238]) and subfigure (b) shows markers mainly for the right leg (from [235]).

Four Kistler force plates (Kistler Instruments AG, Winterthur, Switzerland) were used to record ground reaction forces and gait events such as heel strike and toe off. The analysis software BodyBuilder (Oxford Metrics Ltd., Oxford, UK) was used to reconstruct the limb segments and estimate the joint kinematics and moments.

3.2.2. Experimental procedures

Three able-bodied subjects were recruited with detailed information on the subjects summarized in Table 3.2. The subjects' weight and lengths of leg segments were measured in the upright position. Leg length was measured as the distance between the anterior superior iliac spine and the medial malleolus.

Table 3.2: Subject information.

Subject	S1	S2	S3
Gender	Male	Female	Female
Age (years)	24	42	33
Mass (kg)	94.70	74.40	67.80
Thigh length (m)	0.51	0.49	0.45
Shank length (m)	0.49	0.42	0.43
Ankle joint height (m)	0.08	0.07	0.06
Foot sole length (m)	0.25	0.2	0.18
Leg length (m)	1.00	0.91	0.88

The gait experiment started with a static trial so that the system could estimate the joint centres and axes. Then subjects had five minutes of free walking for familiarization. Subjects walked barefoot along a 10-metre walkway so as to determine their self-selected normal cadence (NC) and suitable starting points for a full step on the force plate. In order to record walking performance at various speeds, subjects walked at 100%, 75% and 50% of their NC, with the actual stepping rate guided by the beats of

an electronic metronome. Each subject walked three times for each walking speed so as to obtain a mean performance. Data for a single stride were collected when subjects passed the centre area of the walkway.

3.2.3. Data analysis

Using a metronome to guide the walking cadence is an accepted method of controlling walking speed [239-241]. With guidance of a metronome, the subjects managed to walk at a constant cadence during each trial. Experimental data over one gait cycle were analysed, commencing with heel strike on the force plate and ending with the next heel strike of the same foot. Calculation of the joint moment requires segment speed and acceleration by differentiation of the segment trajectories. The first derivative of segment trajectory was visually observed to remove outliers, and was then smoothed with the loess or rloess Matlab functions, before further differentiation for the segment acceleration, because outliers or noise makes the second derivative too noisy to carry on further calculation of moment. The embedded Matlab function loess uses a quadratic polynomial to fit the data with a regression weight function. The smoothed value is determined by neighbouring data points defined within the span. The function rloess is a robust version of the loess smoothing method, after an additional calculation of robust weights, which is resistant to outliers (the MathWorks, Inc.). The duration of one gait cycle was normalised to 100%, with heel strikes at 0 and 100%. In defining the kinematic and kinetic features, only mechanical variables in the sagittal plane were considered. Hip, knee and ankle joint angles in the sagittal plane were defined as zero at a neutral still standing position with flexion as positive and extension as negative. Vertical forces, displacements and accelerations in the upward direction, horizontal forces, displacements and accelerations in the forward direction and

moments in the clockwise direction were denoted as positive. Dimensionless scaling strategies [242] were used to minimise the inter-subject variation of gait outcomes. Ground reaction forces were normalised by body weight, while moments were normalised by body mass.

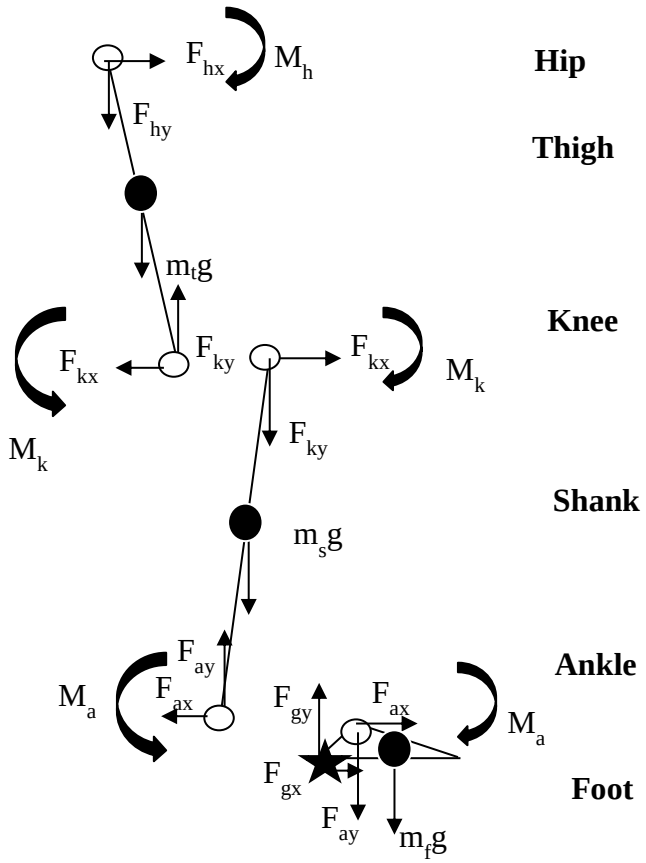

Figure 3.3: Free body diagram of the leg segments.

The BodyBuilder software was used to calculate the joint moments using the inverse dynamics method [1]. The foot was considered as a rigid segment connected to the ankle joint. As depicted in Figure 3.3, the mass of the foot is denoted by m_f. The internal forces and moment in the ankle joint with respect to the foot F_{ax}, F_{ay} and M_a were calculated as:

$$F_{ax} + F_{gx} = m_f a_{fx} \tag{3.1}$$

$$F_{gy} - F_{ay} - m_f g = m_f a_{fy} \tag{3.2}$$

$$M_a - F_{gy} L_{cop} + F_{gx} H_m + F_{ay} L_{aop} + F_{ax} H_a = I_f \alpha_f \tag{3.3}$$

where F_{gx} and F_{gy} are the horizontal and vertical components of the ground reaction forces. The displacement of the centre of pressure (marked with a star in Figure 3.3) from the centre of mass in the horizontal and vertical directions are L_{cop} and H_m, respectively. The displacement of the ankle from the centre of mass in the horizontal and vertical directions are L_{aop} and H_a, respectively. a_{fx} and a_{fy} are the horizontal and vertical components of the displacement acceleration of the foot. I_f is the moment of inertia of the foot and α_f is its angular acceleration. These variables can be determined experimentally or looked up from anthropometric data in Table 3.3. It should be noted that the lever arms in upward and right directions were defined positive.

Table 3.3: Normalised mass and length of lower limb segments (taken from [1]).

Segment	Segment mass/total body mass	Centre of mass/ segment length	
		Proximal	Distal
Foot	0.0145	0.5000	0.5000
Shank	0.0465	0.4330	0.5670
Thigh	0.1000	0.4330	0.5670
Total Leg	0.1610	0.4470	0.5530

The internal forces and moment in the knee joint with respect to the shank F_{kx}, F_{ky} and M_k were calculated as:

$$F_{kx} - F_{ax} = m_s a_{sx} \tag{3.4}$$

$$F_{ay} - F_{ky} - m_s g = m_s a_{sy} \tag{3.5}$$

$$M_k + F_{kx} l_s \lambda_s \cos(\theta_k) - F_{ky} l_s \lambda_s \sin(\theta_k) + F_{ax} l_s (1-\lambda_s) \cos(\theta_k) - F_{ay} l_s (1-\lambda_s) \sin(\theta_k) - M_a = I_s \alpha_s$$

(3.6)

where a_{sx} and a_{sy} are the horizontal and vertical components of the displacement acceleration of the shank. θ_k is the angle between the shank and the vertical axis, with clockwise as positive. m_s, l_s, α_s and I_s are the mass, length, angular acceleration and moment of inertia of the shank. λ_s is the distance between the centre of mass of the shank and the knee joint divided by the shank length. The internal forces and moment in the hip joint with respect to the thigh F_{hx}, F_{hy} and M_h were calculated as:

$$F_{hx} - F_{kx} = m_t a_{tx} \tag{3.7}$$

$$F_{ky} - F_{hy} - m_t g = m_t a_{ty} \tag{3.8}$$

$$M_h + F_{hx} l_t \lambda_t \cos(\theta_h) - F_{hy} l_t \lambda_t \sin(\theta_h) + F_{kx} l_t (1-\lambda_t) \cos(\theta_h) - F_{ky} l_t (1-\lambda_t) \sin(\theta_h) - M_k = I_t \alpha_t \tag{3.9}$$

where θ_h is the angle between the thigh and the vertical axis, with clockwise as positive. m_t, l_t, α_t and I_t are the mass, length, angular acceleration and moment of inertia of the thigh. λ_t is the distance between the centre of mass of the thigh and the hip joint divided by the thigh length.

3.3. Results

Experimental data over one gait cycle were analysed, and duration of one gait cycle was normalised to 100%, with heel strike at 0 and 100%. Detailed results for three subjects walking at 100%, 75% and 50% of NC are presented here. The joint angles, ground reaction forces and the internal joint moments are displayed as means with the shaded areas representing the standard deviations. As the moments in the clockwise direction are denoted as positive, a positive internal moment at the hip, knee and ankle joints with respect to the thigh, shank and foot in the moment figures (Figs 3.10-12)

means a moment from hip extensors, knee flexors and plantarflexors, respectively.

3.3.1. Kinematic performance

Locomotion involves rotation of the hip, knee and ankle joints, as can be seen in Figure 3.4. The hip joint starts with flexion at heel strike and then enters extension. Maximal extension is achieved before the end of the stance phase. Then the hip joint flexes to enter the swing phase, with maximal flexion achieved before heel strike. The knee has flexion and extension twice within one gait cycle. The knee joint is almost fully extended around initial ground contact, followed with flexion after heel strike. This process forms the first "hump" in the knee angle profile. After loading, the leg becomes extended during the mid-stance phase, followed by flexion in the swing phase, which forms the second "hump" in the knee angle profile. In contrast to the hip and knee joints, the ankle starts the gait cycle in a neutral position. After heel strike, the ankle joint extends the foot slightly downwards (plantarflexion) so as to place the whole foot sole on the ground. As walking proceeds, the ankle joint rotates gradually into dorsiflexion. In the second half of the stance phase, the ankle joint pushes the whole leg in preparation for the swing phase by plantarflexion. In the swing phase, the ankle has a small amount of dorsiflexion for toe clearance.

Table 3.4: Walking speeds for subjects (NC: normal cadence).

Walking speed	S1	S2	S3
NC (steps/min)	107	93	112
100% of NC (m/s)	1.42	1.16	1.44
75% of NC (m/s)	0.81	0.79	0.95
50% of NC (m/s)	0.43	0.528	0.61

Individuals with different heights have different cadences. The estimated walking speeds for all subjects are presented in Table 3.4. It should be noted that S3 had the

highest normal cadence (112 steps/min). S2 has a similar leg length to S3 (see Table 3.2), but had a much lower normal cadence (93 steps/min). As the normal walking speeds were defined by the subjects, it is expected that their normal cadences varied.

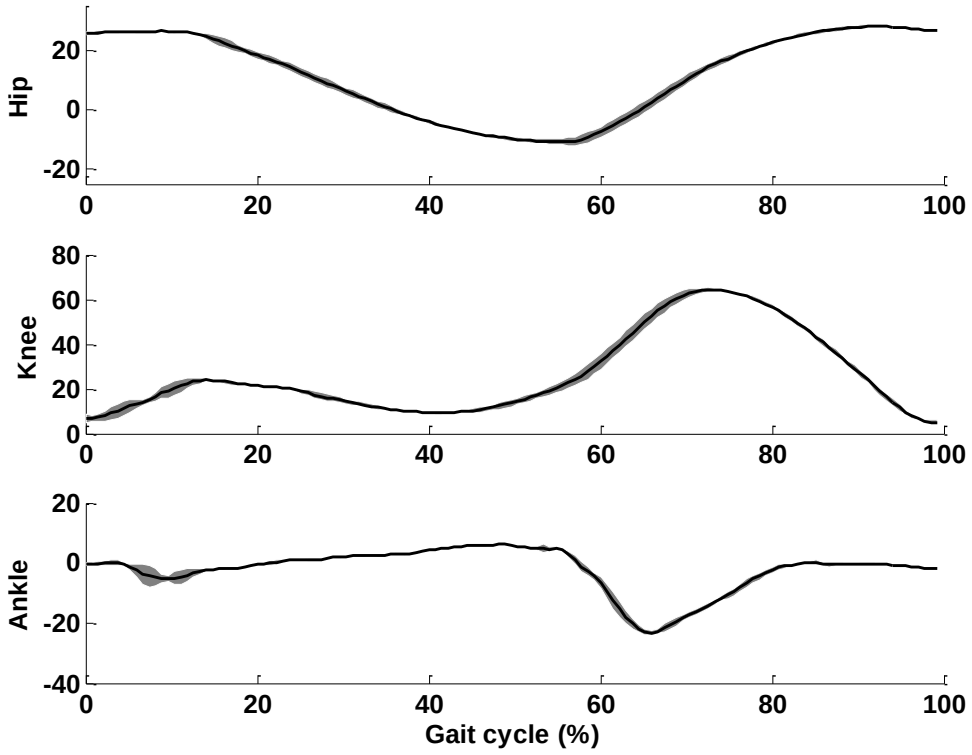

(a) S1.

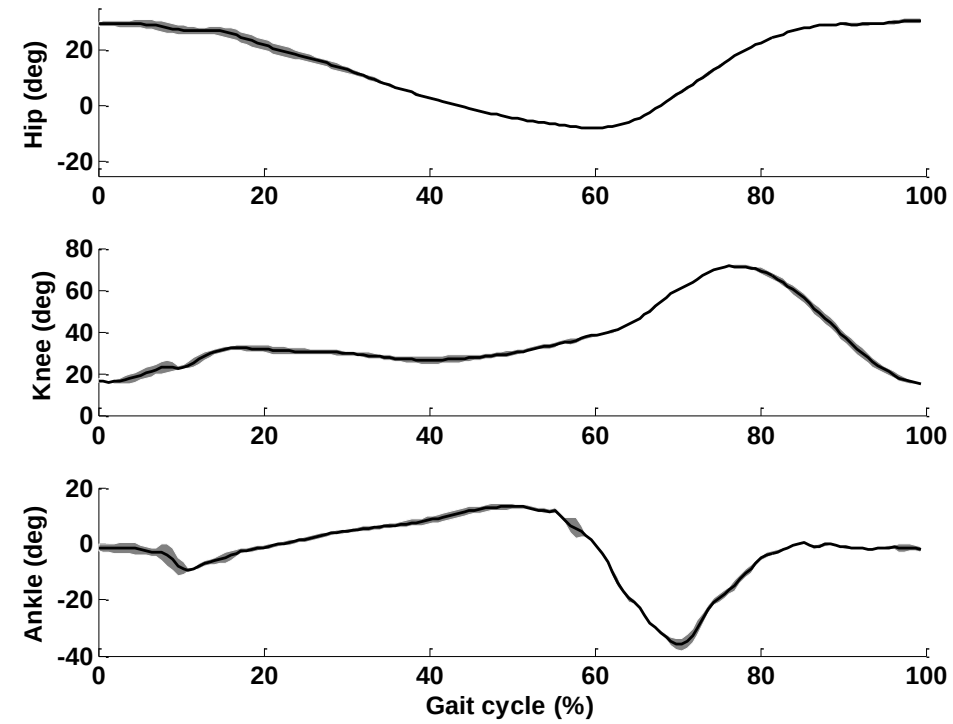

(b) S2.

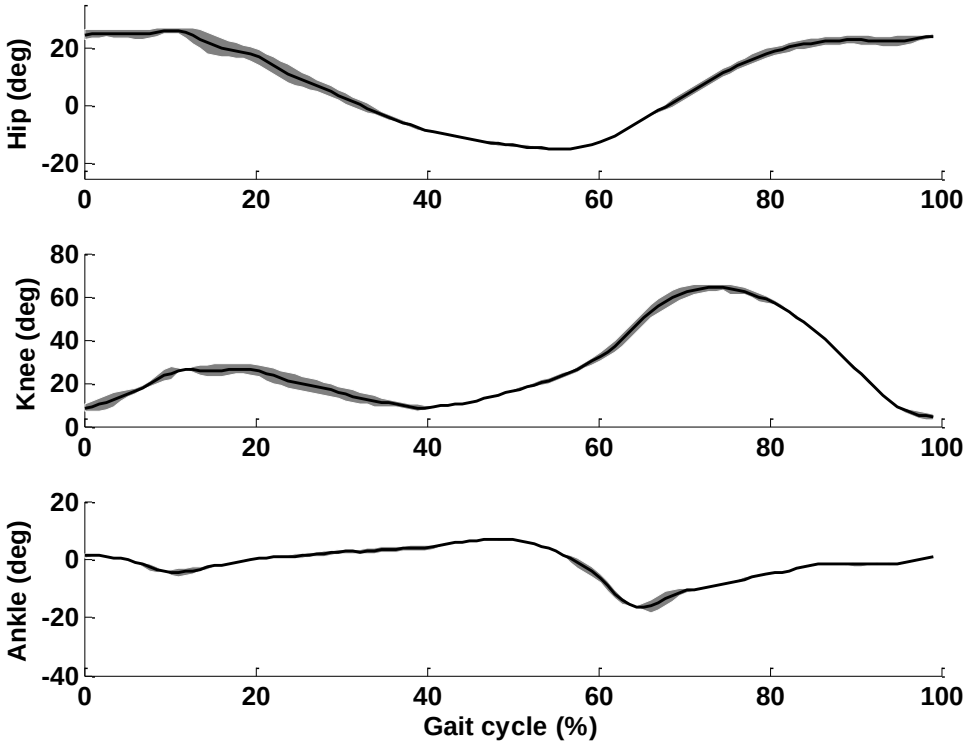

(c) S3.

Figure 3.4: Joint angles for three subjects walking at 100% of NC.

Figure 3.4 shows the mean angles of the hip, knee and ankle joint for the three subjects walking at 100% of NC, from which the typical features of normal walking can be easily observed, such as hip extension and flexion, "double-hump" knee profiles and ankle plantarflexion. S1 has the longest leg length, resulting in the smallest range of motion (ROM) in the hip joint. S2, in contrast to the other two subjects, had a large ROM (50^o) in the ankle joint. She walked with a flexed knee throughout the cycle with 20^o flexion even in the mid-stance phase (see Figure 3.4(b)). This resulted in reduced hip extension at toe off and increased knee flexion during the swing phase. Among the three subjects, S3 had the smallest ROM in the ankle joint (20^o), but her knee joint flexed most during the first-hump flexion at about 15% of the gait cycle. In spite of the small inter-individual differences, all subjects had consistent joint trajectories during overground walking at 100% of NC, which can be seen from the low variability in the angle performance in Figure 3.4. The mean ROMs of the hip, knee and ankle joints for all three subjects were 34^o, 50^o and 31^o, respectively, which are within the physiological ROMs of lower limb joints during overground walking [235].

The mean ROMs of all three joints reduced at lower speeds. The joint angle profiles of three subjects walking at 75% and 50% of NC are displayed in Figures 3.5-3.6. Knee flexion was smaller during the swing phase, and the first flexion hump, which usually occurred at around 15% of the gait cycle during walking at 100% of NC, became weak at 75% of NC, and was hardly observe at 50% of NC. Furthermore, the gait phase ratio (the duration ratio of the stance phase to the swing phase) during slower walking was different from normal walking speed. The mean duration of the stance phase for the three subjects was prolonged from 60% of the gait cycle at 100% of NC to about 74% of the gait cycle at 50% of NC. The maximal ankle extension for S1, which occurred at around 62% of the gait cycle at normal speed, was delayed until 77% of the gait cycle at 50% of NC. The variance increased when the speed reduced.

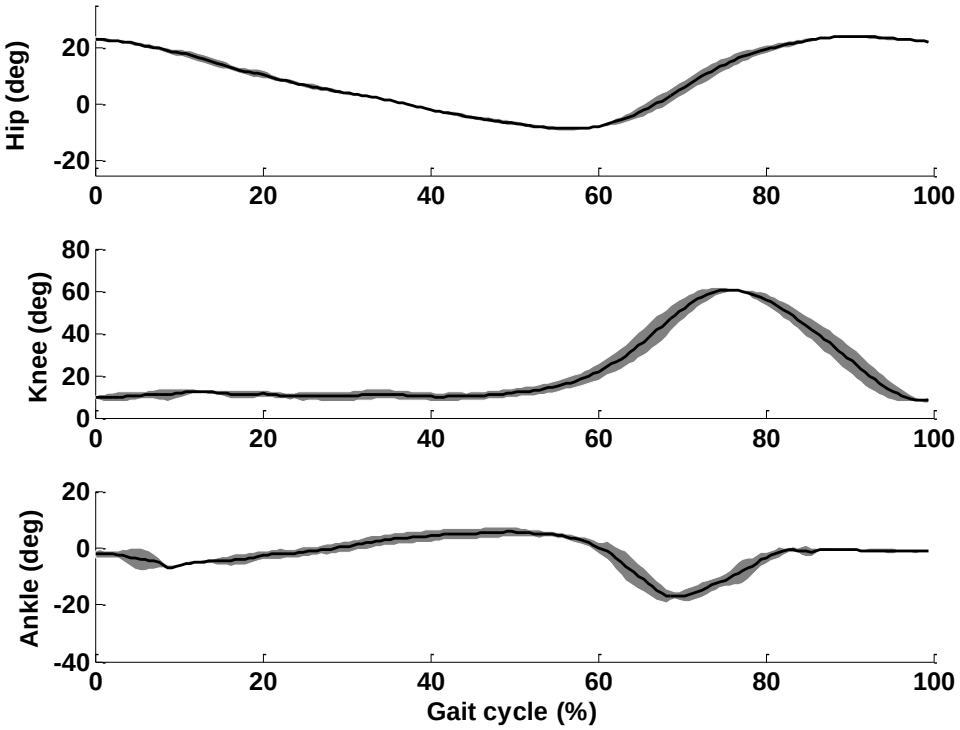
Hip (deg)
20
0
-20
0
20
40
60
80
100
Knee (deg)
80
60
40
20
0
Ankle (deg)
-40
Gait cycle (%)

(a) S1.

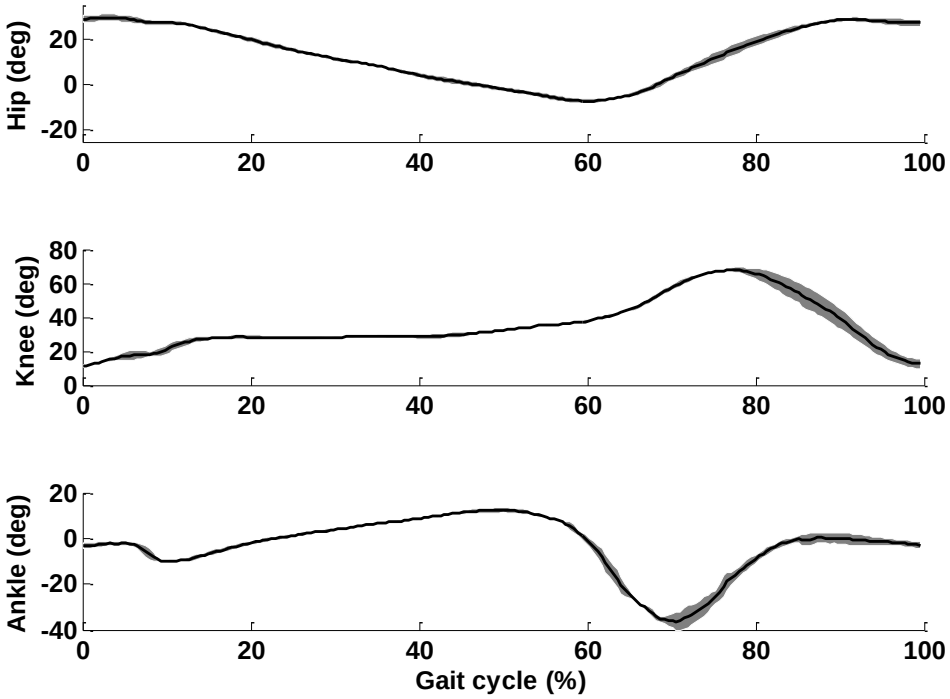
Hip (deg)
20
0
-20
0
20
40
60
80
100
Knee (deg)
80
60
40
20
Ankle (deg)
-40
Gait cycle (%)

(b) S2.

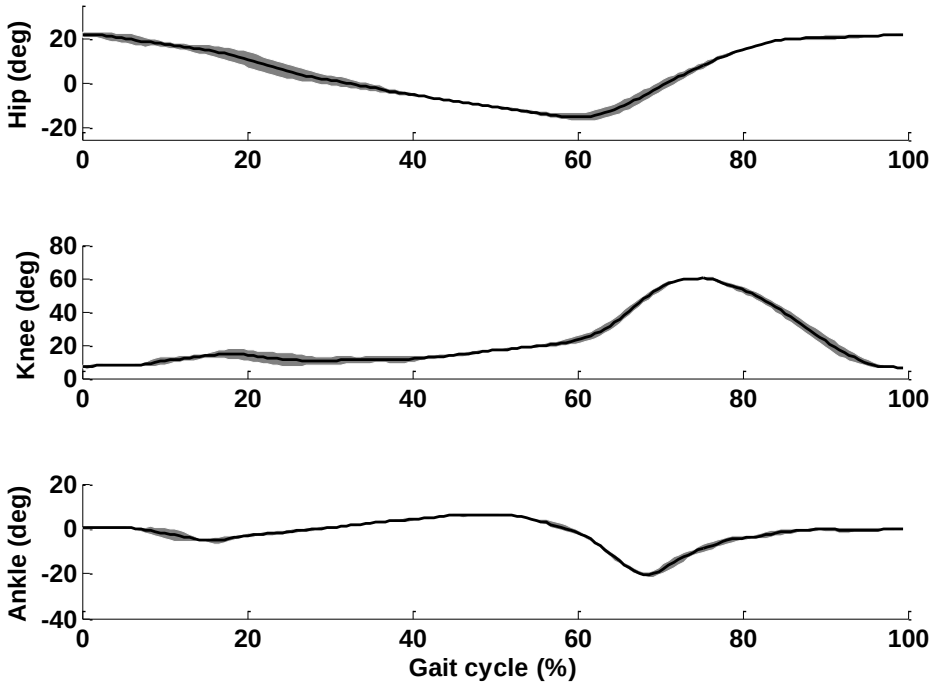

(c) S3.

Figure 3.5: Joint angles for three subjects walking at 75% of NC.

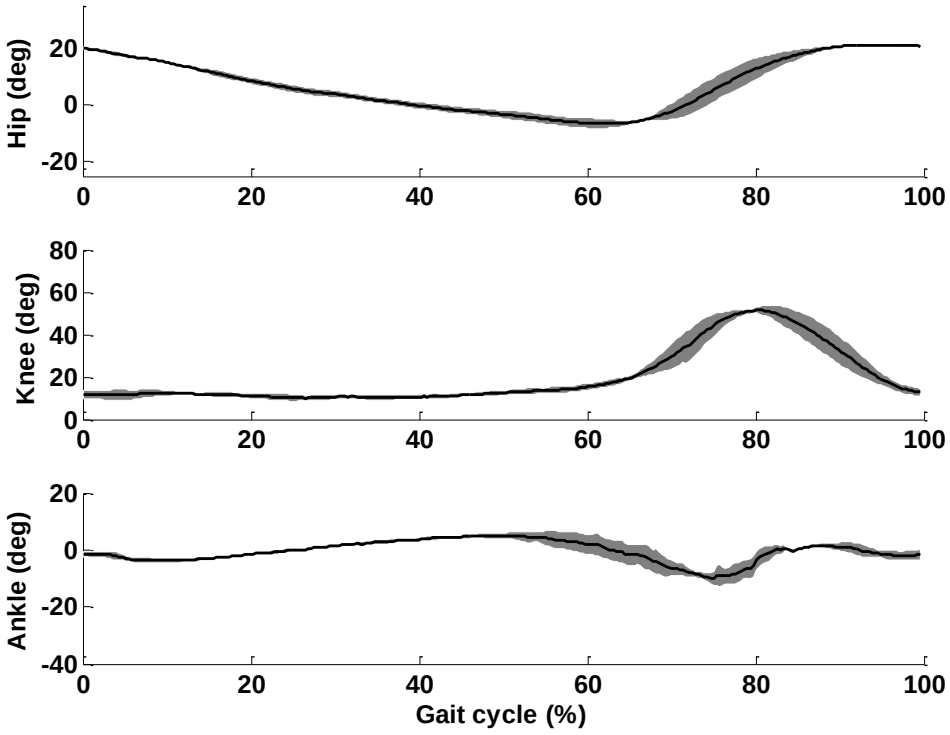

(a) S1.

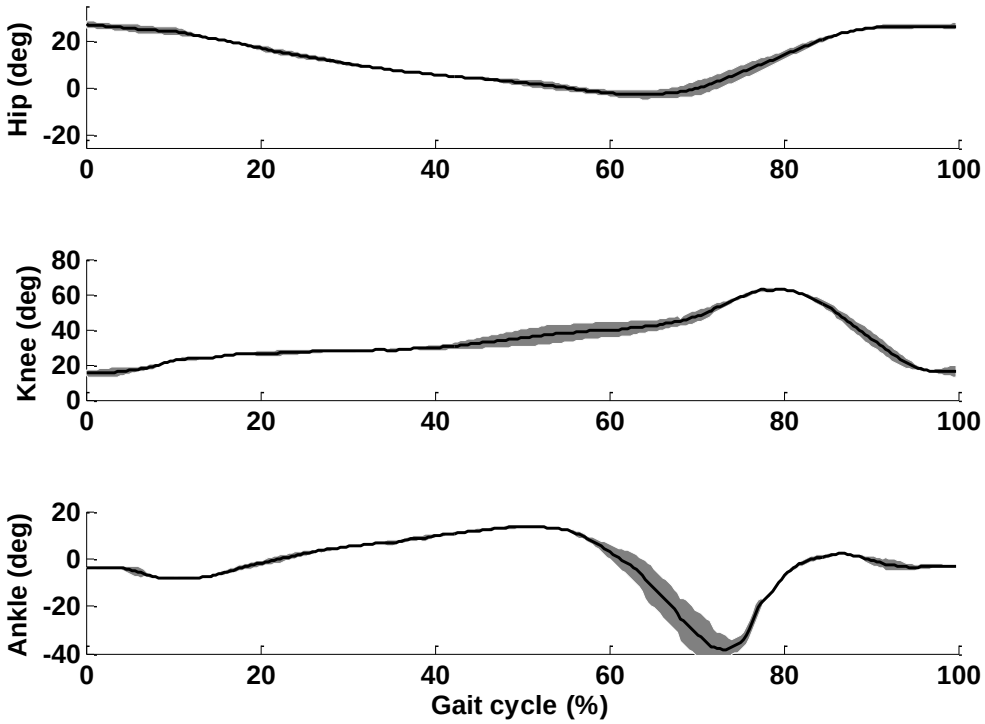

(b) S2.

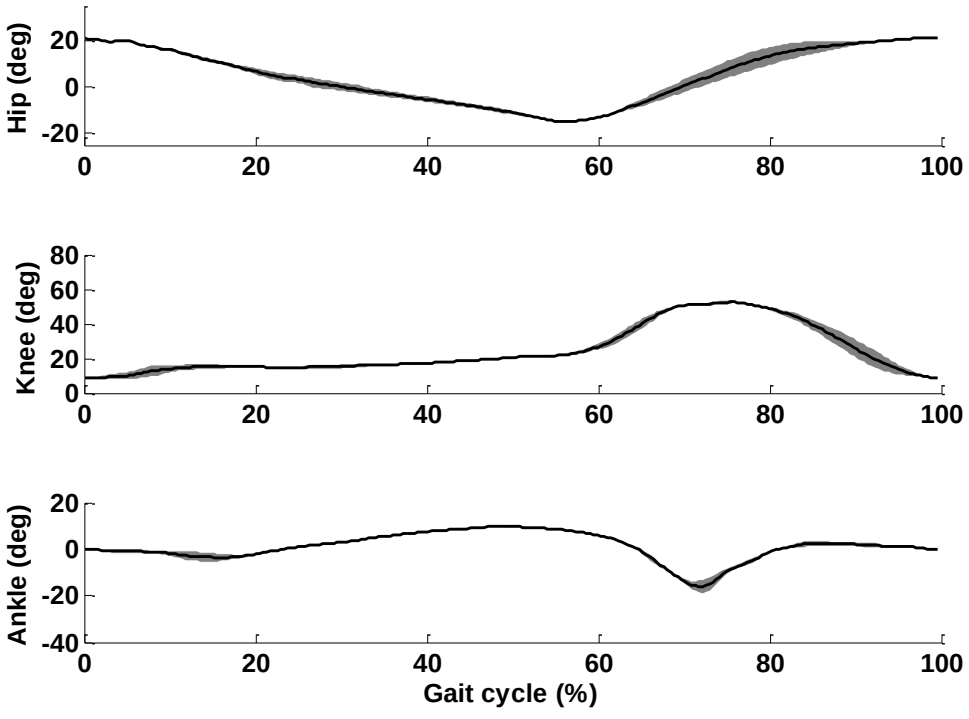

(c) S3.

Figure 3.6: Joint angles for three subjects walking at 50% of NC.

3.3.2. Ground reaction forces

During walking, the ground produces an upward force for body weight support, and horizontal friction for propulsion or braking [235]. The ground reaction forces of all three subjects at 100% of NC are shown in Figure 3.7. Similar to the general description of ground reaction forces in the literature [234], the upward supporting force, shown in the upper figure, demonstrates a double-hump pattern. The upward force increases from heel strike until around 20% of the gait cycle to achieve its first peak. During the latter single-support phase, the upward force reduces slightly and then increases to the second peak around heel off. The double-hump pattern was most pronounced in S3. This was because she walked at the highest cadence among the three subjects, resulting in the largest vertical motion of the centre of body mass. Variations in the upward force profile were observed at around 10% of the gait cycle in S2 and S3. These variations were from the loading of heel strike. Compared to the upward force, the horizontal force showed large variation. This was because different subjects used different walking strategies, producing different levels of friction between the foot and the ground. It is interesting to note that S1 and S2 required more forward propulsion before toe off (see Figures 3.7(a)-(b)) while S3 showed more braking at heel strike (Figure 3.7(c)).

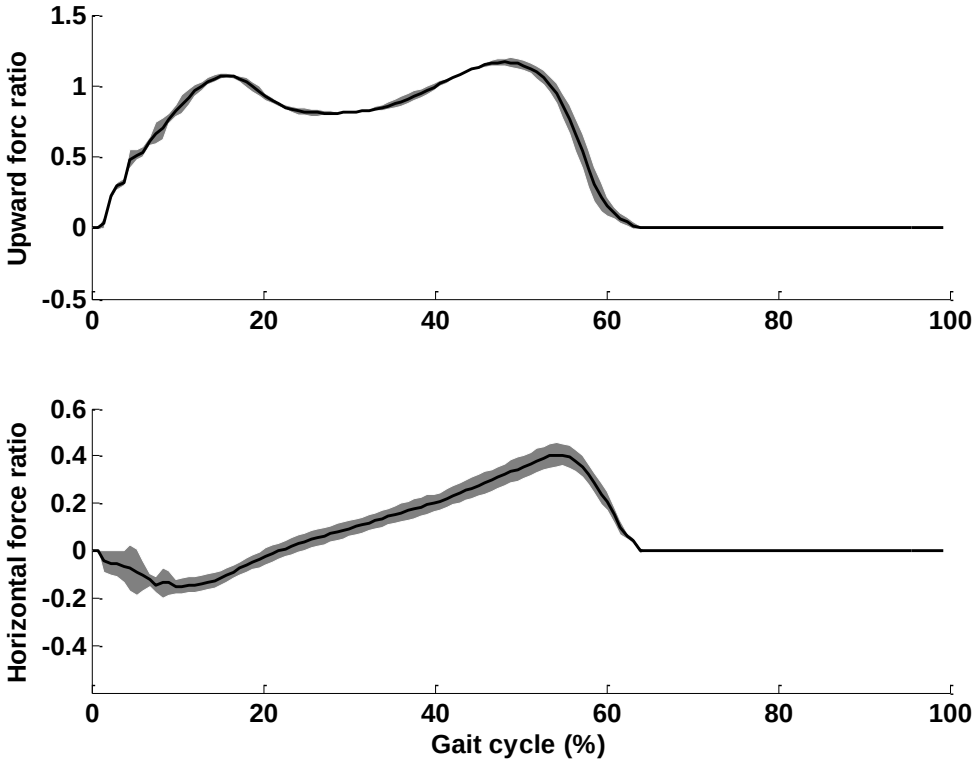
Upward forc ratio
1.5
1
0.5
0
-0.5
0
20
40
60
80
100
Horizontal force ratio
0.6
0.4
0.2
0
-0.2
-0.4
0
20
40
60
80
100
Gait cycle (%)

(a) S1.

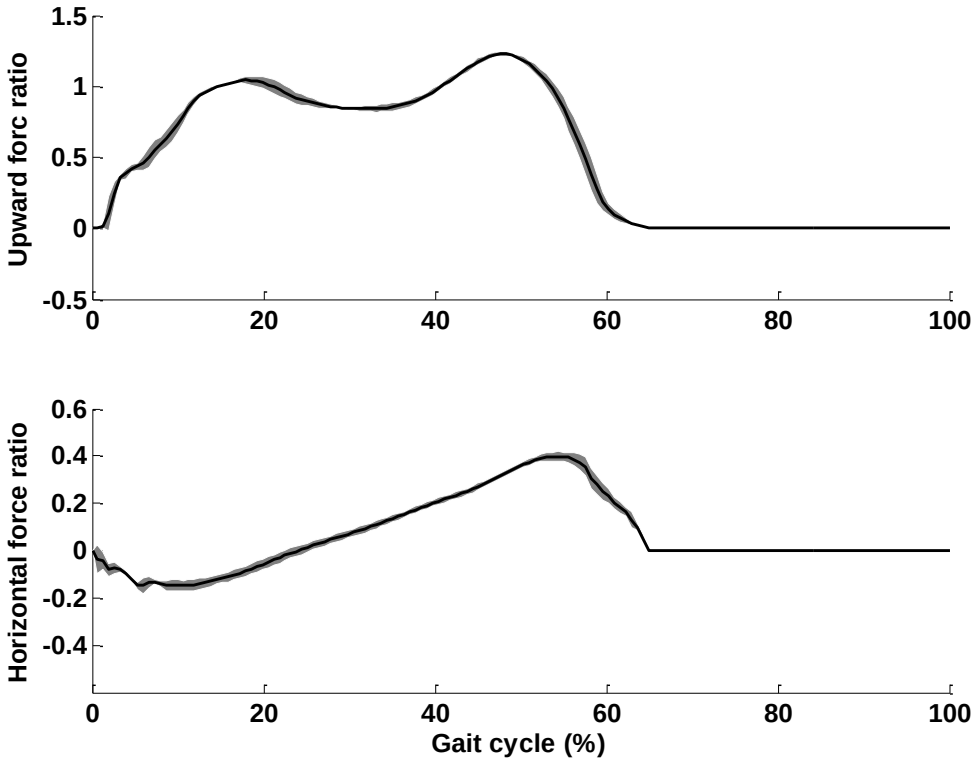
Upward forc ratio
1.5
1
0.5
0
-0.5
0
20
40
60
80
100
Horizontal force ratio
0.6
0.4
0.2
0
-0.2
-0.4
0
20
40
60
80
100
Gait cycle (%)

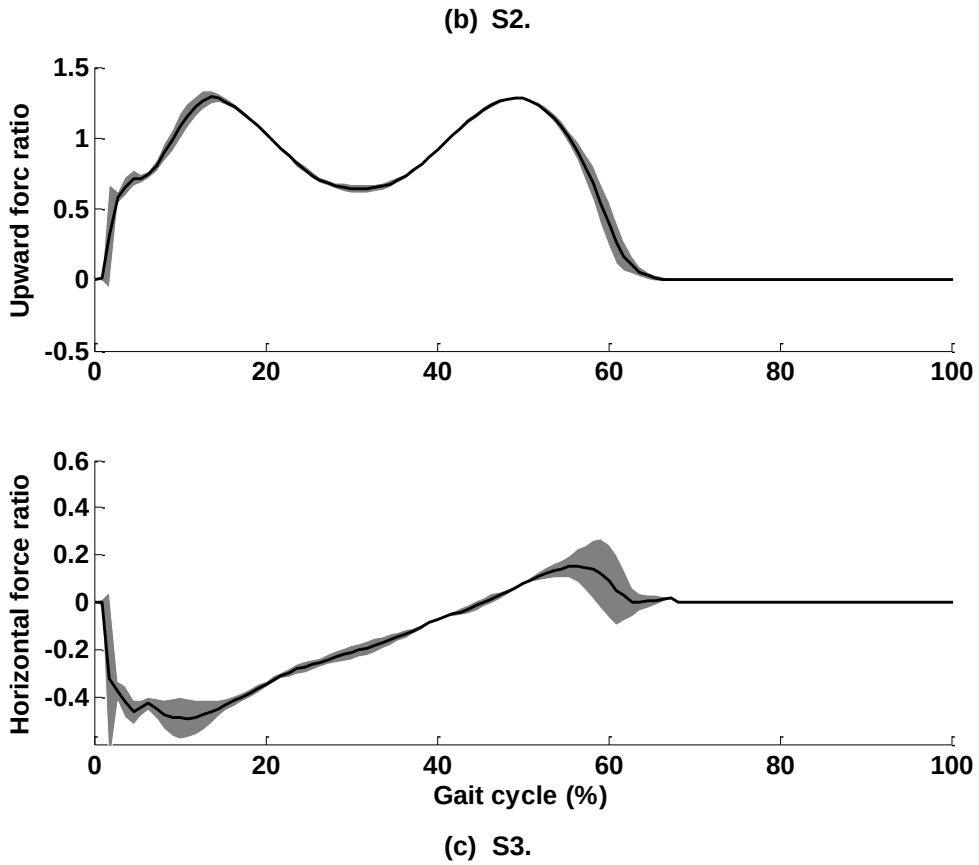

Figure 3.7: Normalised ground reaction forces for three subjects walking at 100% of NC.

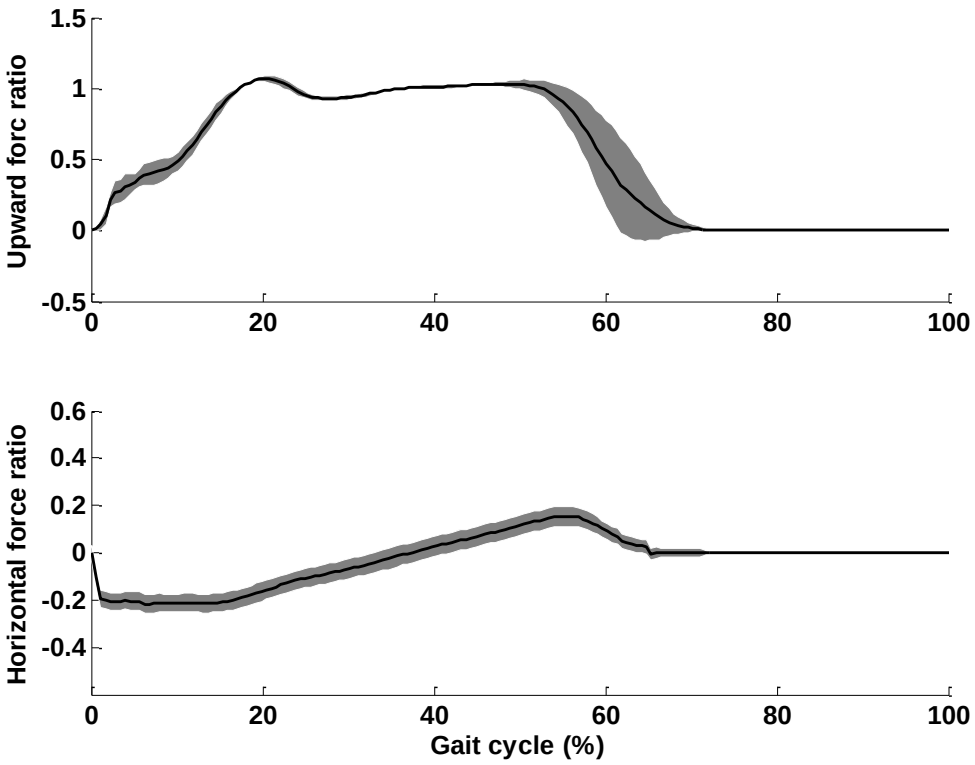
Upward forc ratio
1.5
1
0.5
0
-0.5
0
20
40
60
80
100
Horizontal force ratio
0.6
0.4
0.2
0
-0.2
-0.4
0
20
40
60
80
100
Gait cycle (%)

(a) S1.

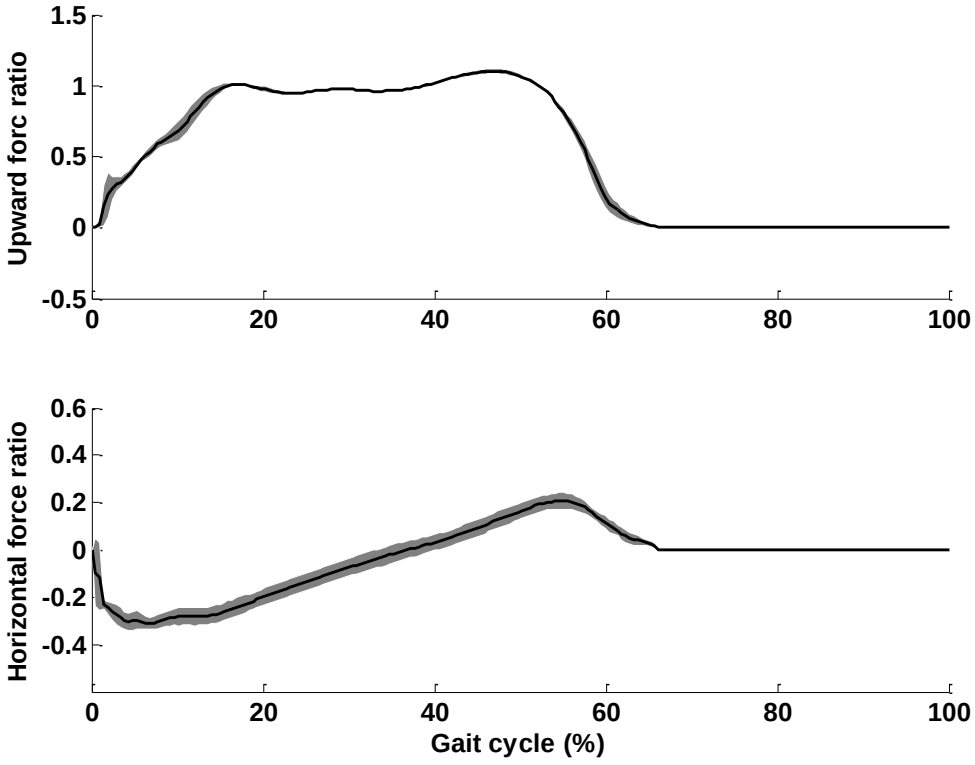
Upward forc ratio
1.5
1
0.5
0
-0.5
0
20
40
60
80
100
Horizontal force ratio
0.6
0.4
0.2
0
-0.2
-0.4
0
20
40
60
80
100
Gait cycle (%)

(b) S2.

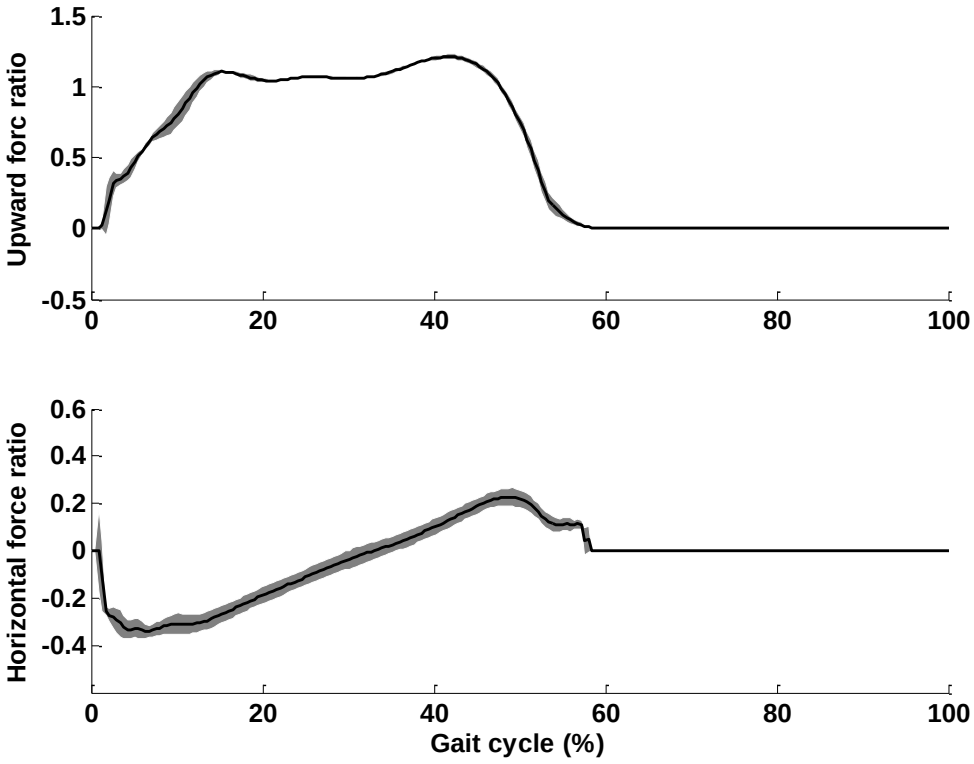

(c) S3.

Figure 3.8: Normalised ground reaction forces for three subjects walking at 75% of NC.

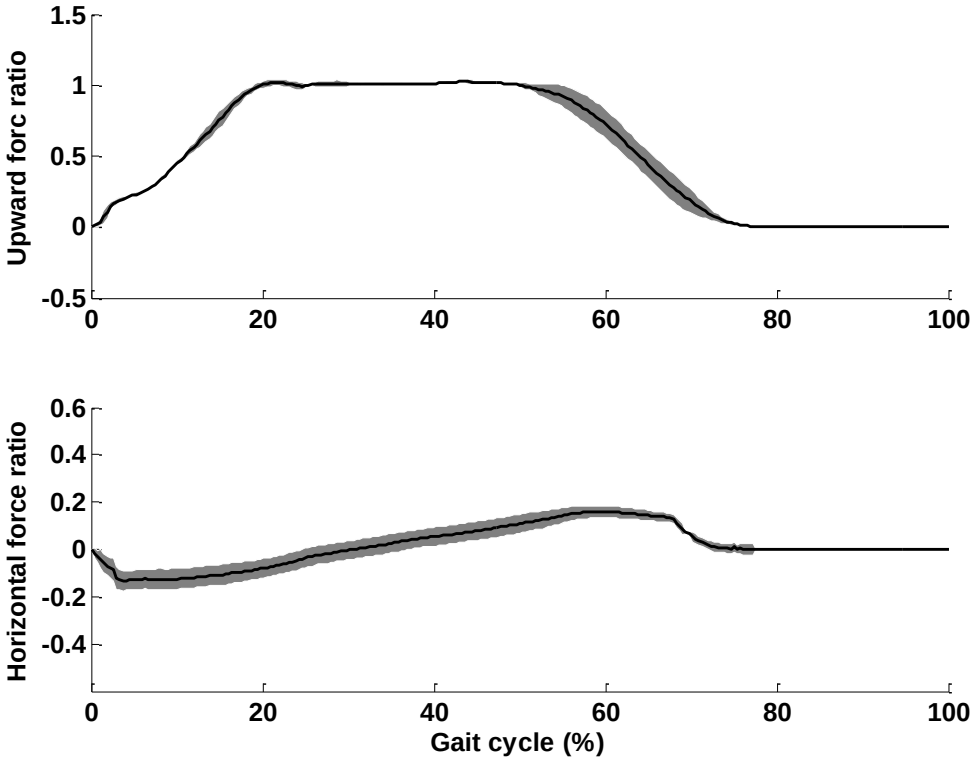

(a) S1.

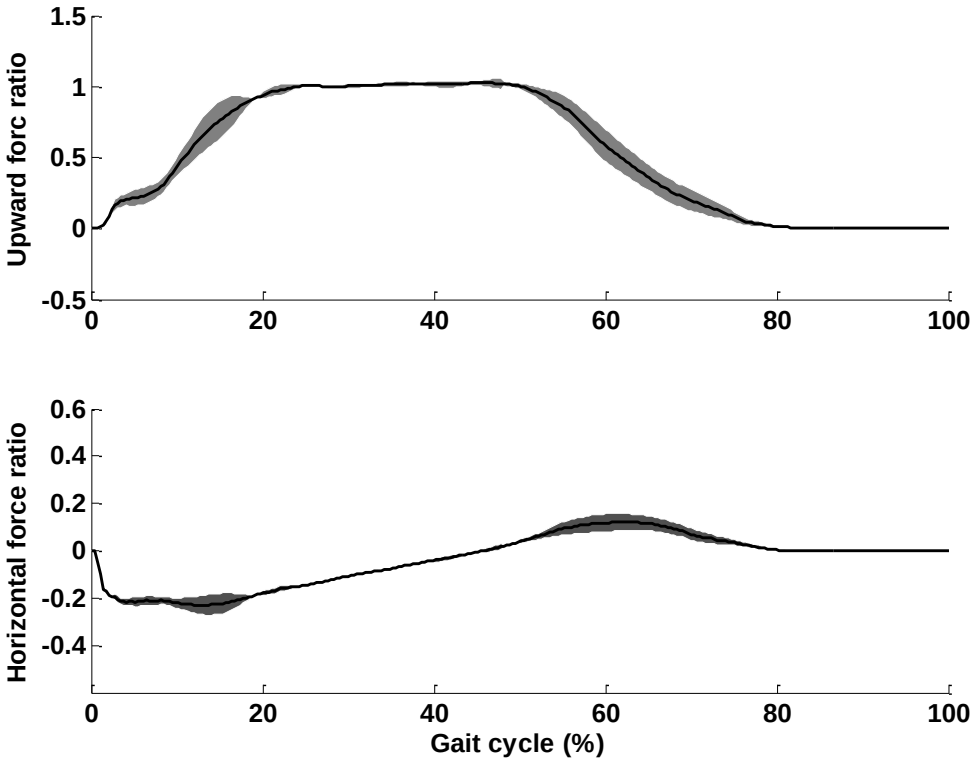

(b) S2.

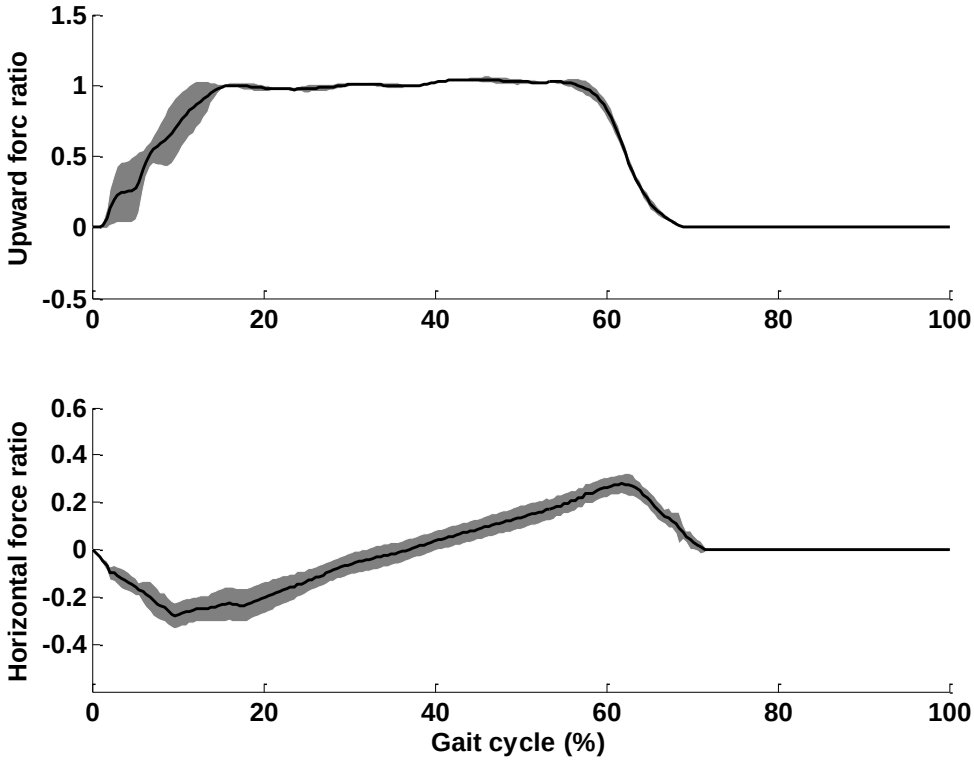

(c) S3.

Figure 3.9: Normalised ground reaction forces for three subjects walking at 50% of NC.

The vertical movements of the centre of body mass were reduced at lower speeds, resulting in the gradual disappearance of the double-hump pattern of the upward force, as depicted in Figures 3.8-3.9, which show forces of three subjects walking at 75% and 50% of NC. When the walking speed reduced to 50% of NC, the upward force was almost constant and equal to the whole body weight (Figure 3.9). The friction was substantially reduced. The ground reaction force duration was obviously prolonged for all subjects in slower walking. The stance phase lasted approximately 75% of the gait cycle in S1 walking at 50% of NC (Figure 3.9(a)). The ground reaction forces at various speeds agree with the description in the literature [243].

3.3.3. Internal moments

The internal joint moments of the hip (positive values mean extension moments), knee (negative values mean extension moments) and ankle (positive values mean plantarflexion moments) in the sagittal plane during a single gait cycle at normal cadence were calculated using Equations (3.9), (3.6) and (3.3), respectively, and are presented in Figure 3.10. The moment patterns in this study are similar to the general description of moment from the gait literature [234, 244]. During the stance phase the ankle joint produced plantarflexion moment to support the body weight. The upright force increased when the body weight transferred to the standing foot. Therefore the moment in the ankle joint increased in this period, as shown in the lowest plot in Figure 3.10. Around heel off, the ankle provided the maximal moment to propel the leg forward. As the foot entered the swing phase, the ground reaction forces were removed, resulting in a rapid reduction in the ankle joint moment. Therefore the ankle moment was quite small in the swing phase, where the ankle joint was in slight dorsiflexion to swing forward.

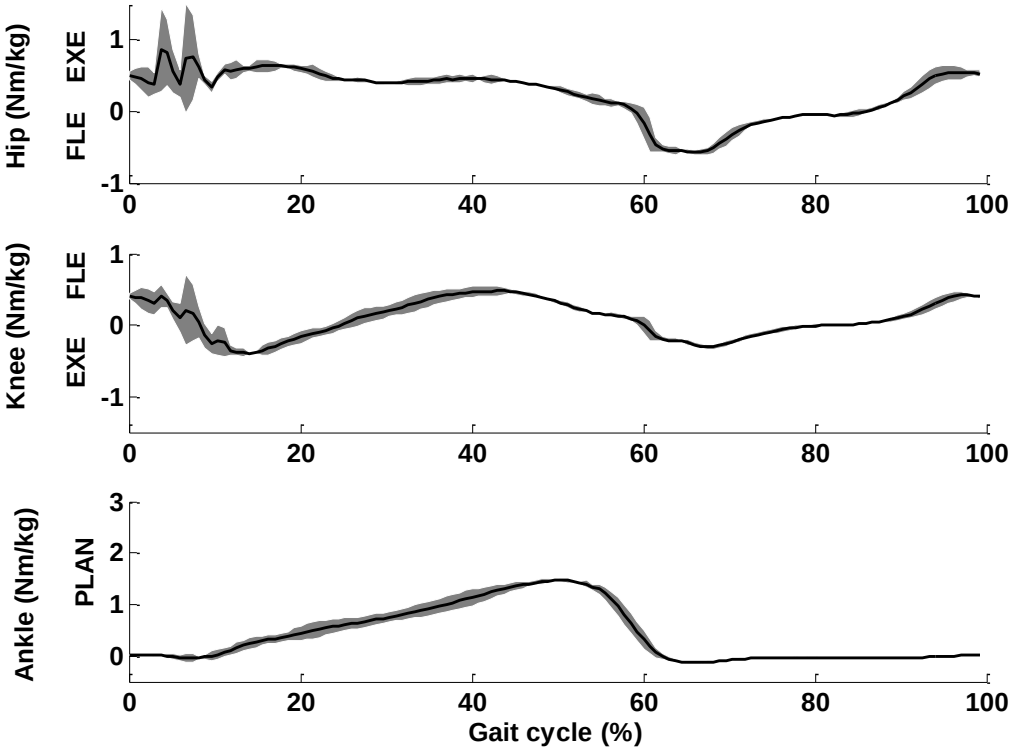
Hip (Nm/kg)
FLE
EXE
1
0
-1
0
20
40
60
80
100
Knee (Nm/kg)
FLE
EXE
1
0
-1
0
20
40
60
80
100
Ankle (Nm/kg)
PLAN
3
2
1
0
0
20
40
60
80
100
Gait cycle (%)

(a) S1.

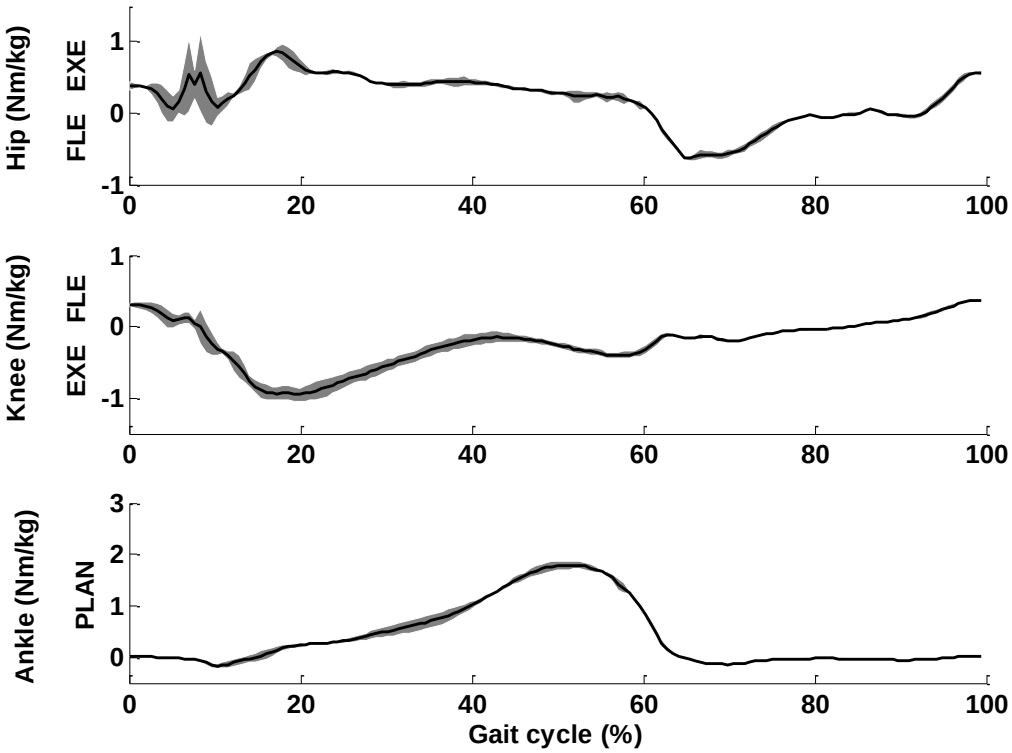
Hip (Nm/kg)
FLE
EXE
1
0
-1
0
20
40
60
80
100
Knee (Nm/kg)
EXE
FLE
1
0
-1
0
20
40
60
80
100
Ankle (Nm/kg)
PLAN
3
2
1
0
0
20
40
60
80
100
Gait cycle (%)

(b) S2.

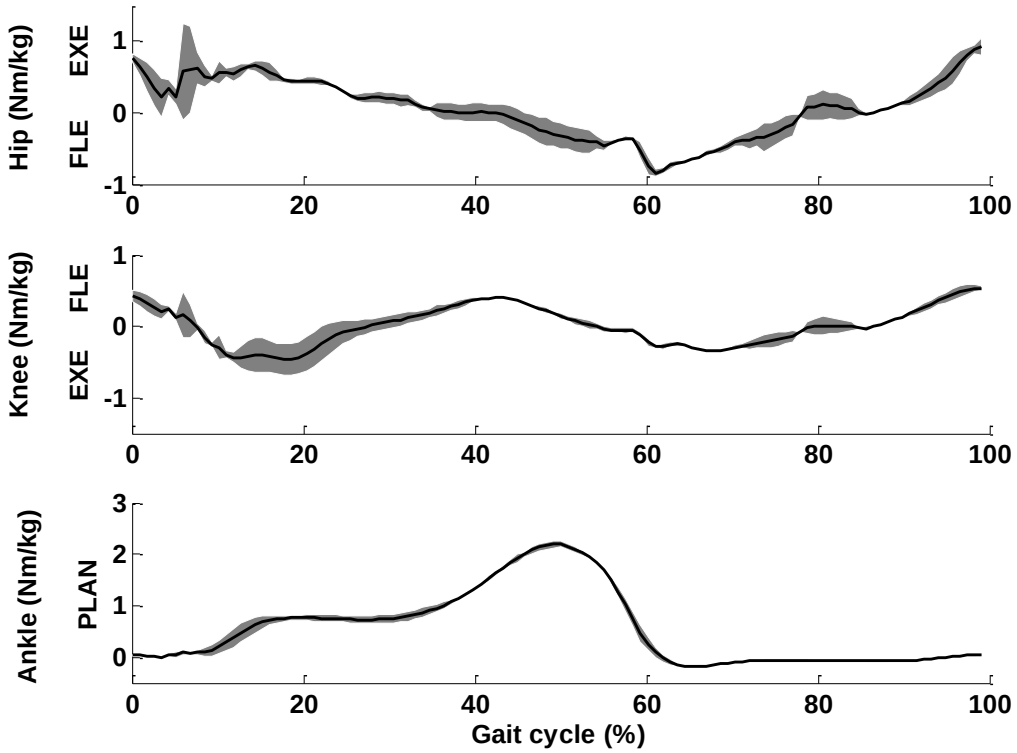

(c) S3.

Figure 3.10: Normalised internal joint moments for subjects walking at 100% of NC.

At heel strike, the ground reaction forces extended the knee joint. Therefore the flexion moment at the knee joint increased to avoid hyperextension, as shown in the middle plot of Figure 3.10. Following the heel strike, an extension moment of the knee joint was produced, so that the leg entered the mid-stance phase. As the body moved forward, the ground reaction forces moved rapidly to the forefoot during the double support phase, resulting in an flexion moment in the knee joint. From toe-off to the mid-swing phase, an extension moment of the knee joint was produced for forward propulsion. During the late swing phase, the knee joint produced a flexion moment so as to reduce the speed of the swing leg and to prepare for the next heel strike.

The hip joint produced an extension moment during the stance phase so as to maintain an upright position and a flexion moment during the early swing phase to move the

whole leg forward (see the top plot in Figure 3.10). The induced kinetic energy from hip flexion was partly transferred to the trunk, resulting in forward motion of the whole body. As the swinging leg was decelerated by the knee flexion moment at the end of the swing phase, the hip joint produced an extension moment to prepare for heel strike and to reduce the forward speed of the whole trunk [234].

Regarding the moments of the three subjects walking at 100% of NC (Figure 3.10), a large standard deviation was observed in the hip around heel strike because of the strike loading. S2, compared to other subjects, had a higher knee extension moment during the stance phase. This was because S2 walked with a more flexed knee joint, as can be seen in the knee angle profile in Figure 3.4(b). S3 had a "flatter" ankle moment (25%-35% of the gait cycle). This was because she had ground forces with the most pronounced double-hump pattern. The ground reaction forces reduced more compared to the other subjects during 25%-35% of the gait cycle, which resulted in a flatter (a lower increase) moment at the ankle joint.

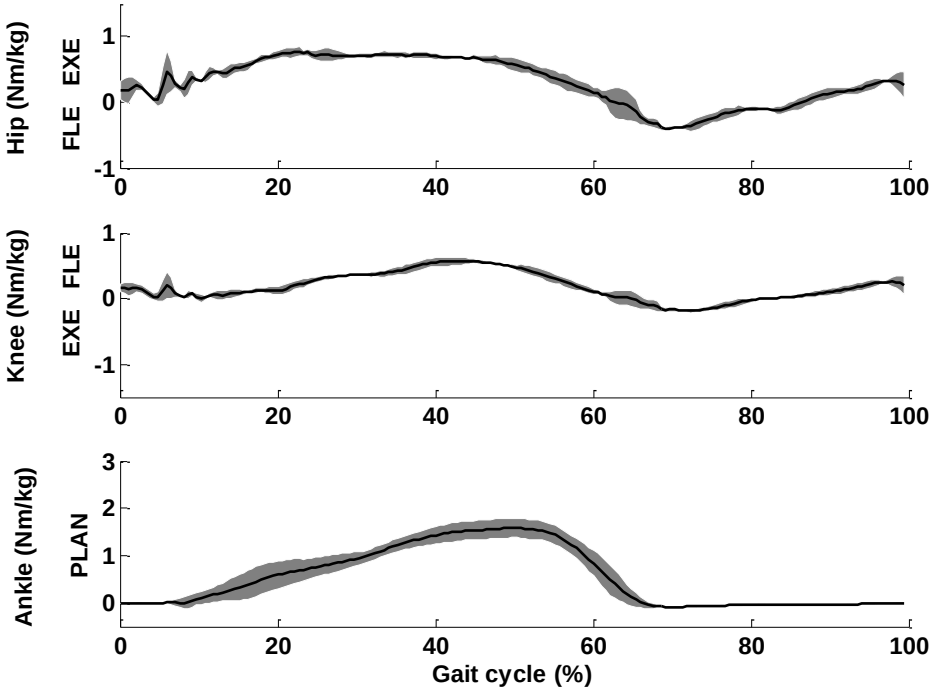

(a) S1.

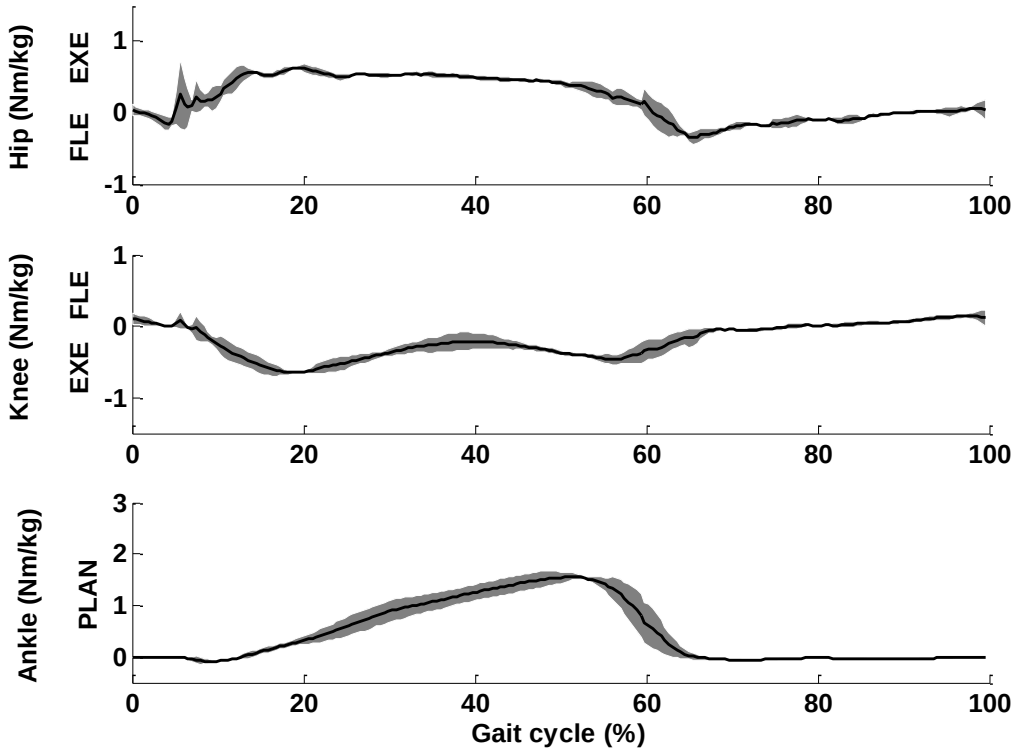

(b) S2.

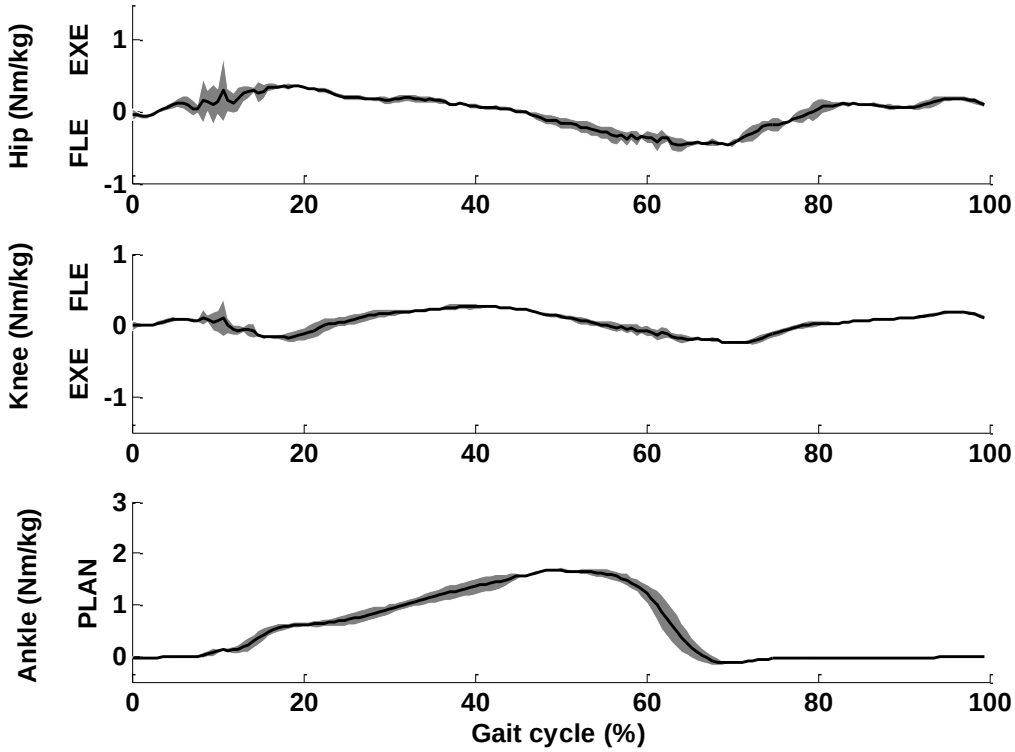

(c) S3.

Figure 3.11: Normalised internal joint moments for three subjects walking at 75% of NC.

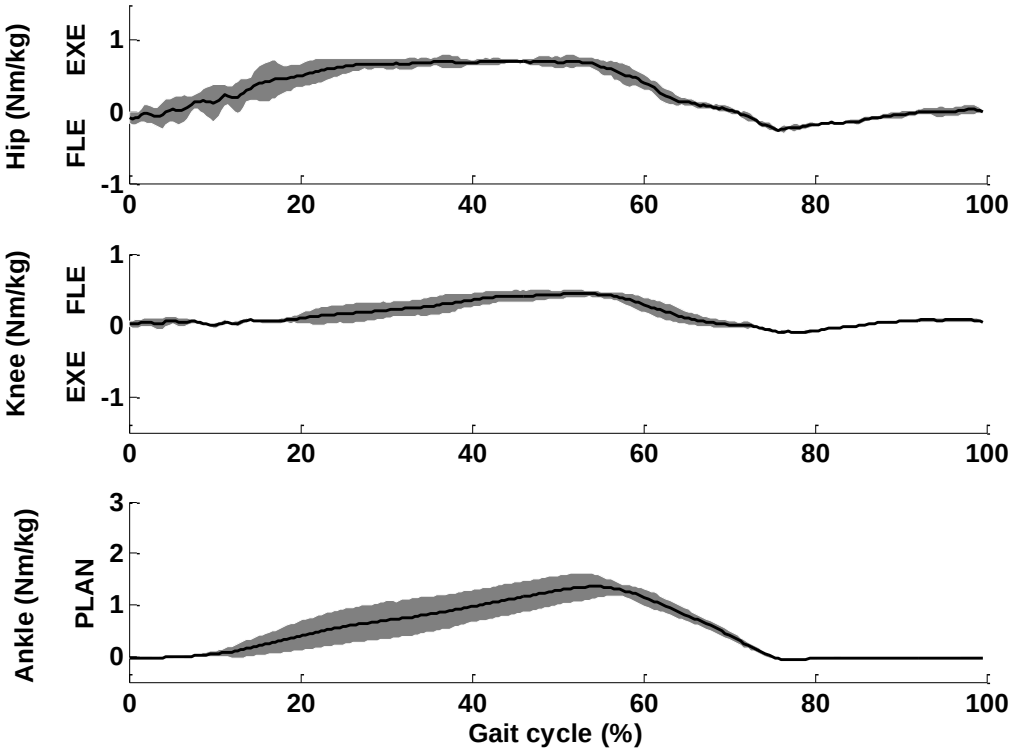
Hip (Nm/kg)
EXE
FLE
1
0
-1
0
20
40
60
80
100
Knee (Nm/kg)
FLE
EXE
1
0
-1
0
20
40
60
80
100
Ankle (Nm/kg)
PLAN
3
2
1
0
0
20
40
60
80
100
Gait cycle (%)

(a) S1.

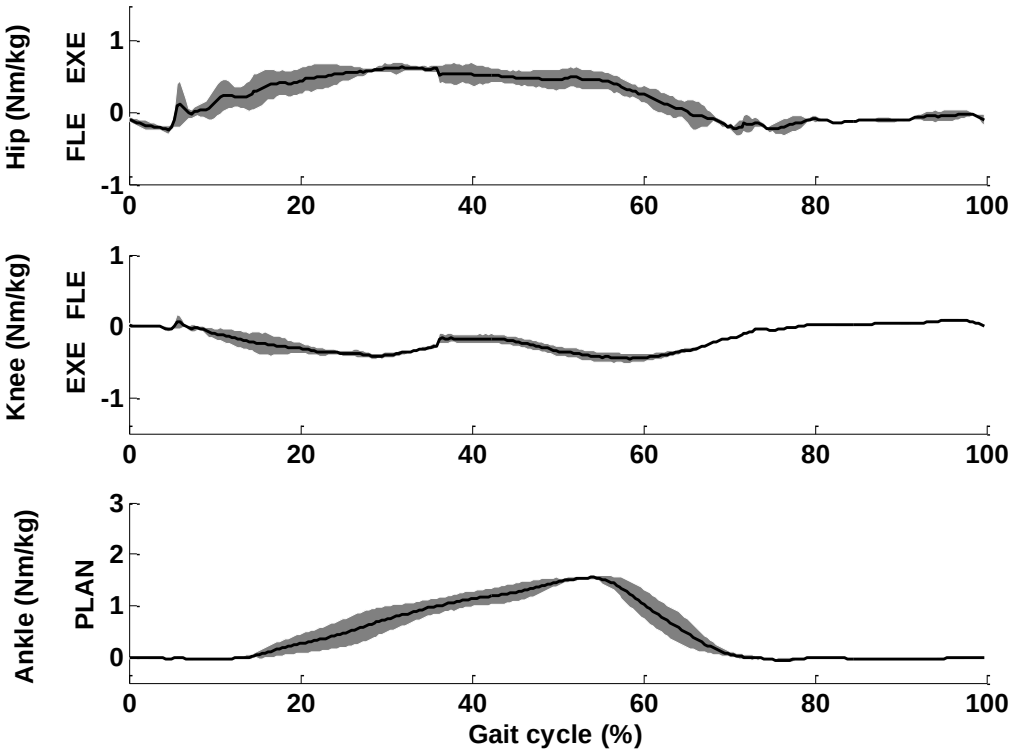
Hip (Nm/kg)
EXE
FLE
1
0
-1
0
20
40
60
80
100
Knee (Nm/kg)
FLE
EXE
1
0
-1
0
20
40
60
80
100
Ankle (Nm/kg)
PLAN
3
2
1
0
0
20
40
60
80
100
Gait cycle (%)

S2.

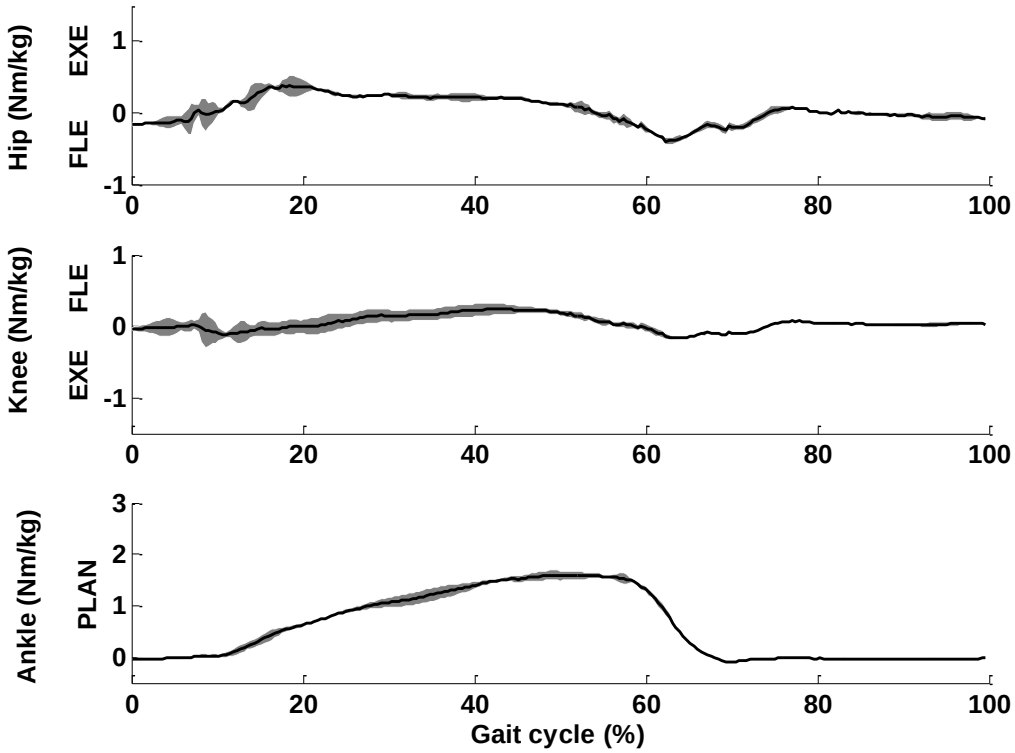

(b) S3.

Figure 3.12: Normalised internal joint moments for three subjects walking at 50% of NC.

The joint moments during slower walking in all three subjects are presented in Figures 3.11-3.12. As the speed reduced, the stance phase lasted longer, which resulted in a prolonged period of hip extension and ankle plantarflexion. The knee joint moment was substantially reduced and was not oscillatory compared to walking at 100% of NC. This was due to the fact that the knee joint was often in extension during the stance phase and had a much reduced flexion in the swing phase at slower walking (as can be seen in Figures 3.5-3.6). The reduced ROM of the knee joint resulted in a lower moment in the knee joint. Furthermore, the ground reaction forces were substantially reduced, especially during walking at 50% of NC, which resulted in a reduced moment in the ankle joint.

3.4. Discussion

The gait experiment recorded walking data at various speeds, to be used for the model development of the GOER system. The joint trajectories and the ground reaction forces from the experiment were selected as the target stepping performance for the GOER system. The joint moments during upright walking were considered as references for the kinetic performance of stepping in the GOER system.

Overground walking at normal speed is a rhythmic sensory-motor task, which does not require much conscious control from the brain [120]. Each of the three subjects could repeat their walking patterns at their self-selected normal walking speeds with small variation (see Figure 3.4). However, it was found challenging for them to walk at a lower speed with a consistent pattern, even though walking was guided by an electronic metronome. A higher standard deviation was observed in the three repeats of each walking session when the speed was further reduced. In contrast to walking at 100% of NC, subjects required voluntary input from the brain to reduce the speed during the subsessions of slower walking, therefore the variance of slow walking increased, especially for the swing phase. In spite of large variance, all three subjects showed coordinated motion in the lower limbs during slow walking.

The peak ground reaction forces reduced at slower walking speeds. Compared to walking at 100% of NC where two large peaks of upward ground force were observed, the force was almost equal to body weight when the subjects walked at 50% of NC. The joint moments, which depend strongly on the reaction forces, achieved their largest peak amplitudes at 100% of NC, compared to the two slower speeds. The moment demonstrates larger variance compared to the kinematic performance, which

is in accordance with previous research studies [243, 245]. Different individuals employ different dynamic skills to achieve the same walking pattern [235]. Therefore, in design of the GOER system, the kinematics patterns such as the joint trajectories were selected as the key criteria to reproduce, while the joint moments were considered as auxiliary features to provide a view of the kinetics of stepping.

The gait analysis described here improved our understanding of overground walking. Moreover, these walking data were able to be utilized for the design of the GOER system. The low variance in kinematics and ground reaction forces justifies their use as the target requirements of stepping in the GOER system. The joint moments could also be compared with those from supine stepping in the GOER system, which provides dynamic differences between upright walking and supine stepping.

One limitation of the experiment is that only three subjects were recruited to walk at three speeds. Although the subjects showed a large range of body mass (68–95 kg) and leg length (0.88-1 m), more subjects should be tested to obtain a general walking pattern. Walking data at slower speeds are desirable for design of a rehabilitation device. However, large variance observed in the walking data at 50% of NC made it challenging to obtain the general features of walking at such a slow speed. Based on the low variance observed at 75% of NC, it is suggested that speeds ranging between 100% and 75% of NC are more suitable for future gait experiments.

3.5. Conclusions

The gait experiment recorded intra- and inter-subject variability in the kinematics and kinetics of overground normal walking for able-bodied subjects. The experimental

performance, such as angle trajectories of the lower-limb joints and the ground reaction forces, can be regarded as the targets for the GOER system. The experimental data can be used in the model development of the GOER system, as discussed in Chapter 4.

Chapter 4. Model Development

Summary: This chapter describes the modelling and simulation of supine stepping. Based on the results of the gait analysis, a circle-fit algorithm was derived to approximate the foot trajectories. A model of a two-bar system was developed to simulate the kinematics of supine stepping at various speeds, which were in similar ranges of motion (ROMs) to experimental overground walking. Furthermore, the kinetic features of supine stepping were analysed through a model of a leg-linkage. These simulation results provide the basis for the design of the GOER system.

4.1. Circle Fit Approximation of the Ankle, Heel and Toe Trajectories

Summary: This study derives a least squares approximation algorithm for analysis of foot trajectories relative to the hip joint in three able-bodied subjects walking overground at various speeds, with focus on three different foot landmarks: the ankle, the heel and the toe. While the study confirmed that the ankle and the heel moved in circular paths in the stance phase, it demonstrated that the toe followed a circular trajectory during the whole locomotion phase. The configuration of these approximated circles was determined, including the circle centre and the radius. This observation provided the basis for model development of the GOER system.

4.1.1. Introduction

Within the biomechanics community, there is a rhetorical hypothesis that the human

performs locomotion through a pendulum strategy. A pendulum concept of walking seems to be a relatively simple and convenient model for analysing the dynamic features of walking. However, there are great variations among the published studies in the configuration of the pendulum, such as the total number of pendula within the model, and the exact locations of the base and the tip of the pendulum. Likewise, while the model is commonly used to describe the stance phase, some studies use it to describe the swing phase.

The centre of the reference system (i.e. the base of the pendulum) can be located on the ground [246, 247], or in some leg segments [248, 249]. Based on the phenomenon that the centre of mass of the human body rises and falls in an arc shape during each stride, Alexander and colleagues developed a simple inverted pendulum model with the base on the ground to describe a leg in the stance phase [246, 247]. The hip joint is chosen as the base of the pendulum models in some other studies such as [248] to simulate overground locomotion. Furthermore, the pelvis was also considered as the base of a pendulum model [249], where the leg was represented by two pendula connected by a hinge at the knee joint.

Most often, the pendulum model was used to describe the stance phase. For example, studies [246, 247] employed a pendulum model to describe the process of a straight leg rolling from the heel to the toe. However, the pendulum concept was sometimes used to describe the swing phase. Study [250] developed a double-pendulum model which simulated the performance of a swinging leg at variable speeds.

In addition to the variability in the pendulum setup, the tip of the pendulum, which is often represented by the foot, is also vaguely defined. Although the foot is a complex

multi-segment structure [251], the pendulum model often regards its tip (the foot) as one segment: a rolling-rocker [249, 251, 252]. The foot is described in the literature [253] to move as ankle, heel and toe rockers during the stance phase. However, this concept does not formally question whether the rocker shape correctly represents the actual foot trajectories.

The typically adopted assumption of the foot as a rigid rocker questions the accuracy of the pendulum model. An often neglected problem is: which points of the foot move along circular trajectories during locomotion? If there are such points moving in circular paths, which can serve as the tips of pendulum models, then what is the configuration of the pendulum, such as the location of its base and the pendular length, or rather the centre and the radius of the circle? Could the assumption about the circular trajectory be extended over the whole gait cycle, rather than only one specific phase? The objective of the study described in this section was to address the exact geometry of the pendulum, i.e. the location of its base and its tip, by finding the best-fit circles of trajectories of the ankle, the heel and the toe at variable walking speeds. As this PhD project aimed to design a system for supine stepping, where the trunk is lying on a bed and the whole leg moves around the hip joint, this study investigated the foot trajectory relative to the hip joint. In this supine position, the foot trajectory is modelled as a normal rather than an inverted pendulum.

4.1.2. Methods

The gait data collected in the experiment described in Chapter 3 were analysed (refer to chapter 3 for a detailed description of the methods and the recorded data). Based on overground walking data from three able-bodied subjects, an algorithm was

developed to find the optimal geometries of circles that could approximate trajectories of the ankle (in the stance phase), the heel (in the stance phase) and the toe (over the whole gait cycle).

4.1.2.1. Gait analysis

The gait experiment captured the moving trajectories of the lower limbs, by recording X and Y coordinates relative to the ground. Among the recorded data, only data of the hip joint, the ankle, the heel and the toe shown in Figure 4.1 were of interest in this study. A new reference system was defined in this study with the centre (0, 0) at the hip joint. Coordinates of the ankle, the heel and the toe in this reference system were obtained by subtracting X and Y coordinates of the hip from their respective coordinates recorded in the experiment. Foot data over one gait cycle were analysed and the duration of one gait cycle was normalised to 100%, with heel strike at 0 and 100%.

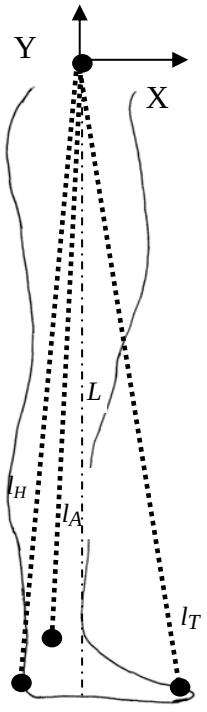

Figure 4.1: Leg position in the new reference system. The X-Y reference centre (0, 0) is

at the hip joint axis. Black dots at the lateral malleolus, calcaneus and second metatarsal head indicate the ankle, heel and toe, respectively. The distances from the hip centre to the ankle, heel and toe are represented respectively by dashed lines as l_A, l_H and l_T. A dash-dot line L represents the vertical distance from the hip to the ground.

4.1.2.2. Circle-fit algorithm

The pendulum model could be determined by searching out circles which approximated the trajectories of the ankle, heel or toe. It was hypothesized that the centre of the fit circle (x_c, y_c) was near to the hip joint (0, 0) and that its radius r was approximately equal to the segment distance l measured from the hip joint (l refers to l_A, l_H and l_T for the ankle, the heel and the toe, respectively).

There were three parameters that could be optimized in order to obtain the best-fit circle: coordinates of the centre of the circle x_c, y_c, and the radius r. Four methods were developed to search for the circular trajectory which approximated the trajectory of the ankle, the heel or the toe with the smallest error:

(1) For the Y coordinate of the pendulum base fixed at the hip ($y_c = 0$), search for the optimal x_c and r;

(2) For the X coordinate of the pendulum base fixed at the hip ($x_c = 0$), search for the optimal y_c and r;

(3) For both X and Y coordinates of the pendulum base fixed at the hip ($x_c = 0$, $y_c = 0$), search for the optimal radius r;

(4) For the radius r of the pendulum equal to the segment distance measured from the hip joint (l_A, l_H or l_T), search for the optimum location for its base x_c and y_c.

It was assumed that each segment analysed had Q data points (x_i, y_i) (i = 1, 2, 3…Q). The distance between each data point (x_i, y_i) and the circle (x_c, y_c, r) was calculated as

$$D(x_i, y_i) = \left| \sqrt{(x_i - x_c)^2 + (y_i - y_c)^2} - r \right|; (i = 1, 2, 3...Q). \tag{4.1}$$

With a least squares algorithm [254], the difference between each data point (x_i, y_i) and the circle can also be represented by

$$f_i(x_i, y_i) = \left| (x_i - x_c)^2 + (y_i - y_c)^2 - r^2 \right|^{0.5}; (i = 1, 2, 3...Q). \tag{4.2}$$

The mean difference between the actual foot trajectories and the circle (x_c, y_c, r) was calculated as

$$F(x_i, y_i) = \frac{1}{Q} \sum_{i=1}^{Q} f_i(x_i, y_i). \tag{4.3}$$

The objective of the best-fit circle was to determine the values of x_c, y_c and r which solved the problem

$$\min_{x_c, y_c, r} F(x_i, y_i). \tag{4.4}$$

The first derivative of Equation (4.3) over r, x_c and y_c yielded the optimal parameters for the best-fit circle:

$$d(F(x_i, y_i))/dr = 0 \tag{4.5}$$

$$d(F(x_i, y_i))/dx_c = 0 \tag{4.6}$$

$$d(F(x_i, y_i))/dy_c = 0 \tag{4.7}$$

The previously described methods to search for the best-fit circle are therefore:

(1) For $y_c = 0$, find $\min_{x_c, y_c, r} F(x_i, y_i)$.

Equations (4.5)-(4.6) yield:

$$\sum_{i=1}^{Q} [(x_i - x_c)^2 + y_i^2 - r^2] = 0 \tag{4.8}$$

$$\sum_{i=1}^{Q}(x_i - x_c)[(x_i - x_c)^2 + y_i^2 - r^2] = 0 \tag{4.9}$$

(2) For x_c = 0, find $\min_{x_c, y_c, r} F(x_i, y_i)$.

Equations (4.5) and (4.7) yield:

$$\sum_{i=1}^{Q}[x_i^2 + (y_i - y_c)^2 - r^2] = 0 \tag{4.10}$$

$$\sum_{i=1}^{Q}(y_i - y_c)[x_i^2 + (y_i - y_c)^2 - r^2] = 0 \tag{4.11}$$

(3) For x_c= 0, y_c = 0, find $\min_{x_c, y_c, r} F(x_i, y_i)$:

$$\sum_{i=1}^{Q}[x_i^2 + y_i^2 - r^2] = 0 \tag{4.12}$$

(4) For $r = l$, find $\min_{x_c, y_c, r} F(x_i, y_i)$:

$$\sum_{i=1}^{Q}(x_i - x_c)[(x_i - x_c)^2 + (y_i - y_c)^2 - l^2] = 0 \tag{4.13}$$

$$\sum_{i=1}^{Q}(y_i - y_c)[(x_i - x_c)^2 + (y_i - y_c)^2 - l^2] = 0 \tag{4.14}$$

Solutions of Equations (4.8)-(4.14) give optimal values for x_c, y_c and r for each method. These four methods were applied to the trajectories of the ankle, heel and toe separately, giving the approximated circle for each foot trajectory. The mean approximation error for each method was calculated using Equations (4.2)-(4.3). In order to keep the results as general as possible, all the equations were normalised with respect to the leg length or the natural gait cycle.

4.1.2.3. Statistical analysis

A one-way ANOVA test was performed in SPSS to see whether there was a significant difference within the four methods ($p = 0.05$). A Bonferroni post-hoc test was performed for each pair of methods to test for differences. An independent one-sided t-test was used to compare whether the mean error of Method 1 is the lowest among the four methods. The method with the smallest error and significant difference from other methods was deemed the best-fit circle algorithm.

4.1.3. Results

Numerical values of foot trajectories are related to the height. However, the shapes of the trajectories are quite similar for most able-bodied adults [255]. The ankle, heel and toe trajectories relative to the hip joint for a representative subject S1 at a normal cadence (NC) of 107 steps/min are shown as thick solid lines in Figure 4.2.

It can be seen that the ankle and heel trajectories, as shown by thick solid lines in Figures 4.2(a) and (b), are similar and have a curved stance phase. Therefore best-fit circles for the ankle and heel trajectories in the stance phase were searched for. The toe trajectory displayed as a thick solid line in Figure 4.2(c) has similar stance and swing phases with a curved shape. Therefore a best-fit circle for the toe trajectory in the whole gait cycle was searched for.

Applying the four algorithms yielded four approximating circles for these three foot landmarks. Figures 4.2 (a)–(c) show the approximation results for S1 walking at 100% of NC. Circles represented by solid, dashed, dotted and dash-dot lines are fit circles

from Methods 1 to 4, respectively. The centres are marked with stars, dots, crosses and plus signs, respectively. It can be seen that Methods 1, 3 and 4 give similar results regarding the centres and the radii of the circles, while Method 2 gives circles (represented as dashed lines) with radii being much smaller (in Figures 4.2 (a)–(b)) or much larger (in Figure 4.2(c)) than the segment distance from the hip. This is because trajectories of the ankle, the heel and the toe have different curvatures. The curvatures of the heel and ankle trajectories at ($x_i = 0$) are in general larger than the curvature of a circle with $r = l$ ($l = l_A$ for the ankle and $l = l_H$ for the heel), so the radius of the fit circle (when only the Y coordinate can vary) is smaller than the segment distance from the hip. Conversely, the curvature of the toe trajectory is smaller than the curvature of a circle with $r = l$ ($l = l_T$ for the toe), so the fit circle has a radius much larger than the segment distance from the hip.

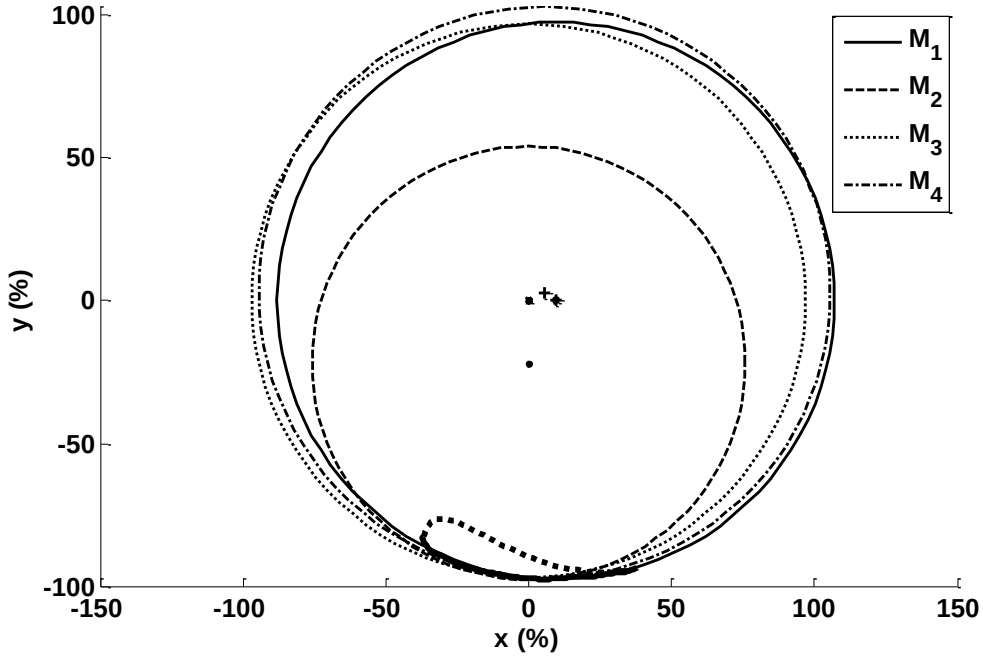

(a) Ankle

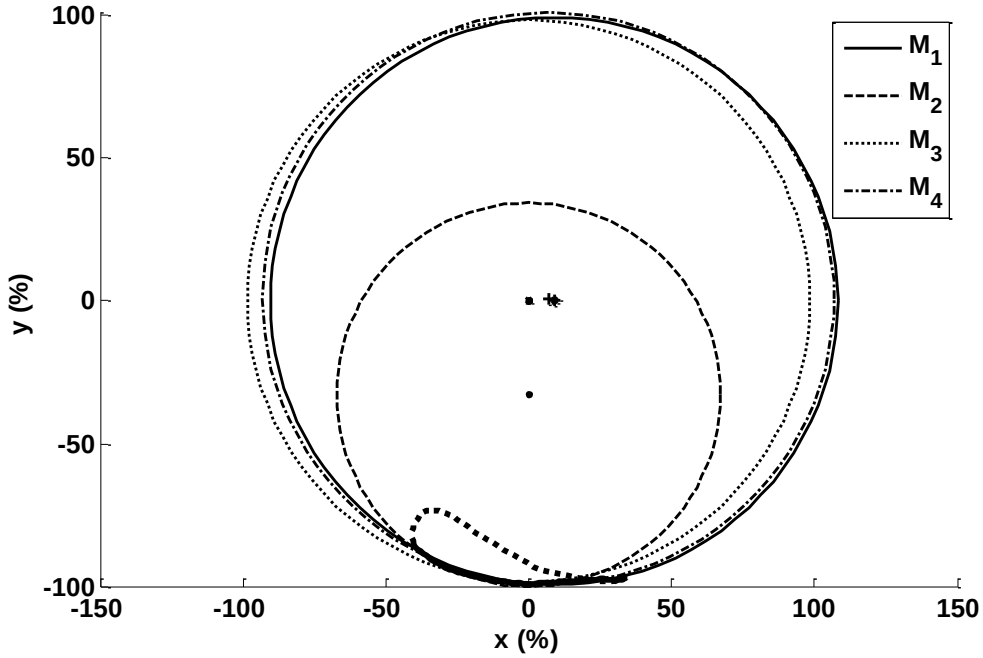

(b) Heel

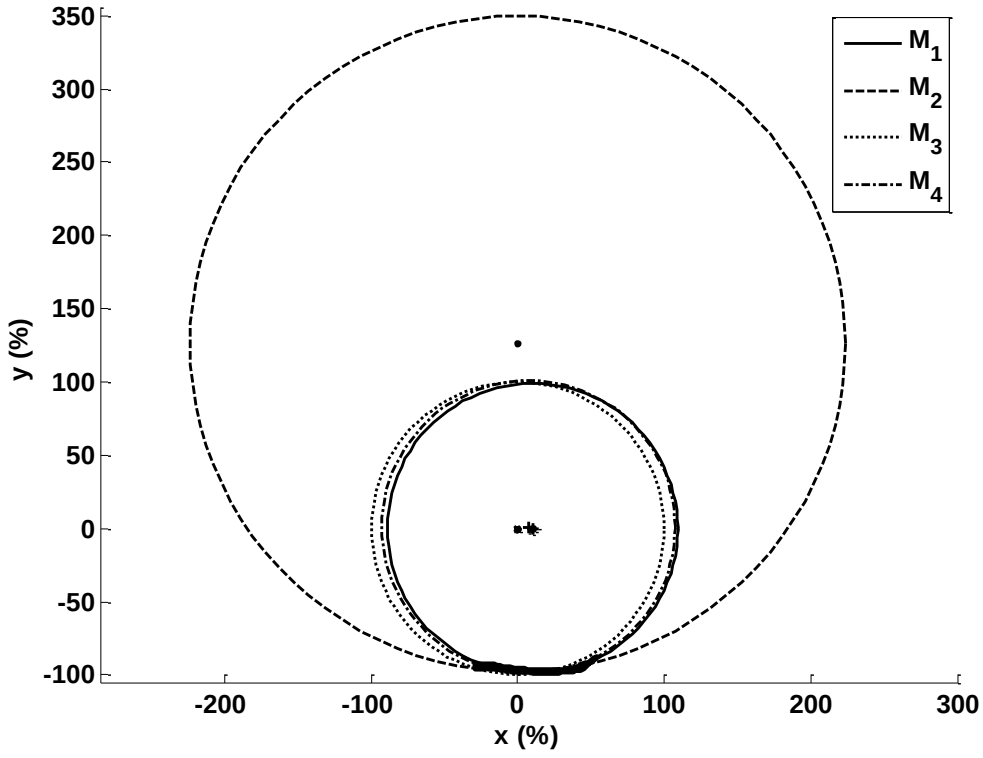

(c) Toe

Figure 4.2: Circle fit approximation of the foot trajectories of S1 walking at 100% of NC. Circles in solid, dashed, dotted and dash-dot lines are fit circles from Methods 1 to 4 (marked as M_1, M_2, M_3 and M_4), respectively. The centres are marked with stars, dots, crosses and plus signs, respectively. The foot trajectories (relative to the hip)

considered for circle approximation are shown as thick solid lines, while those not involved in the approximation (the ankle and heel trajectories during swing) are thick dotted lines.

Using the four circle-fit searching algorithms, the approximating circles for the foot trajectories from the other two subjects were also obtained. The normalised errors between each foot trajectory at 100% of NC and their respective approximating circles are summarized in Table 4.1. The mean and standard deviation (SD) of errors from each method are presented as well.

Table 4.1: Relative error of four methods with respect to the leg length (%) for the ankle, heel and toe trajectories in three subjects walking at 100% of NC.

		Method 1	Method 2	Method 3	Method 4
S1	Ankle	0.42	1.68	1.74	0.65
	Heel	0.77	1.31	1.50	0.12
	Toe	1.21	1.53	2.69	1.76
S2	Ankle	0.52	1.01	1.13	0.93
	Heel	0.82	0.91	1.02	0.99
	Toe	1.44	1.61	2.43	1.74
S3	Ankle	0.59	0.63	1.10	0.83
	Heel	1.05	1.24	1.29	1.17
	Toe	1.56	1.84	2.10	1.91
Mean ±SD		0.93 ±0.41	1.31 ±0.40	1.67 ±0.61	1.12 ±0.59

In all three subjects and for all four methods (12 measurements in total), the trajectory of the ankle, compared to the heel and the toe, had the smallest circle-fit error. Among all the four methods, Method 3, which has the centre of the circle (x_c, y_c) fixed to the hip (0, 0), had the largest approximation error. Method 1, which fixes y_c to the hip and allows x_c and r to vary, had the smallest mean error. A one-way ANOVA test performed in SPSS showed at least one method was significantly different from the other methods (p = 0.031). A Bonferroni post-hoc test showed that Method 1 was

significantly different from Method 3 (p = 0.028). An independent one-sided t-test showed the mean error for Method 1 to be significantly lower than that of Method 2 (p = 0.03). There was no significant difference between Method 1 and Method 4. However, Method 1 yielded errors smaller than Method 4. Therefore Method 1 was selected to search for the best-fit circle forthwith.

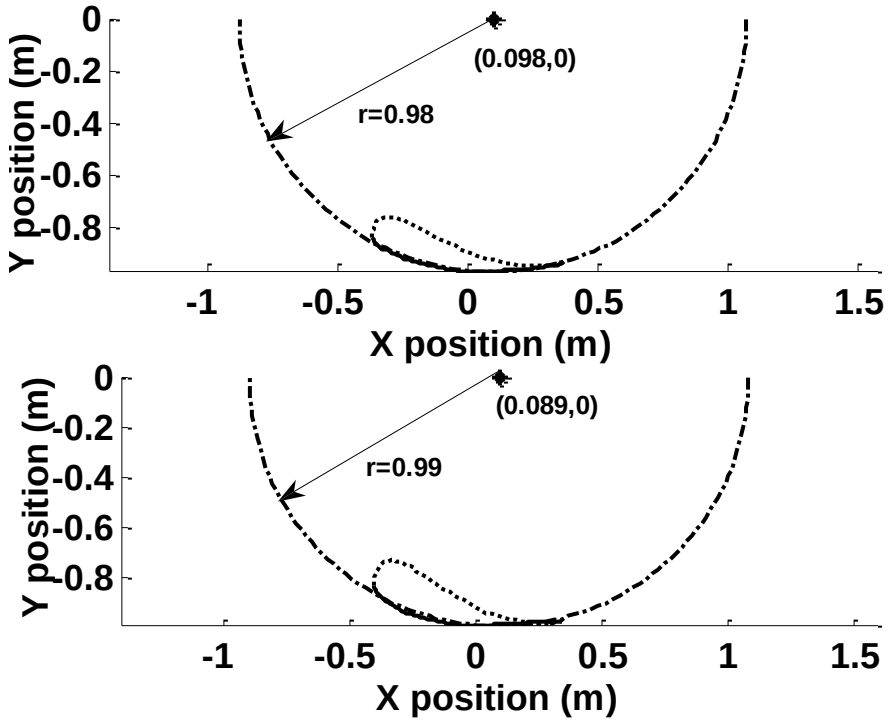

Figure 4.3: Circle fit approximation (Method 1) of the ankle (upper) and heel (lower) trajectories (relative to the hip) in the stance phase of S1 walking at 100% of NC. The best-fit circles are shown as dash-dot lines, with the radius represented as an arrow. The ankle and heel trajectories in the stance phase are shown as solid lines, while those in the swing phase are dotted lines.

The approximation results of Method 1 for the foot trajectories of S1 are displayed in Figures 4.3-4.4. Detailed information about the best-fit circle, including the centre and radius, is also presented. For the foot trajectories in these figures, the parts that were approximated by circles, which are the trajectories in the stance phase for the ankle and heel in Figure 4.3 and the toe trajectory over the whole gait cycle in Figure 4.4, are

represented as solid lines. The parts that were not involved in the circle approximation, which are the swing phase of the ankle and the heel trajectories in Figure 4.3, are displayed as dotted lines. The curved trajectories of the ankle and the heel during the stance phase are fit by the circles (dash-dot lines) closely. The circle approximation of the toe trajectory shown in Figure 4.4 has a larger difference, but it should be noted that this circle quite well approximates both the stance and swing phases of the toe (see zoomed plot in Figure 4.4). The distance between the toe and the hip joint l_T for S1 was 1 m. The centre of the best-fit circle of the toe trajectory was at the point (0.095, 0), which was 9.5% of l_T from the hip joint (0, 0). The radius of the circle was 0.99 m, which was 1% shorter than l_T.

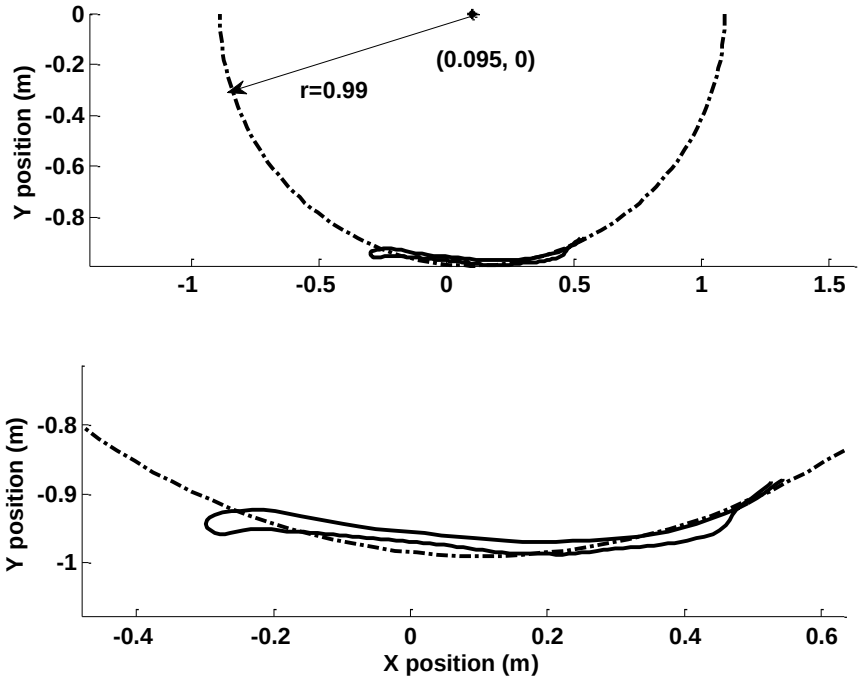

Figure 4.4: Circle fit approximation (Method 1) of the toe trajectory (relative to the hip) in the whole gait cycle of S1 walking at 100% of NC (upper). The best-fit circle is represented by a dash-dot line, with the radius shown as an arrow. The toe trajectories (both the stance and the swing phases) are shown as solid lines. A zoomed view is presented in the lower subfigure.

The foot trajectories during slower walking were also curved, which allowed circle approximation as well. The ankle trajectories of S1 walking at 100%, 75% and 50% of NC are displayed in Figure 4.5. The step length was shortened as the speed decreased. It can be seen that the ankle trajectories in the stance phase at different speeds are similarly curved. The best-fit circles obtained by Method 1 are displayed in Figure 4.5 and are of similar radius.

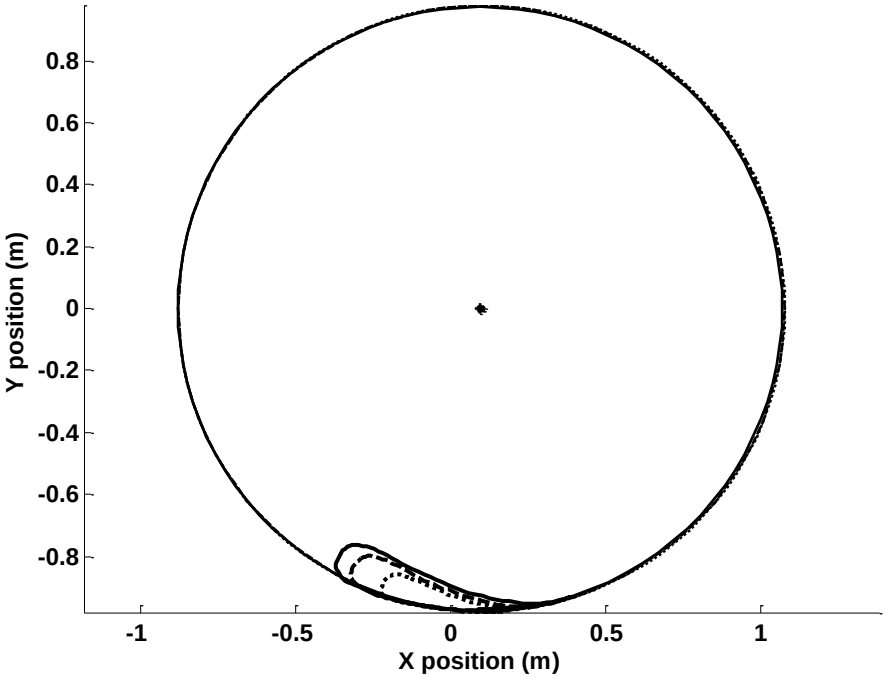

Figure 4.5: Ankle trajectories and the best-fit circles in S1 walking at 100% (solid line), 75% (dashed line) and 50% (dotted line) of NC.

Method 1 was used to find the optimal circles to approximate foot trajectories for slower walking at 75% and 50% of NC for all three subjects. The normalised mean errors of approximation for the trajectories of the ankle (the stance phase), the heel (the stance phase) and the toe (the whole gait cycle) are presented in Figure 4.6, with the centres and radii summarized in Table 4.2. It can be seen that the foot trajectories can be approximated by semicircles with a mean error less than 0.2% of leg length at

variable speeds. The ankle and heel trajectories (in the stance phase) are fit by the circular trajectory with a smaller error than the toe trajectories (in both the stance and swing phases). The circle fit approximation of the ankle trajectory has the smallest error. When the speed decreases, the error reduces as well. Table 4.2 shows that the best-fit circles for the foot trajectories at 100% of NC have the centres closest to the hip while those at 50% of NC have the radii closest to the segment distance from the hip.

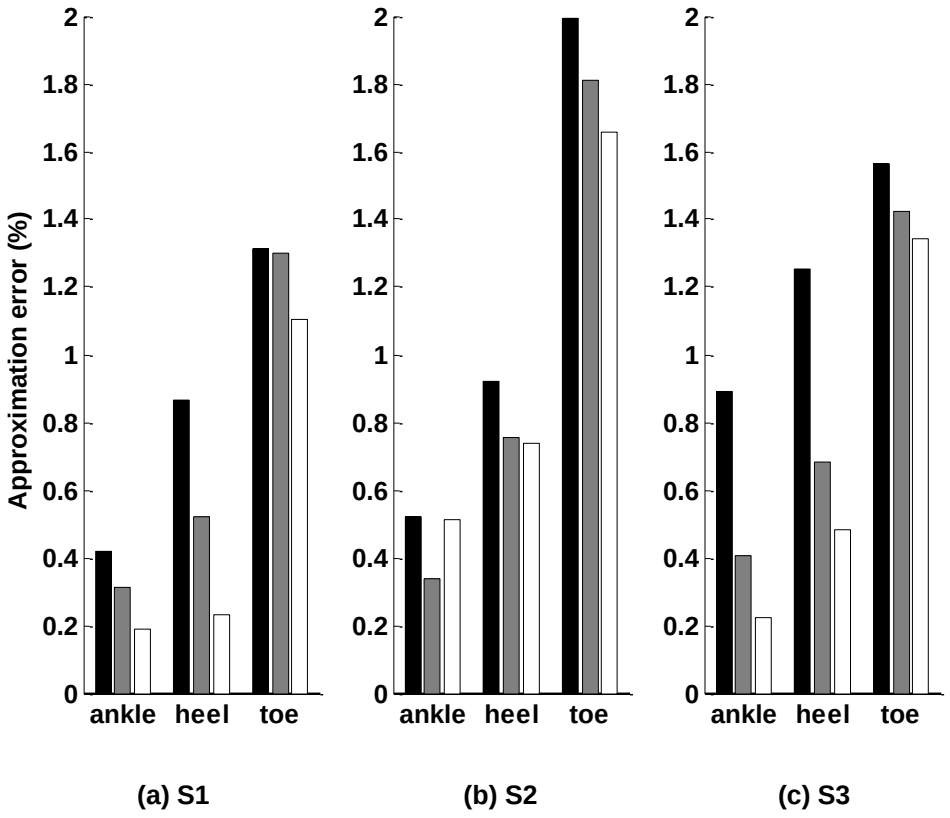

Figure 4.6: Mean errors from the best-fit circle approximation (Method 1) error of three subjects walking at three speeds. Bars in black, grey and white refer to 100%, 75% and 50% of NC, respectively. All errors are normalised to their respective leg length.

Table 4.2: The X coordinates of the circle centres x_c and radii r of best-fit circles with respect to the leg length (%) for the ankle, heel and toe trajectories in three subjects walking at various speeds.

Subject	Segment	100% of NC		75% of NC		50% of NC	
		x_c	r	x_c	r	x_c	r
S1	Ankle	9.80	97.70	10.16	97.85	10.11	97.96
	Heel	8.90	99.25	9.73	99.76	9.59	99.94
	Toe	9.50	99.17	10.10	99.23	11.90	99.00
S2	Ankle	3.87	98.51	5.26	99.15	4.50	99.20
	Heel	3.35	101.17	5.22	101.94	4.35	101.92
	Toe	5.26	101.87	2.61	102.34	3.86	102.28
S3	Ankle	5.82	96.68	5.64	96.81	8.05	98.13
	Heel	4.86	99.68	5.08	99.82	8.03	99.03
	Toe	5.89	100.33	4.16	100.88	5.16	100.55
Mean		6.36	99.37	6.44	99.75	7.28	99.78

4.1.4. Discussion

Locomotion can be described by pendulum models [247, 248]. This study defined the optimal geometry of a pendulum (best-fit circle) which described overground walking by systematically varying the location of its centre and tip. The location of the pendulum centre varied around the hip, while the tip of the pendulum was defined at three different locations on the foot: the ankle, the heel and the toe. Introducing the hip as the reference point was an intuitive choice, but neither of the anatomical points chosen as the tip ideally aligned in the vertical direction with the location of the hip. Therefore the methods which allowed a small variation of the centre of the pendulum

around the hip (Methods 1, 2 and 4) outperformed the method which assumed a fixed circle centre at the hip (Method 3).

It is interesting to note that Method 2 yields that the foot trajectories can be fit by circles with radii much larger (the toe trajectory in Figure 4.2(c)) or much smaller (the ankle and heel trajectories in Figures 4.2 (a) and (b)) than the segment length from the hip. These results are in accordance with previous studies in which the inverted pendulum model has a length longer than the leg in study [256], or a much shorter length in study [257]. The differences in the pendula dimensions resulted from different foci of these studies: study [256] investigated the vertical excursion of the trunk, while study [257] developed a model based on the trajectory of the centre of pressure. The current study focused on the segment trajectories and determined the optimal configuration of the pendula to approximate different segments walking at various speeds. The best-fit circles were found centred close to the hip joint with radii almost equal to the leg length.

All four methods approximated the foot trajectories fairly well. This provided the basis for the simple definition of a pendulum with its centre at the hip and radius equal to the leg length. However, Method 1, which allows horizontal adjustment of the circle centre, obtained the best-circle approximation with the smallest error. The basis for Method 1 is the observation that the lengths of the foot trajectories (step lengths) are not equally divided by the line *L*, which goes vertically from the hip (x_c = 0, y_c = 0) to the ground, but is rather horizontally displaced (see Figures 4.2-4.4). The ankle trajectory has the smallest difference from its best-fit circle, compared to the heel and the toe. This is probably because the only joint between the ankle and the hip (the knee) is almost in constant extension during the stance phase (especially during slow

walking), making the thigh and the shank behave as a bar with a fixed length, while the heel and the toe involves more joints (such as the ankle and subtalar joints) which are rotating slightly during the stance phase. It should be noted that the knee flexion was not ignored during analysis of the foot trajectory. The foot trajectories were experimentally recorded when subjects walked overground with their natural walking patterns, i.e. they could flex their knee joint as much as they normally do. The ankle trajectory during the stance phase relative to the hip joint was found to be well-fit by a circle. This means that the knee joint during this phase was only slightly flexed and could be neglected. This observation was further confirmed by the knee angle during overground walking, which was slightly flexed at normal speed (the middle plot in Fig. 3.4) and hardly flexed at slow speed (the middle plot in Figs. 3.5-3.6).

A novel result of the study was the demonstration that the toe trajectory could be approximated by a circle in both the stance and swing phases. Previous studies commonly assumed that the foot could be approximated with one rigid segment [249, 258] with a semicircle shape [259, 260], and employed the pendulum model for the stance phase only. This study provides the basis for modelling the toe motion within a whole gait cycle using a rigid pendulum. This novel observation could potentially provide a new design approach for gait robots such as the GOER system.

While the exact radius of the optimal circle of the foot obtained in our study might vary among individuals, the conclusion of circle-fit approximation was general, as it depended on typical trajectories of the ankle, heel and toe. The current study also supported the pendulum model concept and foot rocker model at variable speeds, showing that variations in the pendulum model according to the speed change were negligible (error less than 0.2% of the leg length).

A limitation of this study is that only three points on the foot (the ankle, heel and toe) were investigated as the potential tips of the pendulum. There might be certain other points in the foot segment moving in circular paths. It should be noted that the toe trajectory in this study referred to the second metatarsal head. Trajectories of other positions, such as phalanges on the foot, require further investigation. A further limitation of the study is the small number of subjects. The configuration of the best-fit circles might be related to leg length. Although the limited data makes it difficult to generalize the results, all the major observations, such as (i) the circular trajectories of the ankle and the heel during the stance phase, and (ii) the circular trajectory of the toe during the whole gait phase, are consequences of the inherent kinematics of human walking and should be broadly applicable.

4.1.5. Conclusions

This study presented a least squares approximation algorithm for analysis of foot trajectories in normal gait with respect to three different segments: the ankle, heel and toe. It showed that different segments of the foot described different trajectories. This resulted in different configurations of pendula used to describe walking in the stance phase or during the whole gait cycle. Further understanding of the trajectories of different segments of the foot during normal walking might be useful in the design of the GOER system and other foot/lower limb orthoses.

4.2. Kinematic Modelling of the GOER System

Summary: Rehabilitation of walking is an essential element in the treatment of patients with incomplete spinal cord injury (iSCI). During the early period after injury, patients

find it challenging to participate in the training of upright walking. Practising stepping movement in a supine position may be easier and may promote effective rehabilitation earlier. The study described in this section investigated and modelled a Gait Orthosis for Early Rehabilitation (GOER) that does not require the patient to be in an upright position. The model comprised a two-bar mechanical system to provide limb kinematics that approximated normal overground walking. The modelling was based on gait analysis performed on able-bodied subjects walking at 100%, 75% and 50% of normal cadence (NC). Simulated angles of the hip, knee and ankle joints showed comparable ranges of motion (ROMs) to experimental walking data measured in able-bodied subjects. The model provided operating parameters for a prospective GOER system that could be used for early rehabilitation of walking. This study was published in the Journal of Engineering in Medicine [2].

4.2.1. Introduction

Damage to or disease of the central nervous system may result in complete or incomplete loss of motor, sensory and autonomic function below the level of the lesion [261]. To promote restoration of walking in patients with motor impairment, the rehabilitation process should be started as early as possible [262]. Effective restoration of gait requires coordinated movement of the legs [263]. However, for various reasons including injury instability, orthostatic hypotension and muscle weakness, many patients require a period of bed immobilization. In order to promote walking for the patients who cannot maintain an upright position, a Gait Orthosis for Early Rehabilitation (GOER) was designed with the following features:

(1) The patient is able to perform stepping in a supine position;

(2) The ankle joint is activated so as to allow coordinated kinematics of the lower limbs;

(3) Different speeds are accommodated to produce different training modalities.

(4) Haptic feedback on the foot sole is provided to mimic the ground reaction forces during the stance phase.

This study developed a model for the potential GOER system which achieved the first three requirements, i.e. simulation of stepping movement of the lower limbs in a supine position. The fourth requirement will be discussed in Section 4.3.

4.2.2. Methods

The gait data collected in the experiment described in Chapter 3 were analysed. Based on overground walking data from three normal subjects, a model of a two-bar mechanism was developed using Matlab/SimMechanics software (the MathWorks, Inc.) to simulate stepping movement of the lower limb in a supine position.

4.2.2.1. Gait analysis

With the recorded data from the gait experiment, the angle trajectories of the hip, knee and ankle joints were obtained and served as the target performance for the GOER system. Hip, knee and ankle joint angles in the sagittal plane were defined as zero at a neutral still standing position with flexion as positive and extension as negative. The angle α between the line connecting the toe and the ankle and the line connecting the toe and the heel was calculated using the data of the heel, toe and ankle. Experimental data over one gait cycle were analysed, and the duration of one gait cycle was normalised to 100%, with heel strike at 0%.

4.2.2.2. Model development

Computer modelling is an important tool for system analysis and an effective starting point for system development, including exoskeleton design as reported in the literature [190, 232]. SimMechanics software is a modelling environment for mechanical design [264]. It represents physical systems with block diagrams which specify body elements and their mass properties in a coordinated system. The SimMechanics library includes blocks for bodies, joints, force elements, sensors and actuators, which allows simulation of rigid multibody physical systems and their movements. Using standard Newtonian dynamics of forces and torques, modelling in SimMechanics is a tool to present kinematics and kinetic performance directly [264].

Human walking can be described using a pendulum model [258] (see Section 4.1), where the toe is considered to have a semi-circular trajectory with the circle radius approximately equal to the leg length (Figure 4.7(a)). Based on the circle-fit approximation of the toe trajectory described in Section 4.1, a model including a two-bar system and the leg, shown in Figure 4.7(b), was developed using SimMechanics, with the model blocks and parameters presented in Appendix 1. Bar 1 is assumed to rotate at its proximal end P_1, with the distal end (P_2) connected to Bar 2. The foot is placed on Bar 2 with the toe (the second metatarsal phalangeal joint) coincident with P_2. The point P_1 is the centre of the semicircle (dash-dot line) used to approximate the toe trajectory.

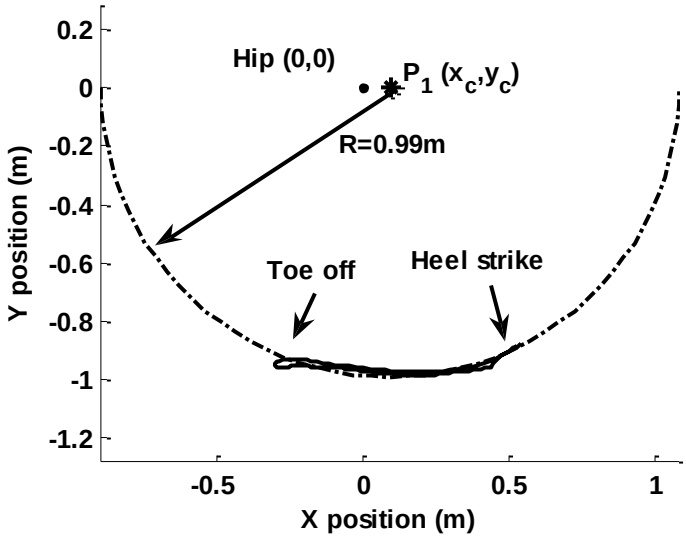

(a) Circle fit approximation of the toe trajectory (in S1 walking at 100% of NC) with the centre at P_1 (x_c,y_c). The hip is at the reference centre (0, 0). The experimental toe trajectory is shown as a solid line and the dash-dot line represents the best-fit semicircle.

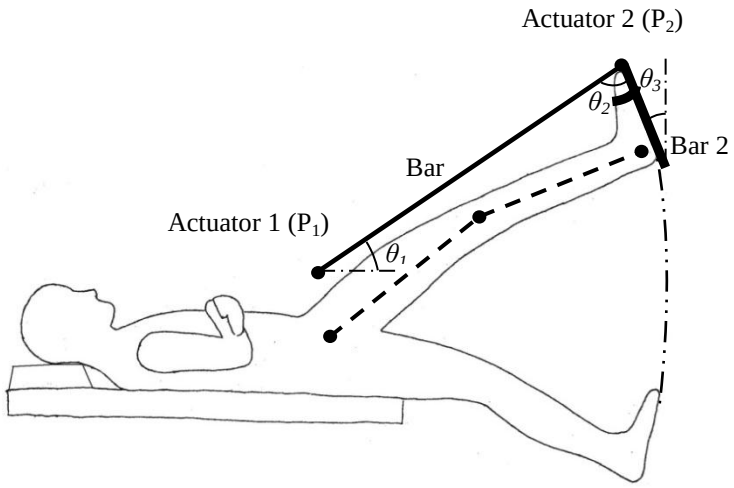

(b) The two thick lines represent Bar 1 and Bar 2. The thin lines represent the thigh and the shank in a supine position. The two bars, thigh, shank and foot are connected through revolute joints, marked with black dots. Actuator 1 is attached to Bar 1 at P_1. Actuator 2 is attached to Bar 2 at P_2. θ_1 and θ_2 are the angles describing the motion of Bar 1 and Bar 2 (θ_2 is the angle between Bar 1 and Bar 2). The dash-double-dot line is the approximated toe trajectory (best-fit semicircle) in Subfigure (a).

Figure 4.7: Development of the two-bar model.

In order to generate the desired toe trajectory, Actuator 1 is mounted on P_1 to control θ_1, the angle between Bar 1 and the horizontal axis. Furthermore, Actuator 2 is attached at P_2 to control foot movement θ_2. The target performance of Actuators 1 and 2 can be obtained from the experimental data of the toe and heel as:

$$\theta_{1j} = \arctan\frac{Y_{Tj} - y_c}{X_{Tj} - x_c}; \quad (j = 1, 2, 3...Q) \tag{4.15}$$

$$\theta_{3j} = \arctan\frac{X_{Hj} - X_{Tj}}{Y_{Tj} - Y_{Hj}}; \left(j = 1, 2, 3...Q\right) \tag{4.16}$$

$$\theta_2 = 90° + \theta_3 - \theta_1 \tag{4.17}$$

where $P_1(x_c, y_c)$ is the centre of the best-fit circle. (X_{Tj}, Y_{Tj}) and (X_{Hj}, Y_{Hj}) are the experimentally obtained toe and heel coordinates within one gait cycle. θ_3 is the angle between the foot sole and the vertical axis, which is obtained from the experimental data. Angles θ_1, θ_2 and θ_3 are defined as zero when they are aligned with the X axis, Bar 1 and the Y axis, respectively. Positive values are defined in an anti-clockwise direction. Combined control of two actuators induces the stance and swing phases with ankle plantarflexion and dorsiflexion, which results in coordinated angle profiles of the lower limb joints. A fixed step solver method ODE3 (Bogacki-Shampine) [265] with a fixed step size of 0.01s was used to simulate the model. The ranges of motion (ROMs) of the hip, knee and ankle joints in the model were constrained within 50^o, 90^o and 50^o, respectively, to prevent excessive flexion or extension [1]. The knee joint angle was constrained as positive to prevent hyperextension.

4.2.2.3. Algorithms for model performance calculation

Once the desired trajectories of Bar 1 and Bar 2 are defined, it is possible to predict the kinematics of the leg driven by the two-bar system. Kinematics of the leg are defined by

trajectories and angles of the hip, knee and ankle joints. The schematic diagram shown in Figure 4.8 is used to demonstrate the calculation algorithm.

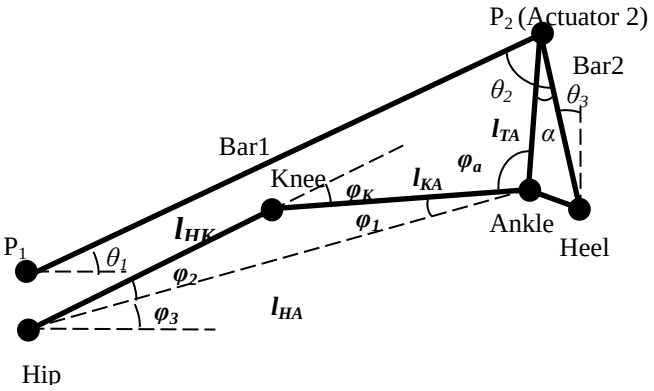

Figure 4.8: Schematic diagram of the model.

The location of the centre P_1 (x_c, y_c) and radius r are obtained using the least squares algorithm described in Section 4.1. Lengths l_{HA}, $l_{HK,}$ $l_{KA,}$ l_{KT} and l_{TA} are the distances between the hip and the ankle, the hip and the knee, the knee and the ankle, the knee and the toe, and the toe and the ankle, respectively. Lengths $l_{HK,}$ l_{KA} and l_{TA} can be measured experimentally. θ_1 and θ_2 are angles of Bar 1 and Bar 2, achieved through Actuator 1 and Actuator 2 in the model, and can be calculated from Equations (4.15)-(4.17). The toe coordinates (x_T, y_T) in the model can be obtained as:

$$x_T = r\cos(\theta_1) + x_c \tag{4.18}$$

$$y_T = r\sin(\theta_1) + y_c. \tag{4.19}$$

The ankle coordinates (x_A, y_A) in the model can be obtained as:

$$x_A = x_T - l_{TA}\sin(\alpha - \theta_3) \tag{4.20}$$

$$y_A = y_T - l_{TA}\cos(\alpha - \theta_3) \tag{4.21}$$

where α is the angle between the line connecting the toe and the ankle and the line connecting the toe and the heel, which is a subject-specific parameter and is calculated from the data collected during quiet standing. With the ankle position determined,

length l_{HA} can be calculated as

$$l_{HA}{}^2 = x_A{}^2 + y_A{}^2. \tag{4.22}$$

The law of cosines in the triangle of the hip, knee and ankle joints yields:

$$l_{HA}{}^2 = l_{HK}{}^2 + l_{KA}{}^2 - 2l_{HK}l_{KA}\cos(\varphi_K) \tag{4.23}$$

$$\varphi_K = \arccos(\frac{l_{HK}{}^2 + l_{KA}{}^2 - l_{HA}{}^2}{2l_{HK}l_{KA}}) \tag{4.24}$$

$$\varphi_1 = \arccos(\frac{l_{HA}{}^2 + l_{KA}{}^2 - l_{HK}{}^2}{2l_{HA}l_{KA}}) \tag{4.25}$$

$$\varphi_2 = \arccos(\frac{l_{HA}{}^2 + l_{HK}{}^2 - l_{KA}{}^2}{2l_{HA}l_{HK}}) \tag{4.26}$$

$$\varphi_3 = \arctan\frac{y_A}{x_A} \tag{4.27}$$

$$\varphi_H = \varphi_2 + \varphi_3 \tag{4.28}$$

where φ_K and φ_H are the knee and hip angles, respectively. φ_1, φ_2 and φ_3 are the related angles in the triangle of the hip, knee and ankle, as shown in Figure 4.8. The knee coordinates (x_K, y_K) in the model can be calculated using Equations (4.29) and (4.30).

$$x_K = l_{HK}\cos(\varphi_2 + \varphi_3) \tag{4.29}$$

$$y_K = l_{HK}\sin(\varphi_2 + \varphi_3) \tag{4.30}$$

In the triangle of the knee, ankle and toe, the law of cosines yields the angle φ_a as

$$\varphi_a = \arccos(\frac{l_{KA}{}^2 + l_{TA}{}^2 - l_{KT}{}^2}{2l_{HA}l_{TA}}) \tag{4.31}$$

with

$$l_{KT}{}^2 = (x_K - x_T)^2 + (y_K - y_T)^2 \tag{4.32}$$

The ankle joint angle φ_A was defined as zero at a neutral still standing position.

Therefore φ_A can be calculated as

$$\varphi_A = \varphi_a - 90^o - \alpha. \tag{4.33}$$

The kinematics of the leg are defined by angle profiles of the hip φ_H (Equation (4.28)), the knee φ_K (Equation (4.24)) and the ankle φ_A (Equation (4.33)).

4.2.2.4. Comparison between experimental and simulated results

Using the experimental data, trajectories of the ankle, knee and hip joints at various speeds were simulated. To compare the simulated and experimental angle profiles of the lower limb joints, their ROM differences and phase shifts were calculated. For the hip joint, the experimental and simulated ROMs are R_{EH} and R_{SH}. The relative differences between the experimental and simulated ROM of the hip joint, R_{errorH}, were obtained as:

$$R_{errorH} = \frac{|R_{SH} - R_{EH}|}{R_{EH}} \times 100\% \tag{4.34}$$

The onsets of maximal hip extension in the experiment and the model within one gait cycle T are T_{EH} and T_{SH} respectively. The phase shift of the simulated and the experimental maximal extension relative to the whole gait cycle T, T_{errorH}, were obtained as:

$$\mathrm{T}_{errorH} = \frac{|T_{SH} - T_{EH}|}{T} \times 100\% \tag{4.35}$$

Similar procedures were adopted to compare the knee and ankle angle profiles from the model and the experiment. In order to obtain the phase shift of the knee joint, the onset of maximal knee flexion was analysed.

4.2.3. Results

Representative angle profiles for Bar 1 and Bar 2 over one gait cycle to achieve stepping at various speeds are shown in Figure 4.9.

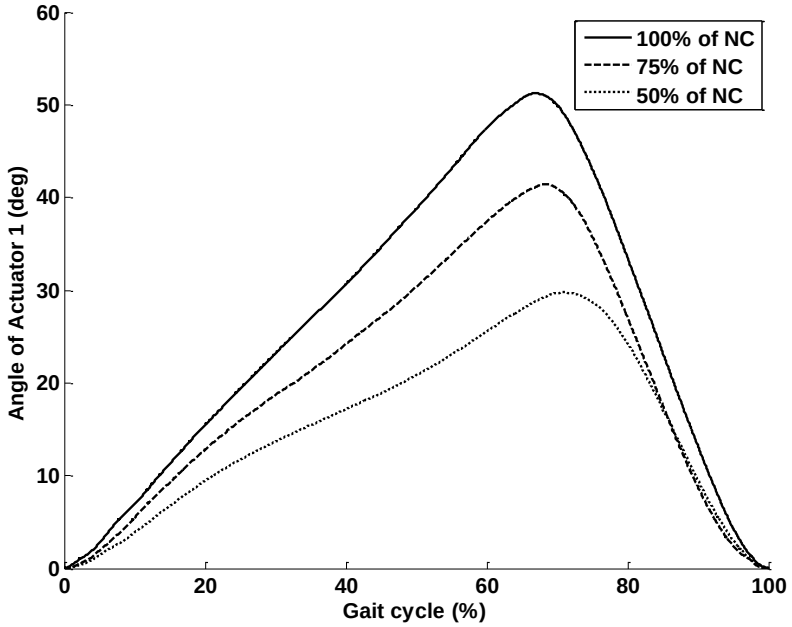

(a) Target angles for Actuator 1.

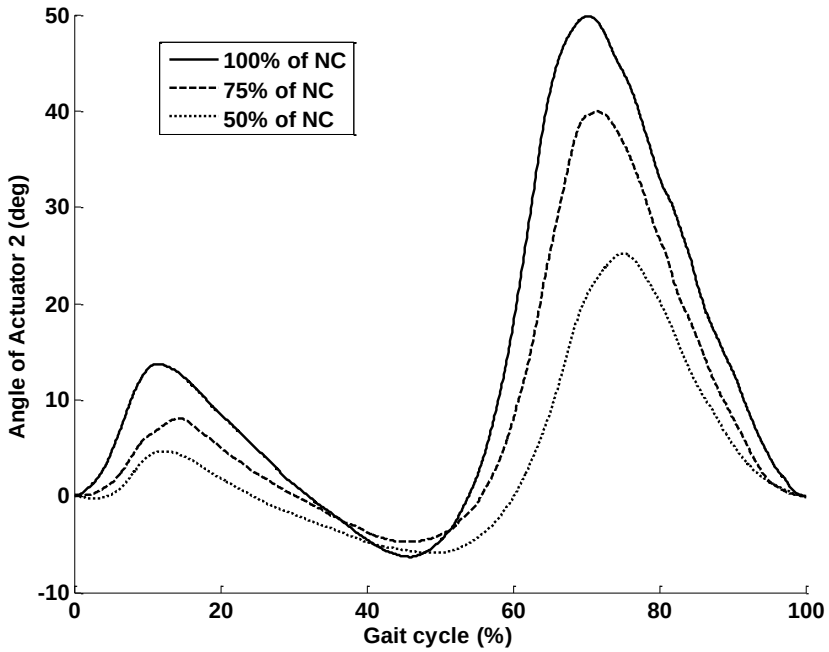

(b) Target angles for Actuator 2.

Figure 4.9: Two actuators profiles to simulate S1 walking at 100%, 75% and 50% of NC.

These are calculated based on walking data of S1 at 100%, 75% and 50% of NC with Equations (4.15)–(4.17). The angle profiles of Bar 1 and Bar 2 for S2 and S3 are similar to those of S1 shown in Figure 4.9, but the ROMs vary by 1-3^{o} to achieve different step lengths.

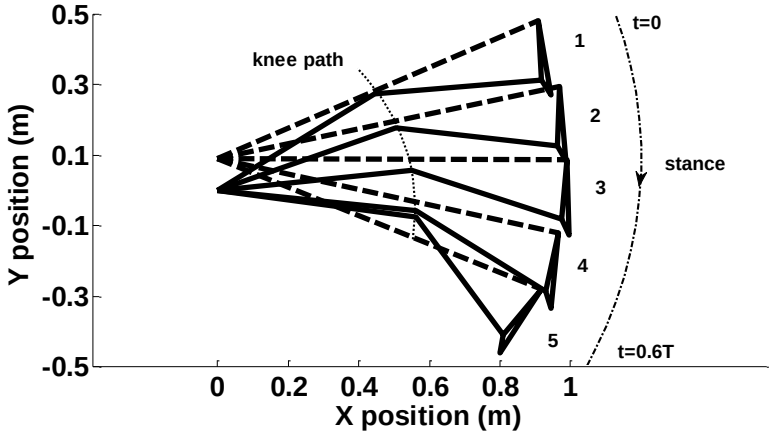

(a) The stance phase (60% of T). Bar 1 moves the leg in a clockwise direction from position 1 (heel strike) to position 5 (toe off).

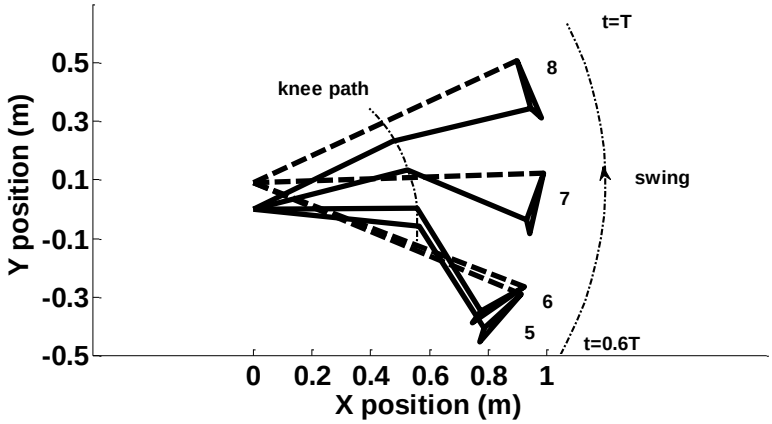

(b) The swing phase (40% of T). Bar 1 moves the leg in an anti-clockwise direction from position 5 (toe off) to position 8.

Figure 4.10: A sequence of eight positions over one gait cycle, showing every 12.5% of the gait cycle. The leg is shown as solid lines while dashed lines represent Bar 1. Bar 2 coincides with the foot sole. T is the duration of the whole gait cycle.

Figure 4.10 shows a sequence of leg positions over one gait cycle, simulating S1 stepping at 100% of NC. Note that unlike overground walking where the hip moves forwards, supine stepping has the hip fixed and the toe moving in the same semi-circular trajectory during the stance and the swing phases. The simulated angle profiles of the hip, knee and ankle joints can be obtained using Equations (4.18)-(4.33).

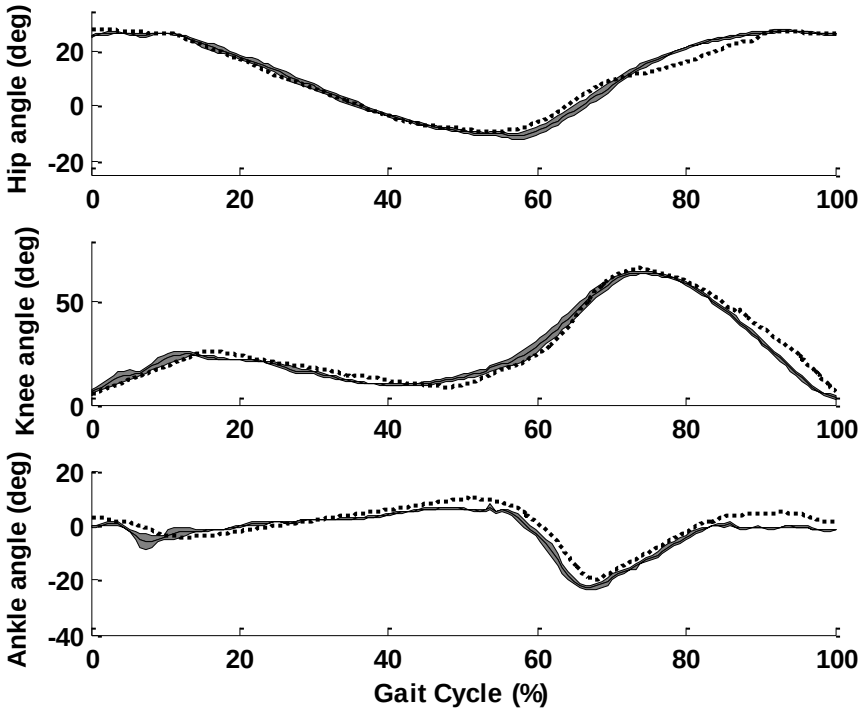

(a) 100% of NC.

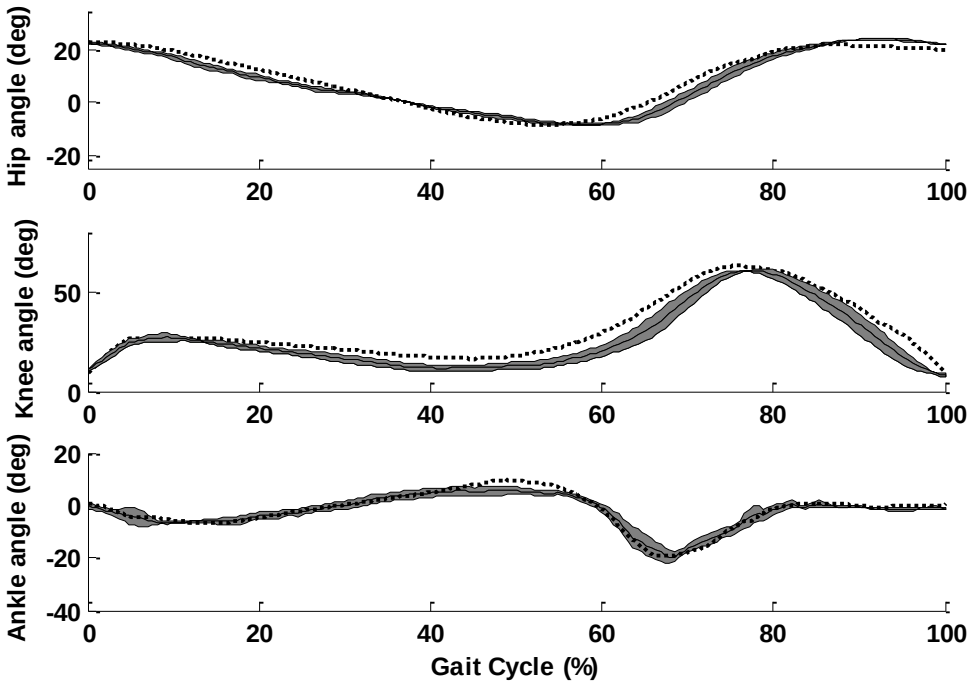

(b) 75% of NC.

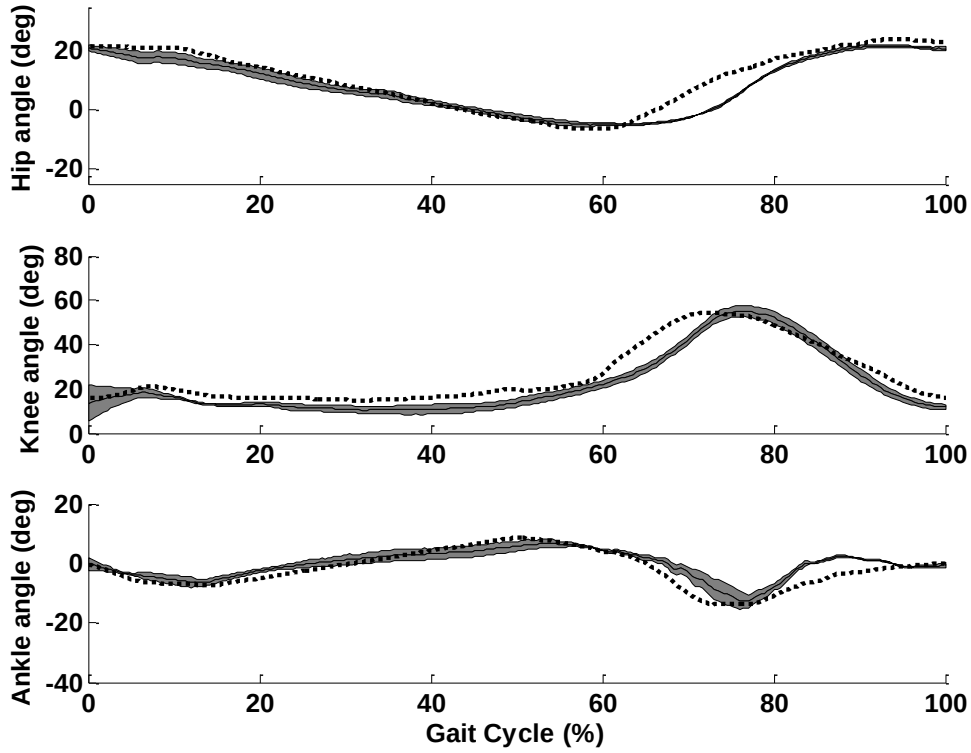

(c) 50% of NC.

Figure 4.11: Kinematics in S1 walking at different speeds. Dashed lines represent the simulated angles while solid lines with shaded areas represent experimental mean angles ±SD.

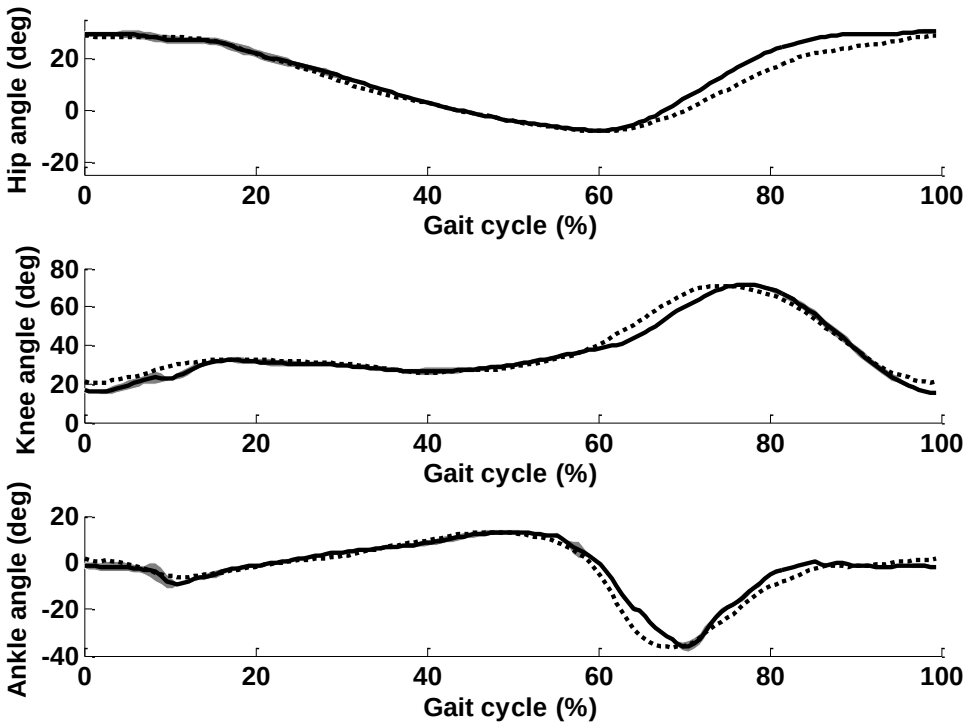

(a) 100% of NC.

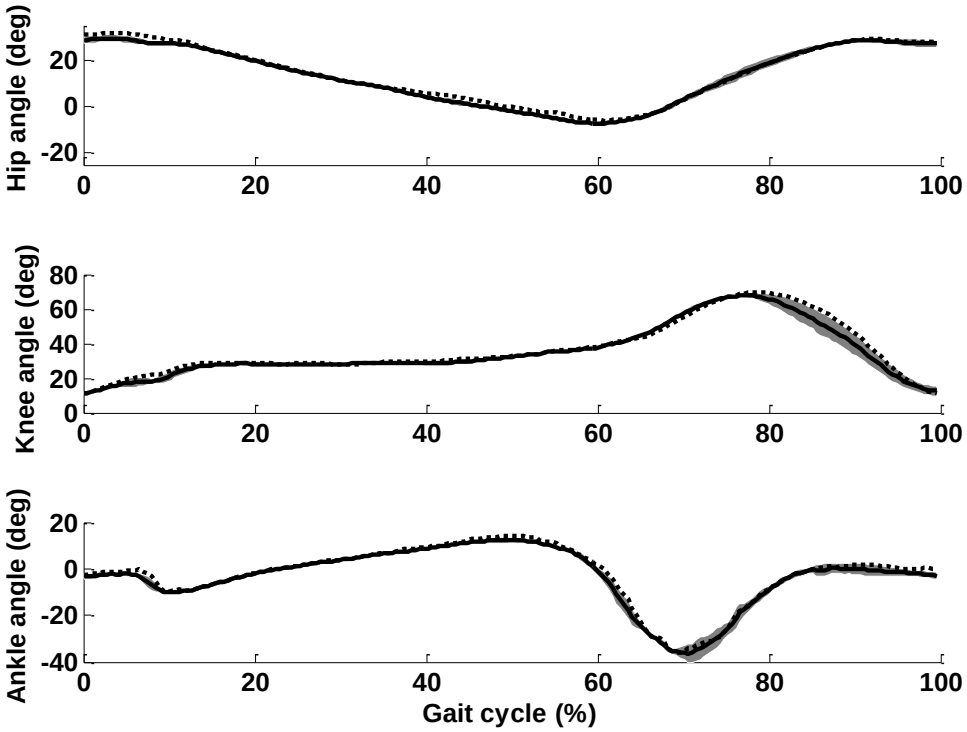

(b) 75% of NC.

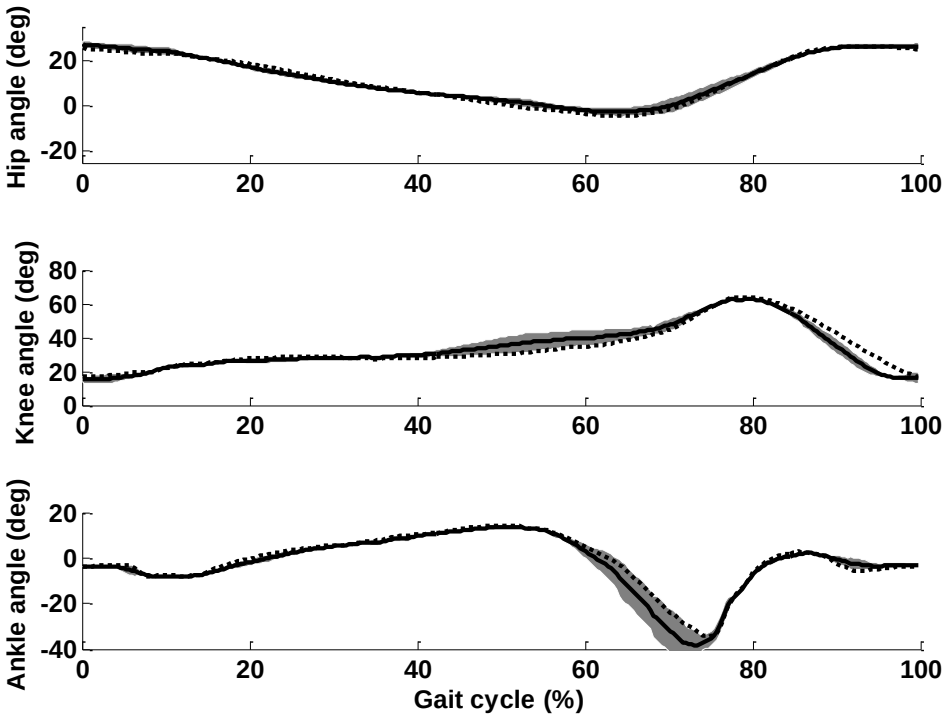

(c) 50% of NC.

Figure 4.12: Kinematics in S2 walking at different speeds. Dashed lines represent the simulated angles while solid lines with shaded areas represent experimental mean angles ±SD.

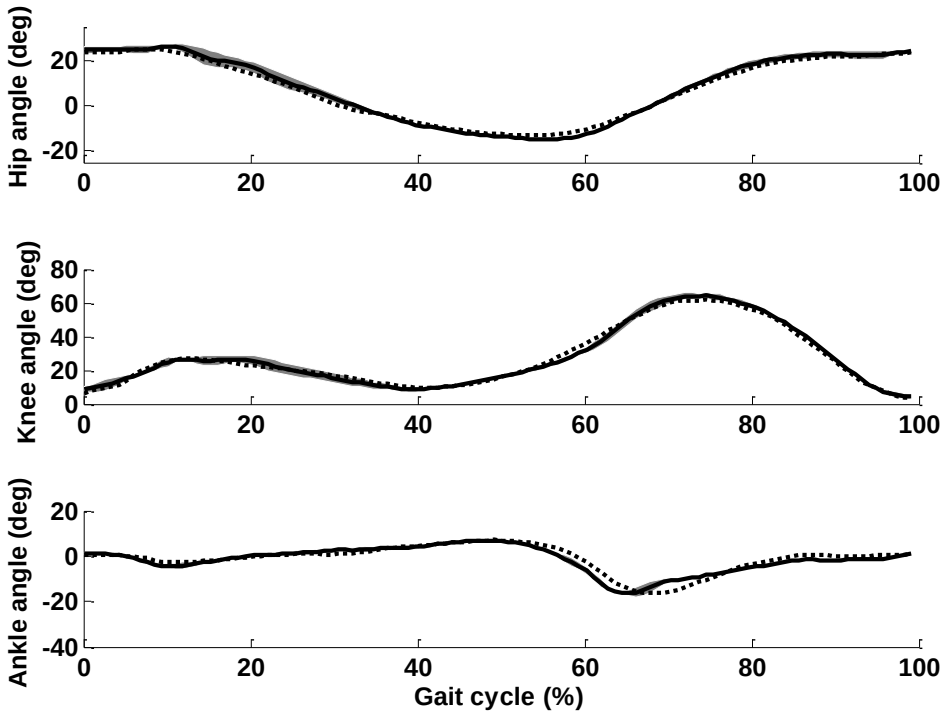

(a) 100% of NC.

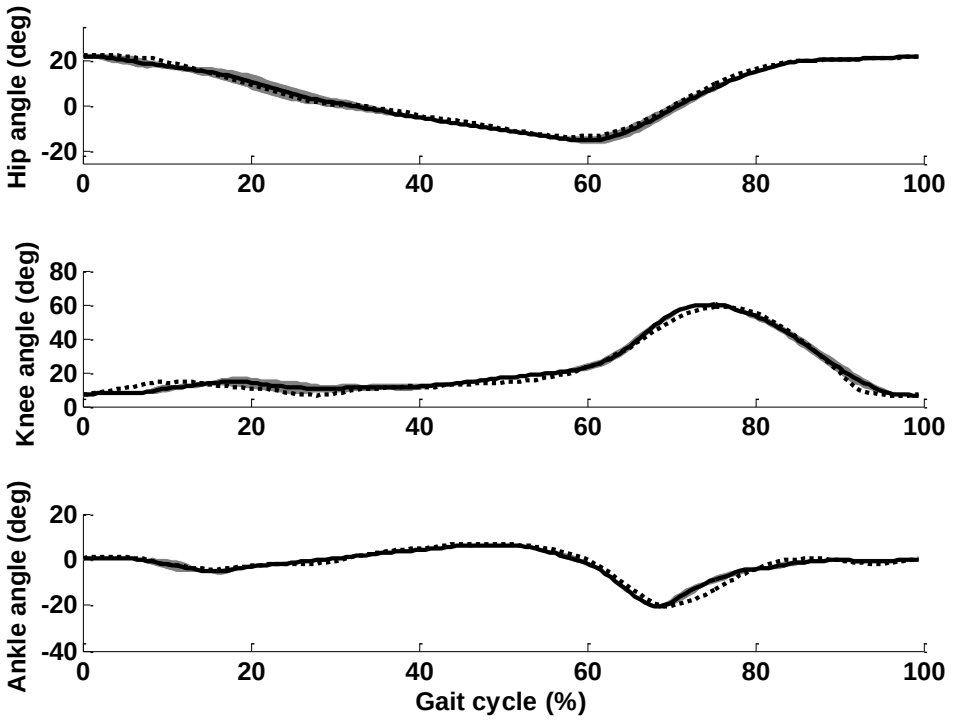

(b) 75% of NC.

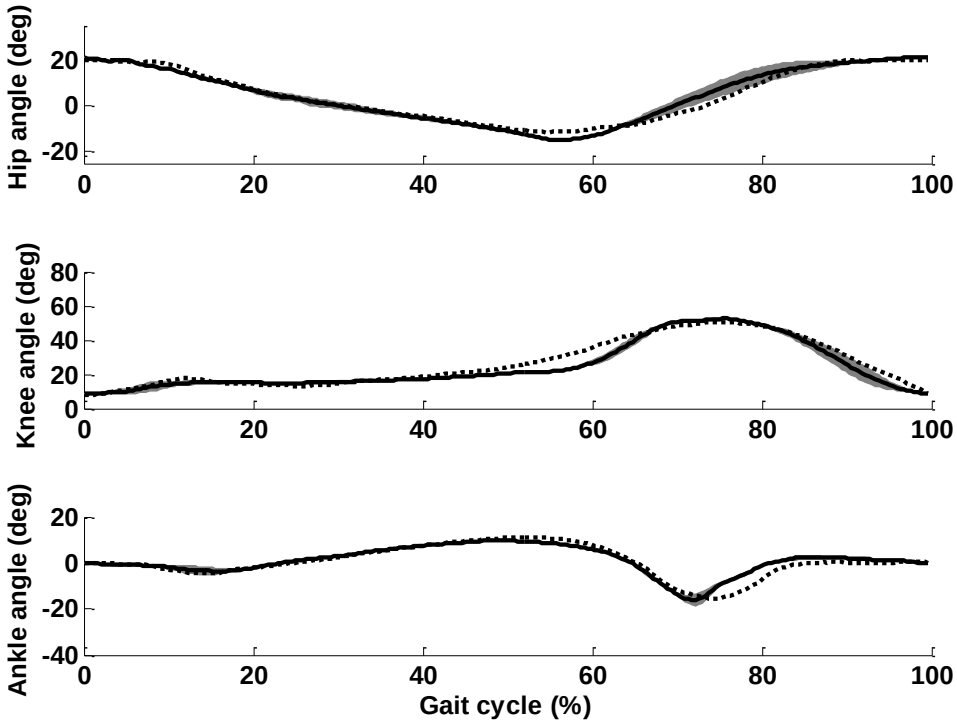

(c) 50% of NC.

Figure 4.13: Kinematics in S3 walking at different speeds. Dashed lines represent the simulated angles while solid lines with shaded areas represent experimental mean angles ±SD.

Table 4.3: The difference (Mean±SD) of the phase shift (%) and ROM error (%) between the model and experimental data of all three subjects.

		100% of NC		75% of NC		50% of NC	
		Phase shift (T_{error})	ROM deviation (R_{error})	Phase shift (T_{error})	ROM deviation (R_{error})	Phase shift (T_{error})	ROM deviation (R_{error})
S1	Hip	4.3±0.4	2.3±1.2	5.2±1.4	3.5±1.6	10. 6±0.9	7.7±2.5
	Knee	2.5±1.1	3.7±1.3	1.7±0.7	3.6±1.9	6.7±0.6	6.2±3.9
	Ankle	4.0±0.8	4.5±2.1	2.6±0.4	10.6±5.9	5.6±1.4	8.4±3.5
S2	Hip	2.0±1.3	3.6±1.9	3.4±1.2	4.3±1.7	3.6±0.9	20.3±3.3
	Knee	5.0±0.3	7.1±1.3	7.6±0.5	1.2±0.6	2.9±1.4	2.6±1.1
	Ankle	6.9±0.1	9.6±3.9	2.9±0.4	2.9±2.1	7.9±1.8	6.15±3.9
S3	Hip	4.4±0.6	5.3±2.3	3.2±0.7	5.9±1.5	9.5±1.1	7.8±3.5
	Knee	6.7±0.9	1.2±0.4	1.7±0.5	1.4±0.8	8.0±0.4	5.1±1.2
	Ankle	8.2±0.2	13.6±3.3	8.5±0.8	4.1±2.3	9.6±1.2	3.7±2.1

Figure 4.11 shows the experimental and simulated angle profiles of S1, walking at 100% of NC (Figure 4.11(a)), 75% of NC (Figure 4.11(b)) and 50% of NC (Figure 4.11(c)). It can be seen that the experimental variability, shown as shaded areas in Figure 4.11, increases with reduction in walking speed. Likewise the deviation between the experimental and modelling data increases with reduction in speed (e.g. the angles of the hip and knee joint), probably due to increased intra-subject experimental variability in these gait parameters. Results from the other two subjects, S2 and S3, stepping at various speeds are shown in Figures 4.12-4.13. Individualized simulated angle profiles for all three subjects closely match the experimental results. The mean values of phase shift and ROM deviation between the simulated and experimental results for all three subjects at the three speeds are summarized in Table 4.3.

4.2.4. Discussion

Dynamic modelling is widely adopted to test the function of gait training devices [190, 232]. However, modelling studies rarely take into account analysis of movement of the foot and the ankle joint. In the current study, simulated and experimental results with detailed analysis of foot trajectories were presented. This study described model development and validation based on experimental data obtained from overground walking. The model successfully simulated supine stepping at three different speeds in three able-bodied subjects.

Based on the approximation of the toe trajectory with a semicircle, a two-bar model was developed and validated by simulation of the angle profiles of the hip, knee and ankle joints, which closely followed the experimental results. The desired toe trajectory is achieved with Actuator 1, placed close to the hip. Actuator 2, located at the toe, moves the foot to simulate the ankle trajectory. The simulated movement of the lower limb is in phase with and have a comparable ROM to the experimental performance at three different speeds, with the best simulation achieved at normal cadence. The joint angles from the model are very close to the experimental results, especially in the stance phase. Some differences can be seen in the swing phase, for example, in the hip joint. This is because the model simulated all human joints as one-dimensional in the sagittal plane, while human walking actually involves three-dimensional joint rotations, especially in the hip. The lack of abduction/adduction simulation in the model induced a minor discrepancy in the joint angles of the model and the experimental results. The simulated joint kinematics at different speeds (Table 4.3) show that there is a small phase variation with variation of speed. Similarly, when the speed reduces, the difference between experimental and simulated ROM increases. This is to be expected because the

kinematic variability during real walking increases with reduction in walking speed [258].

It is believed that repetitive training of coordinated movements of the lower limbs improves neurological recovery following spinal cord injury [66]. Although repeatable movements are essential for recovery, a small degree of kinematic variability might be necessary to prevent training habituation to a fixed pattern of locomotor [211, 266]. In the current study the adaptable kinematics of the lower limbs at variable speeds were achieved through modification of the actuators' parameters. The model provided the control parameters of the actuators necessary to achieve the target profiles of the two-bar linkage system.

The model was validated using data from three subjects. In order to obtain better validity of the model, data from a larger number of subjects is needed. Nevertheless, based on the similarity of simulated results from these subjects, it is expected that the modelled two-bar system would successfully simulate walking of a variety of subjects with different step lengths and walking speeds.

The main scope of this study was kinematic modelling of walking. There were, however, several important issues to be considered to gain a complete picture of robot-assisted walking in a supine position. Coordinated motion of the hip, knee and ankle modelled in this study is only one prerequisite for successful rehabilitation of walking. Another important element is to include simulation of the ground reaction forces during the stance phase [261], which will be investigated in the following section.

Although the motivation for this study came from spinal cord injury, it is believed that the modelled device would be applicable to the other group of patients with injuries to the central nervous system. This modelling study is an important first step towards design of the GOER system, demonstrating technical feasibility of a two-bar mechanism to provide natural walking patterns in a supine position.

4.2.5. Conclusions

A model incorporating a two-bar system which had the capability to simulate stepping with variable kinematics was developed. The model was validated using experimental overground gait data. Simulated results were in good agreement with experimental data for normal and slower walking speeds. The model provided a useful testbed for the conceptual design of the GOER system, which could be used for early neurological recovery of walking, in patients who are still restricted to a supine position.

4.3. Kinetic Analysis of Stepping in a Supine Position

Summary: In order to promote walking in patients who cannot maintain an upright position in the early post-injury phase, a Gait Orthosis for Early Rehabilitation (GOER) was designed to provide stepping training in a lying position. The computer model study described in this section focused on kinetic analysis of supine stepping. A model of leg linkage in an upright position was developed and was validated by simulating dynamic walking which was similar to experimental overground walking. The model was then rotated by 90^{o} to simulate stepping movements in a supine position, which was a useful testbed to investigate the dynamic performance of the GOER system.

4.3.1. Introduction

In our previous study described in Section 4.2 [2], a computer model of a Gait Orthosis for Early Rehabilitation (GOER) was developed. The kinematics of the lower limb were in phase with overground walking, i.e. sharing a similar time for joint flexion or extension. The simulated range of motion (ROM) were similar to normal walking [2]. However, study of locomotion involves not only moving trajectories, but also the dynamic mechanics of progression [267]. As kinetic analysis reveals the cause of the movement, joint kinetics are fundamental for understanding motor patterns of walking. The complex interaction of the leg segments, revealed by the moment of force at each joint, becomes an important issue for investigation.

Dynamic analysis on the motion of the lower limb during supine stepping will be useful for the design process of the GOER system. This study developed computer models to simulate joint dynamics during overground walking and supine stepping, providing an insight into the dynamics of supine stepping in the GOER system.

4.3.2. Methods

A gait experiment was carried out on three able-bodied subjects walking overground at variable speeds as described in Chapter 3. The classical techniques of motion capture and force plate measurement were employed to record dynamic performance: detailed information can be found in Chapter 3. A leg linkage model was developed to simulate upright walking. After the model was validated using experimental walking data, the same model was rotated by 90^{o} to investigate the dynamics of supine stepping.

4.3.2.1. Model development

The human leg can be represented as a linkage system [258]. The leg linkage shown in Figure 4.14 was developed using the SimMechanics toolbox in Matlab (the MathWorks, Inc.), with the actual model shown in Appendix 2.

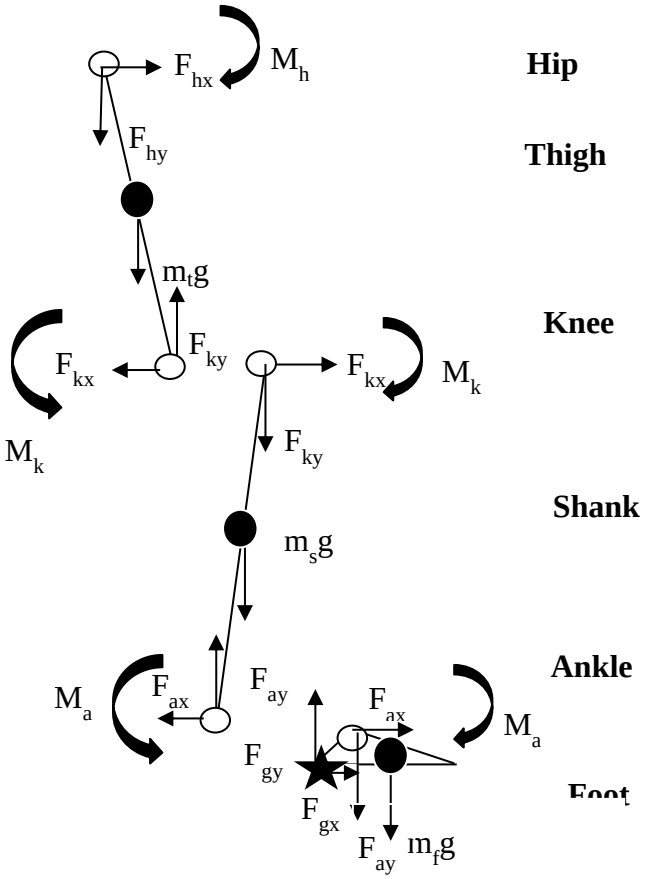

Figure 4.14: Free body diagram of the leg segments in an upright position.

The segments of the thigh, shank and foot are connected through revolute joints, with the centres of mass marked as black dots. Anthropometric data, such as the centre of mass and length of each segment can be found in Table 3.3. In order to simulate human locomotion, three actuators were implemented at the hip, knee and ankle joints. The target angles for these joints were calculated based on experimental data (see

Figures 3.3-3.5). In order to analyse the dynamics of stepping in a supine position, the model was rotated by 90^o as displayed in Figure 4.15, with gravity acting downwards. A fixed step solver method ODE3 (Bogacki-Shampine) [265] with a fixed step size of 0.01s was used to simulate upright walking and supine stepping.

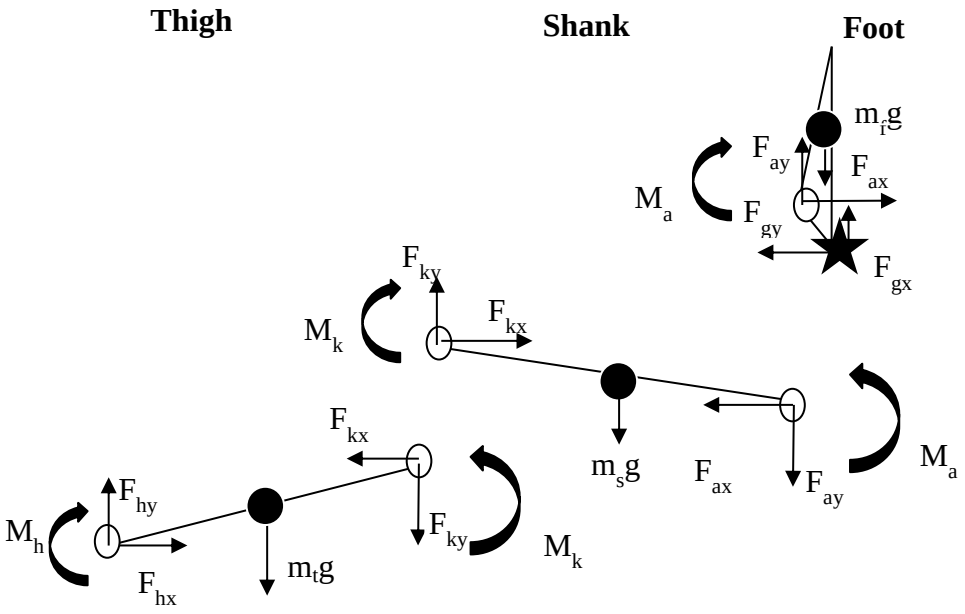

Figure 4.15: Free body diagram of the leg segments in a supine position.

4.3.2.2. Moment calculation algorithm

Using the data collected in Chapter 3, the joint moments at the hip, knee and ankle during upright overground walking can be calculated by the inverse dynamics approach [1]. The gait data were visually observed to remove outliers, and were then smoothed with the loess or rloess Matlab functions. This section presents algorithms to calculate moments of force at the ankle, knee and hip during supine stepping as shown in Figure 4.15. Vertical forces and displacements in the upward direction, horizontal forces and displacements to the forward and moments in the clockwise direction were denoted as positive. Moments were normalised by body mass.

Experimental data over one gait cycle were analysed, and the duration of one gait cycle was normalised to 100%, with heel strike at 0% and 100%.

The mass of the foot is denoted by m_f. The internal forces and moment in the ankle joint with respect to the foot F_{ax}, F_{ay} and M_a were calculated as:

$$F_{ax} - F_{gy} = m_f a_{fx} \tag{4.36}$$

$$F_{ay} + F_{gx} - m_f g = m_f a_{fy} \tag{4.37}$$

$$M_a - F_{gy} L_{cop} + F_{gx} H_m + F_{ax} L_{aop} + F_{ay} H_a = I_f \alpha_f \tag{4.38}$$

where F_{gx} and F_{gy} are the forces applied in the model to simulate the ground reaction forces. The displacement of the ankle from the centre of mass in the horizontal and vertical directions are H_a and L_{aop}, respectively. a_{fx} and a_{fy} are the horizontal and vertical components of the displacement acceleration of the foot. I_f is the moment of inertia of the foot and α_f is its angular acceleration. The displacement of the centre of pressure (marked with a star in Figure 4.15) from the centre of mass in the horizontal and vertical directions are H_m and L_{cop}, respectively. These variables can be determined experimentally or looked up from anthropometric data in Table 3.3. It should be noted that the lever arms in upward and right directions were defined positive. L_{cop} can be calculated using the experimental moment at the ankle joint M_{ae} during stance phase of overground walking. During the stance phase, α_f = 0, the weight of the foot m_f, compared to the ground forces (F_{gx}, F_{gy}), is negligible. M_{ae} during the stance phase can be calculated as [268]:

$$M_{ae} = F_{gy} L_{cop} + F_{gx} H_a'. \tag{4.39}$$

where H_a' is the distance of the ankle joint off the ground. Therefore L_{cop} can be obtained as

$$L_{cop} = \frac{M_{ae} - F_{gx} H_a'}{F_{gy}}. \tag{4.40}$$

The ankle moment during supine stepping M_a can be calculated using Equations (4.36) -(4.40). The internal forces and moment in the knee joint with respect to the shank F_{kx}, F_{ky} and M_k were calculated as:

$$F_{kx} - F_{ax} = m_s a_{sx} \tag{4.41}$$

$$F_{ky} - F_{ay} - m_s g = m_s a_{sy} \tag{4.42}$$

$$M_k - F_{kx} l_s \lambda_s \sin(\theta_k) + F_{ky} l_s \lambda_s \cos(\theta_k) - F_{ax} l_s (1-\lambda_s) \sin(\theta_k) + F_{ay} l_s (1-\lambda_s) \cos(\theta_k) - M_a = I_s \alpha_s \tag{4.43}$$

where a_{sx} and a_{sy} are the horizontal and vertical components of the displacement acceleration of the shank. θ_k is the angle between the shank and the vertical axis, with clockwise as positive. m_s, l_s, α_s and I_s are the mass, length, angular acceleration and moment of inertia of the shank. λ_s is the distance between the centre of mass of the shank and the knee joint divided by the shank length. The internal forces and moment in the hip joint with respect to the thigh F_{hx}, F_{hy} and M_h were calculated as:

$$F_{hx} - F_{kx} = m_t a_{tx} \tag{4.44}$$

$$F_{hy} - F_{ky} - m_t g = m_t a_{ty} \tag{4.45}$$

$$M_h - F_{hx} l_t \lambda_t \sin(\theta_h) + F_{hy} l_t \lambda_t \cos(\theta_h) - F_{kx} l_t (1-\lambda_t) \sin(\theta_h) + F_{ky} l_t (1-\lambda_t) \cos(\theta_h) - M_k = I_t \alpha_t \tag{4.46}$$

where θ_h is the angle between the thigh and the vertical axis, with clockwise as positive. m_t, l_t, α_t and I_t are the mass, length, angular acceleration and moment of inertia of the thigh. λ_t is the distance between the centre of mass of the thigh and the hip joint divided by the thigh length.

Using the experimentally recorded ground reaction forces and proceeding along the lower limb from the ankle to the hip, the leg linkage model shown in Figure 4.15 yielded the moments at the hip, knee and ankle joints during stepping in a supine position. For the sake of safety and in order to avoid eliciting a withdrawal reflex, typically a fraction of force was applied to simulate the ground reaction [261]. Furthermore, it was feasible to apply pressure on the foot sole, while it was impractical to implement friction on the foot physically. Therefore a 30% of upward force was applied on the foot to simulate the kinetics of leg during supine stepping in the GOER system.

4.3.3. Results

Based on the experimentally obtained ground reaction forces and moments at the ankle joint (see Figures 3.6 and 3.9), the COP can be calculated using Equation (4.40). A representative profile of the COP in S1 walking at 100% NC is shown in Figure 4.16. The centre of pressure moves from the heel (0% of the foot length) to the toe (100% of the foot length) during the stance phase. As there is no ground force during the swing phase, the centre of pressure only covers 60% of the gait cycle. The COP profile obtained in this study is similar to the description in the literature [234, 269]. A minor difference can be seen at heel strike (marked with an arrow). This is because of the quick force increase coming from the heel strike loading.

In the simulation of upright walking in S1, the forces, with amplitudes equal to the experimental ground reaction forces (see Figure 3.7(a)), were applied on the foot sole, moving as the experimentally obtained path of the centre of pressure (Figure 4.16). The simulated moments at the hip, knee and ankle joints in S1 walking at 100% of NC are

represented as dashed lines in Figure 4.17(a). The experimental moments are plotted as solid lines for comparison. Similarly the joint moments from the other two subjects can be simulated and presented in Figures 4.17(b) and (c). It can be seen that the simulated moments during upright walking were quite close to the experimental results of overground walking. Minor differences were seen in the stance phase at the knee joint. This might result from approximation error in the centre of pressure and/or the moment of inertia. In spite of these differences, the pattern similarity of the moment profiles at the three joints during upright walking between the model and the experiment satisfactorily validated the model.

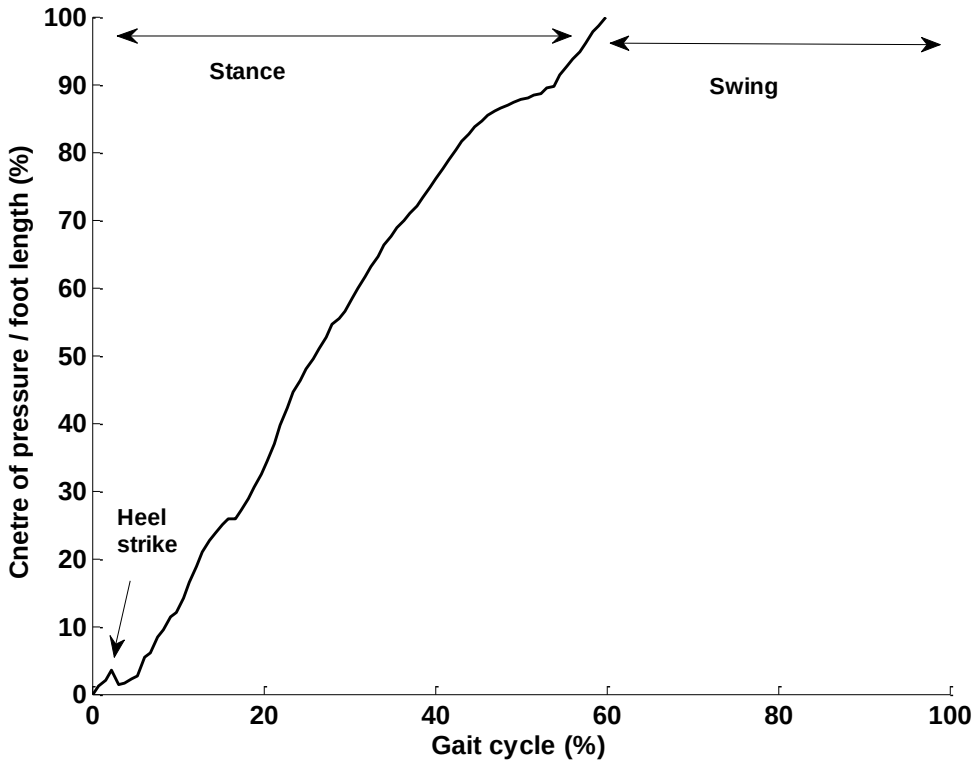

Figure 4.16: Trajectory of the centre of pressure from the heel to the toe in S1 walking at 100% of NC. The foot length of S1 is 0.25 m.

In order to investigate stepping in a supine position, the model was rotated by 90^{o}. The

force induced by gravity was taken to act downwards. The ground reaction forces during overground walking were applied on the foot sole of the supine leg with the same amplitudes, but the upright force was changed into the left direction and the friction was applied vertically. The simulated moments at the ankle, knee and hip joints during supine stepping with full ground reaction forces are shown in Figure 4.17 as dotted lines. The results of 30% of the experimental upward ground reaction force applying on the foot are presented in Figure 4.17 as dash-dot lines. Using similar methods, the joint moments in the three subjects stepping at 75% and 50% of NC were calculated and presented in Figures 4.18-4.19.

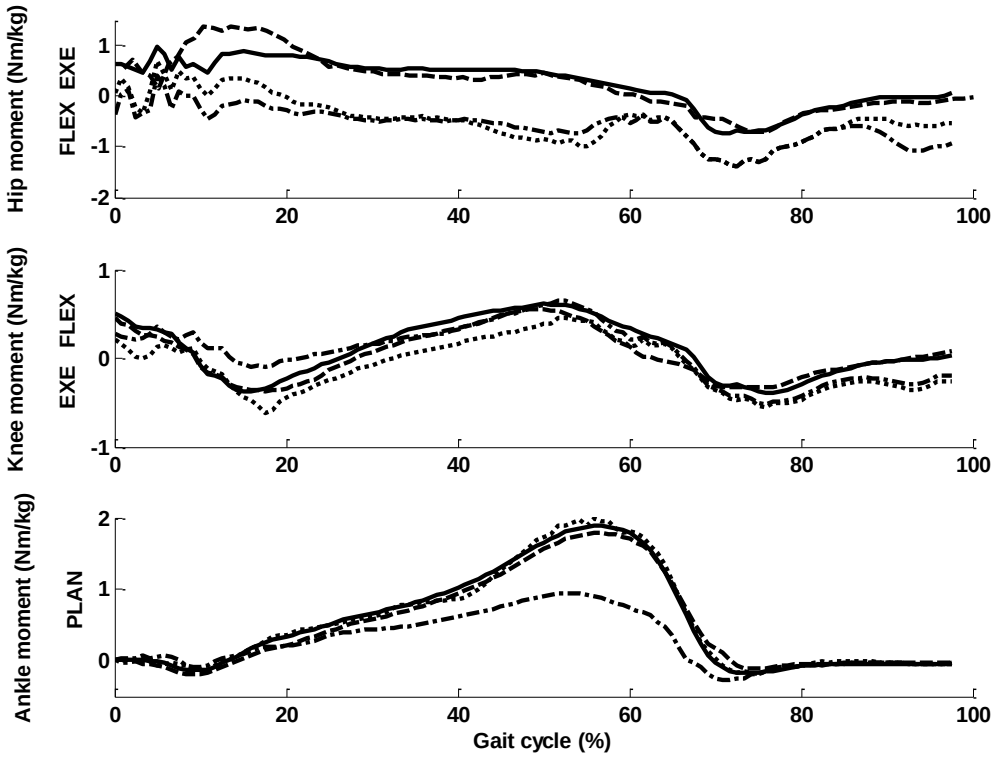

(a) S1.

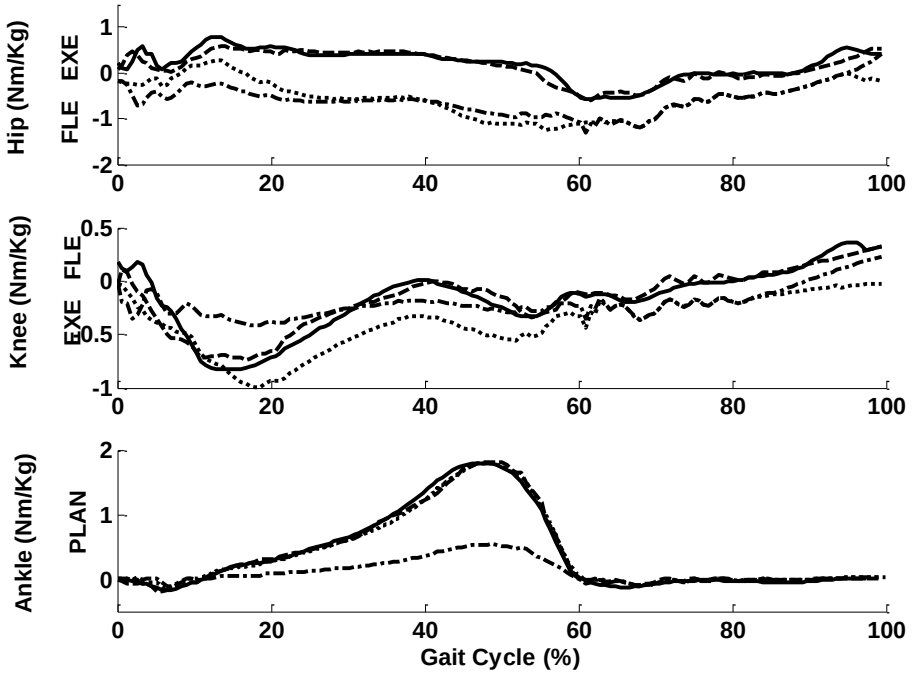

(b) S2.

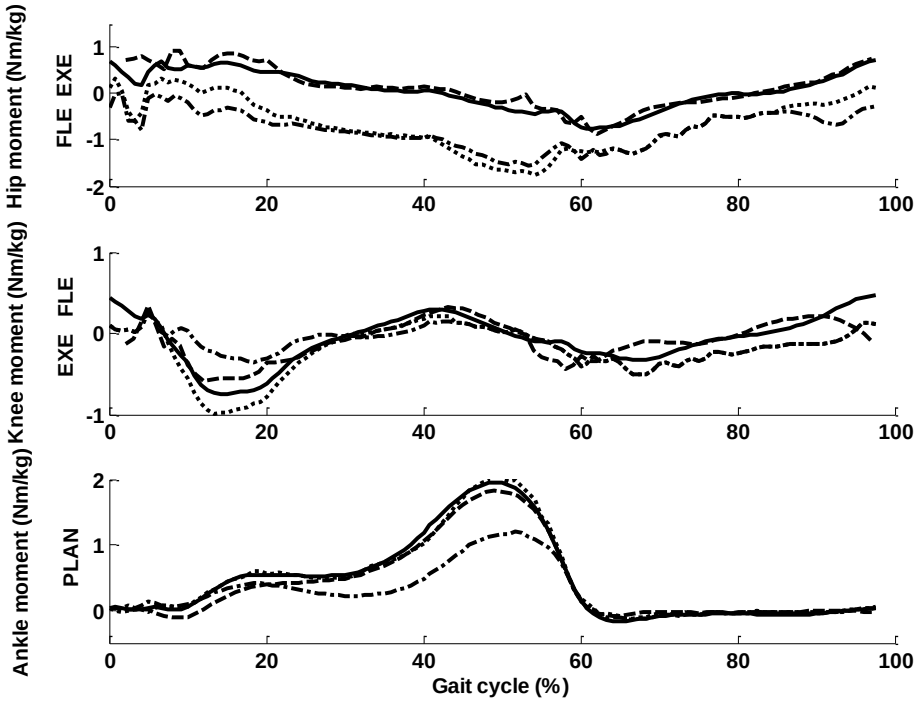

(c) S3.

Figure 4.17: Internal joint moments in three subjects walking at 100% of NC: solid, dashed, dotted and dash-dot lines are respectively the moments during experimental overground walking, simulated upright walking, simulated supine stepping with full ground forces and simulated supine stepping with 30% of upward ground force.

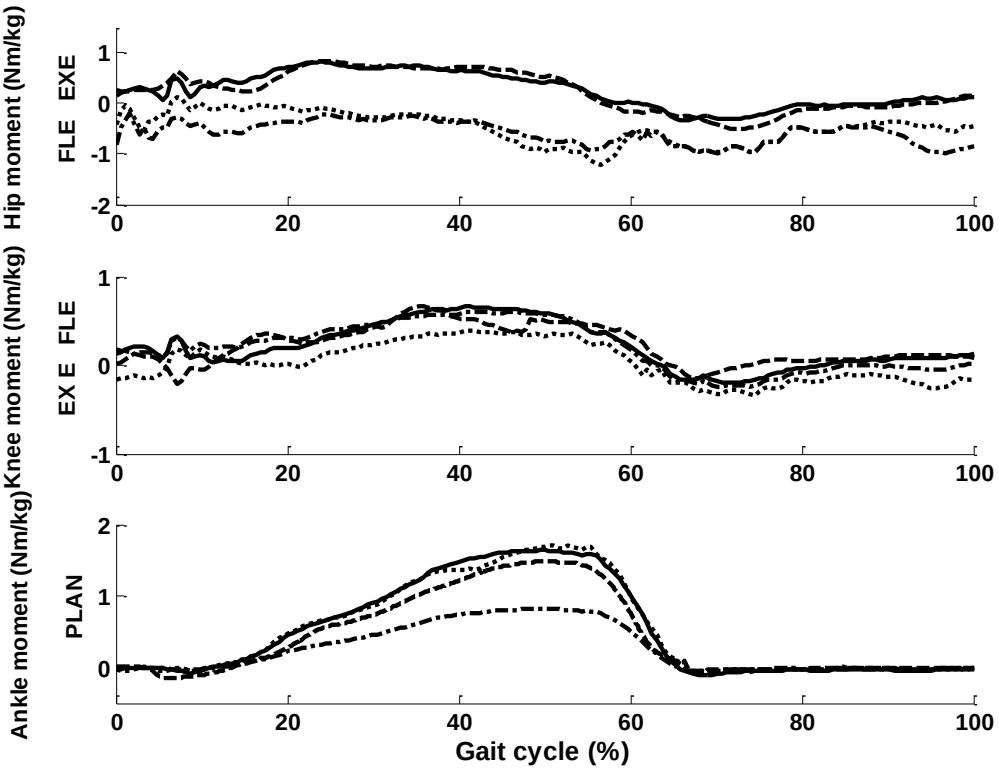
Hip moment (Nm/kg)
FLE EXE
Knee moment (Nm/kg)
EX E FLE
Ankle moment (Nm/kg)
PLAN
Gait cycle (%)

(a) S1.

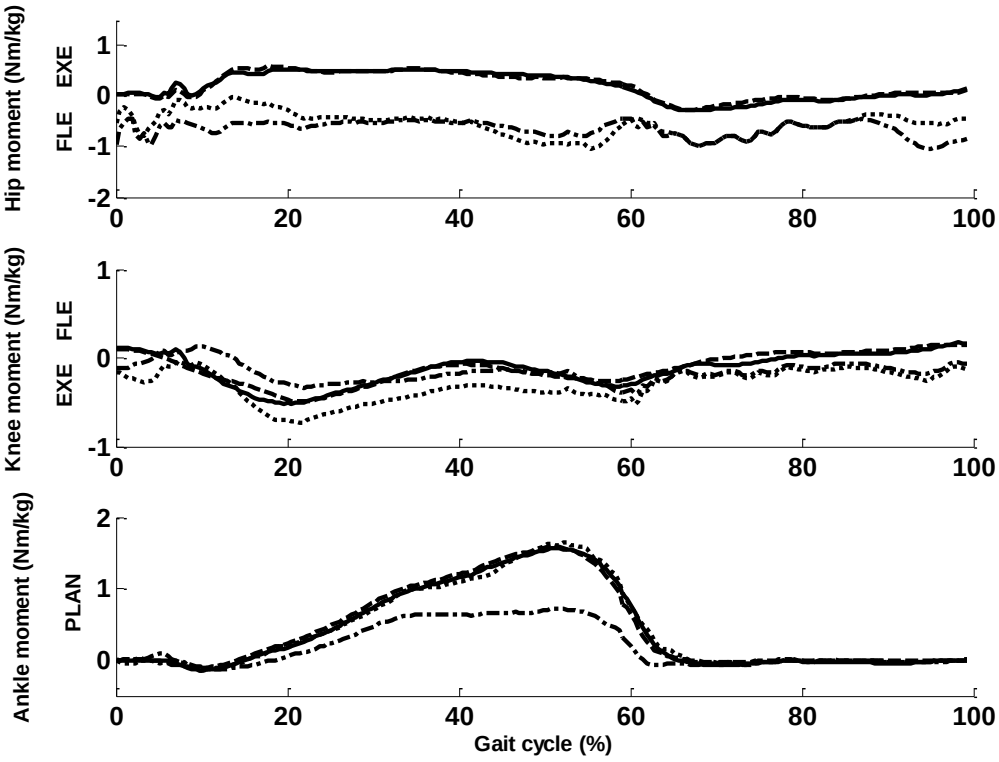
Hip moment (Nm/kg)
FLE EXE
Knee moment (Nm/kg)
EXE FLE
Ankle moment (Nm/kg)
PLAN
Gait cycle (%)

(b) S2.

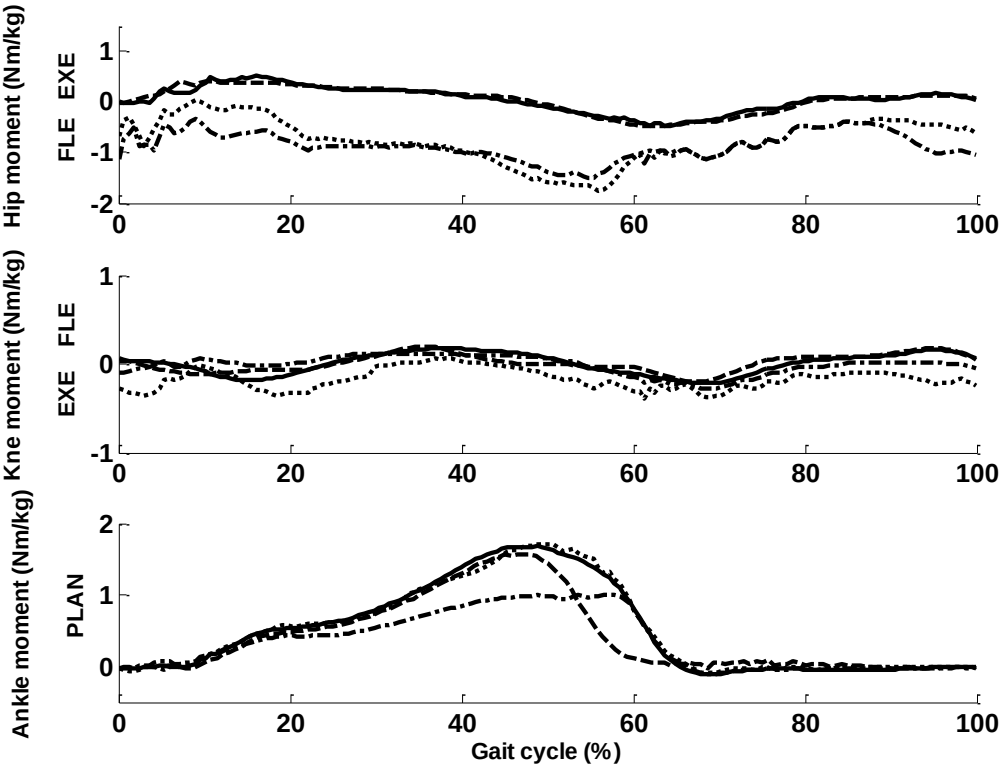

(c) S3.

Figure 4.18: Internal joint moments in three subjects walking at 75% of NC: solid, dashed, dotted and dash-dot lines are respectively the moments during experimental overground walking, simulated upright walking, simulated supine stepping with full ground forces and simulated supine stepping with 30% of upward ground force.

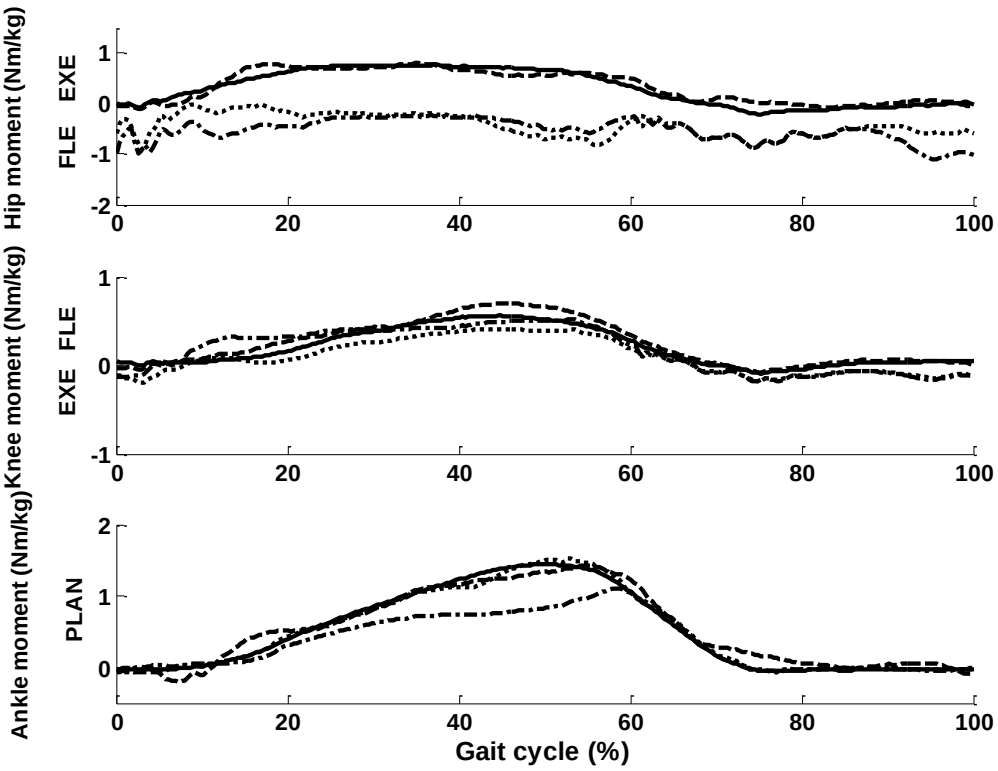
Hip moment (Nm/kg)
FLE EXE
Knee moment (Nm/kg)
EXE FLE
Ankle moment (Nm/kg)
PLAN
Gait cycle (%)

(a) S1.

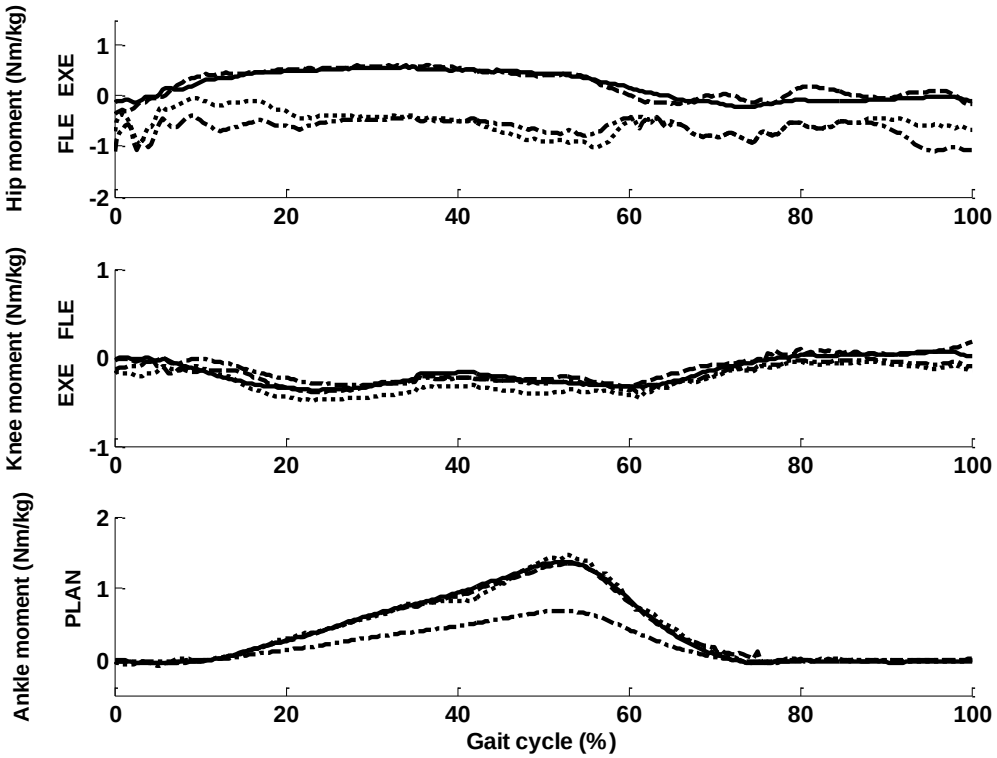
Hip moment (Nm/kg)
FLE EXE
Knee moment (Nm/kg)
EXE FLE
Ankle moment (Nm/kg)
PLAN
Gait cycle (%)

(b) S2.

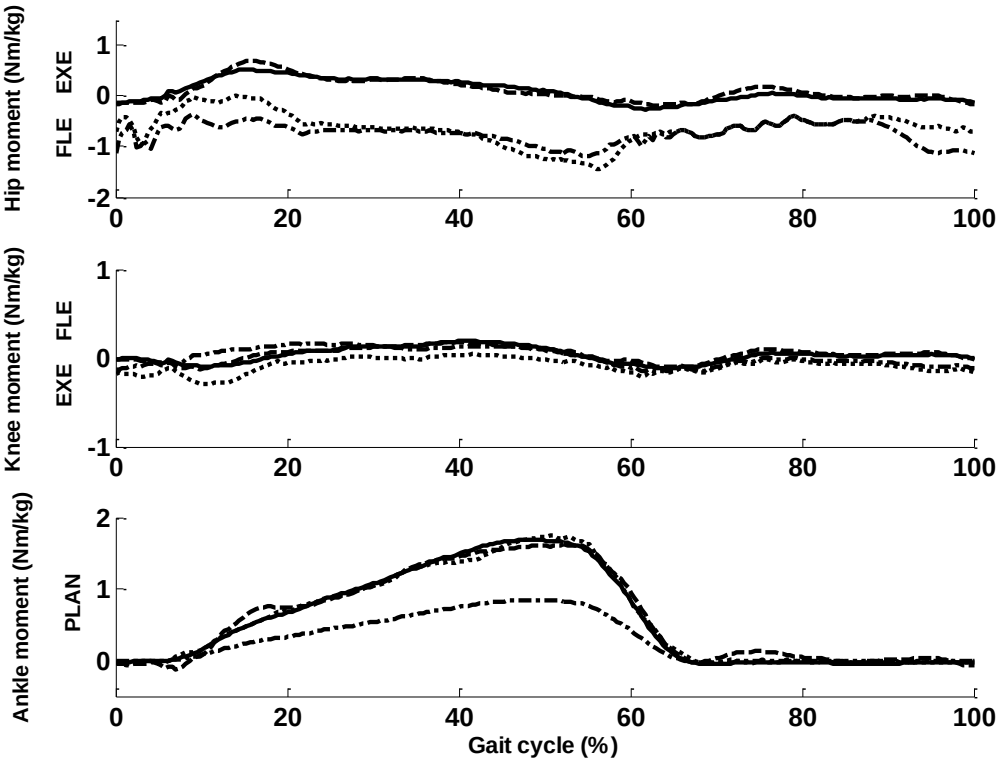

(c) S3.

Figure 4.19: Internal joint moments in three subjects walking at 50% of NC: solid, dashed, dotted and dash-dot lines are respectively the moments during experimental overground walking, simulated upright walking, simulated supine stepping with full ground forces and simulated supine stepping with 30% of upward ground force.

Figures 4.17-4.19 show that the moments at the ankle joint in a supine position with full ground reaction forces are almost equal to those in upright walking, based on the observation that the dashed and the dotted lines in the lowest plot are quite close. However, the differences in joint moments induced by body position became apparent at the knee and the hip joints. Differences between moments in the supine and upright stepping positions were caused by the leg segment weight. During supine stepping, the shank and thigh induced additional external flexion moment at the knee and extension moment at the hip joint. Therefore, the knee joint required more internal extension moment while the hip joint required more flexion moment, compared to upright

walking. This can be observed by the dotted lines being lower than the solid and dashed lines in the top and middle plots of Figures 4.17-4.19.

In contrast to position changes, which influenced the hip joint moment most, the ground reaction forces had significant influence on the ankle joint moment. When the force applied on the foot reduced to 30% of upward ground forces during overground walking, the moment at the ankle joint (the dash-dot line in the lowest plots of Figures 4.17-4.19) reduced to approximately 30% of that during stepping with the whole body weight (the solid, dashed and dotted lines in the same figure). This is as expected, keeping in mind that the ankle joint moment is closely related to the ground reaction forces (Equations (4.38) and (4.39)).

As described in Section 3.3.3, the knee joint produced additional extension moment in the early stance phase (around 15% of the gait cycle) during normal overground walking, which was most pronounced at 100% of NC. This additional extension moment was still observed during supine stepping with full ground reaction forces, but was much alleviated during supine stepping when the ground reaction force was replaced with a value of only 30%. This was because the addition extension came from the heel strike loading. It was expected that the knee joint required less internal extension moment after reduction of the ground reaction forces. Therefore the moment at the knee joint in supine stepping with 30% of upward force was much reduced, based on the observation that dash-dot lines in the middle plots of Figures 4.17-4.19 are close to the neutral position. However, the moment at the hip joint still showed large flexion moment, in spite of a much reduced ground force. As the ground reaction forces only existed during the stance phase, the reduction of force only influenced the joint moments in the stance phase, while those during the swing phase were the same as

those during supine stepping with full ground reaction forces.

When the speed reduced, the differences in the hip moments between supine stepping and upright walking were quite similar to those occurring during walking at 100% of NC. The moments at the ankle and knee joints had a smaller change compared to walking at 100% of NC.

4.3.4. Discussion

In order to investigate the technical feasibility of the proposed GOER device, the kinetic features of supine stepping should be taken into account. Computer modelling is a useful tool for visualization of the dynamic performance at various positions with different levels of ground reaction forces. One of the important elements of this study was the modelling of force transmission between the links (foot, shank and thigh). The moments at the ankle, knee and hip joints were calculated simultaneously using inverse dynamics. The study firstly developed a model to simulate upright walking. The simulated moments at the joints were similar to the experimental data, which confirmed the accuracy of the leg linkage model. Keeping a similar configuration, the model was rotated to simulate stepping in a supine position. Although the same amount of forces as the recorded ground reaction were applied on the foot sole in the supine position, there were differences in the joint moments due to the position change. Differences were closely dependent on the weight of the segments that the joint supports, with the largest difference in the hip joint, which supports the heaviest segments (the thigh, shank and foot), and the smallest difference in the ankle joint.

Joint moments in the lower limbs can be used to quantify forces generated by patients

(reflecting muscle strength) and to assess the clinical rehabilitation process. For patients' safety, only a small force is clinically applied on the foot to stimulate the sensory motor system [261]. Moreover, a low force is selected to prevent reflexes in patients who are more sensitive to stimuli and vulnerable to reflexes compared to able-bodied people [25]. Compared to the simulated moment in the supine position with 100% of body weight applied on the foot sole, the simulated moment at the ankle joint during 30% of upward ground reaction force was significantly reduced. As the foot was not heavy compared to the thigh and shank, the ankle joint moment was closely related to the ground reaction forces. It was expected that a reduced ground reaction force induced a reduced ankle joint moment.

The moment change in the hip joint, which was mainly caused by the position, did not substantially vary at various speeds. However, the knee joint moment during supine stepping during the early stance phase had a smaller difference in slower walking compared to walking at 100% of NC. This might result from the fact that the ground reaction forces during slower walking were lower with less strike loading and were not as dynamically variable as that during normal walking (see Figures 3.7-3.9). Such a reduced force profile induced smaller changes in the moments at the ankle and knee joints, which were more influenced by the ground forces, as discussed above.

It was observed that the hip joint was most sensitive to the change of position while the ankle joint was most sensitive to the forces applied on the foot. The position change from upright walking to supine stepping resulted in a different distribution of forces and a change in the effect of gravity. To avoid excessive forces on the leg joints and to stabilize the leg, the proposed GOER system requires a robust frame which can support the weight of the leg. For the ground reaction force simulation, the system should be

capable of producing a force with an adjustable amplitude, so that the GOER system can initiate the training with a very small force to ensure patient safety, then increase the force amplitude based on the physical condition of the patient, so as to train the ankle joint.

4.3.5. Conclusions

A model of the leg linkage was developed which simulated overground walking with similar dynamics to experimental walking. It utilized experimental gait patterns, such as trajectories and ground reaction forces. The patterns were shown to influence the moments in joints that occur during locomotion. The rotated model allowed analysis of supine stepping with different ground reaction forces. The model proved a useful testbed to investigate the dynamics of supine stepping in the proposal GOER system.

Chapter 5. Prototype Design of the GOER System

Summary: The model of the GOER system with two rotary actuators has a high power requirement for supine stepping, therefore several options for the potential actuation are presented and compared, resulting in a detailed conceptual design of a bar-cam system. The GOER design is then finalised, after suitable materials are selected for each component and a power unit consisting of an electric motor and a gearbox is specified. Furthermore, a pneumatic shoe platform is designed to mimic the ground reaction forces, including analysis of the shoe structure for mechanical stimulation and selection of commercially available pneumatic elements. This chapter ends with a final specification of the GOER prototype.

5.1. Actuation Configuration

Actuation analysis is an important part of system design. This section investigates conceptual design of different actuation configurations for the GOER system.

5.1.1. Power requirements from the two-bar GOER model

Supine stepping was simulated with a model of a two-bar linkage as shown in Figure 4.7. This model employs two rotary actuators to move the bars in semi-circular trajectories periodically. A system with such an actuation setup requires relatively high power input. Supine stepping demands higher peak power than upright walking, because the supine leg needs to accelerate against gravity during the swing phase. It is

expected that the high load combined with the long moment arm of the leg weight results in high power requirements from the two rotary actuators for the two-bar GOER system.

As shown in Chapters 3 and 4, one of the advantages of modelling in SimMechanics / Matlab is that information such as the torque and power can be calculated through the inverse linkage algorithm. The material properties, such as the mass, the length and the moment of inertia of each segment in the model have to be specified, so that SimMechanics model can simulate the dynamics [264]. The properties of the human body segments, including the thigh, the shank and the foot, can be calculated using Table 3.3. The other segments involved in this model are the two bars. The length of the driven Bar 1, as described in Section 4.1.2, is approximately equal to the leg length. Bar 2, which supports the foot, has a length equal to the foot length. The material for these two bars should be selected based on the target performance, which will be discussed in Section 5.1.6. At the current stage of model simulation, the material is provisionally defined as carbon steel with a hollow square cross section (0.025×0.025 m^2 with thickness of 0.003 m).

After the materials of the bars are defined in the model (presented in Appendix 3), the torque of the two-bar GOER system can be calculated as:

$$T_k - T_t = I_t \alpha_t \tag{5.1}$$

$$T_a - T_k - T_s = I_s \alpha_s \tag{5.2}$$

$$T_2 - T_a - T_f = I_f \alpha_f \tag{5.3}$$

$$T_1 - T_2 - T_b = I_b \alpha_b \tag{5.4}$$

where T_k, T_a, T_2 and T_1 are, respectively, the torque at the knee, the ankle, Actuator 2 and Actuator 1. Parameters I_t, I_s, I_f, and I_b are, respectively, the moment of inertia of the thigh, the shank, the foot and Bar 1. Variables α_t, α_s, α_f and α_b are, respectively, the angular acceleration of the thigh, the shank, the foot and Bar 1. T_t, T_s, T_f and T_b are the torques induced by the intersegmental forces with respect to the centre of mass of the thigh, the shank, the foot and Bar 1, respectively. As Bar 2 is relatively short and light (0.25 m in length and 0.5 kg in mass, as can be seen from Section 5.2.2), the torque induced by Bar 2 is negligible in the above torque calculation. The potential user of the GOER system is assumed to have a maximum body mass of 135 kg, which is the upper limit of the user's weight for the Lokomat system[4]. The normal stepping speed of the user in the GOER system is taken to be 1.34 m/s (4.8 km/h), which is an experimentally obtained value from Chapter 3. With all these parameters defined in the model, the movement trajectory of each segment can be simulated, which results in the angular velocity, angular acceleration, torque and power in each joint. Furthermore, the power P can be calculated based on the torque T and the angular velocity w:

$$P = T * w \tag{5.5}$$

The required torque and power for Actuators 1 and 2 for a user with a body mass of 135 kg performing supine stepping at a normal speed of 1.34 m/s are presented in Figures 5.1-5.2. The power from Actuators 1 and 2 are up to 1500 W and 600 W, respectively. In contrast to normal overground walking with power from the hip, the knee and the ankle joints, foot rotation in the GOER system is mainly generated by Actuator 2, which is attached to the tip of the toe. During the heel-off phase, the foot has the largest

[4] Technical Data Lokomat System. http://www.hocoma.com/en/news-events/downloads/. Accessed on 03/01/2012.

plantarflexion and the leg changes from downward movement to upward lifting. As the whole leg is fairly heavy (up to 22 kg for a subject with a mass of 135 kg), the system requires high power to achieve the target performance. When the leg enters the swing phase, the foot moves back into the neutral position. The weight of the horizontally flexed leg tends to push the foot into dorsiflexion. Therefore Actuator 2 works like a generator and provides braking force to prevent further dorsiflexion.

Actuator 1, which moves the whole leg upwards and downwards, has to provide higher power than Actuator 2. During the stance phase when the leg moves downwards, the leg descends by gravity. Actuator 1 works in generator mode so as to slow down the system. However, Actuator 1 has its peak torque at toe off, when it moves the bar and the leg upwards against gravity at a high acceleration (the mean maximal acceleration at 100% of normal cadence for the three subjects during the gait experiment described in Chapter 3 is up to 33.4 m/s^2). It is reasonable that the two-bar GOER system requires high power, especially during the swing phase (1500 W from Figure 5.2).

The high power requirements of the two actuators described above highlight the necessity to reconfigure the drive system. The selection of rotary actuators in the two-bar model is based on the advantage that the target angle profiles for the actuators are easy to obtain from the experimental results (see Section 4.2). However, in the actual physical system, there are many ways to achieve the semi-circular upward and downward movements required in the GOER system.

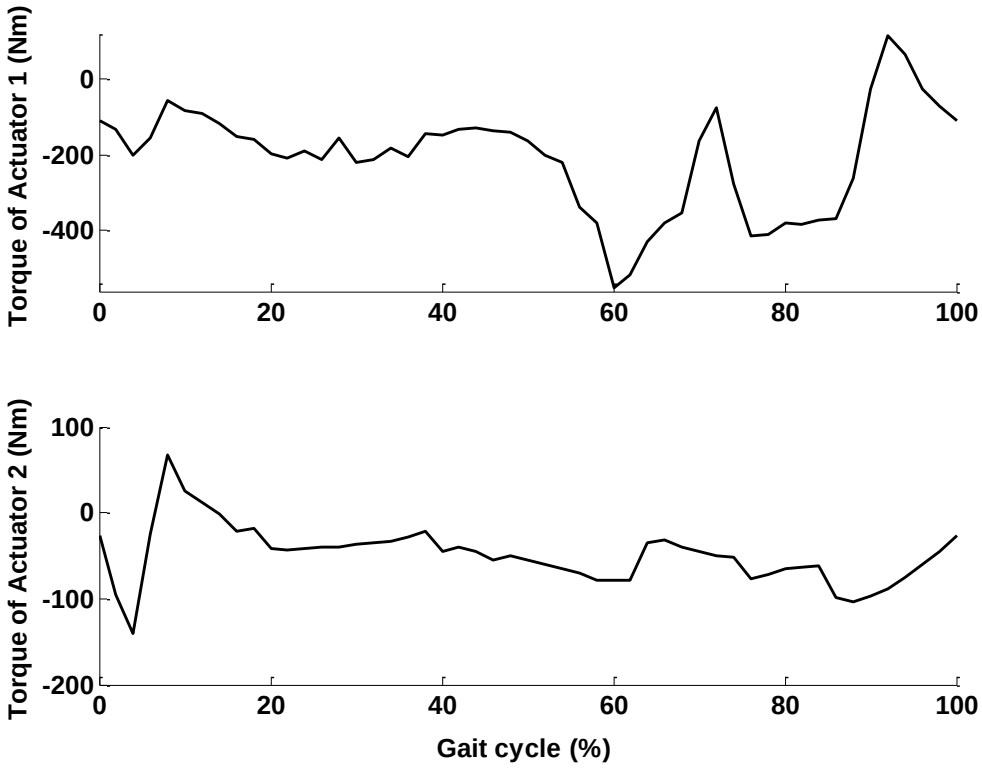

Figure 5.1: Torque requirements.

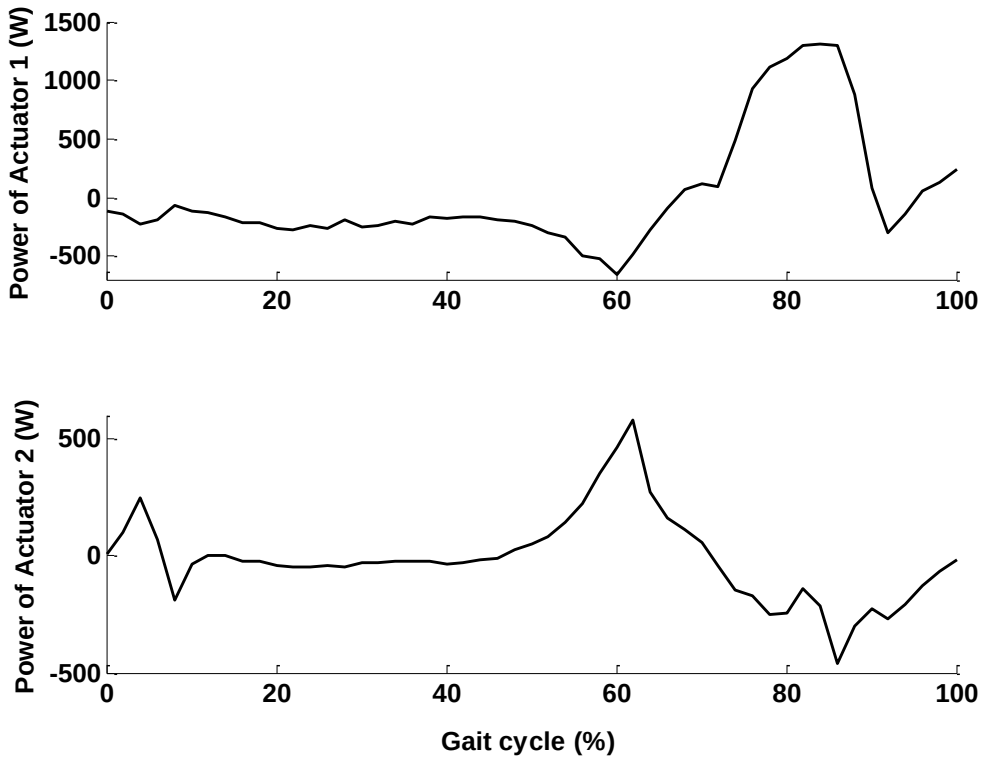

Figure 5.2: Power requirements.

5.1.2. Concept development of Actuation 1

Figure 5.3 displays three configurations for Actuation 1 to achieve semi-circular periodic movements. The simplified diagram in Figure 5.3 presents a pivoted driven bar, with an arrow marking the position of the foot attachment. No information regarding the leg and Actuator 2 is displayed.

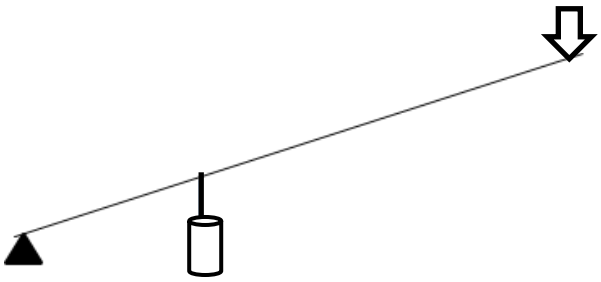

(a) Linear actuation.

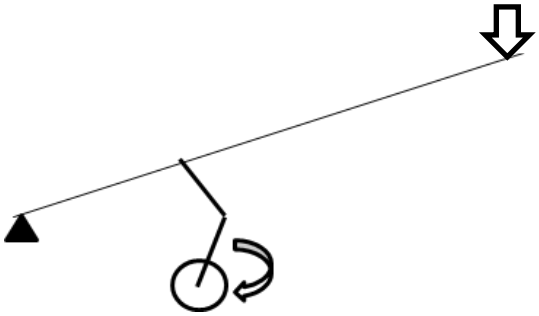

(b) Rotary bar linkage system.

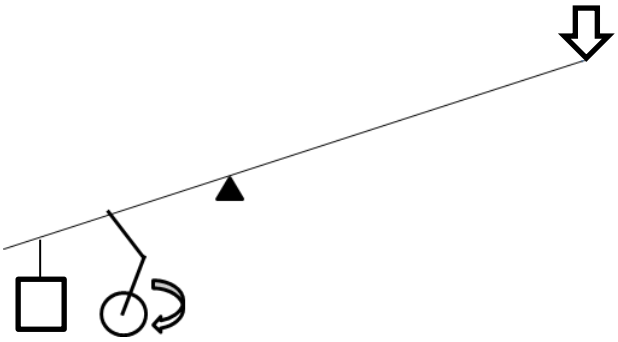

(c) Rotary bar linkage system with a counterweight.

Figure 5.3: Three options for Actuation 1.

The target performance for Actuator 1 is to move the leg up and down repetitively. Linear actuation is an easy method to achieve these periodic movements, as Figure 5.3(a) shows. The linear actuator (marked as a cylinder in Figure 5.3(a)) can induce periodic movements with flexible ranges of motion (ROMs), by changing the stroke. However, linear actuators are often more expensive than rotary actuators. Therefore some relatively cheap options with employment of rotary actuators were further investigated.

A bar linkage is one of the most widely used mechanisms for production of semi-circular trajectories via a rotary actuator [270], which can be seen in Figures 5.3 (b) and (c). Two additional bars are included to move the driven bar, compared to Figure 5.3(a). In contrast to the setup in Figure 5.3(b), the system in Figure 5.3 (c) has the driven bar extended and installs the actuator at the other side of the pivot. Due to the leg attachment, the driven bar in Figure 5.3(b) is out of balance. Extending the driven bar allows attachment of a counterweight (marked as a square in Figure 5.3 (c)) to balance the leg on the other side, resulting in a reduced power requirement.

The bar linkage is a reliable solution to produce periodic movements through constant rotation. Although the GOER system requires a flexible ROM of the driven bar so as to produce stepping at various speeds, a bar linkage can be designed to achieve one ROM for walking at one speed, for example, at 100% of NC, so as to evaluate the design concept of the GOER system. Therefore the bar linkage with a counterweight shown in Figure 5.3(c) is selected as the final setup of Actuation 1.

5.1.3. Design of Actuation 1: a four-bar linkage

Bar linkages can produce different performance with different setups. However, complicated performance requires a complex design. Therefore the target performance for Actuation 1 was simplified based on the simulation performance required by the two-bar model (see Figure 4.9(a)). This section describes synthesis techniques to design a four-bar linkage, which achieves a target ROM of the driven bar with a target phase ratio between the stance and swing phases, i.e. the duration ratio of downward and upward movements.

5.1.3.1. Design parameters of a four-bar linkage

Design of a four-bar linkage requires determination of optimal lengths of the bars so as to achieve the target periodic movement of the rocker from the constant rotation of the crank. As shown in Figure 5.4, a four-bar linkage ABCD is usually based on a fixed frame DA (a thick dash-dot line) and often has a rotational crank AB to move a rocker CD through a coupler BC. The dash-dot line HH' is the horizontal axis. In order to ensure the crank AB performs full rotation, the bar lengths should fulfill [270]:

$$l_s + l_l < l_1 + l_2 \tag{5.6}$$

where l_s and l_l are the lengths of the shortest and the longest bars, while l_1 and l_2 are the lengths of the other two bars.

The bar lengths define the rocker movement: the ROM and the duration ratio of the downward and upward movement. Position ABCD in Figure 5.4 shows that the coupler is aligned with the crank, which allows the rocker tilted at γ_1 ($\angle$CDH) to reach the upper limit CD. When the crank rotates clockwise by γ_2 ($\angle BAB_1$) until it is aligned

with the coupler again, the rocker is tilted at γ_3 ($\angle C_1DH$) to its lower limit C_1D. If the crank further rotates by γ_4 (reflex angle B_1AB, $\gamma_2+\gamma_4 = 360^o$), the rocker moves upward back to its upper limit CD. Therefore the ROM of the rocker is ($\gamma_1+\gamma_3$), with the duration ratio of the downward and upward movements as (γ_2:γ_4). The ROM of the coupler, which is the angle between Bars BC and B_1C_1, is denoted as γ_5 ($\angle CAC_1$).

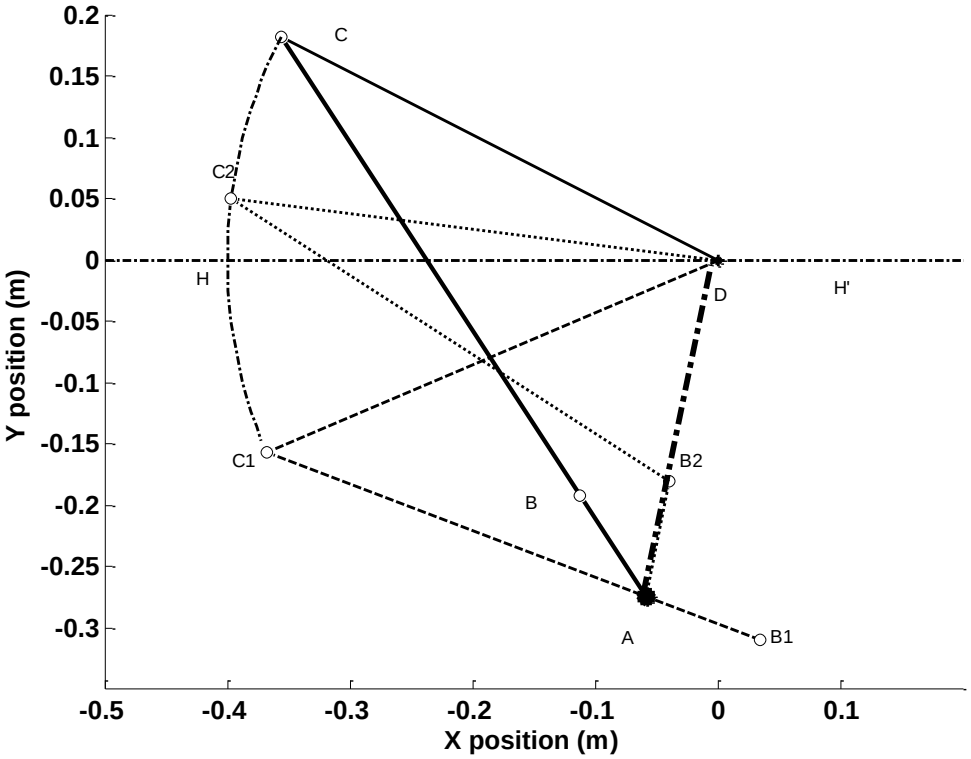

Figure 5.4: A bar linkage ABCD. Bar AB is the crank and Bar CD is the rocker. The trajectory of the rocker tip is shown as a dash-dot curve. Three typical positions ABCD, AB_1C_1D and AB_2C_2D are presented. γ_1: $\angle CDH$; γ_2: $\angle BAB_1$; γ_3 : $\angle C_1DH$; γ_4 : reflex angle $\angle B_1AB$; γ_5: $\angle CAC_1$; γ_6 : $\angle B_2C_2D$.

Bar linkages with different lengths produce different energy transmission efficiencies. The transmission ratio of the input power of the crank to the output power of the rocker is related to the angle between the coupler and the rocker [270]. This angle changes

according to the crank position, such as ∠BCD and $\angle B_1C_1D$ in positions ABCD and AB_1C_1D, which results in different transmission ratios. When the crank is aligned with the frame DA, as shown in position AB_2C_2D of Figure 5.4, the angle of the coupler and the rocker has its minimum value, which is defined as the transmission angle γ_6 ($\angle B_2C_2D$ in Figure 5.4). The transmission ratio of the bar linkage is proportional to the sine of the transmission angle γ_6 [270]. An optimal bar linkage should make the transmission angle γ_6 as large as possible to ensure high power efficiency.

Table 5.1: Target performance of the rocker in the four-bar linkage for stepping at three speeds.

	100% of NC		75% of NC		50% of NC	
	ROM (deg)	Phase ratio	ROM (deg)	Phase ratio	ROM (deg)	Phase ratio
S1	-22.0 to 26.0	6.0 : 4.0	-18.0 to 25.0	7.1 : 2.9	-13.1 to 15.9	7.7 : 2.3
S2	-23.0 to 28.0	6.0 : 4.0	-21.0 to 26.0	7.1 : 2.9	-19.6 to 27.1	7.3 : 2.7
S3	-25.0 to 28.0	6.0 : 4.0	-23.0 to 27.0	6.7 : 3.3	-22.7 to 25.8	7.1 : 2.9
Mean	-23.0 to 27.0	6.0 : 4.0	-21.0 to 26.0	7.0 : 3.0	-18.5 to 23.0	7.4 : 2.6

The ROM and the duration ratio of the rocker combined with the transmission angle are the main parameters for determining the optimal lengths of the bar linkage for the GOER system. The GOER is designed to produce leg movement at variable speeds. The ROMs of the driven bar and the phase (duration) ratios at 100%, 75% and 50% of NC are summarized in Table 5.1, based on the experimental data in Chapter 3.

5.1.3.2. Design of a bar linkage for the GOER system stepping at 100% of NC

Linkage synthesis techniques are described in this section so as to obtain the simplified target performance of Actuator 1 for the GOER system, with stepping at 100% of NC

as an example. According to the requirements of stepping at 100% of NC presented in Table 5.1, the following equations can be derived:

$$\gamma_1 = 23; \gamma_3 = 27 \tag{5.7}$$

$$\gamma_2 + \gamma_4 = 360 \tag{5.8}$$

$$\gamma_2 / \gamma_4 = 2/3 \tag{5.9}$$

$$\gamma_2 + \gamma_5 = 180 \tag{5.10}$$

The law of cosines results in the transmission angle γ_6 as:

$$\gamma_6 = \arccos \frac{l_b^2 + l_c^2 - (l_d - l_a)^2}{2 l_b l_c} \tag{5.11}$$

where l_a, l_b, l_c and l_d are the lengths of bars AB, BC, CD and DA, respectively. Equations (5.8)-(5.10) yield $\gamma_2 = 144°$, $\gamma_4 = 216°$ and $\gamma_5 = 36°$.

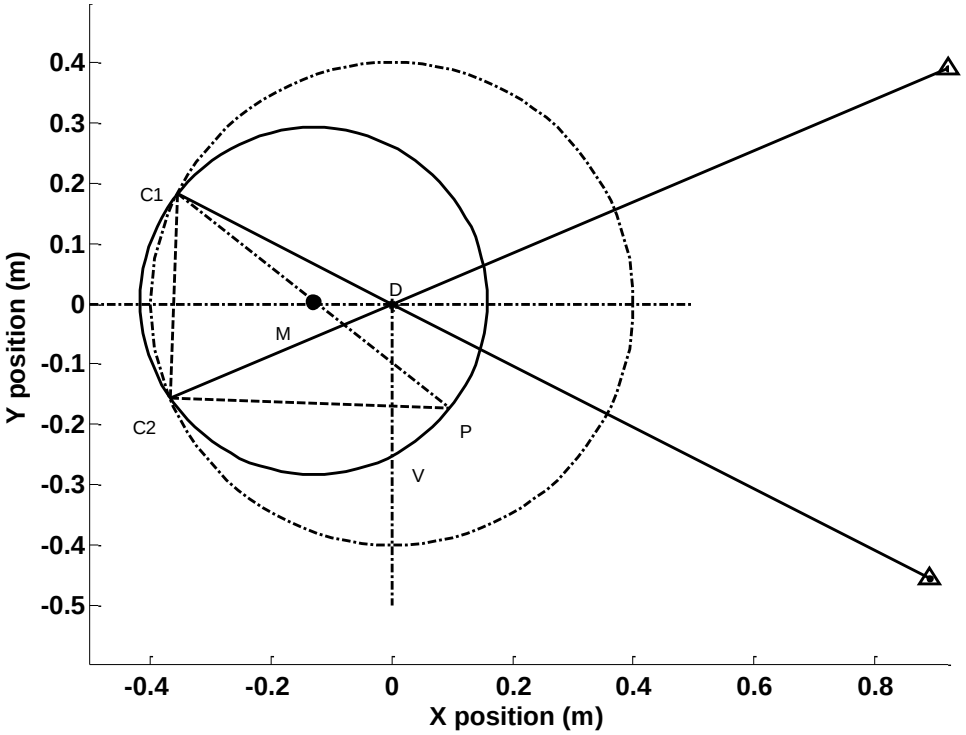

Figure 5.5: Four-bar linkage design. The rocker is lengthened at the other end, with triangles showing the points of foot attachment.

Figure 5.5 shows a rocker rotating at a point D between the range of C_1D and C_2D. The rocker is extended at the other end to represent the driven bar required in the GOER system, with triangles showing the points of foot attachment. In order to ensure the phase ratio of 3:2, i.e. γ_5= 36 °, the possible locations of the crank base A should be part of a circle ***M***, which can be obtained in the following steps:

(1) Choose a point P, which constructs a right triangle C_1C_2P with $\angle C_1PC_2 = \gamma_5 = 36°$.

(2) Draw a circumscribed circle ***M*** with the hypotenuse C_1P as the diameter.

This circumscribed circle ***M***, which is shown in Figure 5.5 as a solid curve, is the potential trajectory for the crank base A to ensure $\gamma_5 = 36°$.

As the minor arc C_1C_2 is the movement of the rocker, it is not suitable for the crank base A. The crank base, which will have an actuator, is better positioned in a low place, such as the lower half circle C_2P, rather than in the upper half circle C_1P. Furthermore, the user of the GOER system aligns the hip joint with the point D for training. Fixing the crank in the minor arc VP will make the training inconvenient (V is the intersection between the circle ***M*** and the vertical line starting at the point D). After consideration of the practical setup of the GOER system, the potential trajectory for the crank base A to ensure the phase ratio of 3:2 is only a small part of the circle ***M***: the minor arc C_2V.

Assuming the rocker with a length of l_c is fixed at D (0, 0), the points C_1 (x_{C_1} , y_{C_1}), C_2 (x_{C_2} , y_{C_2}) and the distance C_1C_2, $l_{C_1C_2}$, can be calculated as:

$$x_{C_1} = l_c \times \cos(180 - \gamma_1) \tag{5.12}$$

$$y_{C_1} = l_c \times \sin(180 - \gamma_1) \tag{5.13}$$

$$x_{C_2} = l_c \times \cos(180 + \gamma_3) \tag{5.14}$$

$$y_{C_2} = l_c \times \sin(180 + \gamma_3) \tag{5.15}$$

$$l_{C_1C_2} = \sqrt{(x_{C_1} - x_{C_2})^2 + (y_{C_1} - y_{C_2})^2}. \tag{5.16}$$

Therefore the possible positions for the crank base A lie on a circle with radius R_A and centre (x_M, y_M) as:

$$R_A = \frac{l_{C_1C_2}}{2\sin(\gamma_5)} \tag{5.17}$$

$$(x_M - x_{C_1})^2 + (y_M - y_{C_1})^2 = {R_A}^2 \tag{5.18}$$

$$(x_M - x_{C_2})^2 + (y_M - y_{C_2})^2 = {R_A}^2 \tag{5.19}$$

Based on the size of the GOER system, the length of the rocker is defined as l_c = 0.40 m. Then the parameters above can be obtained as:

R_A = 0.287; x_M = -0.13; y_M = 0.045.

The position A (x_A, y_A) can be defined via some angle γ_7, which has the zero position aligned with X axis with positive value in anti-clockwise direction, as:

$$x_A = 0.287\cos(\gamma_7) - 0.13 \tag{5.20}$$

$$y_A = 0.287\sin(\gamma_7) + 0.045. \tag{5.21}$$

As the pivot A lies in the arc C_2V, the limits of γ_7, γ_{7_1} and γ_{7_2}, can be calculated as:

$$0.287\cos(\gamma_{7\_1}) - 0.13 = x_{C_2} \tag{5.22}$$

$$0.287\cos(\gamma_{7\_2}) - 0.13 = x_V \tag{5.23}$$

which yields γ_{7_1} = 214 °and γ_{7_2} = 297 °. Therefore the crank base A is in the minor arc C_2V when γ_7 is between 214° and 297°.

The next task is to find the optimal position on the minor arc C_2V for the crank base A

which yields the largest value of the transmission angle. The bar lengths of the four-bar linkage can be defined as:

$$l_{AC_1} = \sqrt{(x_{C_1} - x_A)^2 + (y_{C_1} - y_A)^2} \tag{5.24}$$

$$l_{AC_2} = \sqrt{(x_{C_2} - x_A)^2 + (y_{C_2} - y_A)^2} \tag{5.25}$$

$$l_a = \frac{l_{AC_1} - l_{AC_2}}{2} \tag{5.26}$$

$$l_b = \frac{l_{AC_1} + l_{AC_2}}{2} \tag{5.27}$$

$$l_d = \sqrt{x_A{}^2 + y_A{}^2} \tag{5.28}$$

When γ_7 is between 214^o and 297^o, the length of the crank AB, l_a, the coupler BC, l_b, and the frame DA, l_d, can be calculated as shown in Figure 5.6. The corresponding transmission angle γ_6 can also be calculated using Equation (5.11), as presented in Figure 5.7. It can be seen that the largest transmission angle is obtained when γ_7 = 245^o.

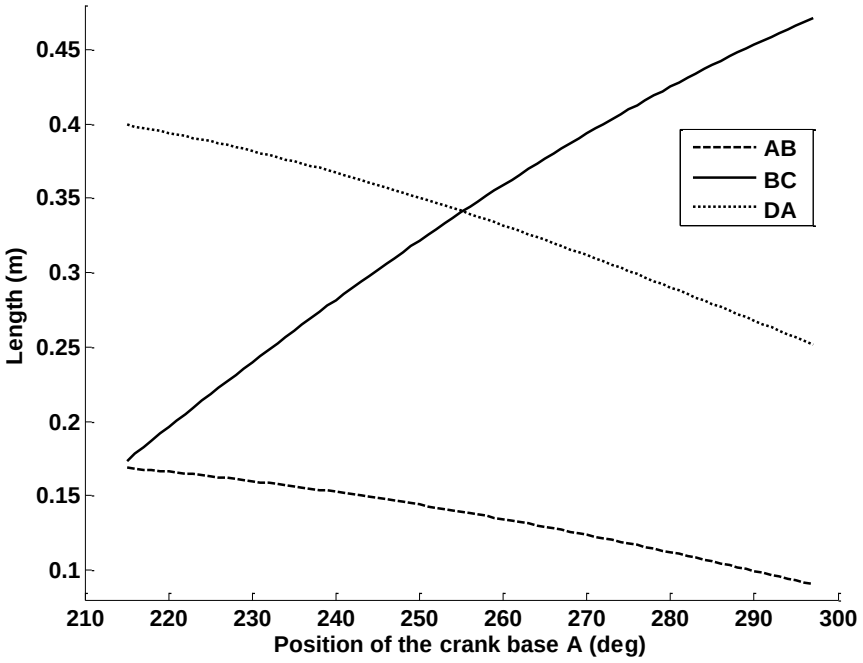

Figure 5.6: Bar lengths as a function of γ_7, which describes the position of the crank base A.

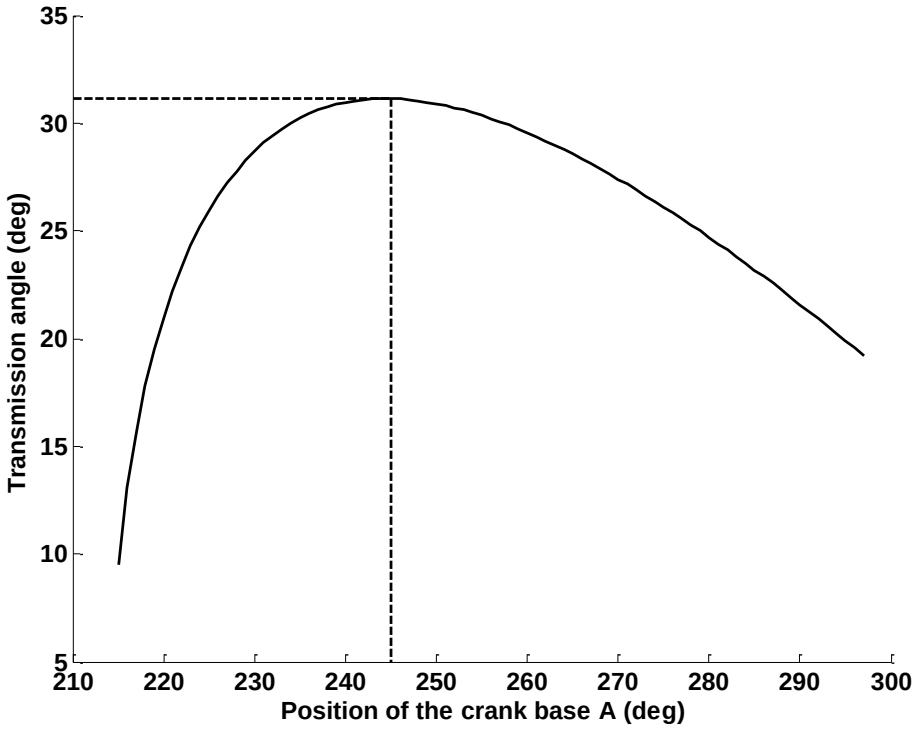

Figure 5.7: The transmission angle as a function of γ_7, which describes the position of the crank base A.

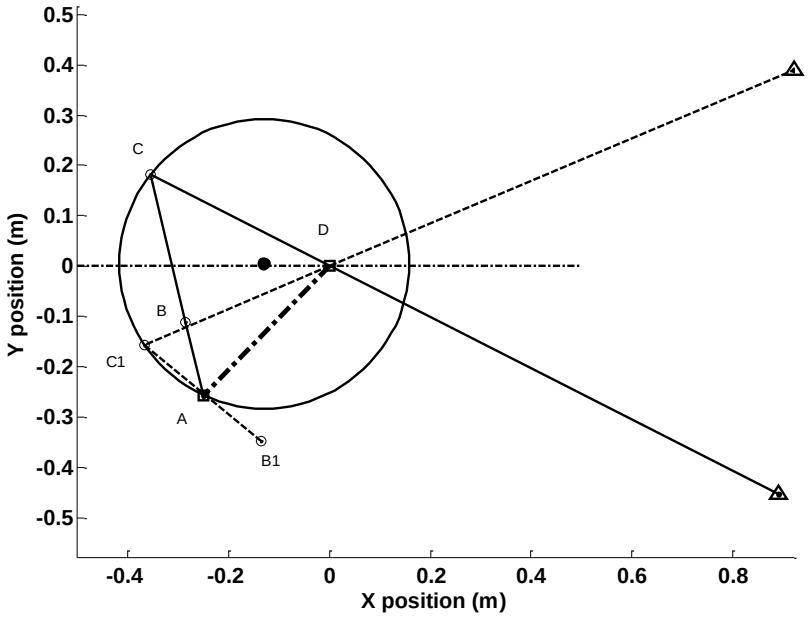

Figure 5.8: The setup of the bar linkage to move the driven bar (ABCD achieves the lowest position of the driven bar for toe off, while AB_1C_1D produces the upmost position of the driven bar for heel strike).

The final setup of the bar linkage system to simulate stepping at 100% of NC can be determined as shown in Figure 5.8, with the lengths as:

l_a = 0.15 m; l_b = 0.30 m; l_c = 0.40 m; l_d = 0.36 m.

The sum of lengths of the shortest and longest bars (0.55 m) is shorter than the combination of the other two bars (0.66 m), which meets the inequality (5.6), allowing full rotation of the crank. The coordinates of ABCD shown in Figure 5.8 are:

A(-0.25, -0.26); B(-0.29, -0.11); C(-0.36, 0.18); D(0, 0).

Using the bar linkage, the target periodic performance can be achieved through constant rotation of the crank, where an electric rotary motor can be used. The final performance of the driven bar induced by the bar linkage is presented in Figure 5.9 as a solid line. The theoretical target angle of Actuation 1 obtained from the two-bar model is shown as a dashed line for comparison. The motion produced by the bar linkage is designed to approximate the target motion by achieving the same ROM and phase ratio. It can be seen that the ROM achieved from the bar linkage is 50^o, and the phase ratio between downward and upward movement is 3:2, which meets the target performance of Actuator 1. However, the angle profile produced by the bar linkage is different from the target angle profile of Actuator 1 during the simulation of the mid-stance and mid-swing phases. These differences occur because the speed is lower at heel strike and higher during the mid-stance and mid-swing phases in the bar linkage setup than the theoretical speeds at the corresponding phase required by the two-bar model. However, these differences are satisfactory as far as the power is concerned. The bar linkage allows the driven bar to change the speed gradually at heel strike, which requires less acceleration, resulting in a reduced power requirement.

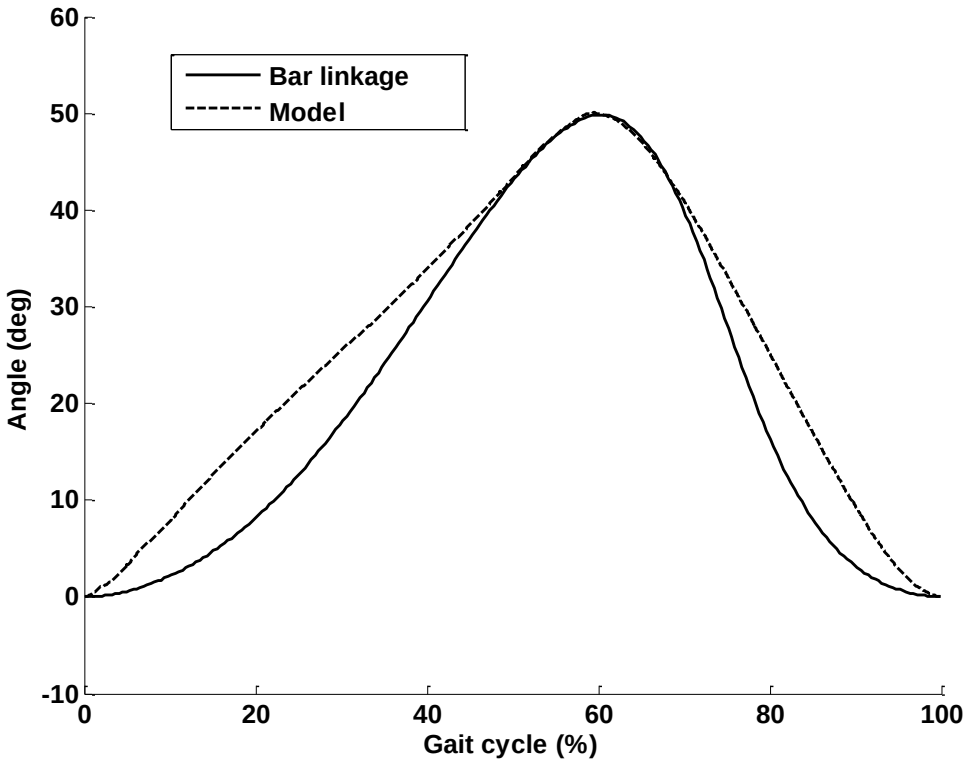

Figure 5.9: The driven bar performance induced by the bar linkage and the target model.

A similar design approach can be employed to obtain the setups of bar linkages for slow walking at 75% and 50% of NC, as defined in Table 5.1. The optimal lengths of the bar linkages for stepping at all three cadences were calculated and are summarized in Table 5.2.

Table 5.2: Configuration of bar linkages for leg motion at all three cadences.

Length (m)	100% of NC	75% of NC	50% of NC
l_a	0.15	0.13	0.07
l_b	0.30	0.20	0.13
l_c	0.40	0.40	0.40
l_d	0.36	0.34	0.34

5.1.5. Design of Actuation 2: a cam mechanism

The model in Figure 4.7(b) shows that the foot segment moves at a high speed (up to 2.2 m/s during the swing phase of walking at 100% of NC). In order to ensure the safety of the drive system, Actuation 2 should be reconfigured so that the power unit is installed in a fixed support, instead of on the moving foot.

The GOER system needs accurate control of the foot movement. The ankle joint changes its rotational direction twice within a gait cycle (from a neutral position to dorsiflexion, plantarflexion and back to the neutral position), which results in a complicated angle profile of Actuator 2, as shown in Figure 4.9(b). In order to generate complex motion, noncircular gears or cams are often adopted [271-273]. Cam devices can provide many arbitrarily-specified movements [274]. The advantage of choosing a cam mechanism to rotate the foot in the GOER system is that a complex trajectory can be achieved through constant rotation, which allows both Actuations 1 and 2 to share the same power unit: a rotary motor. The motor actuates the leg through a four-bar linkage, while it transmits the power to the foot via a chain and rotates the foot through the cam mechanism. Therefore the synchronisation of Actuators 1 and 2 in the GOER system can be achieved mechanically through a bar linkage and a cam mechanism. Another advantage of the cam system is that the cam limits the motion, thus being safer for the patient.

5.1.5.1. Design techniques for the cam mechanism

A cam usually consists of two moving elements: a cam and a follower. The cam fully rotates at its centre, while the follower rotates in a semi-circle at the pivot. In order to

investigate the function of the rotation angles of the follower and the cam, a cam-follower mechanism is employed as shown in Figure 5.10. The cam, which is represented by a solid curve, rotates at its centre ***B***. It is assumed that the follower (the solid straight line in Figure 5.10) pivots at the point ***A***, and has a length L_f equal to the distance AB. The follower contacts the cam rim initially at the point ***C***. There is a corresponding position of the follower so as to ensure contact with each point on the cam rim. In order to explain the motion of the cam and the follower, an example is given to search for the position of the follower which contacts at an arbitrary point $\boldsymbol{D_1}$ on the cam rim (see Figure 5.10).

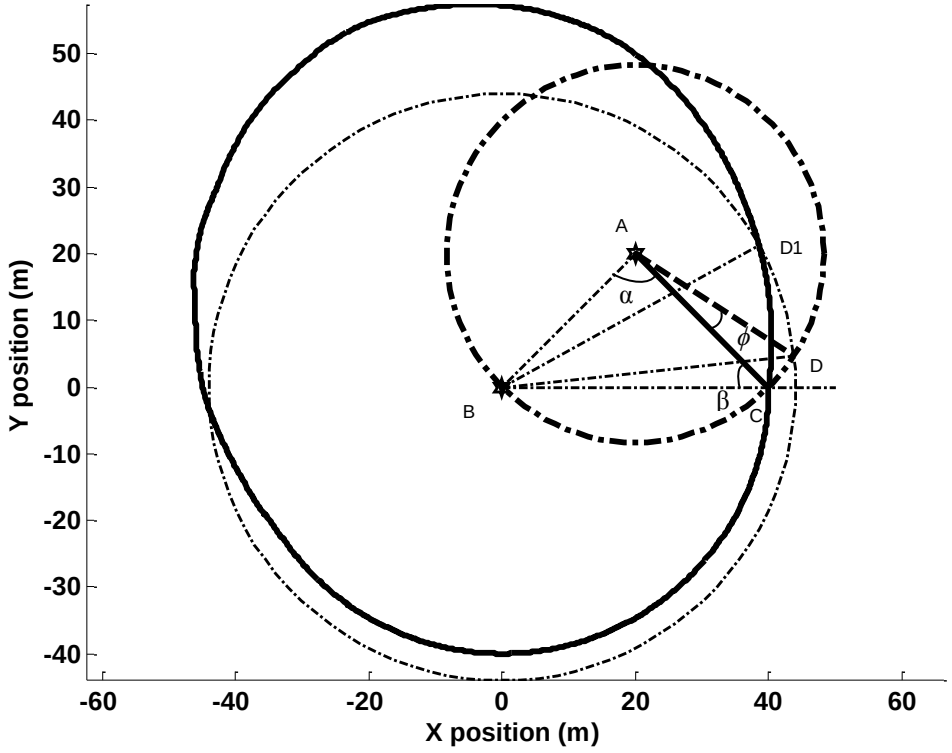

Figure 5.10: The cam-follower mechanism. The solid curve represents a cam, which rotates at the point *B*. The solid straight line represents the follower, pivoting at the point *A*. The follower contacts the cam initially at the point *C*. If an arbitrary point D_1 is to contact with the follower, the cam should rotate from the point D_1 to *D*, so that the follower contacts with the cam at the point *D*, with the position of the follower as the straight dashed line AD. The thick dash-dot circle *A* is the trajectory of the follower, while the thin dash-dot circle *B* is the trajectory of the point D_1 during rotation of the cam.

Suppose the point $\boldsymbol{D_1}$ has a distance L_{D1} from the cam centre ($BD_1 = L_{D1}$). As the cam rotates at the point ***B*** while the follower rotates around the point ***A***, the new contacting position of the follower can be determined as follows:

(1) Draw a circle ***A*** (the thick dash-dot curve in Figure 5.10), with radius L_f, which is the potential trajectory of the follower.

(2) Draw a circle ***B*** (the thin dash-dot curve in Figure 5.10), with radius L_{D1}, which is the trajectory of the target contacting point $\boldsymbol{D_1}$ during cam rotation.

(3) Find the intersection point of circle ***A*** and circle ***B***, which is the new contacting point ***D*** for the follower on the cam.

Assuming in the initial position, ∠BAC is denoted as α, ∠ABC and ∠ACB are equal to β while the distance between the initial contacting point ***C*** and the cam centre ***B***, L_{BC}, is R_b. Assume the follower rotates by an angle ϕ (∠CAD) from the position AC to the new position AD. ∠ABD is defined as δ. Then the relationship between the rotational angle of the follower ϕ and the distance of the cam rim from the cam centre L_H can be described analytically as:

$$\cos(\beta) = \frac{R_b}{2L_f} \tag{5.29}$$

$$\alpha = 180 - 2\beta \tag{5.30}$$

$$\cos(\delta) = \frac{L_H}{2L_f} \tag{5.31}$$

$$180 - 2\delta = \alpha + \phi \tag{5.32}$$

Equations (5.32), (5.30) and (5.29) yield

$$\delta = \frac{2\arccos(\frac{R_b}{2L_f}) - \phi}{2} \tag{5.33}$$

Equation (5.31) yields

$$\delta = \arccos\frac{L_H}{2L_f} \tag{5.34}$$

Equations (5.33) and (5.34) yield

$$L_H = 2L_f \cos(\arccos(\frac{R_b}{2L_f}) - \frac{\phi}{2}) \tag{5.35}$$

Therefore L_H can be calculated based on the target ϕ if R_b and L_f are known.

The transmission efficiency of a cam is related to the pressure angle, which is defined as the angle between the motion direction of the follower and the force between the cam and the follower (common nominal line). The transmission efficiency is proportional to the cosine of the pressure angle [274].

Figure 5.11 shows a cam rotating at a point ***O***, with the rim as a thick solid curve. The follower in the position AB can rotate with the point ***A*** and contact the cam rim at the point ***B.*** For this initial position OAB, the speed of the follower can be represented with the arrow BC. The common nominal line from the cam at the point ***B*** is represented as the thin solid line BD. Therefore $\angle$CBD is the pressure angle θ at the point ***B***. In a cam-follower system, the cam generally rotates (e.g. clockwise direction), while the follower has the pivot ***A*** fixed. However, in the analysis of the pressure angle, it is better to fix the cam and move the point ***A*** in the opposite direction (e.g. anti-clockwise). Under these circumstances the follower has the pivot ***A*** moving along the dash-dot circle ***O*** in Figure 5.11, with the radius as the length of follower AB L_f (keep in mind that the length of OA_1 = AB = L_f).

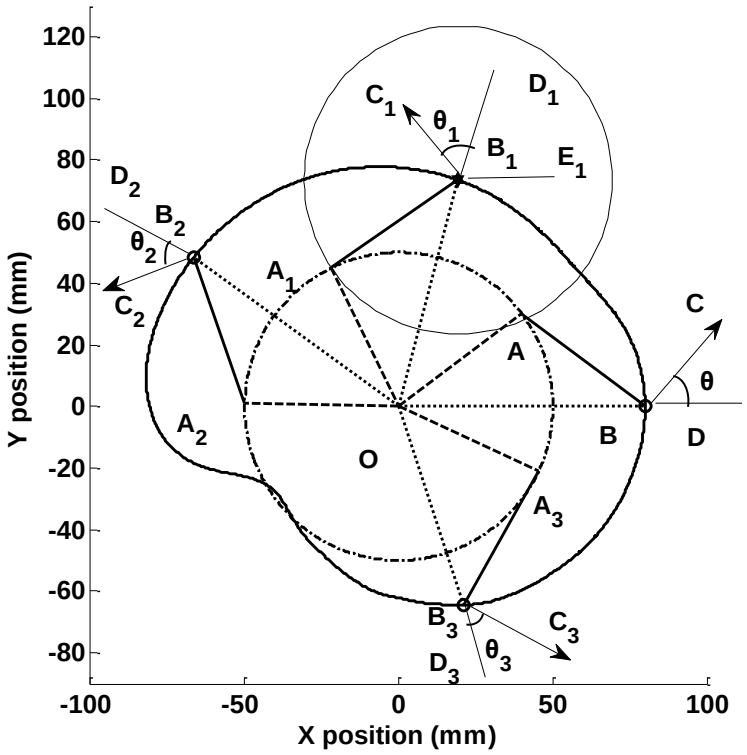

Figure 5.11: The cam and four representative positions of the followers (AB, A_1B_1, A_2B_2 and A_3B_3): the thick solid curve is the cam profile. Circle *O* (thick dash-dot curve) is the potential trajectory of the pivot of the follower. Circle B_1 (thin solid curve) is the potential trajectory of the tip of the follower for contact of the point B_1. The straight lines BD, B_1D_1, B_2D_2 and B_3D_3 represent the common nominal lines. The arrow lines BC, B_1C_1, B_2C_2 and B_3C_3 show the directions of the followers, which are normal to the corresponding lines AB, A_1B_1, A_2B_2 and A_3B_3. Four pressure angles, $\angle CBD$, $\angle C_1B_1D_1$, $\angle C_2B_2D_2$ and $\angle C_3B_3D_3$ are shown as θ, θ_1, θ_2, and θ_3.

In order to find the position of the pivot ***A*** for each contacting point on the cam rim, such as the point B_1, we firstly draw a circle B_1 with radius L_f, which is shown by a dash-dot curve in Figure 5.11. Then the intersection point of circle B_1 and circle ***O*** is the pivot point A_1 for the contacting point B_1. The speed of the follower at the new position A_1B_1 can be represented by the arrow line B_1C_1. The common nominal line from the point B_1 is represented as line B_1D_1. Therefore $\angle C_1B_1D_1$ is the pressure angle

θ_1 at the point $\boldsymbol{B_1}$, which can be calculated as

$$\angle C_1B_1D_1 = \angle A_1OB + \frac{\pi}{2} - 2 \times \angle A_1OB_1 - \angle D_1B_1E_1 \tag{5.36}$$

where the straight line B_1E_1 is in a horizontal position. Using the same technique, the pressure angle of any point at the whole cam rim (such as positions B_2 and B_3) can be calculated (e.g. θ_2 and θ_3). In order to ensure high transmission efficiency, the optimal cam should make the maximal pressure angle as small as possible.

5.1.5.2. Design of a cam for the GOER system stepping at 100% of NC

The cam design techniques, including Equations (5.35) and (5.36), enable the design of a suitable cam to rotate the foot as required in the GOER system. As shown in Figure 4.9(b), the GOER system requires three angle profiles of Actuator 2 to achieve leg performance at three cadences. This section describes the design process for the cam to achieve the target angle profile ϕ at 100% of NC as an example.

The parameters in the function (5.35), such as R_b and L_f, should be determined according to the size of the GOER system. It should be noted that R_b defines the size of the cam. The cam, which is mounted at the tip of the driven bar, should be small and light, so as to reduce the additional load on Actuator 2. Based on a GOER system with a potential foot length of 0.25 m, R_b is defined to be 0.08 m. Therefore the optimal length of follower L_f should be determined to yield the largest transmission efficiency: this makes the maximal pressure angle as small as possible.

In the triangle ABO,

$$l_{OA} + l_{AB} > l_{OB}. \tag{5.37}$$

The follower should be as short as possible to reduce the power. Therefore the follower

pivot is designed to be inside but over the cam area:

$$l_{OA} < l_{OB} \tag{5.38}$$

Equations (5.37)and (5.38) yield the length of follower L_f as

$$0.04 < L_f < 0.08. \tag{5.39}$$

When the follower length L_f varies between 0.04 and 0.08 m, the maximal pressure angle is calculated using Equation (5.36) to be from 71.6^o to 78.8^o, as shown in Figure 5.12. The optimal L_f would be the one giving the smallest maximal pressure angle, which is L_f = 0.05 m. With the parameters R_b = 0.08 m and L_f = 0.05 m, the cam shape can be determined using Equation (5.35) to get the target angle profile ϕ (Figure 4.9(b)) of Actuator 2.

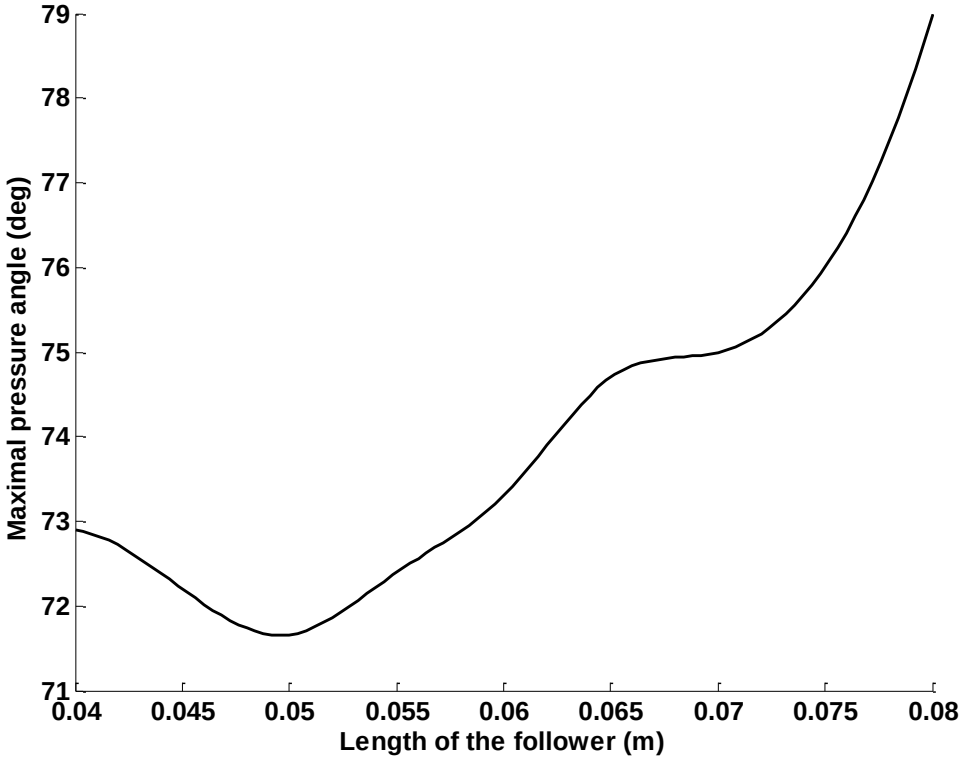

Figure 5.12: The maximal pressure angle according to various follower lengths.

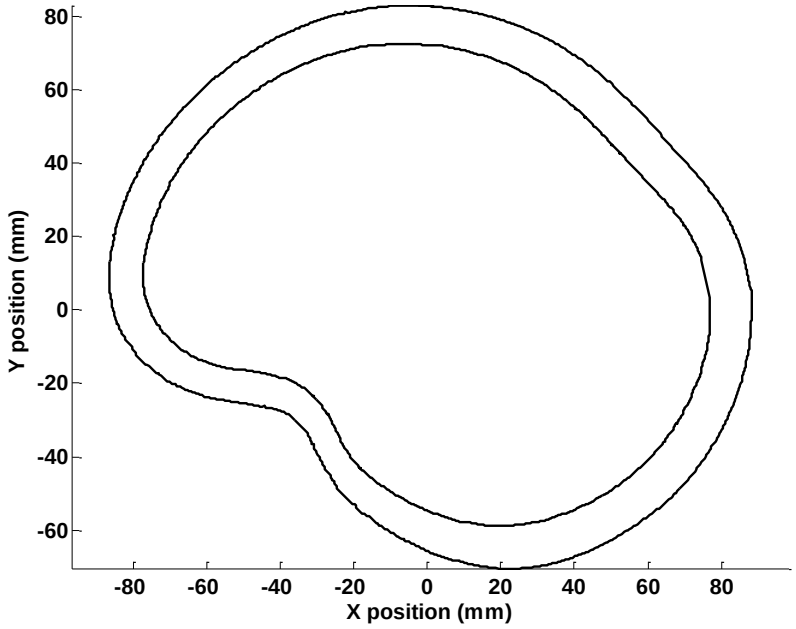

Figure 5.13: The cam for walking at 100% of NC (R_b = 0.08 m, L_f = 0.05 m).

Cam-follower systems often adopt a roller at the tip of the follower to reduce friction during cam transmission. Suppose the roller is 0.01 m in diameter. The final cam takes the shape of a plate with the roller in a groove. The groove follows the cam rim designed with Equation (5.35), but with an offset of 0.005 m on the inner and outer sides of the cam rim. The final cam-roller mechanism has a groove with a width of 0.01 m, as Figure 5.13 shows. The Solidworks presentation of the cam-roller assembly can be found in Appendix 4. The target ϕ for walking at 75% and 50% of NC can be obtained from the experimental data (see Figure 4.9(b)). With similar cam design techniques as described for stepping at 100% of NC, the cams for slower walking can be obtained, as Figure 5.14 shows.

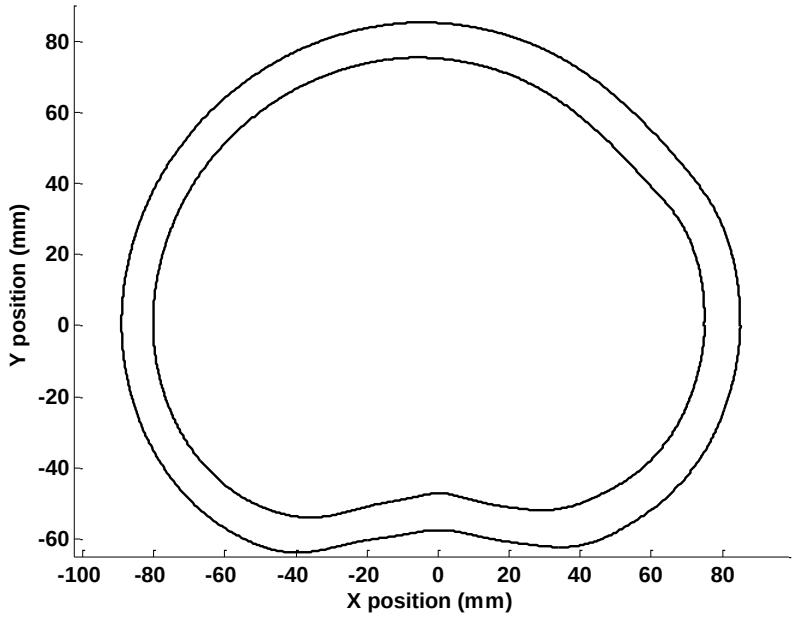

(a) 75% of NC (R_b = 0.08 m, L_f = 0.054 m).

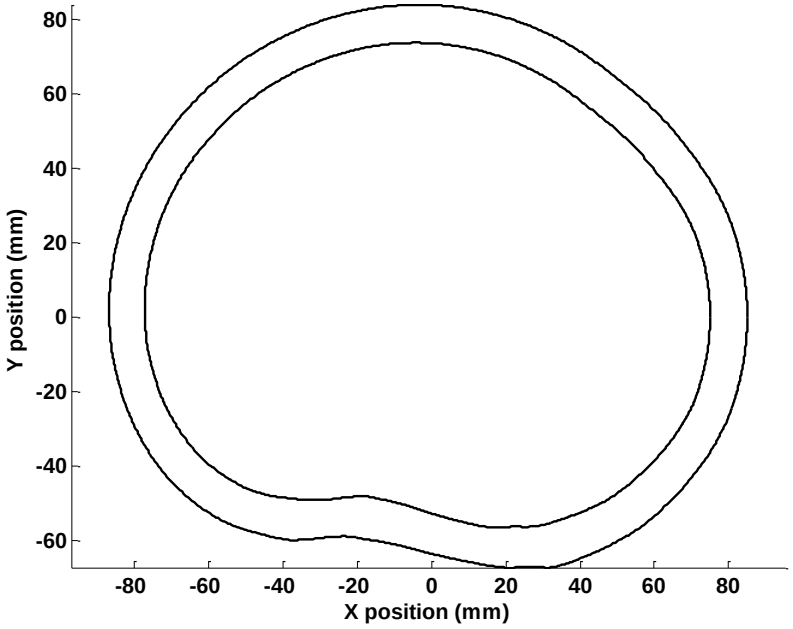

(b) 50% of NC (R_b = 0.08 m, L_f = 0.063 m).

Figure 5.14: Cams for slower walking.

5.1.6. Power requirements from the bar-cam GOER model

The new setup of the GOER system incorporates a bar linkage and a cam mechanism, as Figure 5.15 shows. The motor (installed at the point *A*) rotates the bar linkage ABCD, inducing upward and downward movement of the rocker CD. Therefore the driven bar DE, which is an extension of the rocker CD, produces downward and upward semi-circular movement of the leg. The cam, mounted at the point E, rotates the foot EF to achieve dorsiflexion and plantarflexion. The bar-cam GOER system produces heel-strike (Figure 5.15(a)) and toe-off (Figure 5.15(b)) in a supine leg, with the angles of the hip (H), knee (G), and ankle (F) joints in phase with those during overground walking.

The GOER system with the bar-cam mechanism can be simulated in SimMechanics /Matlab, with the model presented in Appendix 5. The newly included bar linkage and cam mechanism are both initially selected as carbon steel, which is the same as the two-bar model in Section 5.1.1 (the material selection will be discussed in Section 5.1.6). The simulated torque and power for a subject of 135 kg stepping at 100% of NC (crank speed of 50 rpm) is presented in Figure 5.16. It can be observed that the bar-cam GOER system still requires the maximal power at toe off, as in the two-bar setup. Compared to Figures 5.1-5.2, the torque is reduced from 500 Nm to about 150 Nm. The required power is reduced to 670 W, which is only 32% of the power in the two-bar setup (a maximum of 2100 W as can be seen Section 5.1.1). It should be noted that the bar-cam GOER system requires more power in the swing phase (670 W) than in the stance phase (330 W). Therefore a counterweight can be attached on the extended side of the driven bar (the rocker tip C of the bar linkage) to balance the

system. The mass of the counterweight is dependent on the mass of the whole system, which requires determination of the component materials of the GOER system.

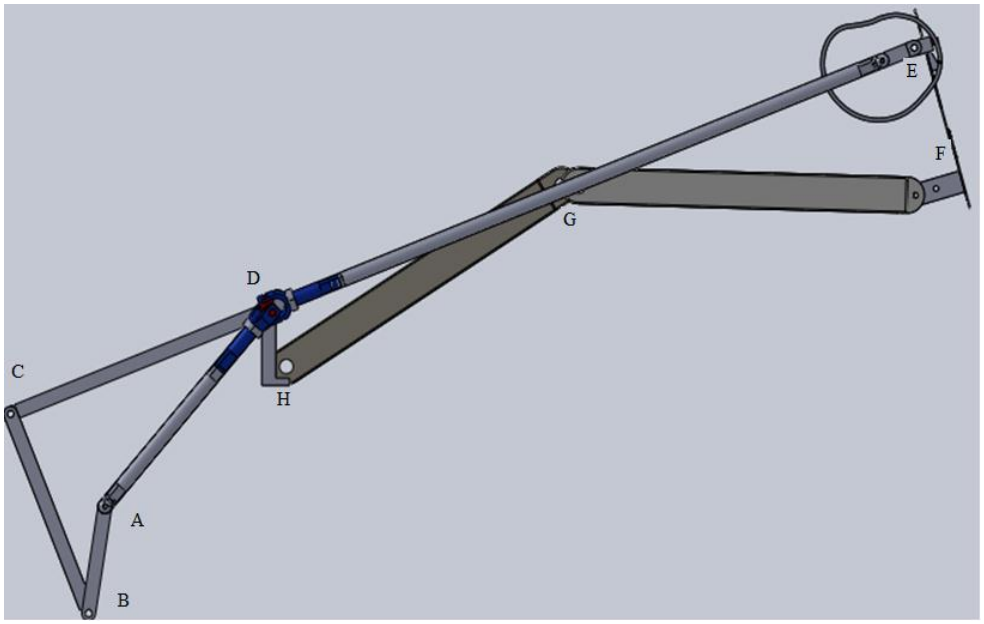

(a) Heel strike.

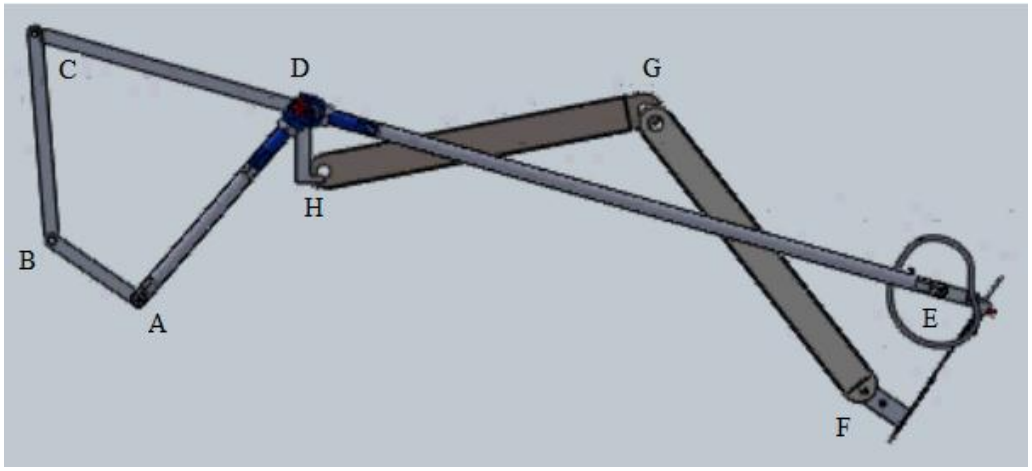

(b) Toe off.

Figure 5.15: The cam-bar linkage setup of the GOER system. The segment ABCD is the bar linkage. The cam is mounted at the point E. The leg segment is represented by EFGH.

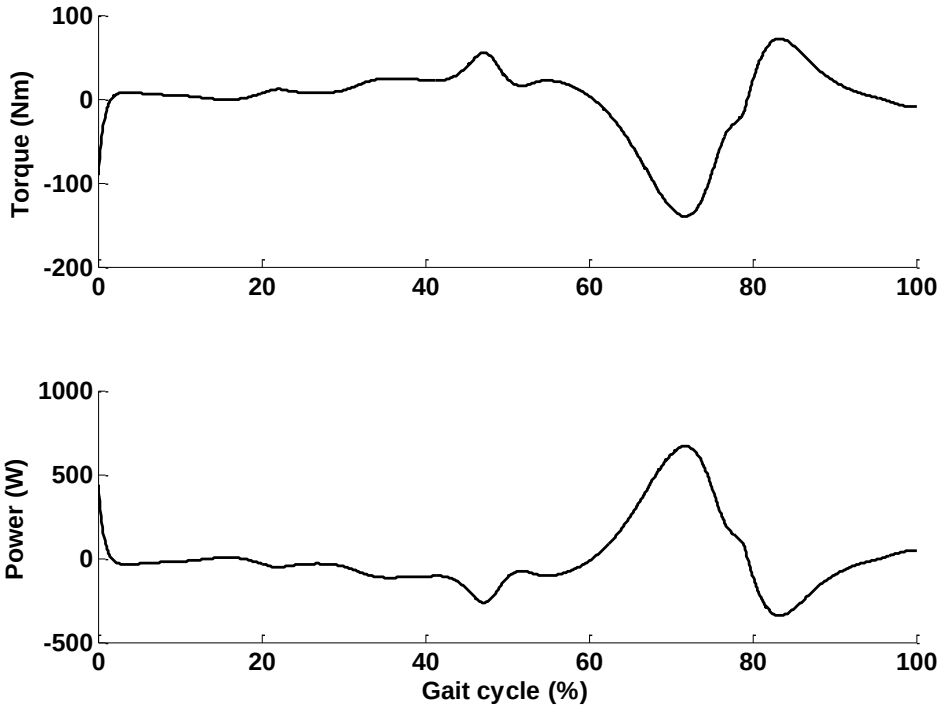

Figure 5.16: The simulated torque and power of the bar-cam GOER system stepping at 100% of NC.

5.1.7. Material selection

In order to simulate the final power requirements of the bar-cam GOER system, the materials and the dimensions of components, including the driven bar, the bar linkage and the cam, should be determined. So far the length of the driven bar, which is determined by the user's leg length, was determined with the least squares algorithm described in Section 4.1. The lengths of the bar linkage and the cam-follower sizes were calculated in Sections 5.1.3 and 5.1.4 respectively. The cross section of the bars and the thickness of the cam (T_c) are to be determined. As described in the dynamic analysis in Section 4.3, a leg frame is important for support of the leg weight. The leg frame consists of a thigh support, a shank support as well as a shoe platform. Each segment length of the leg frame is dependent on the user's leg length and can be

determined based on the anthropometric data in Table 5.3. The length of the leg frame should be adjusted within a range of 0.90-1.20 m so as to fit most people. The cross section of the thigh and the shank bars need to be defined in this section, while the shoe platform will be further analysed in Section 5.2.

Table 5.3: The mass and lengths of body segments for 5% to 95% of the population (taken from [275]).

Segments	Length (m)	
	Male	Female
Height	1.65-1.87	1.50-1.70
Thigh	0.50-0.61	0.46-0.56
Lower leg	0.41-0.50	0.38-0.46
Foot	0.07-0.09	0.06-0.08

The bar segments in the GOER system, such as the driven bar, the bar linkage as well as the leg frame, are designed as hollow square cross sections. In order to choose the materials, the width (W_b) and thickness (T_b) of the cross sections of the bars described above are defined as: W_b = 0.025 m; T_b = 0.003 m.

The driven bar and the bars for the leg frame in the GOER system are up to 1 m in length, therefore bending is a potential cause of failure of these components. The top of the bars has compressive stress, the bottom of the bars has tensile stress, while the neutral plane of the bar has no stress [276]. The bending stress increases proportionally with bending moment, but is also related to the second moment of area of the cross-section of the structural element J. The maximal bending stress σ_b, which takes place at the surface of the bars (the top or the bottom), can be calculated as [277]:

$$\sigma_b = \frac{M_b}{J_b}\frac{W_b}{2} \tag{5.40}$$

where M_b is the maximal bending moment, which occurs at the middle of the bars, and is equal to half of the maximal moment on the bars. J_b is the second moment of area of the hollow square cross section, which can be calculated as

$$J_b = \frac{W_b^4 - (W_b - 2T_b)^4}{12}. \tag{5.41}$$

The maximal moment in the driven bar, the thigh and the shank bars are 140 Nm (Figure 5.16), 135 Nm (dotted line in the top plot of Figure 4.17) and 108 Nm (dotted line in the middle plot of Figure 4.17), respectively. Equations (5.40) and (5.41) yield the bending stresses σ_b of the driven bar, thigh bar and shank bar as 80.65 MPa, 77.77 Mpa and 62.22 Mpa, respectively, which justifies the use of carbon steel AISI1020 (allowable stress for safety is 275MPa) as a suitable material for the driven bar and the leg frame of the GOER system [278]. The CAD drawings of the manufactured driven bar and the leg frame are shown in Appendix 6.

In contrast to the bars, the cam tends to have compressive failure, because it has high pressure on the rim from the roller. The maximal force on the rim F_c can be calculated as

$$F_c = \frac{T_{a2}}{L_f} \tag{5.42}$$

where T_{a2} is the torque required to move the foot, with a maximum of 140 Nm (see Figure 5.1). The length of the roller, L_f, equal to 0.05 m. Therefore the maximal force on the cam rim F_c is 2800 N. It is assumed that the cam has a groove with a depth T_c = 0.05 m. The cam and the roller are theoretically linear with contact area equal to 0. However, in order to estimate the pressure on the rim, the contact width T_w is assumed to be 0.001 m. Therefore the contact area A_c and the compressive strength σ_c can be obtained as:

$$A_c = T_c \times T_w \tag{5.43}$$

$$\sigma_c = \frac{F_c}{A_c}. \tag{5.44}$$

The compressive strength of the cam is 56 MPa. Carbon steel, as mentioned before, can afford such strength. However, due to limited availability of resources, the cam plate was manufactured in plastic. The compressive strength of plastic lies from 150-500 MPa [279].

5.1.8. Electric motor selection

After the materials are determined, the model can be developed with the leg frame included, as shown in Appendix 7. The simulated power of the bar-cam system with the leg frame is shown in Figure 5.17(a).

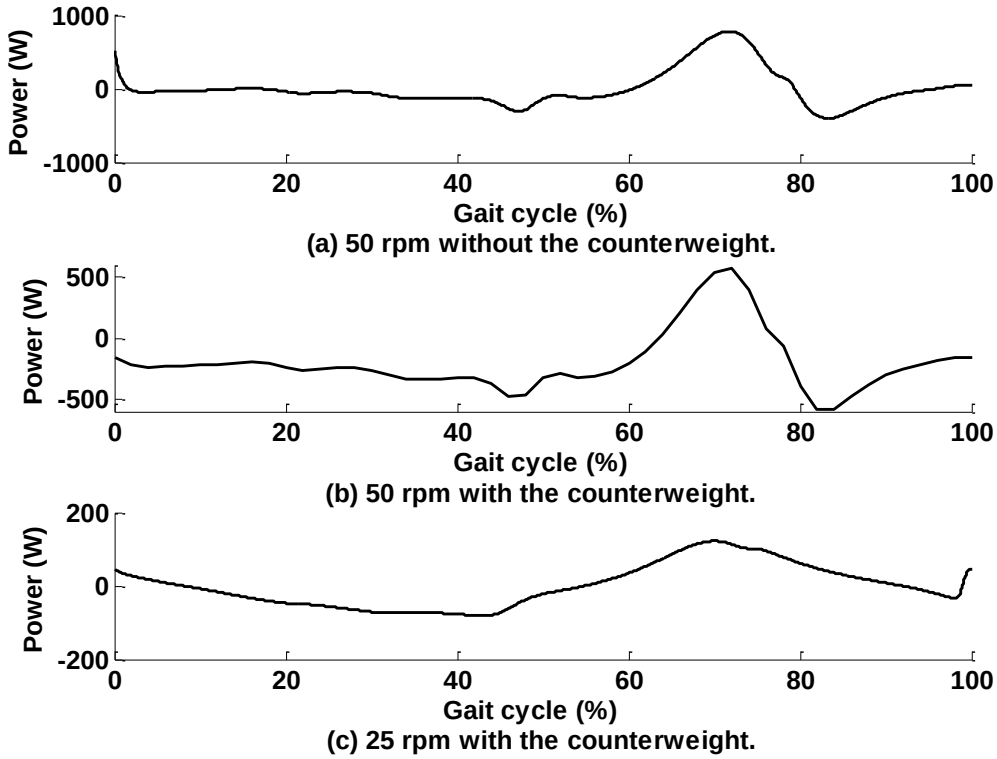

Figure 5.17: The simulated power for the bar-cam GOER system with the leg frame in three different conditions.

Compared to Figure 5.16, the power increased from 670 to 730W (increase of 9%), due to inclusion of a leg frame. A counterweight can be attached on the extended side of the driven bar to balance the system, which reduces the power requirement. Assume the counterweight is mounted at the rocker tip of the bar linkage, which is 0.4 m from the pivot (l_c = 0.4, see Table 5.2). The mass of the counterweight M_{cw} to balance the motionless GOER system can be calculated as

$$M_r g \frac{l_c}{2} + M_{cw} g L_{cw} = M_{lf} g \frac{L_l}{2} + \mathrm{M}_l g \lambda L_l + M_b g \frac{L_b}{2} \tag{5.45}$$

where M_r, M_{lf}, M_l and M_b are respectively the weight of the rocker, leg frame, human leg and driven bar. Lengths l_c, L_{cw}, L_l and L_b are respectively the length of the rocker, the distance of the counterweight from the pivot, the leg length and the length of the driven bar. The variable λ is the ratio of the centre of mass of the leg to the whole leg length, which can be obtained from the anthropometric data in Table 3.3 as 0.447. Assuming the subject has a mass of 135 kg, the weight of the leg M_l can be estimated to be 21.74 kg (135×0.161) based on the anthropometric data in Table 3.3. The mass of the leg frame M_{lf} is calculated as:

$$M_{lf} = \rho_{cs} V_{csl} \tag{5.46}$$

$$V_{csl} = L_l (W_b^2 - (W_b - 2T_b)^2) \tag{5.47}$$

where ρ_{cs} can be taken to be 7850 kg/m^3 [279]. V_{csl} is the volume of the leg frame. Equations (5.46) and (5.47) yield the leg frame mass M_{lf} = 2.1 kg. The mass of the driven bar M_b and the rocker M_r can be calculated as:

$$M_b = \rho_{cs} V_{csb} \tag{5.48}$$

$$V_{csb} = L_b (W_b^2 - (W_b - 2T_b)^2) \tag{5.49}$$

$$M_r = \rho_{cs} V_{csr} \tag{5.50}$$

$$V_{csr} = L_r (W_b^2 - (W_b - 2T_b)^2). \tag{5.51}$$

The driven bar length L_b is almost equal to the leg length L_l, based on the results from Section 4.1. Equations (5.48)-(5.51) yield M_b = 2.1 kg; M_r = 0.8 kg. With the mass of the human leg, the leg frame and the driven bar, the initial mass of the counterweight M_{cw} can be calculated as 29.1 kg using Equation (5.45).

Simulation of the model with a counterweight M_{cw} = 29.1 kg in SimMechanics/Matlab, results in a power profile as in Figure 5.17(b). It can be seen that the maximal required power for 100% of NC decreased from 730 W to 500 W (30% reduction) with the counterweight. However, a power of 500 W is still fairly large. Therefore the crank speed was reduced to half of that at 100% of NC, which becomes 25 rpm, giving a power as in Figure 5.17(c). It should be noted that the ROM of the GOER system is determined by the size of the cam-bar linkage. The current setup is designed to induce stepping performance (ROMs of the joint angles) at 100% of NC, regardless of the speed of the electric motor. Even when the speed reduces to 25 rpm, the simulated stepping performance is the same as that during overground walking at 100% of NC. The simulated power at the slower speed of 25 rpm is 120 W, which is 24% of the power at 50 rpm.

The models aimed to simulate the target trajectory, while the friction between mechanical components was not considered. As the friction in the physical system had potential to increase the power requirements, a Maxon EC 45 motor (with a maximal power of 250 W) and a planetary gearhead GP (a ratio of 236:1) were selected (Maxon motor AG, Switzerland). The CAD drawing of each component and specifications can be found in Appendix 8.

5.1.9. Conclusions

A bar linkage was designed to achieve periodic upward and downward semi-circular movement of the driven bar from continuous rotation of the crank. A cam mechanism was designed to translate constant rotation into semi-circular foot movement mimicking dorsiflexion and plantarflexion. Through computer model simulation a counterweight was determined to balance the system. Slowing down the stepping speed further reduces the required maximal power of the GOER system. The combination of a bar linkage and a cam-roller system enables the GOER system to be driven by only one DC rotary motor.

5.2. Shoe Platform Design

Apart from coordinated movements of the lower limbs, the GOER system aims to stimulate the foot sole to mimic the ground reaction forces which take place during the stance phase of overground walking. As the ground friction is small and is impractical to apply physically on the foot sole, only the upward pressure was considered for simulation of the ground reaction force. Therefore a pneumatic shoe platform was designed as described in this section.

5.2.1. Functional shoe requirements

The target performance of the dynamic shoe platform was determined based on the gait analysis results described in Chapter 3. Figure 5.18 presents the trajectory of the centre of pressure moving along the foot sole (excluding the toe) and the force amplitude profile when a representative subject (S1) walked at 100% of NC. The two

dashed lines in Figure 5.18(a) divide the foot sole into the heel, the arch and the forefoot based on the assumption that these three parts are of the same length. Figure 5.18(b) shows the upward force amplitude applied on the corresponding area of the foot over the gait cycle (GC).

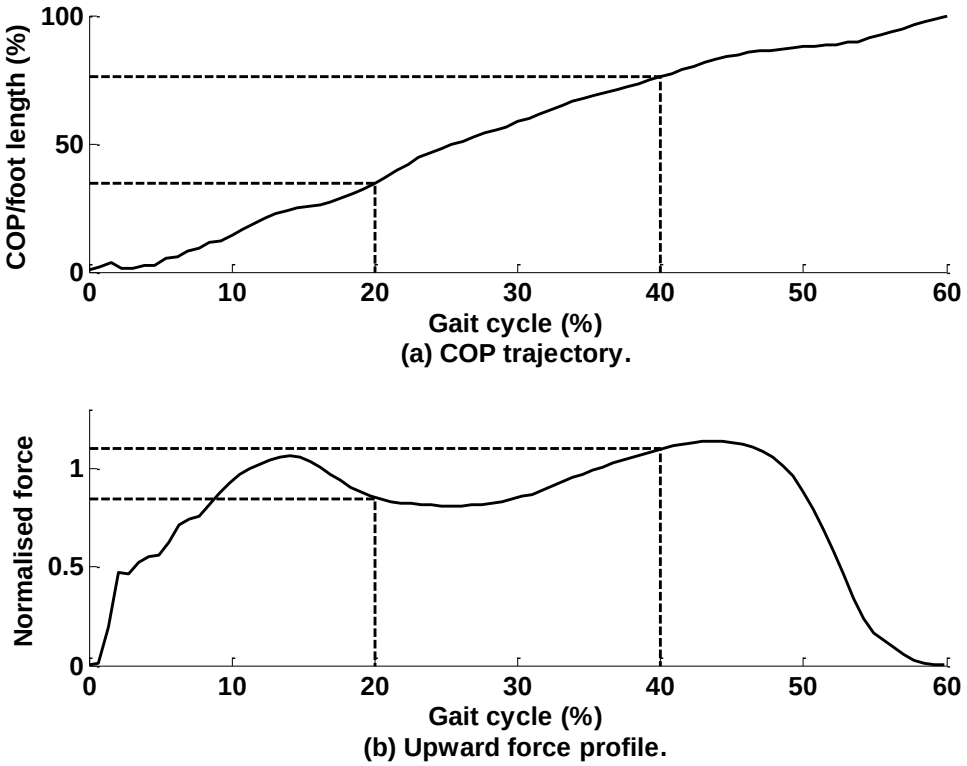

Figure 5.18: Ground reaction force during the stance phase (COP: centre of pressure).

As the foot arch seldom contacts the ground, the arc area does not share the ground force. From heel contact to 25% of GC, the ground reaction force is mainly applied on the heel, with a first peak of 1.04 times body weight, occurring at around 15% of GC. In mid-stance (25% to 35% of GC), the centre of pressure moves from the heel through the arch to the forefoot. The resultant force on the foot sole reduces from 1.04 to 0.85 times body weight. The force on the heel reduces from 1.04 times body weight to 0, while the force on the forefoot increases from 0 to 0.85 times body weight. From 35%

to 45% of GC, the force is mainly applied on the forefoot and increases to 1.2 times body weight. From 45% to 60% GC, the force on the forefoot reduces quickly from 1.2 times body weight to 0.

Based on the force data in all three subjects walking at 100% of NC (Figure 3.7), the force profile during overground walking is simplified as in Figure 5.19, with the left Y axis as the amplitude. The force on the heel, as the dashed lines show, increases to a maximal value of 1.2 times body weight at 5% of GC. This force maintains its maximal value until 20% of GC, and then reduces to 0 at 35% of GC. The force on the forefoot, on the other hand, increases from 0 to 1.2 times body weight from 25% to 40% of GC, maintains the maximal amplitude until 55% of GC, and then reduces to 0 at around 60% of GC.

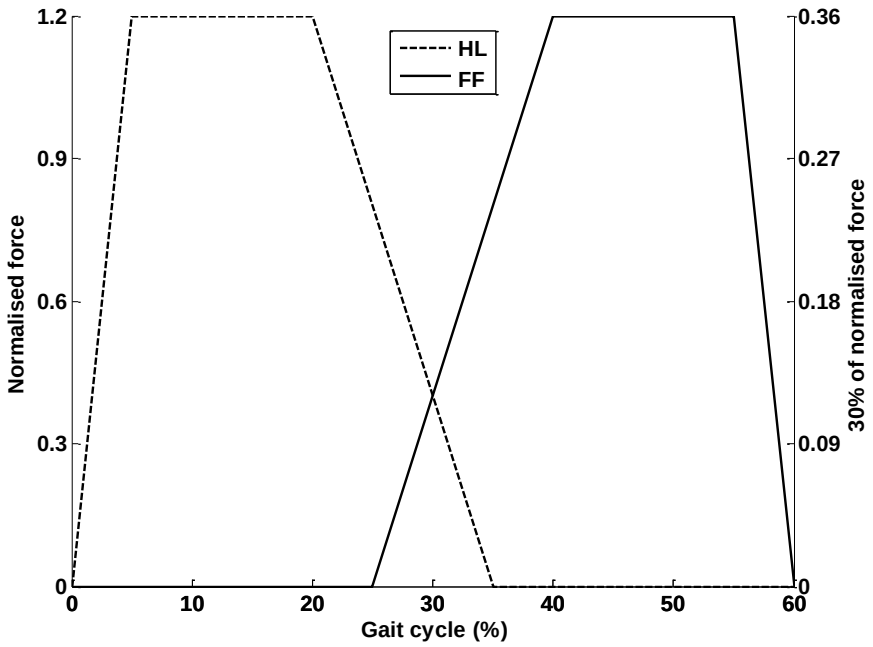

Figure 5.19: The simplified upward force profile on the foot sole to simulate walking at 100% of NC: the dashed line is the force for the heel (HL) while the solid line is for the forefoot (FF). The left Y axis shows the amplitude of the force taking place during overground walking, while the right Y axis shows the target amplitude for the shoe platform (30% of ground reaction force).

As the dynamic shoe platform is designed for patients who are vulnerable to injury, the force amplitude should be carefully designed to avoid activation of reflexes and uncontrolled spastic movements of the leg [280], to ensure safe usage. Upright walking rehabilitation programmes typically use body weight support to reduce the load on the patient's foot according to the physical condition of each patient. 30% of body weight is often adopted to activate the loading receptors on the foot soles of the patient [7, 261]. Therefore the force amplitude produced by the shoe platform is designed to be limited to 30% of that taking place during overground walking. The target force amplitude for the shoe platform is shown in the right Y axis in Figure 5.19, with the maximum as 0.36 times body weight.

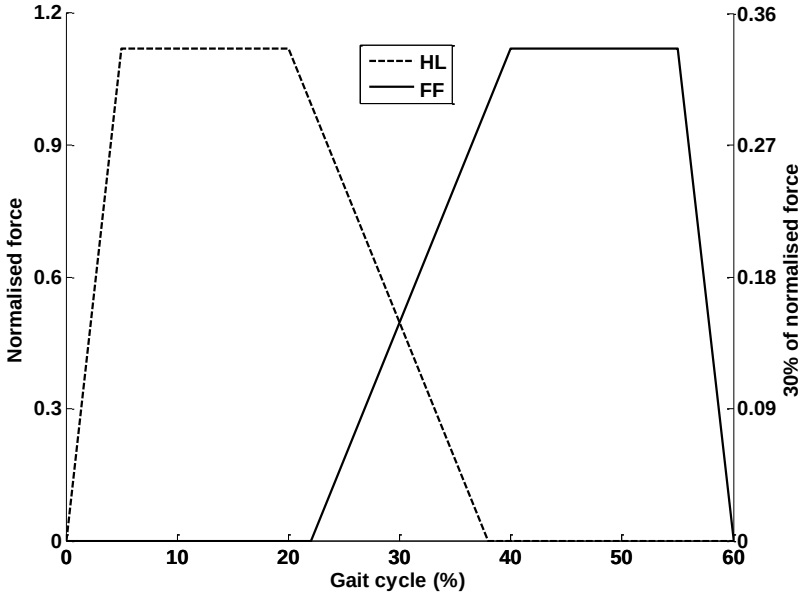

(a) 75% of NC.

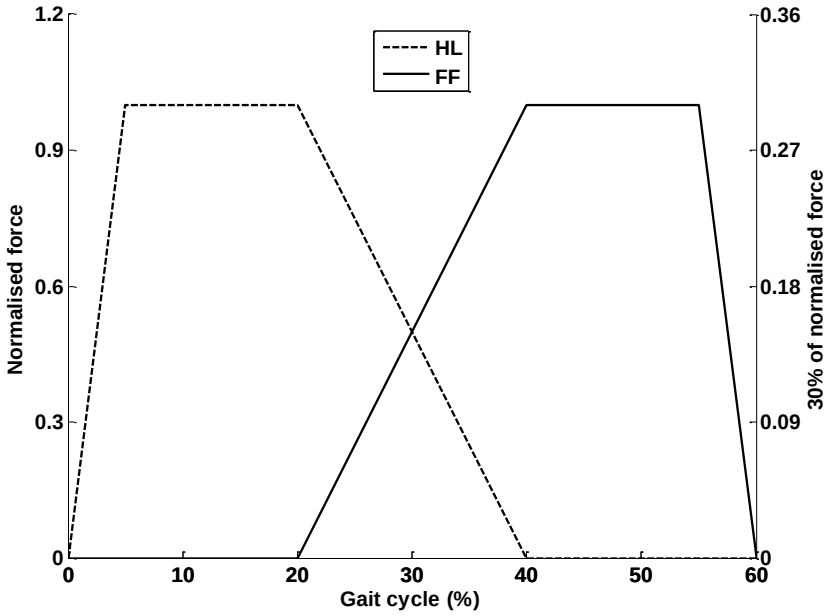

(b) 50% of NC.

Figure 5.20: The simplified upward force profile on the foot sole to simulate walking at 75% and 50% of NC: the dashed line is the force for the heel (HL) while the solid line is for the forefoot (FF). The left Y axis shows the amplitude of the force taking place during overground walking, while the right Y axis shows the target amplitude for the shoe platform (30% of ground reaction force).

The force profiles for slower walking, based on the experimental data in Chapter 3, are quite similar to that during 100% of NC, but the amplitudes of double peaks reduce as the speed reduces. Furthermore, the force during the mid-stance phase is close to the body weight. Therefore the simplified force profile for slower walking is designed as in Figure 5.20. The differences between the simplified force profiles at slower speeds from those at 100% of NC have two aspects. Firstly the constant value on the heel and the forefoot reduces from 1.2 times body weight at 100% of NC to 1.12 and 1.05 times body weight at 75% and 50% of NC. Furthermore, the time for the force on the heel starting to reduce and for the force on the forefoot starting to appear reduces from 25% of GC at 100% of NC, to 23% and 20% of GC at 75% and 50% of NC, respectively, resulting in a force which is only 0.8 times body weight at 100% of NC, increasing to

0.99 and 1.05 times body weight during mid-stance at 75% and 50% of NC.

According to the anthropometric data in Table 5.4, body weight for 95% of men is below 94 kg and that for 95% of women is below 81 kg [281]. Thus, 30% of maximum force is 332 N for 95% of men and 286 N for 95% of women. The target forces for the shoe platform simulating stepping at three speeds are summarized in Table 5.4.

Table 5.4: Anthropometric data and target maximal force requirements of the shoe platform [281].

	Anthropometric data for 95% of population			Target maximal force (N)		
	Foot length (m) (without the toe)	Foot breadth (m)	Maximal mass (kg)	100% of NC	75% of NC	50% of NC
Men	0.21 to 0.25	0.08 to 0.11	94	332	310	290
Women	0.17 to 0.22	0.07 to 0.10	81	286	267	250

5.2.2. Shoe platform components

The anthropometric data in Table 5.4 show that the length of the shoe should be adjustable from 0.17 to 0.25 m. The shoe width varies by only 0.04 m among 95% of the population. Therefore the shoe width is designed with a mean value of 0.09 m to suit most of the population. As shown in Figure 5.21(a), the shoe platform is made of two foot plates (grey) and two pressure plates (purple). The two foot plates can be connected using different nut positions, resulting in an adjustable total length. The two pressure plates, one for the heel and the other for the forefoot, can be moved up and down by two pneumatic cylinders (see Figure 5.21(b)), which are fixed at the bottom of the shoe (see Figure 5.21 (c)).

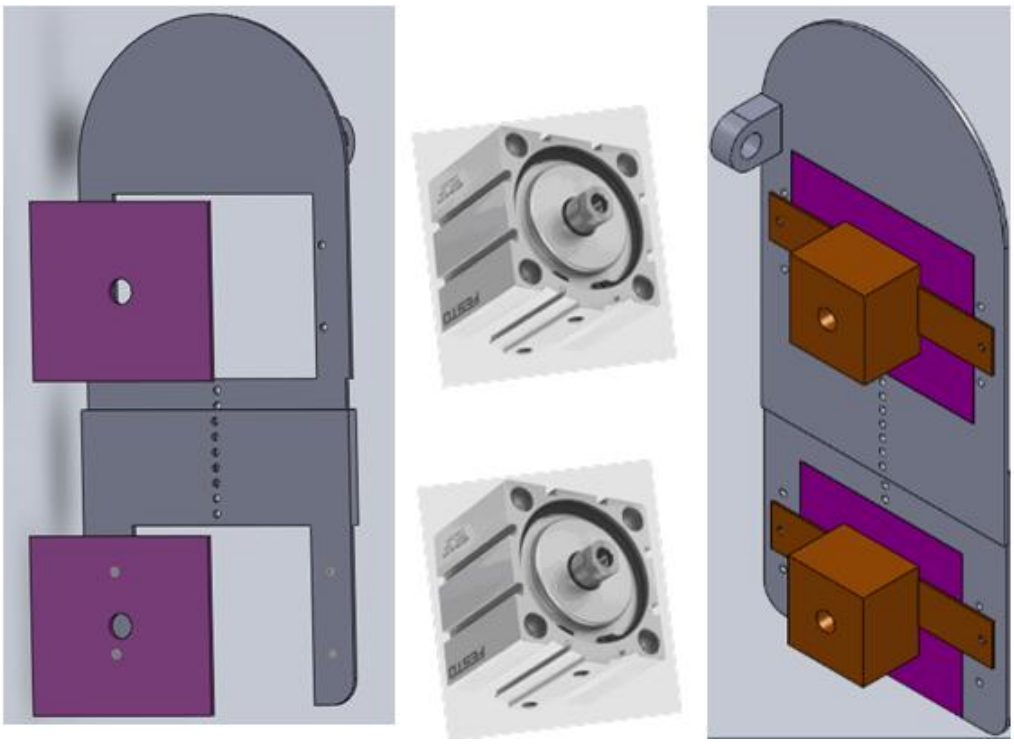

(a) Exploded view. **(b) Cylinders.** **(c) Bottom view.**

Figure 5.21: Pneumatic shoe platform.

We assume each pressure plate is 0.002 m in thickness (T_p) and 0.07 m in length (L_p). The pressure plate can endure a force up to 330 N. The compressive stress of the pressure plate σ_p can be calculated to be 2.36 MPa with the following equation:

$$\sigma_p = \frac{F_p}{L_p T_p} \tag{5.52}$$

Such a small value of σ_p allows aluminium alloy (the compressive strength of Aluminum 2014-T6 is 470 MPa[5]) to be used as potential materials for the shoe platform. The CAD drawing of each component can be found in Appendix 9.

[5] Available from http://www.matweb.com/. Accessed on 16/05/2012.

The technical specifications and geometries of the foot platform enable selection of pneumatic components. The upward and downward movement of the foot induced by the mechanical motion of the pressure plate should be as small as possible, to reduce influence on the target motion profile of the ankle joint. Therefore pneumatic cylinders with a short stroke of 10 mm are desirable. The available compressor can provide a constant pressure (P_p) of 0.6 MPa. Therefore two cylinders which can induce forces up to 330 N at 0.6 MPa are required.

Two types of cylinder (FESTO Ltd., Germany) had specifications meeting our target. Cylinder One was 32 mm in piston diameter and 20 mm in stroke, which can normally generate forces up to 483 N at 0.6 Mpa. This cylinder could achieve the target force amplitude (maximum of 332 N), but the stroke of 20 mm was very long, which might induce too much movement on the foot and disturb the target ankle rotation. Cylinder Two, which was one size smaller than Cylinder One, had a piston with 25 mm in diameter and 10 mm in stroke. It could normally generate forces up to 295 N at 0.6 MPa, which was 11% lower than the target maximal amplitude. Currently no study confirms how much force is required on the foot sole to mimic the sensation of ground reaction forces without activation of a withdrawal reflex. The theoretical basis is lacking regarding how much stroke is acceptable for mechanical stimulation of the foot without inducing measurable disturbances to the ankle angle. Therefore, a Cylinder One and a Cylinder Two were chosen, which allows investigation of suitable force amplitude and acceptable stroke for mechanical stimulation of the foot.

5.3. Prototype Presentation

In order to prove the design concept, the GOER mechanism with a shoe platform was manufactured. Theoretically the GOER system should have mechanisms for both legs. However, a simplified mechanism for one leg only was manufactured to test the design concept.

The GOER prototype, as shown in Figure 5.22, included a leg frame (1) to fix and support the user's leg. The leg frame was made of carbon steel and weighed 2.1 kg. The shoe platform (2), which was made of aluminium alloy and weighed 0.5 kg, was connected to the leg frame through a hinge around the ankle joint and to the driven bar (3) around the toe area. The bar linkage (4), mounted on the other end of the driven bar, moved the leg upwards and downwards. Foot rotation (plantarflexion and dorsiflexion) was achieved by a cam (5). The compound movements of the bar and the cam, as shown in Figure 5.24(a), produced walking-like stepping movements of the lower limb in a supine position. The shoe platform, as shown in Figure 5.23, had a foot plate and two pressure plates connected through two cylinders. Solenoid valves were employed to provide air through the blue air supply tube, so as to apply mechanical force stimulation on the foot sole, with force profiles shown in Figure 5.24(b).

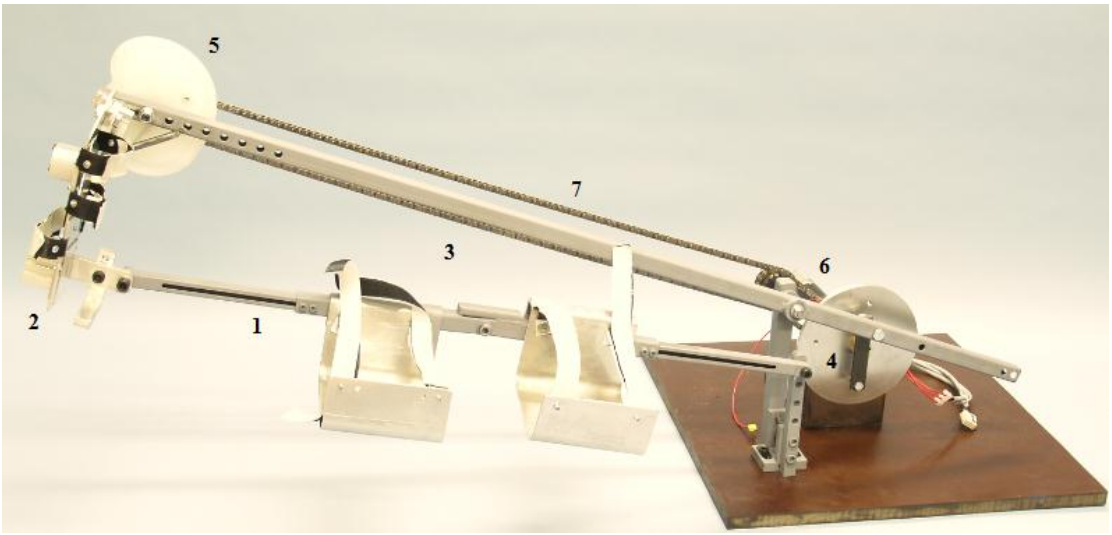

Figure 5.22: The GOER prototype. The user places the leg in the leg frame (1) and the foot on the shoe platform (2). The leg is moved by a driven bar (3), which is moved via a bar linkage (4). The foot is rotated by a cam (5). The electric DC motor (6) rotates the bar-linkage and transmits rotation to the cam via a chain (7).

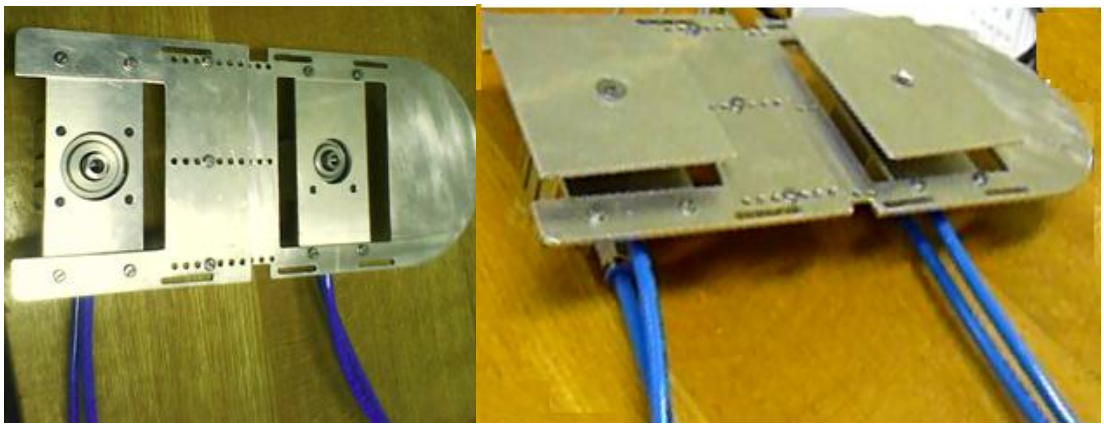

(a) The foot plate. **(b) The two pressure plates rise for mechanical simulation.**

Figure 5.23: The shoe platform.

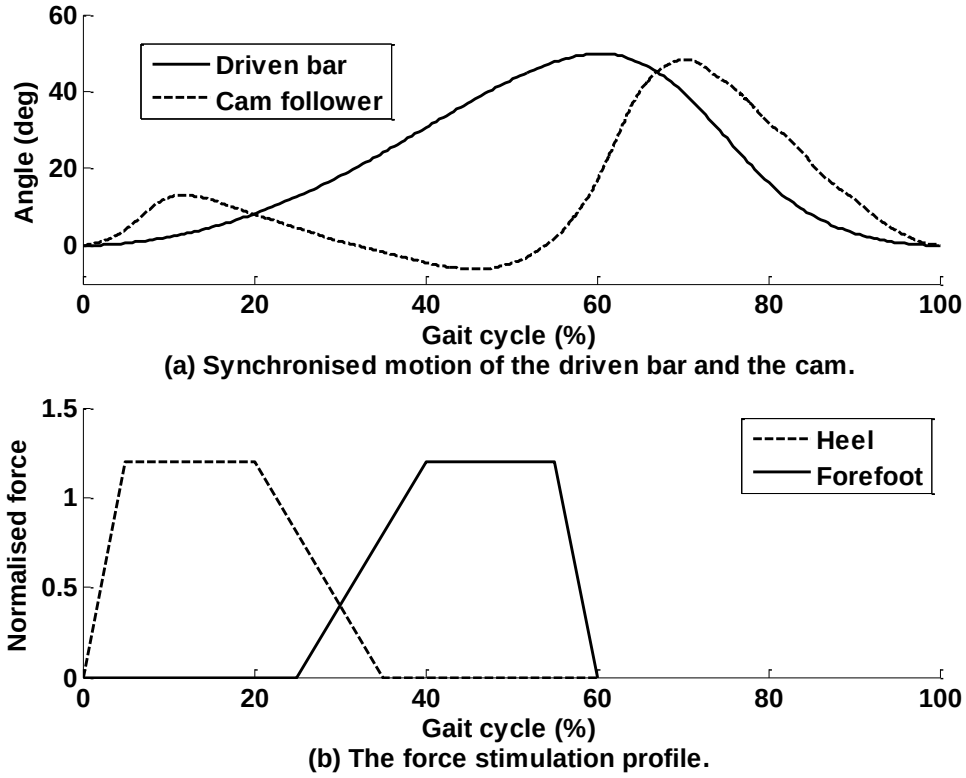

Figure 5.24: The prototype performance.

The GOER prototype has an adjustable length of the driven bar and the leg frame. However, the cam and the motor are connected by a chain with a fixed length for motion transmission. Therefore the distance between the cam and the fixing point of the driven bar is set at 1 m, which constrains the potential users of the GOER prototype to a leg length of 1 m. Nevertheless, the GOER prototype with a fixed leg performance (joint angles targeting those occurring at normal walking speed only) can still be used to investigate the design concept of the GOER system.

5.4. Conclusions

Computer simulation showed a high power requirement for the simple two-bar GOER system. After a bar linkage and a cam-roller mechanism were designed, the simulation

results showed a reduction in the power requirement for the system. The dynamic shoe platform was designed with pneumatic elements selected for force application. These design concepts allowed manufacture of the prototype for further experimental evaluation, as detailed in Chapter 6.

Chapter 6. Experimental Evaluation of the GOER Prototype: the Bar-cam System

Summary: The GOER prototype has two main elements: a bar-cam system to move the lower limbs in the coordinated manner of walking and a dynamic shoe platform to provide mechanical stimulation on the foot sole for imitation of the ground reaction forces. This chapter evaluated the performance of the first element. The second aspect is evaluated in Chapter 7. Driven by an electric motor, the GOER prototype produced supine stepping performance. The kinematics of stepping were investigated through a preliminary test of the GOER prototype with an empty leg frame, followed by a test on three able-bodied subjects whose legs were moved by the GOER prototype. The angles of the hip, knee and ankle joints during supine stepping were measured and compared with the corresponding target values during overground walking. The ranges of motion (ROMs) of the lower limb joints were found to be within the physiological ranges of overground walking.

6.1. Introduction

Patients with spinal cord injuries often have impaired function in the lower limbs. With the aim of improving walking ability, they participate in rehabilitation programmes to practise synergistic walking. It is contended that practising movement within the physiological range of motion (ROM) promotes the integrated function of locomotion control [235]. The GOER system was designed to promote early rehabilitation of walking with patients in a supine position. Computer simulation showed that the GOER model induced physiological ROMs in the joints of the lower limb [2], which

provided a basis for the design and manufacture of a GOER prototype.

This experimental study evaluated performance of the GOER prototype, with focus on the leg motion. The performance of the prototype was initially investigated with an empty leg frame which served as a mechanical model of the leg. After the prototype was able to induce physiologically acceptable ROMs of the joint kinematics in the leg frame, three able-bodied subjects were recruited to use the GOER prototype for passive supine stepping. The ROM of the hip, knee and ankle joints were compared with overground walking.

6.2. Methods

The mechanical components, especially the drive system, of the GOER prototype are described, followed by a description of the experimental procedure for the evaluation of the lower limb motion.

6.2.1. The GOER system description

The GOER prototype, as shown in Figure 6.1, includes a leg frame (1) and a foot platform (2). The upward and downward periodic movement of the leg is produced by the driven bar (3), which is rotated via a bar linkage (4). The ankle rotation is driven by a cam (5). The main driver is an electric motor (6), which rotates the bar linkage and transfers power to the cam via a chain (7). The user puts the leg in the leg frame, with the hip, knee and ankle joints aligned at positions A, B and C. The leg frame is attached to the tip of driven bar D. The bar linkage is arranged to induce 50^{o} rotation of the driven bar at the point E, resulting in fixed ROMs in the leg (frame) joints

which correspond to the ROMs occurring during walking at normal speed, which are 34^o, 51^o and 30^o in the hip, knee and ankle joints, respectively (see Chapter 3 for mean ROM of each joint). As the distance between the cam and the fixing point of the driven bar is set at 1 m, the GOER prototype is best suited to users with a leg length of 1 m to practise stepping with a fixed step length of 0.85 m (normal speed of 1.42 m/s from Table 3.4). A detailed description of the GOER prototype is in Section 5.3.

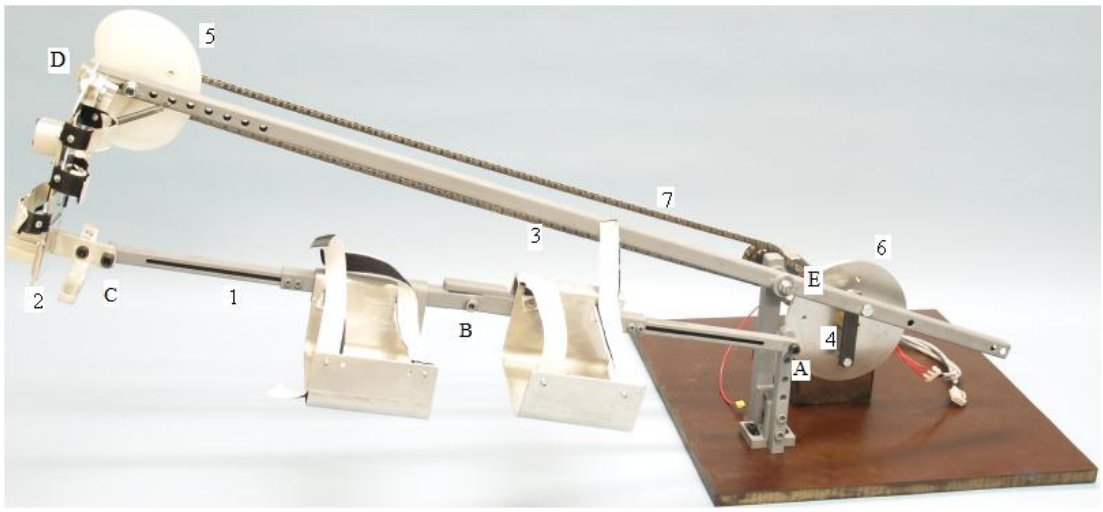

Figure 6.1: The GOER prototype. The user places the leg in the leg frame (1) and the foot on the shoe platform (2). The leg is moved by a driven bar (3), which is actuated by a rotary bar linkage (4). The foot is rotated by a cam (5). The DC motor (6) rotates the bar-linkage and transmits rotation to the cam via a chain (7). The trajectories of the leg frame (including the joints of the hip (A), knee (B) and ankle (C)) and the driven bar (including the tip (D) and the pivot point (E)) are recorded to investigate the motion induced by the GOER prototype.

The drive system in the GOER prototype includes a Maxon motor and a gearbox (Maxon motor AG, Switzerland), with specifications provided in Appendix 8. The motor incorporates a speed measurement device: an encoder HEDL 9140, which has three channels with a maximal operational frequency of 100 kHz. The motor controller system was provided by Mr. Calum Cossar from the SPEED Laboratory, University of

Glasgow[6]. The controller FCIV (FC represents the flexible controller and IV means the fourth generation), as shown in Figure 6.2, consists of a hardware control unit connected to a PC with a standard RS 232 serial interface. A control panel (Figure 6.3) is designed with Visual Basic software, which allows input of the target speed, and displays the actual motor speed. The controller system and the power electronics are described in Appendix 10.

Figure 6.2: FCIV motor controller platform.

[6] SPEED lab. *Scottish Power Electronics and Electric Drives Consortium*. Available from: http://www.gla.ac.uk/departments/speed/. Accessed on 15/05/2012.

Figure 6.3: The controller panel.

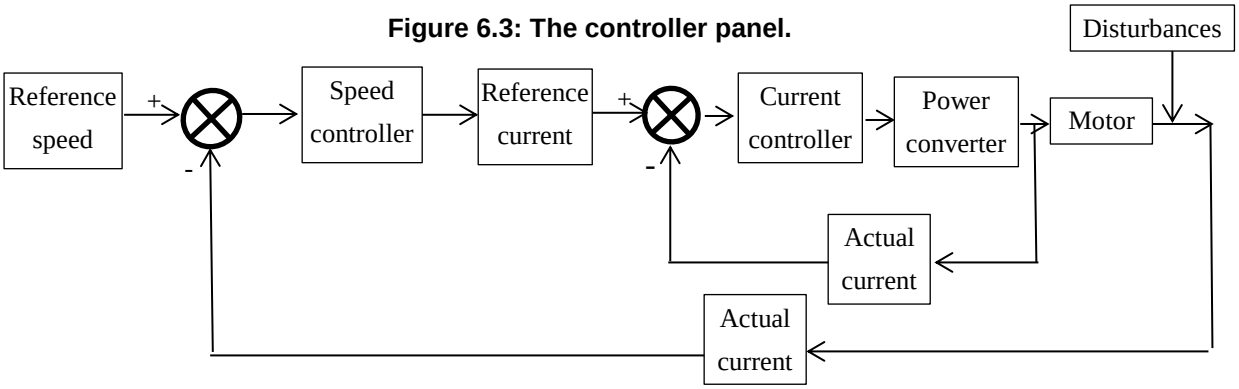

Figure 6.4: The control loop.

The speed controller algorithm, which is programmed with Code Composer Studio software, includes a speed loop and a current loop (see Figure 6.4). Based on the actual position measured by the encoder in the motor unit, the speed loop gives out the reference current by calculating the difference between the actual speed and the reference speed. Then, the current loop calculates the current input for the motor by comparing the difference between the reference current and the actual current measured by the current sensor [282]. The control loops adopt PI control algorithms, with parameters Speed K1, Speed K2 for the speed loop and iK1, iK2 for the current

loop. The parameters Speed K1 and Speed K2 are constant at 18 and 15. Parameter iK1 adjusts the speed rise time, while the difference between the two parameters iK1 and iK2 modifies the steady-state error, i.e. the smaller the value of (iK1-iK2), the closer the actual speed approaches the reference speed. The two parameters iK1 and iK2 are tuned through testing to achieve constant speed rotation, which is documented in the next section.

6.2.2. Experimental procedures

In order to control the GOER prototype, the controller parameters iK1 and iK2 were tuned to achieve constant-speed rotation. Then evaluation procedures were initiated which included two parts: a preliminary test on the GOER system with a leg frame model (model-leg-only) and an experiment with three able-bodied subjects using the GOER system without employment of the leg frame (subject-leg-only). Ethical approval was obtained from the Ethics Committee for Non Clinical Research, Faculty of Biomedical & Life Sciences, University of Glasgow.

Tuning of the controller parameters

Given the requirements for the GOER prototype, the controller performance was defined to achieve the reference speed in less than 10 s with an error less than 1%. Two reference speeds of 1000 rpm and 1500 rpm were tested. During the parameter tuning, the GOER prototype was connected to an empty leg frame. As the GOER system was designed for users with incomplete SCI, who might produce voluntary movements during training, the controller of the GOER prototype needs to be robust to such disturbances. A 2 kg object was added to the knee joint of the frame at a random phase of the gait cycle so as to simulate a disturbance on the GOER system.

Preliminary test on the model-leg-only system

A leg frame as shown in Figure 5.22 was used to simulate a human leg with a thigh length of 0.56 m and a shank length of 0.53 m. In order to prevent hyperextension of the knee joint, which could easily take place in a supine position because of gravity, the length of the leg frame (1.09 m) was arranged to be larger than the target leg length (1 m), so that the whole leg frame was slightly flexed throughout the gait cycle.

As discussed in Chapter 5, the GOER system needs a counterweight, the mass of which needs to be determined for the model-leg-only system. As discussed in Section 5.1.7, the counterweight for the model-leg-only system M_{cwm} can be determined as

$$M_r g \frac{l_c}{2} + M_{cwm} g L_{cw} = M_{lf} g \frac{L_{lf}}{2} + M_b g \frac{L_b}{2} \tag{6.1}$$

where L_{cw} is the distance between the counterweight and the supporting point of the driven bar, which is 0.4 m. M_r is the mass of the rocker, which is 0.8 kg, while M_{lf} is the mass of the leg frame, which is 2.1 kg (see Section 5.1.7). L_l is the leg length, which is 1 m. L_b is the length of the driven bar, which is almost equal to the leg length, while M_b is the mass of the driven bar, which is 2.1 kg. Therefore M_{cwm} is calculated to be 4.78 kg for the model-leg-only system.

After balancing with the counterweight, the GOER prototype with an empty leg frame was actuated to produce motion. The ROMs of the driven bar and the leg frame were measured by an ultrasound system (zebris Medical GmbH, Allgäu, Germany), which is a commonly used device for motion capture based on the travel time of ultrasound

waves[7]. As shown in Figure 6.1, the marker placements of the zebris system were at the joints of the hip (point A), the knee (point B) and the ankle (point C) on the leg frame as well as at the tip of the bar near the toe area (point D) and the pivot (point E) on the driven bar. Furthermore, potential failure modes of the GOER prototype were investigated and are described in Appendix 11.

Subject-leg-only sub-test

After the GOER prototype was confirmed to induce safe ROMs in the leg joints, three male able-bodied subjects (detailed information provided in Table 6.1) were recruited to use the GOER prototype. Although a leg frame was designed in the GOER system to support the user's leg weight, this sub-test was performed without the frame so that the overall load on the GOER prototype was reduced to avoid damage to the plastic cam.

This subject-leg-only system required readjustment of the mass of the counterweight, denoted now as M_{cws}. The leg frame was not included. Furthermore, the human leg, which was actively supported by the subjects, was assumed not to put additional load on the system. Therefore the mass of the counterweight M_{cws} can be calculated as

$$M_r g \frac{l_c}{2} + M_{cws} g L_{cw} = M_b g \frac{L_b}{2} \tag{6.2}$$

which gives M_{cws} = 2.19 kg for the counterweight adopted in the subject-leg-only system.

[7] Zebris system: Available from: http://www.zebris.de/. Accessed on 18/05/2012.

Table 6.1: Subject information (all male).

Subject	Age (years)	Thigh length (m)	Shank length (m)	Foot sole length (m)	Body mass (kg)
S1	26	0.48	0.52	0.26	85
S2	24	0.51	0.55	0.28	84
S3	23	0.52	0.58	0.28	86

During the test, the subject lay down on a mattress, as shown in Figure 6.5. The subject supported himself with the right leg on the ground. The left foot was attached to the foot platform using Velcro straps. The subject was encouraged to support the weight of the left leg voluntarily, but to follow the motion induced by the GOER prototype. In order to record the motion of the driven bar, the first zebris marker was placed at the pivot point E. As the presence of the foot on the foot plate would disrupt ultrasound recording of the toe point, the second zebris marker was placed at the point D on the driven bar, which was 0.9 m away from the pivot point E. In order to record the leg motion produced by the GOER prototype, zebris markers were placed at the joints of the knee B and the ankle C on the subject's leg, as shown in Figure 6.5. In order to estimate the position of the hip joint, a fixed point A on the frame, which was 0.13 m above the hip joint, was selected to place a further zebris marker.

The sampling frequency of the zebris system was set to be 100 Hz in all experiments. Two different motor speeds of 1000 and 1500 rpm were tested for the GOER prototype, resulting in stepping cadences of 4 strides/min and 6 strides/min, and stepping speeds of 0.41 km/h and 0.61 km/h, respectively. Each stepping session was repeated three times to calculate the mean performance. The subjects filled out a form describing their experience of using the prototype (see Question Sheet in Appendix 12).

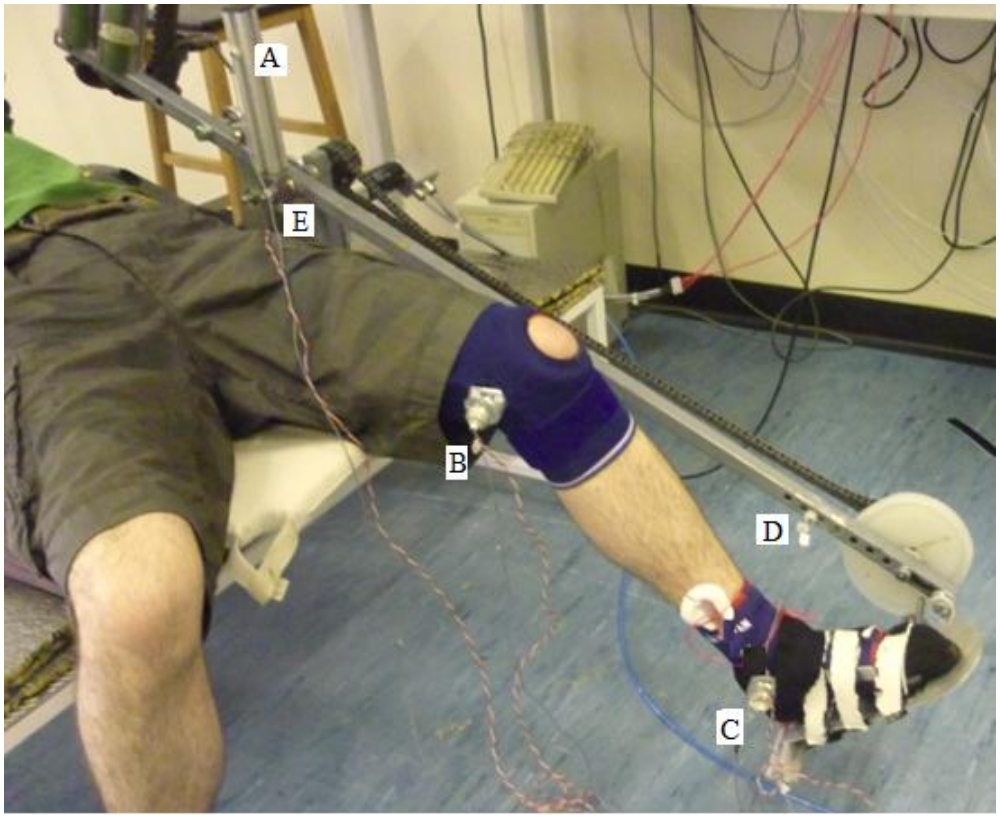

Figure 6.5: The test setup with a subject.

The angle trajectories of the hip, knee and ankle joints within a stepping cycle were analysed. The recorded data were visually observed to remove outliers, and were filtered with a window size of 5 to remove noise, and were finally smoothed with the loess or rloess Matlab functions. In order to make the joint performance easier to interpret, stick diagrams were plotted to show the stepping performance of Subject S1. The supine stepping was rotated 90^{o} to be upright in the diagram so as to be comparable with overground walking. The performance of the same subject walking overground (collected in the gait analysis experiment in Chapter 3) is provided for comparison. The kinematics of the leg frame and subjects' legs in the GOER system were simulated with the bar-cam model developed in Section 5.1.5. The simulated results are presented for comparison.

6.3. Results

Results of the preliminary test with an empty leg frame are presented, followed by the experimental results on three male able-bodied subjects. Model simulation results are presented for reference.

6.3.1. Preliminary test

With a counterweight of 4.78 kg, the model-leg-only system was balanced. It was observed that when iK1 = 100 and iK2 = 90, the controller criteria were met, i.e. the motor reached the reference speed in less than 10 s and followed the reference speed with an error less than 1%, regardless of the disturbance to the GOER system. As shown in Figure 6.6, the motor achieved constant rotation speed for the reference speeds of 1000 rpm and 1500 rpm after acceleration for 5 s and 7.3 s respectively. The motor rotated at 998 rpm and 1495 rpm during the steady state, with errors of 0.2% and 0.33% for their reference speeds. The downward and upward arrows in Figure 6.6 showed the time when the disturbance (an object of 2 kg) was added and removed from the prototype. The disturbance did not affect the constant speed rotation. The speed profile at 1000 rpm in Figure 6.6(a) is smooth, while that at 1500 rpm has regular jitterings, which are marked with stars in the speed curve of 1500 rpm in Figure 6.6(b).

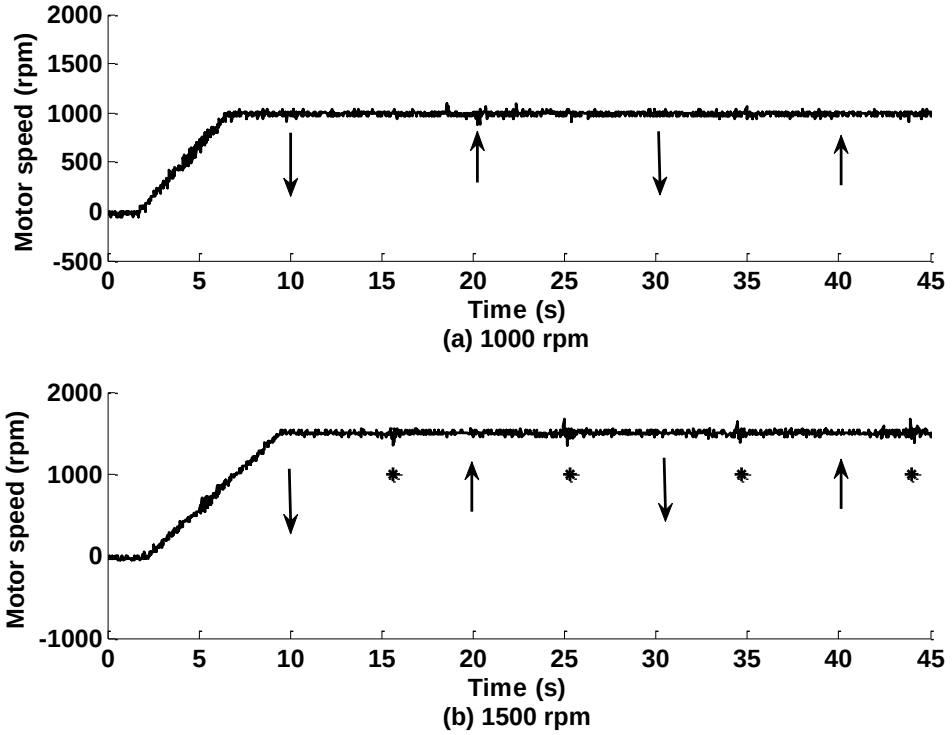

Figure 6.6: The motor speed with an empty leg model (leg frame). The downward and upward arrows show the time when the disturbance was added and removed from the leg frame. The stars mark the observed jittering.

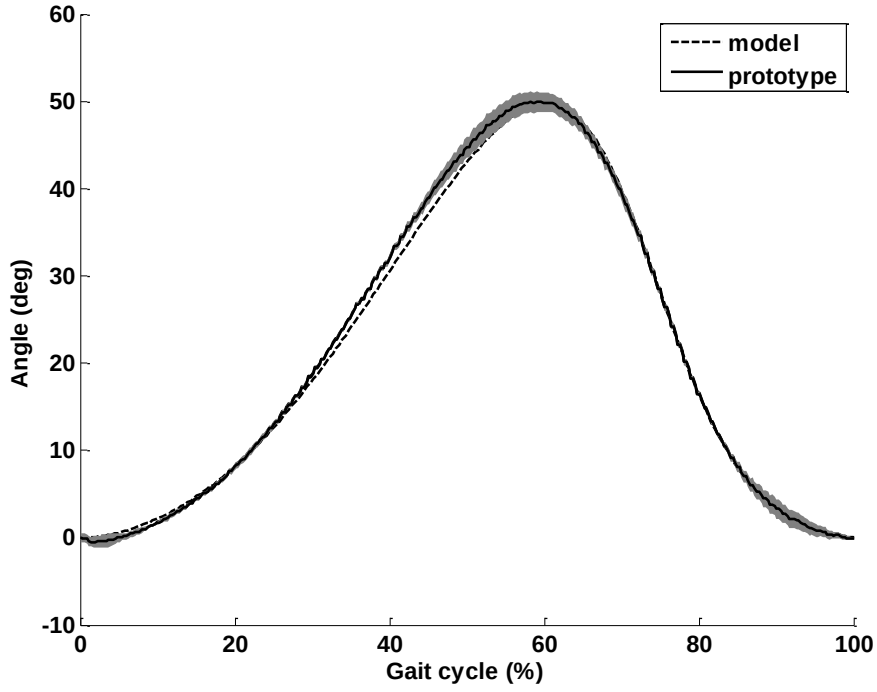

Figure 6.7: The performance (mean ± SD) of the driven bar. The solid line is the performance from the test while the dashed line shows the model simulation of the bar-cam system as described in Figure 5.9.

The mean performance of the driven bar at motor speeds of 1000 rpm and 1500 rpm is displayed in Figure 6.7, with the standard deviation (SD) shown as a shaded area. The simulated performance from the bar-cam model (the solid line in Figure 5.9) is shown in Figure 6.7 as a dashed line for comparison. The mean ROM from the GOER prototype was 50^{o}, which was similar to the simulated target performance from the model. The GOER prototype moved the driven bar slightly faster during the stance phase, but it did not interrupt the target phase ratio of 3:2.

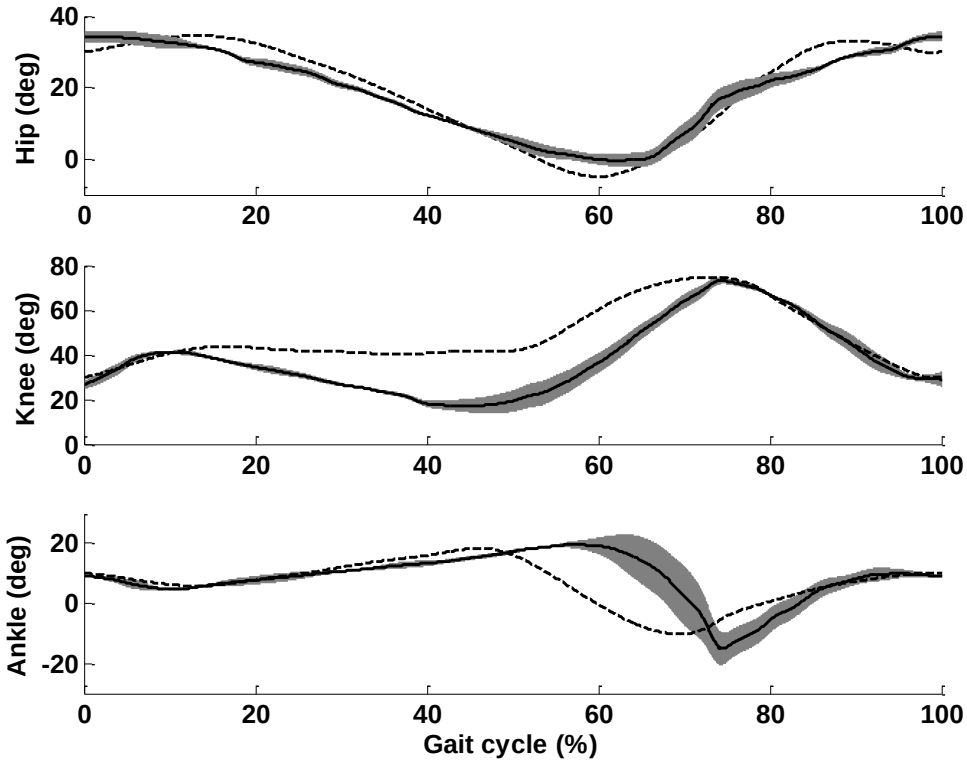

Figure 6.8: The joint performance of the leg frame. The solid lines show experimental mean values while the shaded areas are standard deviations. The dashed lines are model simulation results.

The GOER prototype induced coordinated motion of the leg frame, with the joint angles (mean ± SD) presented as solid lines and shaded areas in Figure 6.8. The model simulation results are shown as dashed lines. The hip and the knee joints of the

leg frame in both the experiment and the model were always in flexion. The knee and ankle joints of the leg frame showed jerky motion around maximal ankle plantarflexion. The experimental ROMs of the hip, knee and ankle joints were respectively 34^o, 57^o and 34^o, which were of similar ranges to the simulated results, but the experimental ankle plantarflexion happened later than the simulated ankle trajectory.

6.3.2. Test on subjects

In order to reduce the load on the cam of the GOER prototype, the subjects were encouraged to follow but not to disturb the shoe position by actively supporting their own leg weight. Due to lack of leg support, subjects reported the pelvis was not very comfortable during supine stepping (see subjects' feedback in Appendix 13). It was reported that the leg motion produced by the GOER prototype was 70% similar to walking (0 means not similar at all while 100% means identical). In contrast to joint motion measured on the empty leg frame, the tests with subjects demonstrated smooth leg movement but with large variation.

Figure 6.9 shows the joint angles (mean $\pm$ SD) of Subject S1 as solid lines and shaded areas. The model simulation results are shown as dashed lines. S1 is the same subject S1 as in the gait analysis experiment described in Chapter 3. This study took place two years after the study in Chapter 3. This subject lost weight within these two years, resulting in different masses. The stepping performance can be compared with that during overground walking. As shown in Figure 6.9, the GOER prototype induced ROMs of 29^o, 47^o and 25^o respectively in the hip, knee and ankle joints of S1, which were similar to the ROMs during overground walking (see Figure 3.4(a)). Walking performance in these two conditions is further presented in Figure 6.10.

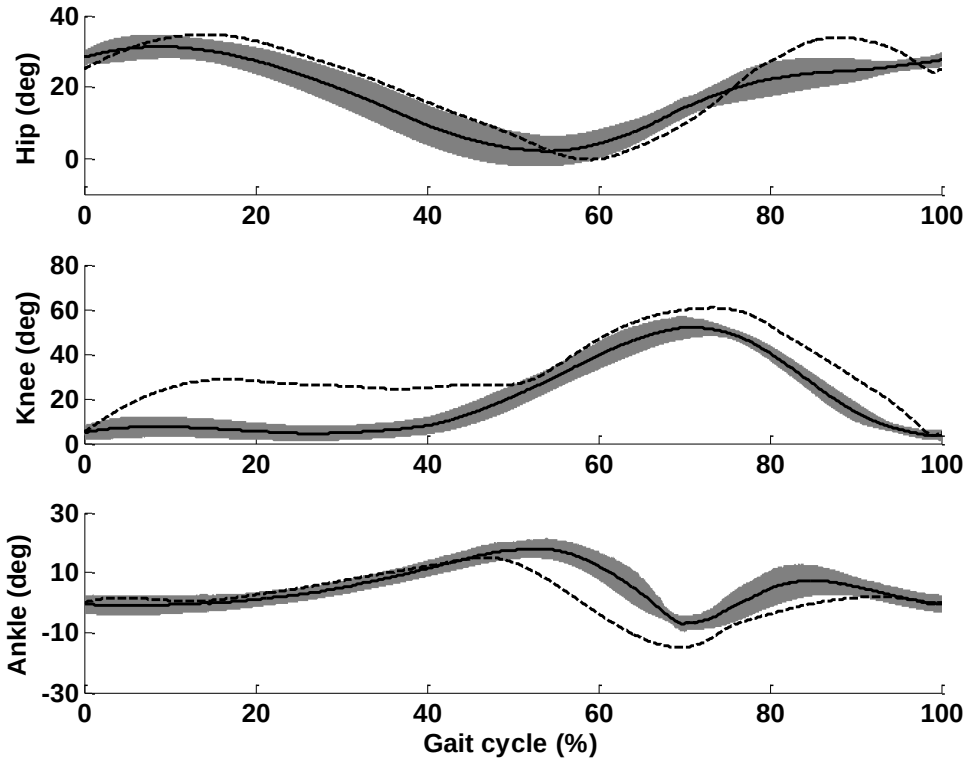

Figure 6.9: The leg performance of S1. The solid lines show experimental mean values while the shaded areas are standard deviations. The dashed lines are model simulation results.

Stick diagrams presented in Figure 6.10 show five different phases of a whole gait cycle through six sticks. The performance of supine stepping is presented in Figure 6.10(a) while that of overground walking in the same subject (results collected in the gait analysis experiment in Chapter 3) is plotted in Figure 6.10(b) for comparison. The stick diagrams start and end with heel strike, with the first four sticks as four typical positions during the stance phase, while the remaining two sticks are the swing phase. The red lines represent the thigh and shank segments, with the black circles as the centres of gravity. The red triangle at the bottom is the foot. The black circle in the middle of the foot sole represents the centre of mass, while the other one denotes the centre of pressure, which moves from the heel at heel strike to the toe during toe off. As there is no ground pressure during the swing phase, the centre of pressure is not marked in Stick 5 in either diagram of Figure 6.10.

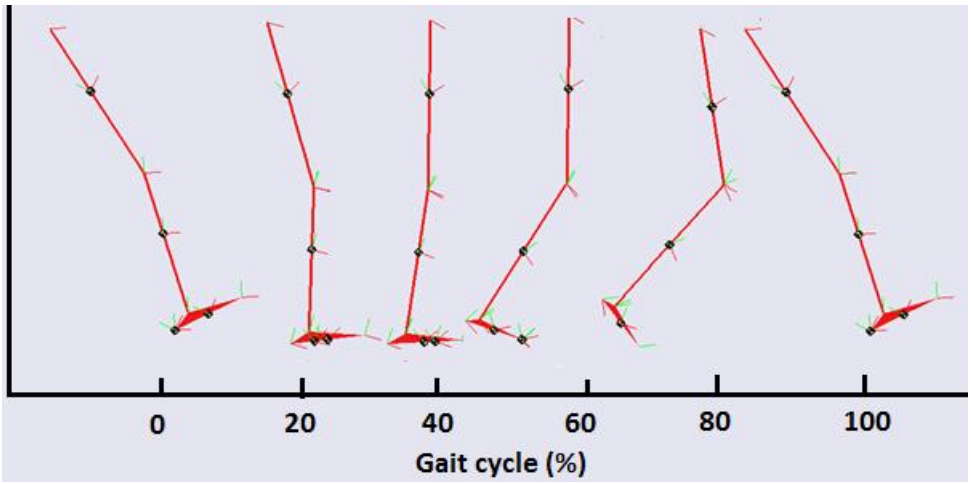

(a) Stepping in the GOER system.

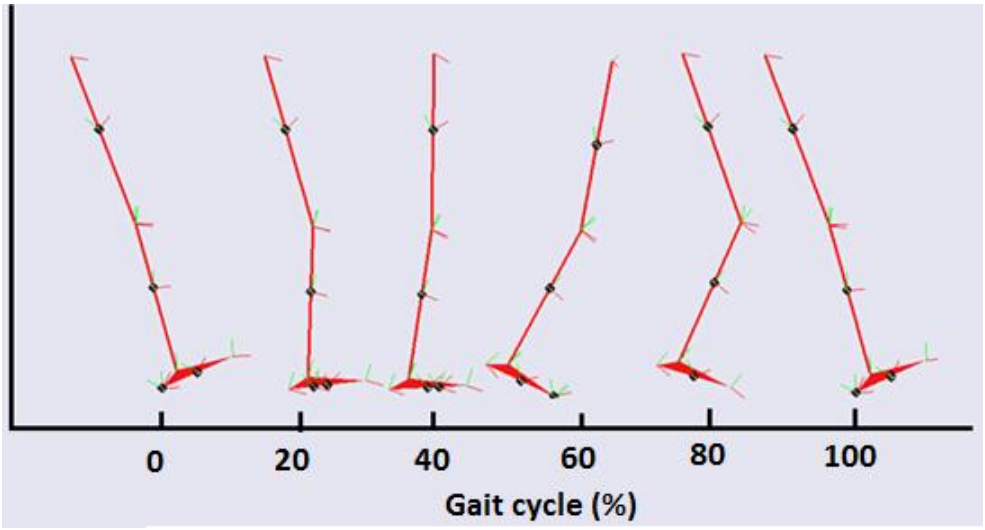

(b) Overground walking.

Figure 6.10: Stick diagram of movement in S1.

In spite of the similar ROMs, some differences between supine stepping in the GOER prototype and overground walking were observed in the hip and ankle joints. Figure 6.10 shows that supine stepping had 8^{o} more flexion in the hip joint at heel strike (Stick 1) than overground walking. Furthermore, the hip joint in the GOER prototype was hardly in extension during the toe off phase (Stick 4) compared to 9^{o} extension during overground walking. In contrast to the maximal extension taking place around toe off during overground walking, the GOER prototype delayed the maximal plantarflexion

into the mid-swing phase (Stick 5). All these differences between the motion induced by the GOER system and overground walking were also observed in Figure 6.9, by comparing the difference between experimental and simulated results.

The stepping performance of S2 and S3 in the GOER system is displayed in Figure 6.11, with simulated results presented as well. Both subjects had the hip joint in flexion throughout the gait cycle. Regarding the knee joints of all three subjects, S1 showed double-hump flexion in the knee joint with 20^{o} flexion in the mid-stance phase, while S2 and S3 showed flexion in the knee joint over the whole gait cycle, with about 30^{o} flexion even in the mid-stance phase for S3. The delay in ankle plantarflexion was more pronounced in S2 and S3 than S1.

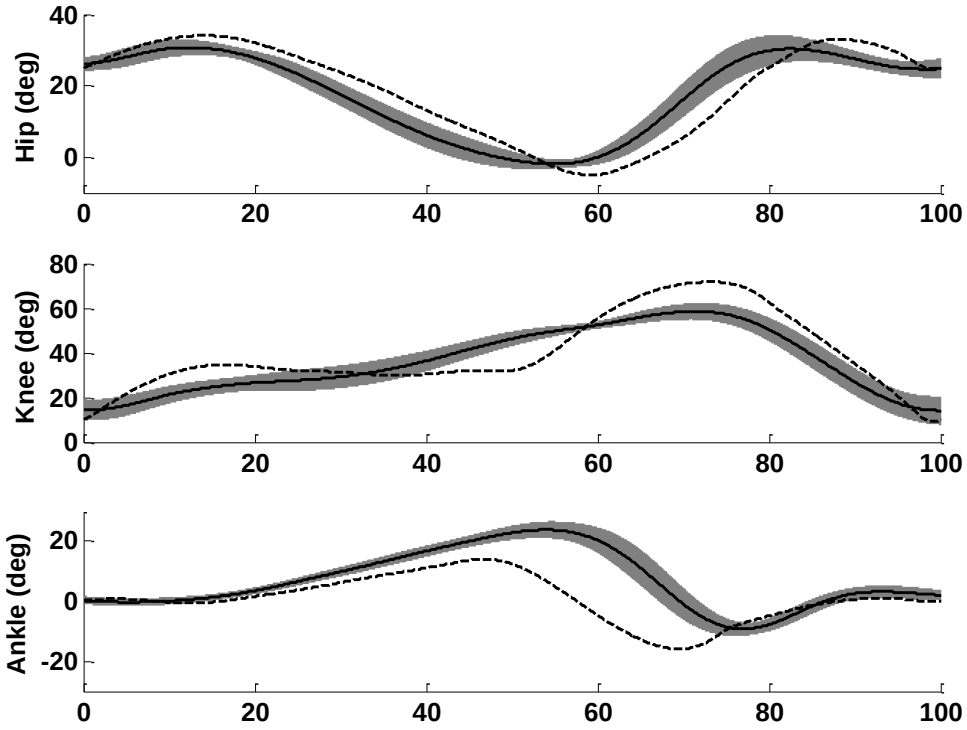

(a) S2 (mean ± SD).

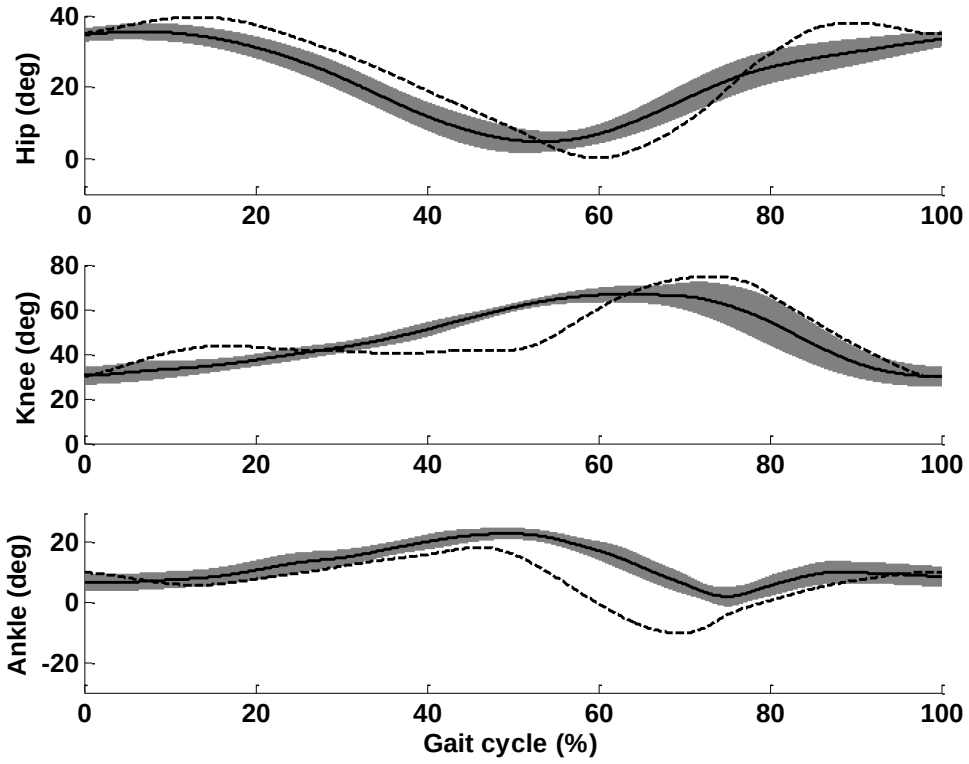

(b) S3 (mean ± SD).

Figure 6.11: The leg performance of S2 and S3. The solid lines show experimental mean values while the shaded areas are standard deviations. The dashed lines are model simulation results.

6.4. Discussion

The aim of this study was to investigate the performance of the GOER prototype and to analyse the technical feasibility of the GOER system as a rehabilitation device. The GOER system should have mechanisms to coordinate stepping of both legs. Here, the prototype was manufactured for only one leg stepping. However, the prototype under study with one stepping leg allowed evaluation of technical feasibility of the overall GOER system.

Balanced with a counterweight of 4.78 kg, the GOER prototype with an empty leg

frame was actuated with a DC motor rotating at a constant speed. These preliminary results firstly confirmed the methods of counterweight calculation (Equation (6.1)), and secondly validated the tuned controller parameters iK1 and iK2. Two different rotation speeds (1000 rpm and 1500 rpm) were tested, which resulted in different stepping speeds of 0.41 km/h and 0.61 km/h in the GOER prototype. The selection of these slow speeds was based on the properties of the weak plastic cam. Higher speeds would induce larger power transmitted from the electric motor to the leg via the cam, which would give higher load on the cam. Furthermore, low speeds are usually adopted in the early phase of walking rehabilitation. Therefore low speeds were selected in this study for the GOER prototype.

The motor achieved rotation at constant speeds of 1000 rpm and 1500 rpm. However, the speed profile at 1500 rpm demonstrated jittering (marked with stars in Figure 6.6). Compared to rotation at 1000 rpm, the motion at 1500 rpm demanded much higher power, especially at heel off, which can be seen from the power requirements of the GOER system at different speeds presented in Figures 5.17(b) and (c). Therefore the demand of a fast power increase in this phase disturbed the system, resulting in regular jittering phenomena in the speed curve at 1500 rpm. By reducing the speed to 1000 rpm, the motor rotated without jittering. The prototype was manufactured with the bar linkage and the cam to induce ROMs in the leg joints approximating those during walking at 100% of NC only. Although two different speeds were tested in the experiments, the ROM of the driven bar was theoretically the same, and was close to the simulation result, as shown in Figure 6.7.

The GOER system aimed to induce sensory inputs to the leg joints so as to promote the rehabilitation process. Therefore achieving physiological ROMs of the leg joints and

coordination of the leg segments during supine passive movements were the key objectives of this study. The preliminary test of the GOER prototype induced synchronised movements in the leg frame, with ROMs similar to simulated performance. Due to the presence of gravity, the supine leg frame tended to fall into hyperextension. Therefore the leg frame was purposely designed with a length (1.09 m) larger than the target leg length of 1 m. Keeping this in mind, it was expected to observe flexion in the hip and knee joints of the leg frame throughout the gait cycle, as shown in Figure 6.8.

The leg frame showed a jerky period in the swing phase, which was demonstrated with pointed angle curves of the knee and ankle joints at heel off (see Figure 6.8). This was because the high load applied on the weak cam disturbed constant rotation of the cam. In contrast to the bar linkage which had a counterweight to reduce the power requirement, the cam system, which did not have any specific power reduction mechanism, endured high load from the leg frame. As discussed above, the highest power requirement taking place at heel off caused a jerky rotation of the cam at this time. Largely dependent on the cam rotation, the ankle joint showed a pointed angle trajectory (jerky plantarflexion) in Figure 6.8. This problem could be alleviated by reducing the load on the cam, i.e. by reducing the leg weight. In spite of these problems, the ROMs of the hip, knee and ankle joints in the physical leg frame were within the physiological ROMs during overground walking [235], which provides a basis for safe usage.

In order to reduce the jerk problem caused by cam rotation, the test with subjects was carried out without the leg frame. Therefore the joint angles in subjects showed a smooth profile, as can be seen in Figures 6.9 and 6.11. However, reduction of load was

not a satisfactory solution, because the load, although reduced, still disturbed the cam rotation, which resulted in delayed ankle plantarflexion in all three subjects, compared to the simulated results (see Figures 6.9 and 6.11). Replacing the material of the cam with aluminium alloy might remove the jerky rotation. Compared to preliminary results of the leg frame in Figure 6.8, large variation was observed in the kinematics of the human leg, which came from the voluntary input of the subjects. It was challenging for the subjects to support their own leg weight and to follow the rotation of the shoe platform. The voluntary support of the leg weight inevitably affected the final joint motion, which resulted in large standard deviations. S1 had the best knee performance among the three subjects with double-hump flexion, mainly because his leg length was 1 m, which fitted the user requirement of the GOER prototype. S3 had a leg length 0.1 m longer than the required leg length, which resulted in flexion in the knee joint throughout the gait cycle, even during the mid-stance phase. In spite of these differences, all three subjects achieved coordinated motion of the leg, with ROMs similar to physiological motion during overground walking [235].

A limitation of this study is that the subjects were asked to support their leg weight by themselves, which caused voluntary interference to the target joint angles. Due to the simplified structure of the GOER prototype, which is best suited to people with a leg length of 1 m, three people with long leg length were recruited in this study and only one of them had exactly the right leg length. Results from more subjects would be needed for an extensive evaluation. Further testing is required in subjects with SCI.

The cam mechanism of the GOER prototype, which enabled the prototype to be driven by only one DC motor, had some drawbacks. The cam induced jerky motion at high load (see Figure 6.8) and delayed the ankle plantarflexion (see Figures 6.9-6.11).

Although the cam-chain method is a simple way to induce foot movement, a new actuation setup, such as a linear actuator, needs to be employed for a flexible and smooth ankle rotation. Furthermore, a flexible pelvic support should be used in the GOER system, which supports the bottom, but does not interrupt hip extension. In order to create an easy usage environment, a stronger system for two-leg stepping with a proper pelvic support needs to be developed.

6.5. Conclusions

This study investigated the passive leg movements produced by the GOER prototype. Test results from three subjects showed that the GOER prototype was capable of inducing coordinated leg motion with ROMs of the leg joints similar to those during overground walking at normal speed (a normal speed for a subject with a leg length of 1 m is 1.42 m/s from Table 3.4). The combination of the bar linkage, counterweight balance and the cam transmission enabled the GOER prototype to be driven by only one electric motor. The experimental results of leg motion confirmed the model development process of the GOER system in Matlab, and proved the technical potential and feasibility of the GOER system as a device for early rehabilitation of walking.

Chapter 7. Experimental Evaluation of the GOER Prototype: the Shoe Platform

Summary: This study presents experimental results for the shoe platform which was designed for users in a lying position to mimic the ground reaction forces occurring during overground walking. Mechanical stimulation of the foot sole produces pressure sensation as well as reflexes. Stimulation with high intensity produces strong reflexes, which induces additional perturbations in the ankle joint. This should be prevented to ensure safe usage of the shoe platform. The aim of this study was firstly to determine the parameters of the dynamic shoe platform which avoided activation of reflex-induced perturbations and secondly to collect users' feedback about the sensation produced by the shoe platform. The experiment had two sub-tests: single stimulus and cyclic walking simulation. The shoe platform firstly produced single mechanical stimulation forces on the heel or on the forefoot to investigate the effect of mechanical forces on the reflex response and the ankle angle. Stimulation parameters which did not generate reflex-induced ankle perturbations were determined in the single-stimulus sub-test and were used in the second sub-test for cyclic walking simulation, where both the heel and the forefoot were stimulated. The platform produced pressure sensation in able-bodied subjects which was similar to the ground reaction occurring during upright walking. Weak reflexes were observed in the tibialis anterior (TA) and soleus (SOL) muscles. It is concluded that the dynamic shoe platform has the potential to be incorporated with the GOER system to provide walking-like load sensation on the foot sole during stepping rehabilitation of patients in a supine position.

7.1. Introduction

The GOER prototype was manufactured to produce stepping movement in a supine position for those who cannot maintain an upright position during rehabilitation. Apart from coordinated leg movement described in Chapter 6, suitable stimulation of the load receptors in the lower limbs is another key factor for successful neurological recovery [84].

Load can be detected by a wide variety of receptors, including cutaneous receptors on the foot sole and stretch receptors in the muscles [283]. Loading input derived from cutaneous and proprioceptive afferents is important for regulation of stepping [118]. Load receptors in the soleus and gastrocnemius muscles are thought to detect changes in the body's centre of mass with respect to the feet, which provides proprioceptive feedback for maintenance of balance during walking [284]. The cutaneous load receptors detect support surfaces [283], which enables modulation of the kinematic performance of human walking, such as corrective reactions to stumbling [285]. In order to practise stepping in a supine position in the GOER system [2], an appropriate loading input should be implemented in the lower limbs to mimic the ground reaction forces occurring during overground walking. Therefore a dynamic shoe platform was designed using pneumatic components to stimulate the foot sole, so that users of the GOER system sense their feet moving in the air during the swing phase and contacting the ground during the stance phase.

The shoe platform stimulated the foot sole by small movements of the pressure plates (see Section 7.2.1), which changed the ankle angle. In addition to pressure sensation, mechanical stimulation on the foot soles produced reflexes [23, 29, 286]. Strong

reflexes induced additional observable movements in the ankle joint [29]. Due to the lack or reduction of control from the brain, patients with upper motor neurone lesions often have exaggerated reflexes in response to stimulation, which might interrupt training or ambulation [62, 63, 280]. The GOER system should avoid these observable reflex-induced movements to facilitate training and to prevent injuries to potential users (acute patients), whose legs are fixed in the leg frame while the motion is guided by the bar linkage.

The first aim of this study was to define the shoe parameters which prevent strong reflexes. The motivation of EMG recording in this study was to investigate muscle responses, thereby determining the mechanical stimulation intensities which were not high enough to activate strong reflexes. The second aim of the study was to record the sensation in the leg induced by the dynamic shoe platform.

7.2. Methods

This section introduces the structure of the shoe platform and gives a detailed description of the experiment. The shoe platform firstly applied single mechanical stimulation forces with different patterns on the heel or on the forefoot, and then produced cyclic mechanical stimulation on both the heel and the forefoot to mimic the forces occurring during overground walking. EMG signals and the ankle angle were investigated and users' sensation feedback was documented.

7.2.1. Equipment description

Figure 7.1 shows the shoe platform under study. A detailed description of the shoe

design can be found in Section 5.2. Although not all the gait analysis results in Chapter 3 show that the heel endured larger force than the forefoot, most publications show the heel has higher force than the forefoot during normal gait [253, 269]. Furthermore, the heel has thick skin, which makes it less sensitive to stimulation than the forefoot [25], therefore it is desirable to induce higher force stimulation on the heel than on the forefoot, so as to produce the heel-strike sensation for overground walking simulation [234]. The pressure plate for the heel is actuated by a cylinder with a piston stroke of 20 mm and a diameter of 32 mm, while the forefoot pressure plate is actuated by a cylinder with a stroke of 10 mm and a diameter of 25 mm. Each cylinder is controlled by a solenoid valve (see Figure 7.2) to control the movement of the pressure plate. If the solenoid valve is activated, the air is transmitted to the cylinder, resulting in upward movement of the pressure plate. If the solenoid valve is deactivated, the cylinder retracts, producing downward movement of the pressure plate.

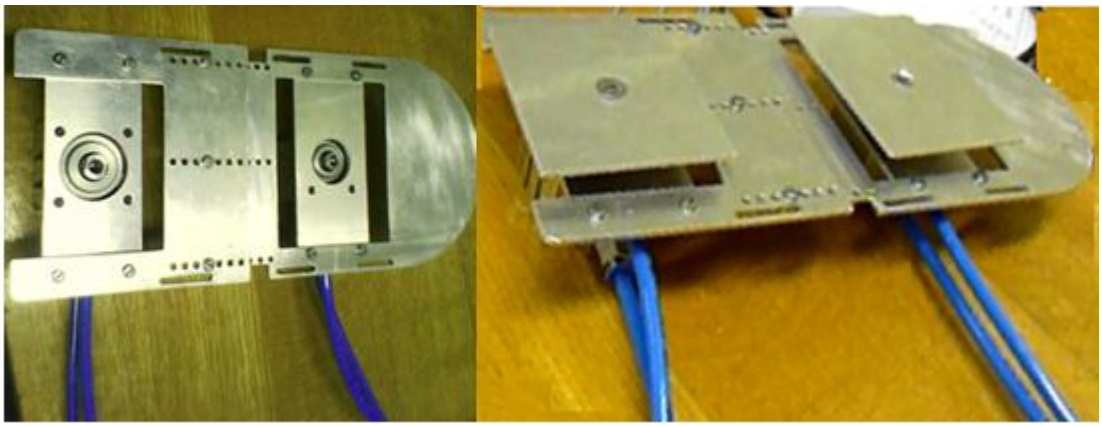

(a) The foot plate. **(b) The two pressure plates rise for mechanical simulation.**

Figure 7.1: The shoe platform structure.

As shown in Figure 7.2, the laptop produces voltage signals via a DAQ card to activate or deactivate the solenoid valve, thereby controlling the movement of the pressure

plate. This achieves mechanical stimulation of the foot sole. A one-way flow control valve is employed to regulate the rise time of each pressure plate. Both pressure plates can be controlled independently, so that the timing of mechanical stimulation can be adjusted to mimic the dynamics of the ground reaction forces which occur during overground walking. The force stimulation in this study focused more on the timing of the force, i.e. controlling the displacement of the pressure plate rather than the actual force amplitude, as the rise time of the mechanical stimulation has a larger influence on the muscle response than the actual force amplitude (see Section 7.3).

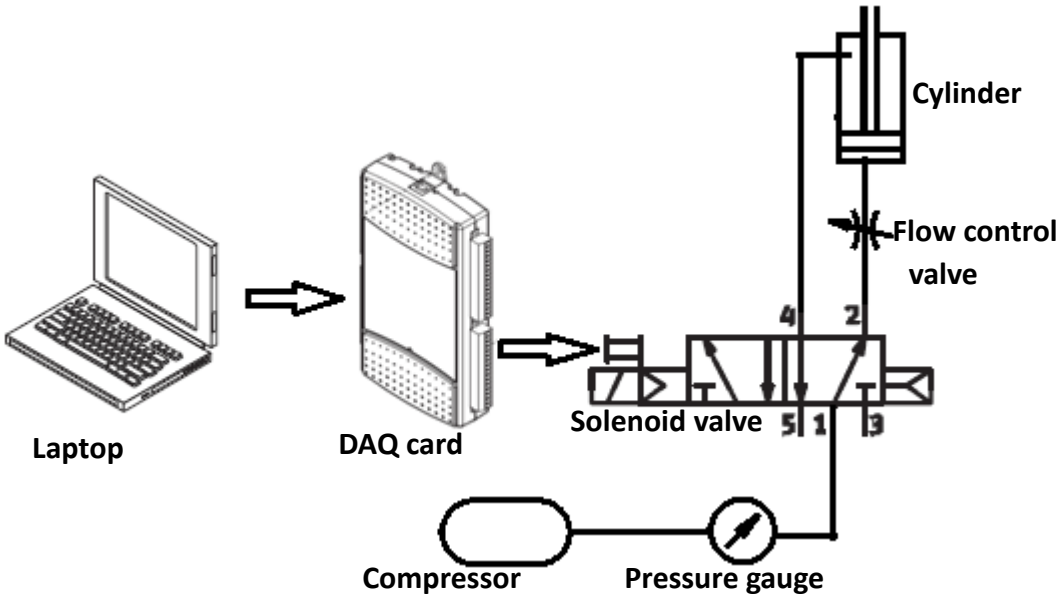

Figure 7.2: The pneumatic system for mechanical force stimulation.

7.2.2. Subjects and measurement devices

In order to evaluate the effect of mechanical stimulation on the foot sole, ten able-bodied subjects were recruited (Table 7.1). Ethical approval was obtained from the Ethics Committee for Non Clinical Research, Faculty of Biomedical & Life Sciences, University of Glasgow.

Bipolar EMG signals from the tibialis anterior (TA) and soleus (SOL) muscles were recorded by a GTEC amplifier (Guger technologies, Austria) via Matlab/Simulink (the MathWorks, Inc.). The sampling frequency of the EMG recording was 1200 Hz. An ultrasound system (zebris Medical GmbH, Allgäu, Germany) was employed to record foot motion at a frequency of 100 Hz. Two zebris markers were used to measure the coordinates of the medial knee joint (x_k, y_k) and the medial ankle joint (x_a, y_a) of the right leg. The right foot was fixed to the shoe platform using Velcro straps. Subjects gave feedback whether the Velcro was strapped tightly enough while remaining comfortable. In order to record foot motion, a third zebris marker was fixed on the Velcro strap over the first metatarsal head (x_m, y_m). The ankle angle θ_a, which was defined as the angle between the shank and the dorsum of the foot, is calculated as:

$$L_{ka} = \sqrt{(x_k - x_a)^2 + (y_k - y_a)^2} \tag{7.1}$$

$$L_{am} = \sqrt{(x_a - x_m)^2 + (y_a - y_m)^2} \tag{7.2}$$

$$L_{km} = \sqrt{(x_k - x_m)^2 + (y_k - y_m)^2} \tag{7.3}$$

$$\theta_a = 180 + \arccos\sqrt{\frac{L_{ka}^{\ 2} + L_{am}^{\ 2} - L_{km}^{\ 2}}{2L_{ka}L_{am}}} \tag{7.4}$$

where L_{ka}, L_{am} and L_{km} are the lengths between the knee and the ankle, the ankle and the first metatarsal head and the knee and the first metatarsal head, respectively. To ensure synchronous recording of the stimulation signal and the EMG response, the voltage signals for controlling the movement of the pressure plates were delivered through a digital output port of a DAQ card to a digital input port of the GTEC amplifier. In this way the command signals for mechanical stimulation and muscle activity were synchronised and recorded in the same file.

Table 7.1: Subject information.

Subject	Mass (kg)	Height (m)	Foot length (m)
S1	47	1.54	0.18
S2	53	1.60	0.20
S3	54	1.59	0.18
S4	56	1.62	0.18
S5	60	1.68	0.23
S6	72	1.70	0.23
S7	72	1.73	0.20
S8	72.5	1.82	0.24
S9	74	1.76	0.24
S10	88	1.94	0.25

7.2.3. Test procedures

Subjects wore the dynamic shoe platform on the right foot. After the EMG sensors were fixed on the TA and the SOL of the right leg, the subject lay down on a mattress. The subject firstly performed maximal dorsiflexion and plantarflexion of the right foot three times to produce reference EMG signals during maximal voluntary contraction (MVC). The subject was then asked to lie relaxed. A pillow was put under the right leg to flex the knee joint at approximately 30^{o}. The angle of the foot sole and the shank was about 150^{o}. Minor adjustments were made to ensure that the subject lay comfortably on the mattress during the whole test.

Table 7.2: Force amplitudes at various pressures (manufacturer's data[8]).

Pressure (bar)	Force on the heel (N)	Force on the forefoot (N)
2	160	100
2.5	200	125
3	240	150
3.5	280	175

Four different pneumatic pressures were tested, with the corresponding force amplitudes presented in Table 7.2. The maximum force generated by the cylinder was 280 N (3.5 bar$\times$80 N/bar). This force amplitude corresponds to approximately 30% to 60% of the body weight of the subjects tested. The force range of 30% to 60% of the body weight is similar to the force experienced by patients practising treadmill walking with body weight support [261].

Mechanical stimulation was firstly applied in the single-stimulus sub-test (on either the heel or the forefoot) to investigate the reflex responses, and then in the cyclic-stimulation sub-test (on both the heel and the forefoot) for walking simulation to record users' sensation.

(a) Single-stimulus sub-test

This sub-test evaluated the influence of different parameters of the mechanical stimulus, including the rise time of the pressure plates (long (0.20 s) and short (0.05 s)), location of the mechanical stimuli (the heel and the forefoot) and the pressure amplitude (2, 2.5,

[8]Available from: http://www.festo.com/cms/de_de/index.htm. Accessed on 20/06/2012.

3 and 3.5 bar). All of these parameters were combined, resulting in 16 types of stimulation taking place in a random order. Each type of stimulation was performed four times for averaging purposes. Each of these 64 stimuli was applied every 30 s and lasted for 0.8 s. The subjects had 5 minutes of rest after 32 stimuli to prevent habituation. This single-stimulus sub-test lasted for about 45 min.

(b) Cyclic-stimulation sub-test

In order to mimic dynamic ground reaction forces during walking, cyclic stimulation was applied on both the heel and the forefoot in this sub-test. The pressure plates used the long rise time of 0.20 s for full extension, which meant the force took 0.20 s to achieve the target amplitude for stimulation of the foot sole. Two gait cycles of 2 s and 5 s were chosen to simulate walking at fast and slow speeds. For a person with a height of 1.80 m and a step length of 0.85 m, these two selected gait cycles corresponded to walking speeds of 3 and 1.2 km/h respectively, which are close to normally adopted walking speeds for patients during treadmill training [129].

The shoe mechanism induced the force pattern in Figure 7.3 to simulate walking. The heel had mechanical stimulation for 40% of the gait cycle, and the forefoot was stimulated during 20-60% of the gait cycle. The heel and the forefoot were stimulated together for 20% of the gait cycle to simulate the mid-stance phase. Four pressures mentioned above (2, 2.5, 3 and 3.5 bar) combined with two cycle periods resulted in 8 cyclic-stimulation tests. Each test started with 5-second rest, followed by 9 stimulation sequences (9 strikes).

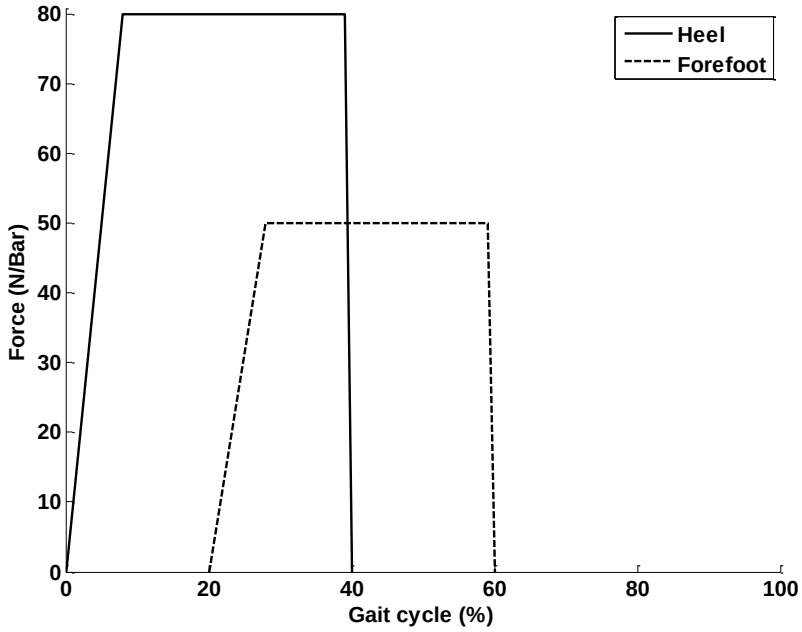

Figure 7.3: Force profile for walking simulation.

After the whole test, the subject filled out a questionnaire (Appendix 14) about the sensation on the sole induced by cyclic walking simulation. The sensation focuses more on the timing of the force and location of stimulation rather than the actual force amplitude.

7.2.4. Data analysis

EMG signals, which were recorded with a band-pass filter (5-500 Hz) and a notch filter at 50 Hz, were full-wave rectified and saved synchronously with the trigger signal for the pressure plate stimulation. The EMG data and zebris recordings were visually observed to remove outliers. The EMG data with high background noises were discarded. The zebris data were further filtered with a window size of 5 to remove noise, and were finally smoothed with the loess or rloess Matlab functions.

Muscle activity during MVC was collected mainly for normalisation of EMG signals

from different subjects. The raw EMG signals during MVC are usually processed by calculating root mean square (RMS) values to remove the non-reproducible information in the raw EMG recordings [287, 288]. For the EMG data during MVC, the RMS amplitude in a 500 ms time window centred at the maximal peak of the EMG signals was calculated [287, 288]. The maximal MVC_{RMS} (RMS during MVC) within the three repetitions was used as the reference for EMG normalisation. For the EMG data from the single-stimulus sub-test, the RMS value during the mechanical stimulation (0.8 s) was calculated to investigate EMG responses. For the cyclic walking simulation data, the mean RMS amplitude of the total duration of the mechanical stimulation on the foot sole was calculated and compared to that of a 5 s pre-stimulation period to investigate the effect of walking simulation on muscle response.

As reported in Section 7.3, large EMG bursts were observed in the single-stimulus sub-test. As the subjects were told to relax without exerting voluntary movement during the whole test, these large bursts were considered as reflexes, and their latencies were investigated. In contrast to the RMS representation of muscle activity during MVC, a reflex is often represented by the raw EMG signal instead of the RMS value, because calculation of the RMS value employs a moving window, which introduces a delay in the EMG signals, thereby affecting determination of the reflex onset. The mean amplitude and standard deviation (SD) of the baseline raw EMG signals during 0.8 s pre-stimulation were calculated and the reflex threshold was defined as mean + SD of the baseline EMG [289]. The reflex latency was initially searched for by computer programming, where the onset of each EMG burst was determined as the first signal component larger than the reflex threshold and with a duration longer than 10 ms [289]. As automatic computer programming cannot account for artefacts [290], visual

observation is often employed to detect the onset of reflexes [23, 291]. This method is proven to be accurate and reliable [289, 292, 293]. Visual observation was performed through an interactive graphics method [292, 293], where the EMG signals during the mechanical stimulation (0.8s) along with the values mean + SD and mean + 2SD were plotted and zoomed. The onset of the reflex was visually determined as the earliest detectable increase in the EMG signal which stayed continuously above the resting state [294]. The results from the visual observation were determined as the final latencies.

In the results below, all EMG data are normalised with respect to MVC_{RMS} to enable a valid comparison of stimulation responses from different subjects. This resulted in the reflex amplitude expressed by the raw EMG signal as a percentage of MVC_{RMS}. Although different representations of EMG signals are used, this is an often adopted method of EMG normalisation [288]. For the single-stimulus sub-test, EMG signals during the pre-stimulation period (0.8 s) and the mechanical stimulation (0.8 s) are presented. The mechanical stimulation periods are marked as dashed lines in the EMG figures. The amplitudes of the dashed lines are the reflex thresholds. It is defined that a reflex with a raw EMG amplitude lower than 100% of MVC_{RMS} is called a weak reflex, while that larger than 100% of MVC_{RMS} is called a strong reflex. An independent t-test was performed in SPSS to see whether the stimulation with a long and short rise time produced significantly different EMG responses ($p = 0.05$). For the cyclic walking simulation, the responses of each sub-test are presented, including 5 seconds of rest and 9 repetitions of stimulation. In order to make the EMG figure for the cyclic-walking sub-test readable, the data were resampled at 100 Hz.

In order to test whether the mechanical stimulation caused ankle movement, the ankle

angle is presented together with the EMG signals. If reflex-induced ankle movement is observed, the ankle perturbation is marked with a dashed arrow.

7.3. Results

The RMS amplitudes during MVC and rest are presented in Table 7.3. Subjects had large variance in MVC_{RMS} but had similar values at rest.

Table 7.3: RMS during MVC and at rest (μV).

Subject	MVC		Rest	
	TA	SOL	TA	SOL
S1	162.81	126.52	1.16	1.11
S2	347.23	91.43	1.24	1.46
S3	211.12	54.08	1.86	1.52
S4	69.16	74.23	1.29	1.75
S5	255.32	31.28	1.07	1.03
S6	100.04	66.12	1.01	1.05
S7	220.45	115.57	1.15	1.58
S8	109.36	31.91	1.35	1.05
S9	97.78	50.26	1.04	1.18
S10	318.28	47.53	1.41	1.49
Mean±SD	189.16±97.33	68.89±33.08	1.26±0.25	1.32±0.27

Different mechanical stimulation patterns produced different EMG responses. The results from single-stimulus tests and cyclic walking simulation are presented separately in the following two subsections.

7.3.1. Single-stimulus sub-test

Sixteen stimulation patterns as described above were applied in this sub-test. Weak and strong reflexes were observed corresponding to stimulation with the long and short

rise times.

(a) Stimulation by the pressure plate with a long rise time

When the pressure plate took 0.2 s to reach full extension for mechanical stimulation, reflexes were observed in one or both of the lower leg muscles. Figure 7.4 shows the responses of Subject S3 after heel stimulation at 2 bar. The stimulation produced a weak reflex in the SOL with a raw EMG (peak) amplitude of 20.2% of MVC_{RMS} and a latency of 55 ms.

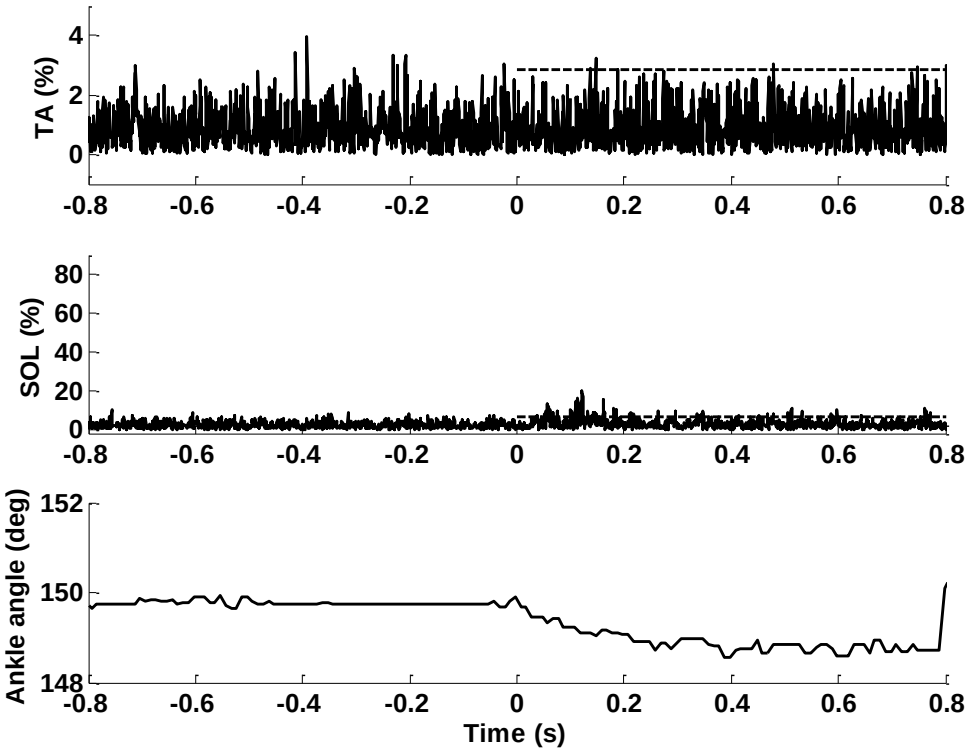

Figure 7.4: Heel stimulation at 2 bar in S3 with a long rise time. The dashed lines show the mechanical stimulation periods with the amplitudes as the reflex thresholds.

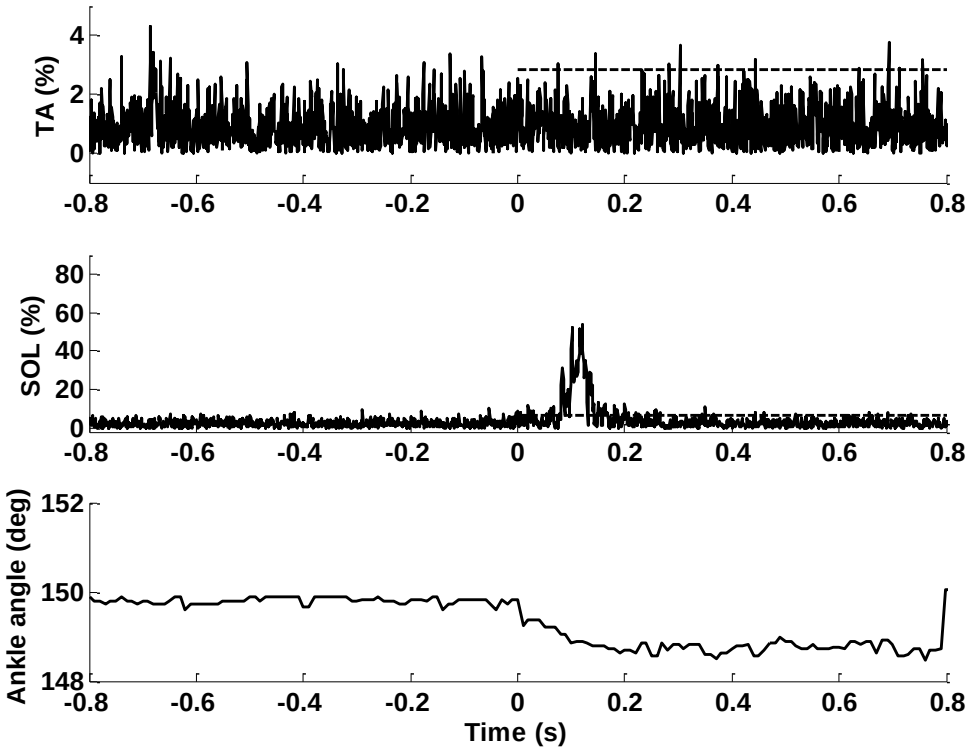

Figure 7.5: Heel stimulation at 3.5 bar in S3 with a long rise time. The dashed lines show the mechanical stimulation periods with the amplitudes as the reflex thresholds.

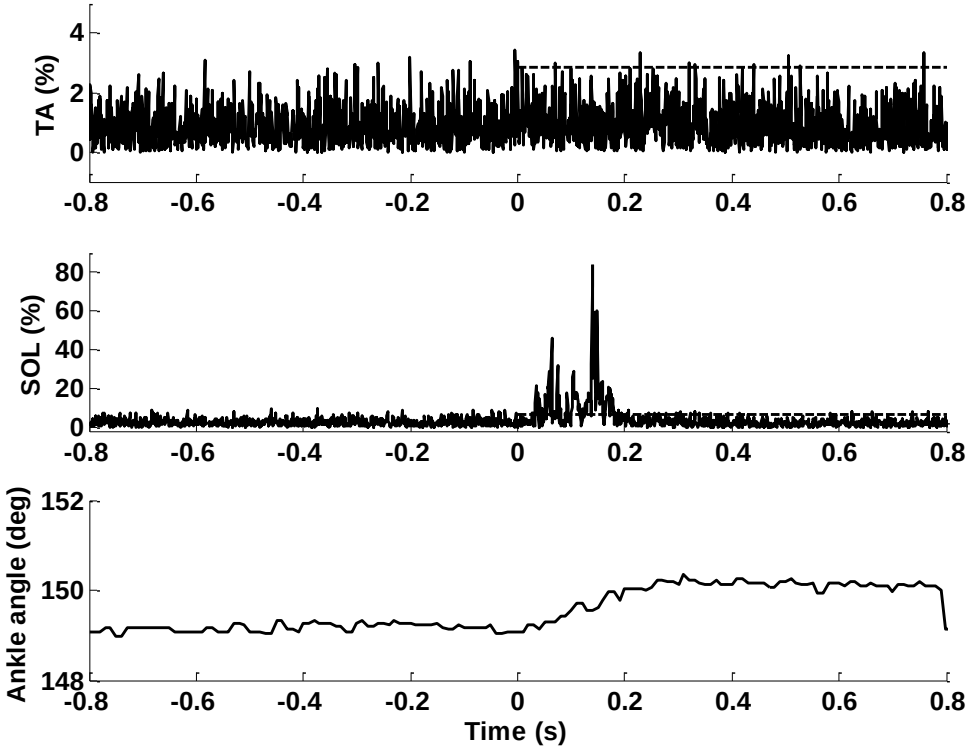

Figure 7.6: Forefoot stimulation at 3.5 bar in S3 with a long rise time. The dashed lines show the mechanical stimulation periods with the amplitudes as the reflex thresholds.

When the pressure increased, a higher EMG amplitude was observed. Figure 7.5 shows the responses when the pressure of the heel stimulation increased to 3.5 bar. Compared to Figure 7.4, a weak reflex of about 54% of MVC_{RMS} in peak amplitude with a latency of 78 ms was observed in the SOL. The ankle angle of S3 reduced by about 0.9^{o} in response to heel stimulation, regardless of the pressure amplitude. As the piston rose slowly, the ankle angle changed gradually. It was observed by comparing Figures 7.4(c) and 7.5(c) that the ankle angle changed more slowly at 2 bar than at 3.5 bar. The rising movement of the pressure plate at 2 bar was more easily reduced, probably because the upward force at 2 bar was lower (160 N) than at 3.5 bar.

Stimulation on the forefoot induced similar reflex responses in the lower leg muscles, but increased the ankle angle. Figure 7.6 shows the results of S3 in response to slow forefoot stimulation at a pressure of 3.5 bar. Compared to Figure 7.5(b), forefoot stimulation induces a 36% higher reflex in the SOL than heel stimulation in S3. Forefoot stimulation increased the ankle angle gradually by 0.8^{o}.

Stimulation with a long rise time produced weak reflexes in six out of ten subjects. Subject S1, S3 and S7 had reflexes in the SOL only, S4 and S10 had EMG increase in the TA only, while S2 had reflexes in both muscles. Each type of stimulus was repeated four times. The mean RMS amplitudes during mechanical stimulation at 3.5 bar with a long rise time for all subjects are presented in Table 7.4. It can be seen that all subjects had small RMS amplitudes (less than 4.5% of MVC_{RMS}).

The movement of the ankle joint during stimulation with a long rise time was induced by upward physical movement of the pressure plate, and did not change with the pressures. The mean ankle angle changes are presented in Table 7.5. The slow movement of the pressure plate during mechanical stimulation induced a mean change

of about 1.33^{o} in the ankle angle, with a maximal change of 2.45^{o}.

Table 7.4: Mean RMS at stimulation of 3.5 bar with a long rise time (%MVC_{RMS}).

Subject	Heel stimulation		Forefoot stimulation	
	TA	SOL	TA	SOL
S1	0.91	1.14	0.89	1.05
S2	0.46	3.12	0.89	2.30
S3	1.19	3.42	1.20	4.02
S4	3.21	2.77	2.48	2.21
S5	1.70	2.37	1.07	2.06
S6	4.41	2.02	3.26	2.10
S7	2.89	2.41	2.98	1.33
S8	1.51	2.73	1.53	2.38
S9	1.38	1.19	1.31	1.22
S10	3.50	1.85	0.52	1.01
Mean±SD	2.12±1.30	2.30±0.76	1.61±0.95	1.97±0.90

Table 7.5: The ankle angle change (degrees) induced by the upward movement of the pressure plate during mechanical stimulation.

Subject	Heel stimulation	Forefoot stimulation
S1	-1.98	2.37
S2	-1.41	0.51
S3	-1.08	0.89
S4	-1.15	1.42
S5	-0.46	0.61
S6	-2.45	0.89
S7	-1.81	1.15
S8	-1.44	1.14
S9	-0.97	0.91
S10	-0.51	0.82
Mean±SD	-1.33±0.63	1.07±0.53

(b) Stimulation by the pressure plate with a short rise time

When the pressure plate was adjusted to achieve full extension within 0.05 s, reflexes with various amplitudes were observed in nine out of ten subjects, when either the heel or the forefoot was stimulated. Some subjects had strong reflexes with raw EMG amplitudes larger than 100% of MVC_{RMS}. Stimulation with a high pressure induced a reflex with a large amplitude, therefore the responses at a pressure of 3.5 bar are presented in this section.

Figure 7.7 shows the responses of S3 to heel stimulation at 3.5 bar. Similar to stimulation with a long rise time, the SOL was more active than the TA during stimulation with a short rise time. A strong reflex was produced in the SOL with the raw EMG (peak) amplitude up to 120% of MVC_{RMS} and a latency of 44 ms, while a weak reflex was observed in the TA with a latency of 115 ms. The ankle angle reduced by 1.2^{o}. As the pressure plate rose quickly, the ankle angle should reduce quickly. However, the ankle angle was disturbed as the dashed line shows. This disturbance was considered as an additional ankle perturbation induced by the strong reflex.

Reflexes had large variance between different subjects. Subject S6, in contrast to S3, had more activity in the TA in response to stimulation. Figure 7.8 presents responses of S6 to heel stimulation at 3.5 bar. This stimulation pattern induced a strong reflex in the TA with a raw EMG (peak) amplitude up to 200% of MVC_{RMS} and a latency of 66 ms, while no obvious reflex was observed in the SOL. The heel pressure plate reduced the ankle angle in S6 by about 2.3^{o}. An additional change of 1^{o} in the ankle angle (marked with a dashed arrow) was observed and was also considered as an additional

perturbation induced by the strong reflex. Figure 7.9 displays the results of S6 for forefoot stimulation. An even stronger reflex was induced in the TA with a latency of 46 ms, while no additional ankle angle change was observed.

Figure 7.10 shows the responses of Subject S7 after heel stimulation. In contrast to the responses of S6 in Figure 7.8, S7 had activity in both lower leg muscles in response to heel stimulation: a strong reflex in the TA and an observable weak reflex in the SOL. The heel stimulation reduced the ankle angle by 1.89^{o}. A reflex-induced ankle perturbation of 0.3^{o} was observed in S7, as shown by the dashed arrow.

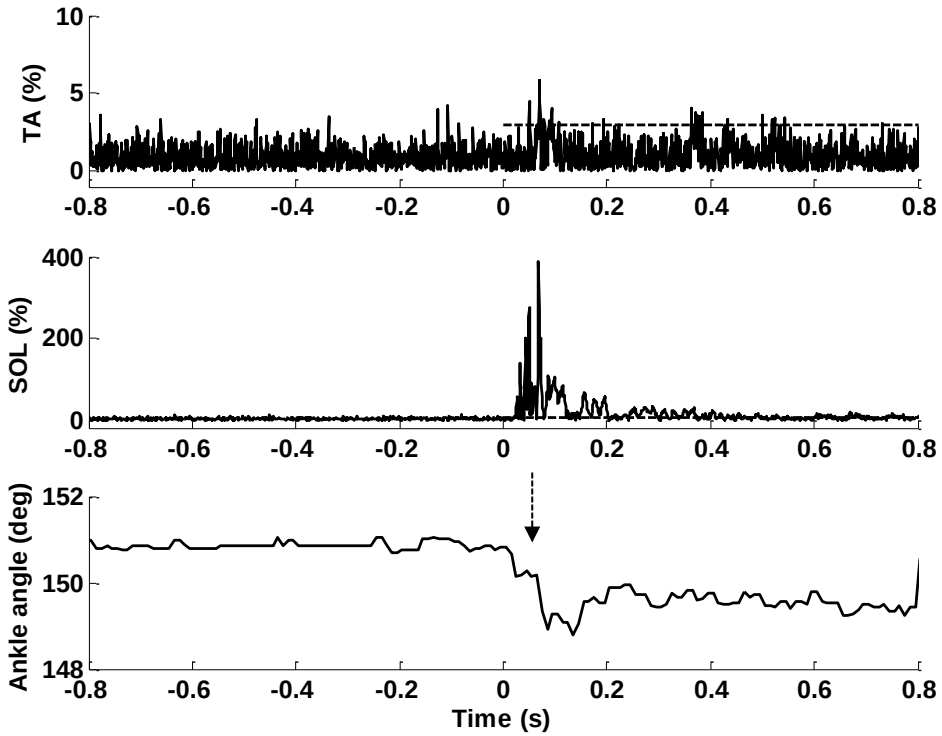

Figure 7.7: Heel stimulation in S3 with a short rise time. The dashed arrow shows reflex-induced ankle perturbation. The dashed lines show the mechanical stimulation periods with the amplitudes as the reflex thresholds.

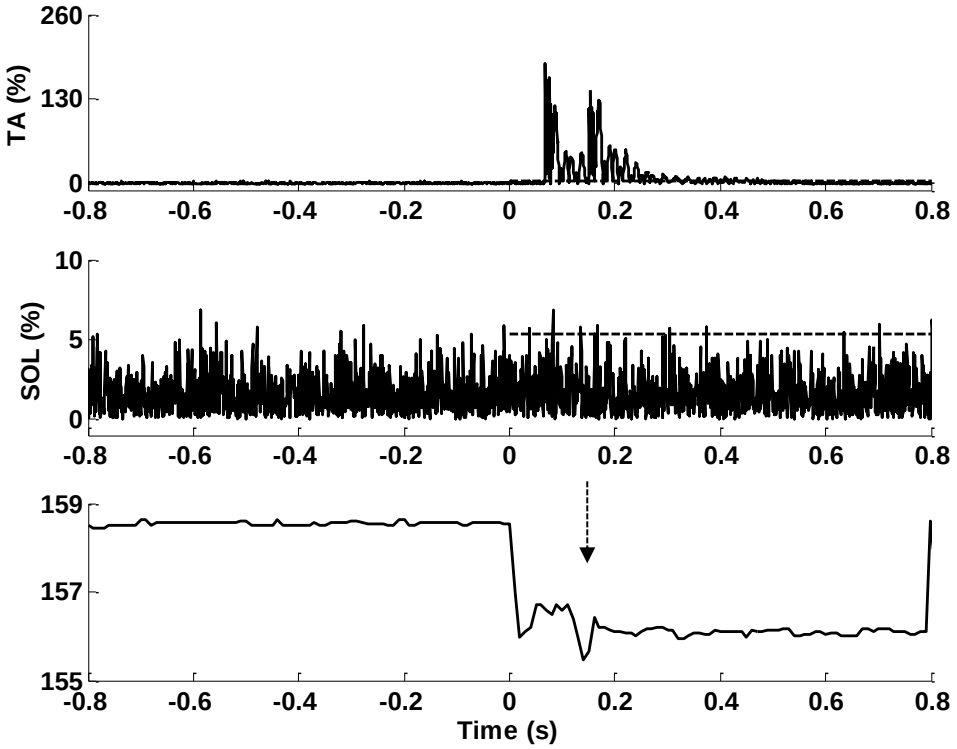

Figure 7.8: Heel stimulation in S6 with a short rise time. The dashed arrow shows reflex-induced ankle perturbation. The dashed lines show the mechanical stimulation periods with the amplitudes as the reflex thresholds.

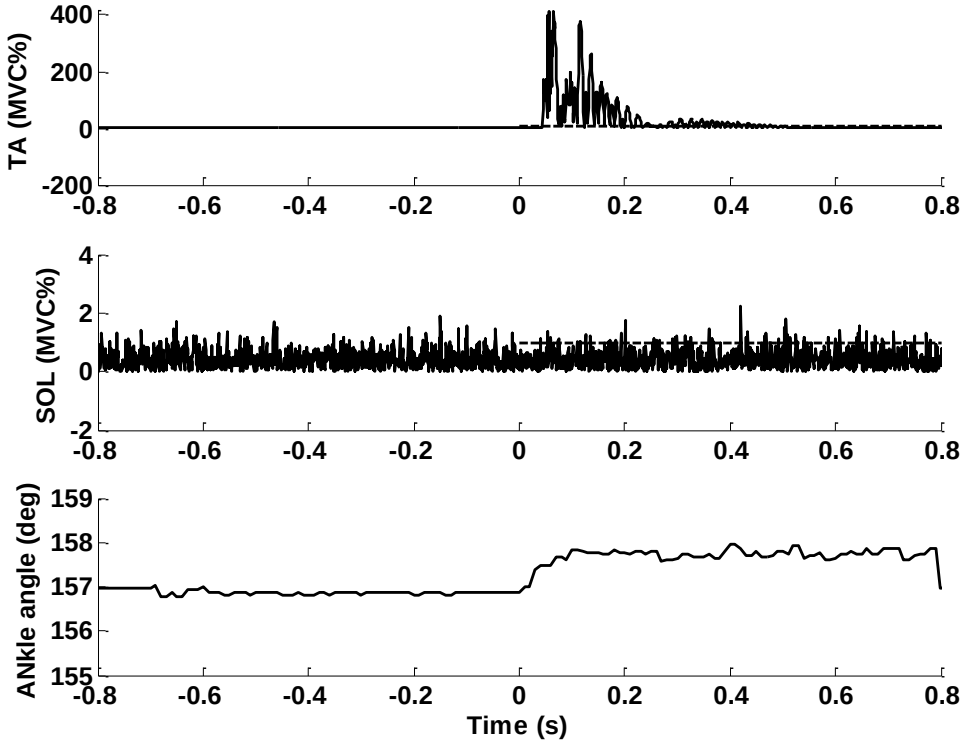

Figure 7.9: Forefoot stimulation in S6 with a short rise time. The dashed lines show the

mechanical stimulation periods with the amplitudes as the reflex thresholds.

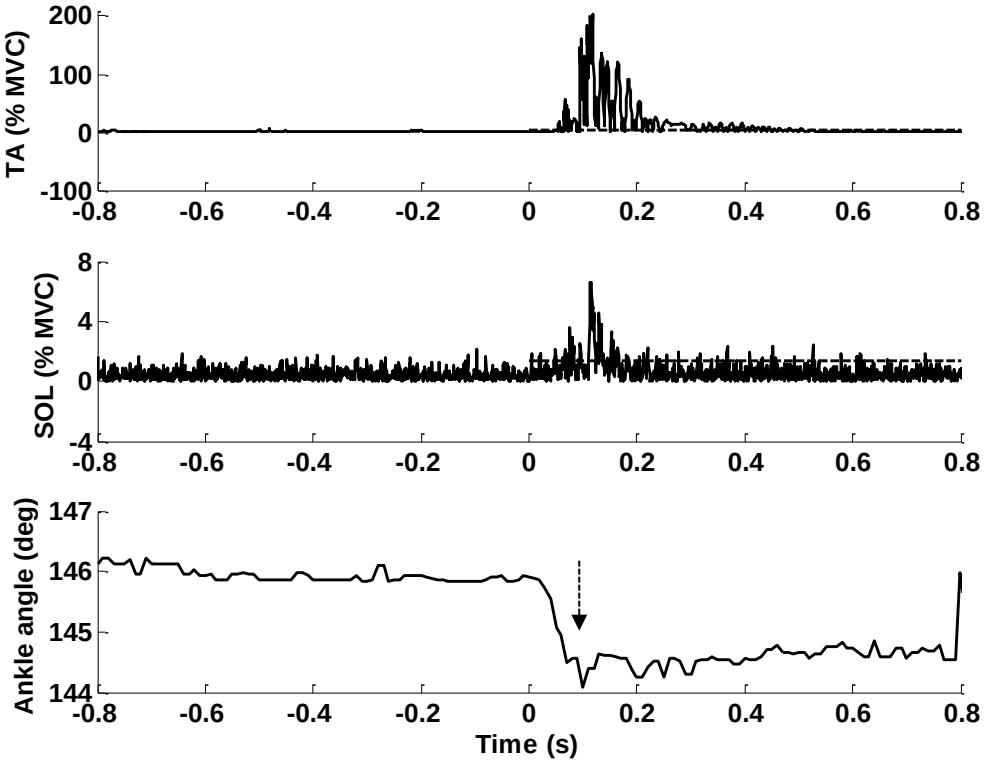

Figure 7.10: Heel stimulation in S7 with a short rise time. The dashed arrow shows reflex-induced ankle perturbation. The dashed lines show the mechanical stimulation periods with the amplitudes as the reflex thresholds.

Table 7.6: Mean RMS for stimulation by a short rise time (%MVC_{RMS}).

Subject	Heel stimulation		Forefoot stimulation	
	TA	SOL	TA	SOL
S1	1.17	2.11	8.82	6.58
S2	0.49	6.68	0.46	2.63
S3	3.52	13.34	1.32	8.02
S4	7.86	6.75	3.31	2.65
S5	6.52	3.23	2.88	4.61
S6	13.78	2.16	17.00	1.96
S7	11.67	4.83	1.58	1.95
S8	1.73	4.87	1.65	4.39
S9	1.47	1.27	1.45	1.29
S10	11.19	8.36	0.67	1.88
Mean±SD	5.94±4.97	5.36±3.64	3.33±4.90	3.22±2.00

Strong reflexes were observed in five subjects (S1, S3, S6, S7 and S10). Three of them (S3, S6 and S10) had strong reflexes at four test pressures. Additional reflex-induced perturbation in the ankle joint was observed in three subjects (S3, S6 and S7). The mean RMS amplitudes during mechanical force stimulation at 3.5 bar for all subjects are presented in Table 7.6. Compared to the stimulation with a long rise time (Table 7.4), much higher RMS amplitudes were observed if the pressure plate rose quickly, with the maximal RMS amplitude up to 17% and 13% of MVC_{RMS} in the TA and the SOL respectively. An independent t-test on the data of Table 7.4 and 7.6 showed the RMS values from the stimulation with a long and short rise time were significantly different ($p = 0.003$).

Table 7.7: Reflex latencies (ms) for stimulation by the pressure plate with a short rise time. NA means no reflex was observed.

Subject	Heel stimulation		Forefoot stimulation	
	TA	SOL	TA	SOL
S1	93.33	95.42	94.79	90.00
S2	73.33	38.13	101.67	35.52
S3	98.12	45.83	106.87	47.08
S4	40.63	49.38	57.71	81.67
S5	62.50	59.37	132.92	92.08
S6	65.83	NA	46.46	NA
S7	66.87	76.04	98.13	81.04
S8	57.71	43.54	115.00	53.33
S9	NA	NA	NA	NA
S10	88.96	104.58	68.75	NA
Mean±SD	71.92±18.61	64.04±25.16	91.37±28.17	68.67±22.82

In order to investigate the origin of the reflexes, the reflex latencies were calculated. Each stimulus was repeated four times, resulting in 64 stimuli in the whole single-stimulus sub-test for each subject. Although some subjects had strong reflexes in some stimuli, most subjects showed very limited reflexes. Subjects S5 and S8 had

very weak reflexes even at a high pressure of 3.5 bar. S9 had no reflex throughout the test, although he felt obvious sensations of stimuli. The mean latencies of reflexes induced by the stimulation of a short rise time at 3.5 bar are presented in Table 7.7. The subjects showed latencies ranging from 36 to 133 ms.

7.3.2. Cyclic-stimulation sub-test

During walking simulation, the piston was adjusted to fully extend within 0.20 s (long rise time). Cyclic stimulation was applied with two cycle times of 2 s and 5 s in each subject to simulate walking at fast and slow speeds. Figure 7.11 shows responses in S7 during the simulation of fast walking at 3.5 bar. Weak reflexes were observed in the TA and the SOL, but no additional ankle perturbation was produced by the reflexes as shown in the enlarged Figure 7.12. The ankle angle changes induced by the cyclic mechanical stimulation were 1.7^{o} from heel stimulation and 0.9^{o} from forefoot stimulation, which were similar to those during single stimuli with a long rise time of the pressure plate (Table 7.5).

Cyclic stimulation induced neither strong reflexes nor additional ankle perturbations in any of the subjects. Weak reflexes were observed in nine out of ten subjects. Muscle activity during stimulation was increased compared to the resting situation. The RMS amplitudes relative to the resting state for all ten subjects at variable pressures are presented in Figure 7.13. It can be seen that higher pressures induced larger reflexes, with the largest amplitudes occurring in the SOL during simulation of fast walking, and the smallest amplitudes observed in the TA during slow walking simulation.

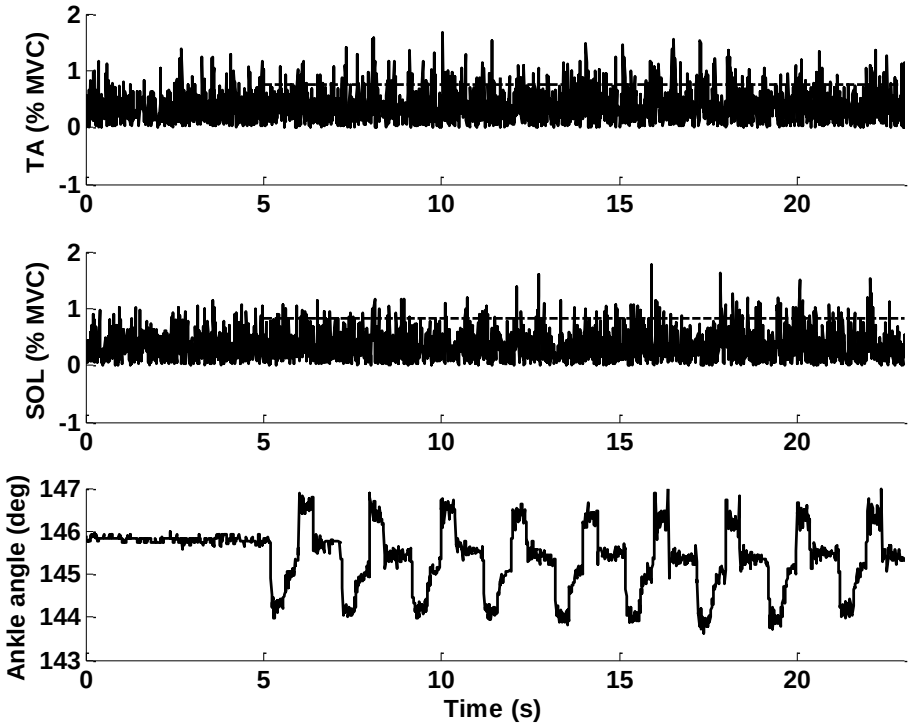

Figure 7.11: Walking simulation responses of S7. The dashed lines show the mechanical stimulation periods with the amplitudes as the reflex thresholds.

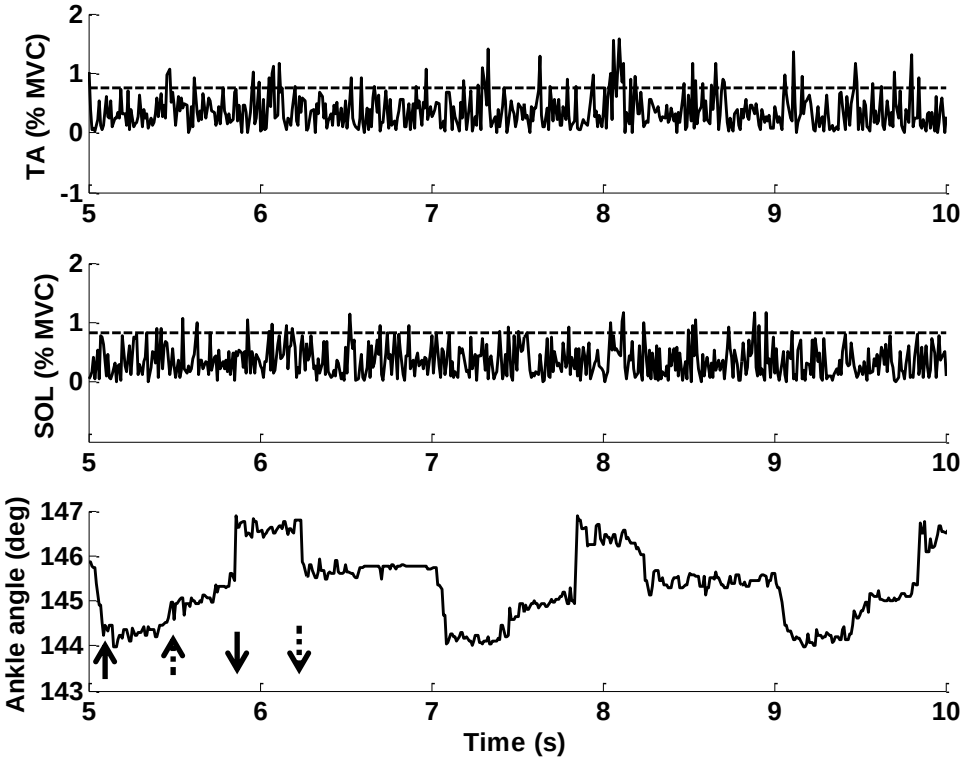

Figure 7.12: Zoomed version of Figure 7.11. The upward and downward arrows show the start and end times of stimulation on the foot sole. The solid arrows represent the

heel pressure plate and the dashed arrows indicate the forefoot pressure plate. The dashed lines show the mechanical stimulation periods with the amplitudes as the reflex thresholds.

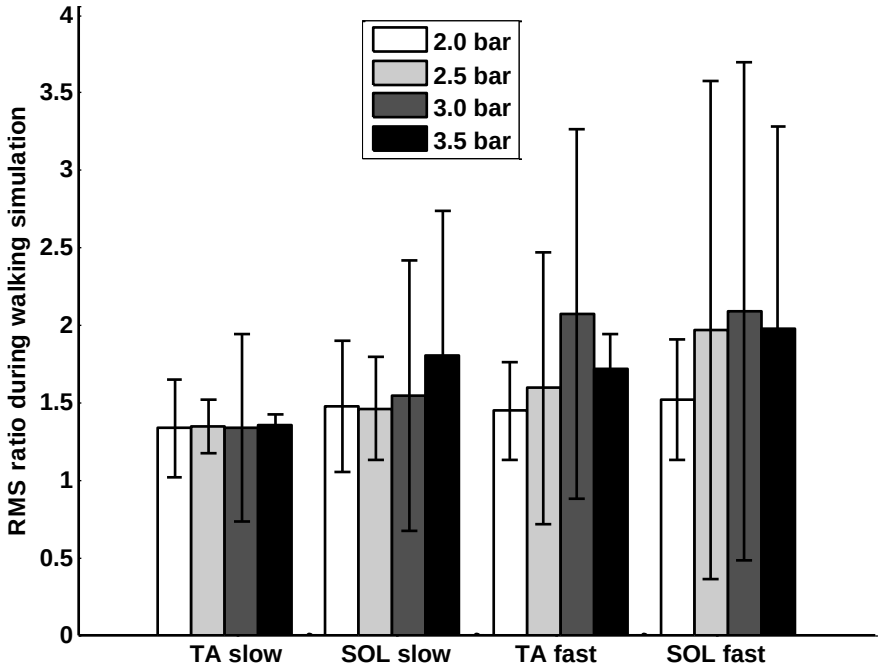

Figure 7.13: RMS values (relative to resting state) during walking simulation tests.

Subjects provided subjective feedback of using the shoe platform (see Appendix 15). All ten subjects felt cyclic force patterns on the foot sole. Nine subjects thought the shoe platform had the right location of stimulation for walking simulation, while one thought the pressure on the top of the foot caused by the Velcro straps made the feeling different from walking. Six subjects thought the stimulation had similar force timing to walking. Among the four subjects who perceived different timings from walking, two subjects thought the delay between the heel and forefoot stimulation was too long, while the other two subjects did not give a reason why they felt different. Seven of the ten subjects considered the rising speed of force on both the heel and the forefoot to be similar to overground walking, two thought the force on the heel had a better feeling than on the forefoot, while one subject thought the force on the forefoot had a better feeling. Seven subjects thought the shoe platform was comfortable to use

while the other three subjects were neutral (neither comfortable nor uncomfortable). Six subjects described the stimulation as pressing, two subjects described it as punching and two subjects described it as walking.

7.4. Discussion

The pneumatic shoe platform applied mechanical stimuli on the foot sole of users in a supine position. Accompanied with pressure sensation, mechanical stimulation produced reflexes in the leg muscles. As strong reflexes had potential to induce ankle perturbation, the reflex amplitudes were investigated in the single-stimulus sub-test, through which the parameters of the shoe platform were determined to produce mechanical stimulation without reflex-induced perturbation in the ankle joint. Then in the cyclic walking simulation, the shoe platform provided dynamic mechanical stimulation on the heel initially to simulate heel strike, and then on both the heel and the forefoot to mimic mid-stance and finally on the forefoot only to represent heel off, which succeeded in producing walking-like sensations.

Stimulation achieved by upward movement of the pressure plate changed the ankle angle by about 1.3^{o} on average regardless of pressures, which represents less than 5% of the target ROM of an ankle joint that goes between -20^{o} (plantarflexion) and $+10^{o}$ (dorsiflexion) (see Chapter 3). Heel stimulation changed the ankle angle more than forefoot stimulation, because the piston under the heel has a longer stroke (20 mm) than that under the forefoot (10 mm). Six out of ten subjects experienced weak reflexes during stimulation with a long rise time. When the rising speed of the pressure plate increased, nine out of ten subjects experienced reflexes. Five subjects had strong reflexes, and three of them had additional ankle perturbation induced by

the strong reflexes.

The reflexes recorded in the single-stimulus sub-tests had latencies ranging from 36-133 ms, which implies that the reflexes are spinal in origin [26]. The shoe platform stimulated the cutaneous mechanoreceptors by dynamic forces. The movement of the pressure plate changed the ankle angle, resulting in stretch of the TA and the SOL muscles. The dynamic pressure induced polysynaptic cutaneous reflexes while the muscle stretch generated monosynaptic reflexes. Studies on stretch reflexes in the SOL displayed latencies of 35-50 ms due to ankle angle disturbances [23, 295]. The latencies of stretch reflexes in the SOL were found to be related to the ankle angle, and could be prolonged up to 80 ms with an ankle joint in plantarflexion [296]. Research on cutaneous reflexes through non-nociceptive electrical stimulation on different areas of the sole reported latencies of cutaneous reflexes ranging from 50-90 ms [286, 297] and normally prolonged at weak stimulation [26]. The reflexes induced by the shoe platform in the current study are likely a combination of both stretch and cutaneous reflexes as described above, given the latency range from 36-133 ms. Both of these responses act as protective strategies: to prevent overstretching by stretch reflexes and to withdraw the foot after stimulation of cutaneous reflexes.

The SOL generally has a higher occurrence of stretch reflexes than the TA [296]. This agrees with the observation in S3 (see Figure 7.7), who had more reflexes in the SOL than the TA. S6 produced double-burst reflexes in the TA (see Figures 7.8-7.9), which agrees with previous descriptions of cutaneous flexor reflexes [26]. Cutaneous flexor reflexes are often observed in the TA [298], therefore it is not surprising to see that S6 had reflexes with peak amplitudes twice MVC_{RMS} in the TA, while no reflex was observed in the SOL. However, it is not unexpected to see reflexes in both the TA and

the SOL as shown in S4 and S7, which is in accordance with study [297]. Although the same pressure was employed during heel and forefoot stimulation, S3 and S6 had higher reflex amplitudes during forefoot stimulation than heel stimulation (see Figures 7.5-7.6 and Figures 7.8-7.9). This might be because the forefoot is usually more sensitive to stimulation than the heel [25]. Reflexes have a tendency towards a decrease in latency for increasing stimulus intensity [26, 297, 299], which explains the shorter mean latency in the TA of S6 for forefoot stimulation than for heel stimulation (see Table 7.7). It was also expected that the limited weak reflexes observed in the TA of S5 and S8 during forefoot stimulation had long latencies (up to 133 and 115 ms, respectively).

The rising speed of the pressure plate combined with the pressure amplitudes had a large influence on the reflex amplitudes. Stimulation with a short rise time at 3.5 bar produced a reflex with a raw EMG amplitude larger than 100% of MVC_{RMS}. It should be noted that the MVC_{RMS} value is smaller than the raw maximal EMG value during MVC (about 75% smaller in this study). Therefore a reflex with a raw EMG amplitude larger than 100% of MVC_{RMS} does not mean that the reflex is larger than MVC, rather it is observed to be strong enough to perturb the ankle joint in some subjects. Strong stretch reflexes in the SOL are considered to cause ankle plantarflexion (increase the ankle angle). The EMG burst in Figure 7.7 after heel stimulation by a pressure plate with a short rise time was considered to be a stretch reflex, based on the short latency of 46 ms. Therefore the reflex-induced plantarflexion reduced the dorsiflexion caused by the upward movement of the heel pressure plate, resulting in the ankle perturbation as seen in Figure 7.7. Ankle flexion (ankle angle reduction) is reported to be the dominant flexor reflex [297], therefore it is expected to see ankle dorsiflexion during strong flexor reflexes, as shown in Figure 7.8 and Figure 7.10. Comparing Figure 7.8

and Figure 7.9, it can be seen that forefoot stimulation produced stronger flexor reflexes, but induced no additional perturbation in the ankle angle. This might be because the potential reflex-induced dorsiflexion was reduced by the ankle plantarflexion caused by the upward movement of the forefoot pressure plate. In summary, the cause and effect of reflex and ankle angle are: (i) the movement of the pressure plate changed the ankle angle, which caused a stretch reflex. The shoe platform stimulated the cutaneous mechanoreceptors by dynamic forces; (ii) when the stimulation intensity was high, the reflex became strong enough to induce a withdrawal reflex; (iii) the stretch reflex increased the ankle angle, while the withdrawal reflex decreased the ankle angle.

Weak reflexes in the muscles are considered to be a satisfactory reaction to stimulation induced by the shoe platform. However, strong reflexes that induce additional ankle perturbation might cause injury to users (especially for patients with spinal cord injury who often have spasticity) and should be avoided in the GOER system. Walking simulation by the dynamic shoe platform delivered the force gradually by adopting the pressure plate with a long rise time. The mechanical stimulation under these circumstances still changed the EMG activity from the lower leg muscles in able-bodied subjects, with increased EMG amplitudes during stimulation compared to the resting period. A higher pressure produced stimulation with a higher intensity, resulting in higher EMG signals in the lower leg muscles. No additional ankle perturbation was observed. Six subjects thought the stimulation had similar force timing to walking, and seven subjects considered the rising speed of force on both the heel and the forefoot to be similar to overground walking.

This study evaluated the performance of the shoe platform, which was confirmed to

be an effective device to produce walking-like sensation. The limitation of this shoe platform is that the mechanical stimulation changes the ankle angle, which is unavoidable if a pneumatic cylinder is employed for stimulation, but can be further reduced by choosing a cylinder with a piston shorter than 10 mm. Another limitation of the shoe platform is that the timing of the force on the heel and the forefoot as shown in Figure 7.3 is different from the target profiles displayed in Figure 5.19. During the design stage, it was thought that a fast rising speed of force should be applied on the heel to simulate the large loading at heel strike. Therefore, only two one-way control valves were employed, which were intended to regulate the downward speeds of the two pressure plates. However, the observation of reflexes during the tests revealed the requirement of reducing the upward speed of the pressure plates to prevent reflex-induced ankle perturbation. Therefore the final force patterns in the walking simulation had a slow increase and fast decrease in amplitude (see Figure 7.3). Although most subjects reported that the force profile was similar to the ground reaction forces occurring during walking, two more control valves would be required to reduce the downward speed of the pressure plates for a better simulation of walking-like performance. The pneumatic system was easy to control, but noise should be reduced by adopting noise silencers.

One limitation of this study relates to the measurement of the ankle angle. The right foot was fixed to the shoe platform using Velcro straps. In order to record the ankle motion produced by the shoe platform, especially the ankle perturbation induced by strong reflexes, the foot as well as the shoe platform was not fixed to allow free rotation. Subjects gave subjective feedback whether the Velcro was strapped tightly enough while remaining comfortable. During the mechanical stimulation, the rising pressure plate rotated the foot, and also pushed the shoe platform away from the foot.

The distance the shoe platform should be pushed away was influenced by how tight the Velcro straps are, i.e. the tighter the straps are, the shorter distance the shoe moves. The tightness of the Velcro was not specifically controlled but was determined to such that the subjects remained comfortable. Therefore, the recorded ankle angle was a combination of movements from the foot and the platform. The extension of the pressure plate pushed the footplate further from the foot sole, which reduced the ankle angle at heel stimulation and increased the ankle angle at forefoot stimulation. Another limitation is that the shoe mimicked the force by controlling the displacement of the pressure plate instead of the actual pressure applied on the foot. The four pressures were read from the pressure gauge as shown in Figure 7.2 while the actual pressure/force on the foot was not measured. To overcome this shortcoming, pressure sensors are required to be inserted between the pressure plates and the foot sole so as to record how much pressure is actually applied by the shoe platform. Proportional valves should be adopted to control the pressure amplitude.

This study also evaluated sensation from users' feedback. Reflexes, to some extent, reflect the stimulation intensity, which is believed to be related to sensation intensity. However, reflexes have large individual variance. A better quantitative measurement of sensation is required.

The current study demonstrated technical feasibility of the dynamic shoe platform for ground force simulation and investigated the influence of different stimulation parameters on physiological responses from able-bodied subjects. The target users of the shoe platform are patients with incomplete spinal cord injury, who are more sensitive to stimuli and more vulnerable to reflexes than able-bodied subjects. Further tests should be carried out in patients in order to investigate the potential clinical usage.

7.5. Conclusions

The study demonstrated the technical feasibility of a dynamic shoe platform applying walking-like mechanical force stimulation on the foot sole of able-bodied subjects in a supine position. The shoe platform applied cyclic mechanical forces on the foot sole, which induced physiological responses in the lower leg muscles and produced pressure sensation which was similar to overground walking. The shoe platform is a useful tool to stimulate the foot sole. It can be incorporated in the GOER prototype to stimulate load receptors, thereby promoting the rehabilitation process of patients with impaired lower limb function.

Chapter 8. Discussion

Summary: With experimental walking data, the circle approximation approach for the toe trajectory was developed. The kinematics and kinetics of supine stepping were analysed through model simulation. The performance of the GOER prototype was evaluated in able-bodied subjects and was proved to be a promising device for early rehabilitation of walking. This section provides an overall discussion (advantages and limitations) of this work regarding the gait data analysis, model development, the general features and the potential application of the GOER prototype compared with current early rehabilitation devices.

In order to promote walking restoration for patients who cannot maintain an upright position, a Gait Orthosis for Early Rehabilitation (GOER) was developed in this project with the following target requirements:

1. Patients are able to perform stepping in a supine position;
2. The ankle joint is activated so as to allow coordinated kinematics of the lower limb;
3. Different speeds are accommodated to produce different training modalities;
4. Haptic feedback on the foot sole is provided to mimic the ground reaction forces.

The detailed performance requirements of the GOER system, including the ROMs of the lower limb joints and the force patterns on the foot sole, were defined using the overground walking performance from able-bodied subjects.

8.1. Gait Data Requirements and Recording Process

A gait analysis experiment was performed to record the kinematic and kinetic features of overground walking, as described in Chapter 3. Apart from providing target motion

of the GOER system, the walking data, especially the segment trajectories and ground reaction forces, were indispensable for model development in Chapter 4, because the walking performance was required to define the actuation profiles in the model for supine stepping. Therefore the requirements for input gait data to design an adequate system are the segment trajectories and the ground reaction forces during overground walking. As these required data are not available in the literature on gait performance, a gait experiment was performed, where three able-bodied subjects walked overground at three different speeds.

Treadmill walking is not suitable to produce the target gait data in this project, because (i) it is a matter of contention whether treadmill walking produces a normal gait pattern or not and (ii) the treadmill requires an additional force plate to measure the reaction forces during walking, which brings additional technical work. Therefore overground walking rather than treadmill walking was recorded in a standard gait laboratory using the Vicon motion analysis system in this project.

The three subjects recruited in the gait analysis experiment had a large range of body mass (68–95 kg) and leg length (0.88-1 m). We believe they represent the general gait pattern for healthy people. With a metronome guiding their cadence, three different speeds were tested: 100%, 75% and 50% of normal cadence (NC). Although the test results show large variability in the walking pattern at 50% of NC, walking at a slow speed is of great interest for rehabilitation devices. Since the recommended starting speed of initial clinical gait training is 1.5 km/h[9] (0.42 m/s), walking at 50% of NC

[9] Available from: http://www.hocoma.com/stroke/. Accessed on 27/11/2012.

was specially arranged in the gait analysis experiment, which managed to generate walking performance at a speed of 0.43 m/s (see Table 3.4)

The use of cadence control, which is a widely adopted method for gait analysis [239-241], was a good way to collect data in this project. The metronome helped the subjects walk at a constant speed during each trial. Subjects generated a constant movement pattern when walking at their preferred normal speed. They did not report any difficulty in following the metronome rhythm during slow walking.

8.2. Computer Design of the GOER System

The design process of the GOER system was achieved through computer simulation as documented in Chapters 4 and 5. Analysis of the foot trajectory during normal gait revealed a circular feature of the toe trajectory. Therefore computer models were developed to investigate kinematics and kinetics of supine stepping. The final structure of the GOER prototype was implemented as a bar-cam system.

8.2.1. Circle approximation of the toe trajectory

Analysis of overground walking at various speeds revealed that the foot trajectories relative to the hip joint centre were curved. It was hypothesized that the foot trajectories could be approximated by semi-circles. A least squares algorithm was developed, which managed to calculate the centre and the radius of the best-fit circles for the foot trajectories. This algorithm can be universally adopted to find the best-fit circle of any curved trajectory.

We focused on the novel approach of approximating the toe trajectory with a circle because: (i) there is a theoretical basis that walking is often described by a pendulum; (ii) the toe trajectory within the whole gait cycle is similarly curved; and (iii) the circle approximation provides a practical approach of producing the toe trajectory. Although the toe is on the ground during the stance phase, the toe trajectory relative to the hip joint is far from a straight line, as the hip joint centre moves like an inverted pendulum during the stance phase [235, 256]. Therefore it is feasible to simulate the toe trajectory relative to the hip in the stance phase using a pendulum or a circle. During the swing phase the toe lifts off the ground with a minimal distance of 5 cm [255] while the hip joint rises about 4 to 5 cm [256]. There is a limited change in the distance between the toe and the hip during the swing phase as well. These observations justify the approach in this work to approximate the toe trajectory over the whole gait cycle with a circle. The toe trajectory might be well-fit by a parabola or a complicated polynomial function, but we choose circle approximation because this method yields a small approximation error and more importantly, allows us to use a swaying rigid bar to generate the toe movement.

The circle successfully models the toe trajectories during locomotion at variable speeds, with negligible variations in the circle setup. As data from only three subjects walking at three different speeds were used to develop the circle approximation methodology, the circle configuration cannot be claimed to be general. However, after being tested using these data, we believe that the circular trajectory of the toe during the whole gait phase is a consequence of the inherent kinematics of human walking and should be broadly applicable.

8.2.2. Kinematic simulation of supine stepping

The circle approximation concept for the toe trajectory provided the basis for development of a two-bar model to simulate walking in a supine position. One actuator was employed to move the rigid bar upwards and downwards to produce the toe trajectory while a second actuator was used to control ankle dorsiflexion and plantarflexion. The combined actuation managed to produce the target foot trajectory. Although three joints (hip, knee and ankle) are active during normal walking, we focused on this two-bar model, because two actuators are enough to produce the target leg motion. According to the end-effector control method [212], if the foot follows the target trajectory relative to the hip, the leg linkage can produce a synchronised walking pattern in the lower limbs. Therefore the two-bar model provided an efficient structure for supine stepping.

The model simulated kinematics at various walking speeds, which were in good agreement with the experimental data. The kinematic simulation results demonstrated that it was feasible to approximate the toe trajectory with a semi-circle, thereby confirming the hypothesis of semi-circular foot trajectories. The experimental gait data on kinematic features of walking helped develop the model and are useful in confirming the accuracy of the two-bar model for supine stepping.

The model results implied that the two-bar system was capable of inducing supine stepping, which met the first three target requirements of the GOER system. The two-bar model was validated using data from only three subjects walking at three different speeds. Due to the limited data, the model cannot be claimed to be general. However, we believe that the model has potential to simulate walking patterns for a

large population, since the model basis, i.e. circular toe trajectory, is an inherent feature of human walking. The methodology of the two-bar model was confirmed to have potential application in gait rehabilitation systems such as the GOER system.

8.2.3. Kinetic analysis of supine stepping

The fourth requirement of the GOER system was investigated by computer modelling of a leg-linkage model, which was capable of simulating stepping at various positions with different amplitudes of the ground reaction forces.

In contrast to the kinematics of walking which are directly recorded from the gait experiment, the kinetic modelling used the estimated values of segment properties, including the moment of inertia and centre of mass, to calculate the joint moments. However, the estimation of segment properties does not influence the general patterns of moments, because the moment patterns are closely related to the ground reaction forces. The forces, which were directly recorded from the gait experiment, agree with the general description of ground reaction forces from the gait literature [243]. Therefore the moment patterns in this work were similar to the general patterns from the gait literature [243].

The kinetic model used the same data as in the experimental kinetic calculation to define the segment properties, such as the centre of mass and moment of inertia. The model was simulated using the experimental data, including the joint angle profiles and the ground reaction forces. The model reproduced the joint moments during upright walking. This confirmed the assumption of model segment properties and validated the accuracy of the leg-linkage model for kinetic analysis.

After the model with the same segment properties was rotated by 90^{o}, it became a useful tool for investigation of the kinetics of supine stepping. It was observed that the position change from upright to supine altered the moment of the hip joint during locomotion. It was observed that a simplified ground reaction force reduced the moment at the ankle joint. The position change and a simplified application of load on the model for supine stepping resulted in different moment patterns in the lower limb. These simulation results highlighted the importance of a leg frame with a dynamic shoe platform in the GOER system.

The observation of kinetic differences during supine stepping also provides important clinical guidelines for training programmes for patients, especially the strategies for training the muscles at the hip and ankle joints for patients on bed rest.

8.2.4. Simulation of the bar-cam GOER system

These computer modelling studies provided a useful basis for the conceptual design of the GOER system, as they allowed determination of the important structures and components including the bar-leg setup, the leg frame and proper mechanical force stimulation on the foot sole. In order to obtain a GOER system with efficient power transmission, a synthesis process was carried out for the design of a four-bar linkage and a cam-roller mechanism, which succeeded in generating target periodical movements of the driven bar and the foot using a constantly-rotating motor. Another advantage of using the bar-cam structure is that the cam limited the motion range, thus making the system safer for potential users, especially SCI patients. Employment of a counterweight reduced the power requirements of the bar-cam GOER system.

These simulation results confirmed the design process of the cam-bar mechanism and provided the basis for the prototype manufacture. The design techniques of the bar-cam mechanisms and the counterbalance concept were successfully applied in the GOER system and have potential application in general mechanical design.

8.3. Evaluation of the GOER Prototype

The performance of the GOER prototype was evaluated in able-bodied subjects, as shown in Chapters 6 and 7. Specific attention was paid to the joint angles and foot sole stimulation.

8.3.1. Joint angles induced by the bar-cam system

By controlling one electric motor, a combined motion in the bar linkage and the cam was achieved, which enabled the GOER prototype to produce supine stepping. Preliminary investigation of the passive leg movements in the users showed that the GOER prototype was capable of inducing coordinated leg motion in a supine position with ROMs of the leg joints similar to overground walking at normal speed. The GOER prototype was manufactured after analysis on the suitable materials. Based on the calculation of bending failure mode, the material of the driven bar was carefully selected to prevent elastic deformation. Furthermore, the test did not include a leg frame and the subjects were encouraged to support their leg weight voluntarily, therefore the load on the GOER prototype was fairly small. The driven bar did not show elastic deformation during the tests.

These experimental results confirmed the efficacy of the model development of the

GOER system in computer simulation in Chapter 4 and 5, and demonstrated that the prototype met the first two requirements of the GOER system. Although the fixed foot path generated by the bar-cam mechanism kinematically limited ROMs in the hip, knee and ankle joints, different stepping speeds were produced in the GOER prototype by changing the rotation speed of the motor. The third requirement of the GOER system, i.e. different training modalities such as adaptable ROMs of the lower limb joints, can be achieved by further investigation of new actuation concepts, where linear actuators serve as a potential solution.

8.3.2. Foot sole stimulation induced by the shoe platform

A pneumatic shoe platform was developed to apply forces on the foot sole with users in a supine position for simulation of the ground reaction forces. Preliminary tests results in Chapter 7 showed that the shoe platform managed to apply cyclic mechanical forces with adjustable amplitudes on the foot sole, and produced walking-like sensation (force timing) in able-bodied subjects with physiological responses from the lower leg muscles. The force profile can be further improved by adopting more cylinders, so that different forces can be applied on different areas of the foot sole, so as to mimic the load as seen in the gait cycle. The shoe platform should incorporate force sensors to record interaction forces between the shoe platform and the foot sole, thereby providing feedback for the force control.

The mechanical pressure deformed the soft tissues on the foot sole, which resulted in loading (pressure) that was sensed by the subjects. Although the actual force applied on the foot sole was not measured, the maximum force that can be generated by the cylinder is 280 N. This force amplitude corresponds to approximately 30% to 60% of

the body weight of the subjects tested. We believe the system is safe for load application to the foot when constrained by Velcro strapping.

The shoe platform met the design target and is a useful tool for application of mechanical stimulation on the foot soles. It can be incorporated in the GOER prototype to fulfill the fourth requirement of load stimulation.

8.4. Overall Evaluation of the GOER System

There are currently several rehabilitation devices focusing on lower-limb training which do not require the user to be in an upright position, including recumbent tricycles [220], the MotionMaker [221], the MoreGait system [222] and the commercially available Erigo device [219]. However, none of these devices can produce coordinated walking-like movement in the lower limbs. Furthermore, the first two devices have no dynamic loading on the foot sole. The Erigo implements force on the foot sole via gravity, but the force patterns are different from walking. The MoreGait system provides walking-like stimulation on the foot sole, but like many other rehabilitation devices such as the Lokomat, the ankle joint is not actuated in the way required during walking.

Stepping of the lower limbs in a walking manner is therefore a key novel feature of the GOER system and is believed to promote recovery of locomotion by inducing proprioceptive feedback from the leg joints [65]. Cyclic mechanical stimulation on the foot sole with cutaneous sensation similar to walking, as demonstrated by the shoe platform of the GOER prototype, is considered to promote the integrated functions of the neuromuscular and musculoskeletal systems [1]. The GOER system, which

combines coordinated walking-like supine stepping in the lower limbs with synchronised cyclic force stimulation on the foot sole, has been demonstrated to be a technically promising system for rehabilitation of walking for users who are restricted to a supine position, and it provides functionality not available in current rehabilitation devices.

Chapter 9. Conclusions

With an activated ankle joint, the GOER system was developed, which allows users to practice walking in a supine position with synchronised mechanical stimulation on the foot sole for ground force simulation.

Analysis of overground walking at various speeds revealed that the foot trajectories relative to the hip joint centre were curved, which inspired approximation of the foot trajectories by a circle via least squares optimisation. The ankle and the heel move in circular paths in the stance phase, which agrees with the pendulum concept of locomotion described in [246, 247]. Furthermore, a novel demonstration was that the toe trajectory relative to the hip joint centre followed a circular path in the whole gait cycle. This observation justified simulation of the toe motion over the whole gait cycle using a rigid bar, which provided a new approach for the design of gait robots.

Based on the circle-approximation of the toe trajectory, a computer model of a two-bar mechanical system was developed, which produced supine stepping at various speeds. Kinetic analysis on a leg linkage model revealed that a leg frame was required to compensate the position change during supine stepping and a dynamic shoe platform was indispensable for simulation of ground reaction forces.

With information on mechanical design obtained from computer modelling, a bar-cam GOER prototype was manufactured with a pneumatic shoe platform. The GOER prototype induced synchronised motion in the hip, knee and ankle joints in three able-bodied subjects, which was similar to overground walking. The dynamic shoe platform produced walking-like sensation on the foot sole and physiological responses

from the leg muscles in ten able-bodied subjects. Therefore the GOER prototype was proven to be technically feasible for supine stepping.

In conclusion, we have developed the GOER system which combines coordinated walking-like supine stepping in the lower limbs with synchronised force stimulation on the foot sole. This research demonstrated technical feasibility of the GOER system. It is a promising device for early rehabilitation of walking.

Chapter 10. Future Work

Summary: Future development of the GOER system is discussed based on the design of and experimental evaluation of the GOER prototype. A gait analysis experiment recruiting more subjects walking at a new speed range is desirable so as to further validate the circle-fit approximation algorithm and generalise the target performance of the GOER system. Manufacture of the second leg for the GOER prototype and employment of a powerful electric motor are required so as to investigate coordinated movement of two legs with synchronised mechanical stimulation of the foot soles. An improved GOER system with new actuation concepts has been proposed to obtain a multifunctional mechanism. Potential employment of sensory electrical stimulation is discussed. Moreover, some recommendations are given for improvement of the dynamic shoe platform. With these modifications and the evaluation, the GOER system can be further developed to produce adaptable stepping in various positions with synchronised loading on the lower limbs for patients who cannot maintain an upright position.

10.1. Gait Analysis Experiment

Upright walking is a challenging task which involves sensing the dynamic ground reaction forces on the foot soles for maintenance of balance and synchronising complex intersegmental motion of the lower limbs for forward progression [300]. A gait analysis experiment was performed in three able-bodied subjects to record the kinematic and kinetic features of overground walking in three able-bodied subjects. A further gait analysis experiment is desirable with more subjects. Foot trajectories, especially the toe trajectory from a large subject group with different leg lengths, should be investigated so as to obtain general results for the best-fit circle: the circle

configuration (the circle centre and radius) as a function of the leg length. Under these circumstances, applicability of the two-bar GOER model can be generalised.

Walking parameters such as the step lengths, ranges of motion (ROMs) of the lower limb joints and intersegmental dynamics vary according to the speed. Therefore future gait experiments should also investigate walking performance at various speeds. Most patients cannot perform training of high intensity due to their physical weakness. Therefore slow walking is of great interest in designing robotic rehabilitation devices. However, the speed of walking during the experiment should not be as slow as 50% of normal cadence (NC). The human performs overground locomotion at normal speed subconsciously, resulting in a walking pattern at 100% of NC with high consistency and reproducibility (see Figures 3.3 and 3.6). However, the performance variance increases when the speed reduces. This is because the human produces conscious voluntary input to purposely reduce the speed and this voluntary input has intra- and inter-individual variability. Therefore the gait experiment described in Chapter 3 showed that walking at 50% of NC, which is equivalent to only one third of normal walking speed (see Table 3.4), had high variability (see Figures 3.5 and 3.8). Based on the relatively low variance observed at 75% of NC, the speed range for further gait experiments is suggested to be between 75-100% of NC. Slow walking can be guided by an electronic metronome, and the speed can be reduced by 10 or 20 steps/min for each session, such as in the study [243]. Then the changing trend of walking performance within the speed range of 75-100% of NC will be obtained and can be used to predict walking patterns at an even slower speed. Regression analysis serves as a good method for prediction, judging by its successful application in predicting walking performance in children who have different normal walking speeds [236].

10.2. The Bar-cam GOER Prototype for the Other Leg

The current GOER prototype allowed preliminary evaluation of the performance of one leg only. However, the whole bar-cam GOER system for two legs needs to be manufactured for extensive functional investigation. The combination of the bar and cam mechanisms in the GOER prototype managed to generate target motion in the lower limb, which confirmed the accuracy of the design process and provided the basis for the manufacture of the robotic system for the other leg. The relevant systems for the other leg, such as the driven bar, shoe platform and bar-cam mechanism, are of the same specification documented in Chapter 5.

This bar-cam setup reduces the complexity of motor control, because movement synchronisation of the hip, knee and ankle joints is achieved through the mechanical systems of the bar linkage and the cam mechanism, which are driven by a constantly-rotating motor. The potential bar-cam system for the other leg can be driven by the same electric motor, as long as the motor is powerful enough to move two legs. However, the selection of materials requires further investigation. The plastic cam was observed to wear down gradually during the experimental evaluation of the prototype. Therefore the cam should be manufactured with a strong but light material, such as aluminium alloy, to rotate the highly-loaded foot via the shoe platform. Furthermore, subjects reported the pelvis was not comfortable at hip extension during the preliminary test of the GOER prototype (see Chapter 6). Therefore a soft and rotatable pelvic support is desirable to allow clinical application.

Driven by a powerful motor unit, the updated GOER prototype would allow attachment of the leg frames and the shoe platforms for both legs. This provides the

opportunity to evaluate supine stepping with synchronised mechanical stimulation on the foot sole when the users are supported in a comfortable position.

10.3. Investigation of New Actuation Concepts

By employing only one constantly-rotating electric motor, the bar-cam GOER prototype described in Chapter 6 reduced the complexity of the movement control strategies. The disadvantage of the prototype is that the fixed foot path limits the adaptability of the stepping pattern, i.e. the step length and ROMs of the lower limb joints cannot change according to the stepping speed. Although intensive repeatable movements are essential for recovery, training with a small degree of kinematic variability in different modalities might be necessary to prevent training habituation to a fixed locomotor performance [211, 266]. Therefore, alternative actuation concepts should be investigated to increase the potential for clinical application.

Linear actuators, as shown in Figure 5.3(a), serve as good options to produce adaptable kinematics of the lower limbs. Continuous walking at various speeds with adjustable ROMs can be achieved by changing the stroke length of the linear actuators. Furthermore, an additional linear actuator can be adopted to change the bed position as in adjustable tilt tables, so that different training positions can be achieved.

A linearly-actuated GOER system could produce adaptable stepping with various training positions, which could serve as a device to progress patients from supine to upright walking training.

10.4. Electrical Stimulation for Sensory Feedback

Electrical stimulation can be implemented in the GOER system. Functional electrical stimulation (FES) is a widely used modality for muscle training [301] and movement control of weak or paralysed limbs [220]. FES has been applied on the muscles around the ankle joint to assist ankle rotation during upright walking [168]. Apart from providing additional power for walking, FES trains the muscles in the way required during overground walking, which is believed to promote walking restoration [180]. However, FES was not adopted to move the leg in the GOER system, because the required torque profile to move the leg in the GOER system (Figure 5.1(b)) is different from the torque in the ankle joint during overground walking (Figure 3.10), especially during the swing phase. Overground walking requires low torque to dorsiflex the foot for toe clearance, while supine stepping requires plantarflexion torque to prevent hyperflexion of the ankle joint (see Section 5.1.1). The use of FES to rotate the ankle in the GOER system might train the muscles in a way that is different from the normal performance during overground walking.

Nevertheless, electrical stimulation can be employed in the GOER system to provide sensory feedback. Patients might perform passive training in the GOER system due to physical weakness in the early phase after injury. As visual and vestibular sensory organs do not provide feedback of stepping training, additional methods such as cutaneous and proprioceptive feedback should be exploited to indicate the leg motion. Sensory electrical stimulation can be employed in the GOER system by stimulating muscles which synchronise walking at different gait phases, thereby providing benefit. The application of electrical stimulation is of interest and requires further research.

10.5. Improvement of the Dynamic Shoe Platform

Ground reaction forces provide important information related to walking. A pneumatic shoe platform was designed in this PhD work to stimulate the foot sole for cutaneous feedback of walking. Evaluation of the shoe platform described in Chapter 7 revealed several issues for further research.

The shoe platform adopted two one-way control valves to adjust the rising speed of the two pressure plates (one for the forefoot and one for the heel). Although walking-like sensations were induced in able-bodied subjects, the shoe platform requires two additional one-way control valves for regulation of the descending speed of the pressure plates. By reducing both the rising and descending speeds of the pressure plates, the final force patterns generated by the shoe platform will be close to the ground reaction forces as shown in Figure 5.18(b). The force profile can be further improved by adopting more cylinders, so that different forces can be applied on different areas of the foot sole, thereby mimicking the moving path of the centre of pressure on the foot sole (see Figure 5.18(a)). Proportional valves should be adopted to control the force amplitude and to coordinate the force with the leg motion. The shoe platform should incorporate force sensors to record interaction forces between the shoe platform and the foot sole, thereby providing feedback for the force control. After further development the shoe platform would finally be able to produce adaptable forces initially on the heel and lastly on the toe, which resemble the ground reaction forces occurring during overground walking.

Research on active usage of the shoe platform is of great interest. Able-bodied subjects reported pressure on the foot sole when using the shoe platform in a relaxed

situation (see Chapter 7). It is believed that active resistance against the mechanical stimulation will transmit the load to the lower limb joints, resulting in a similar loading situation during the stance phase of overground walking. Last but not least, the updated shoe platform should be safe to use in patients. Muscle activity at different stimulation intensities, including different force amplitudes and force rising rates, should be investigated. The clinical response should be evaluated before it is incorporated in the GOER system.

10.6. Conclusions

Further research will allow the GOER system to induce adaptable stepping patterns at various positions with increased functional potential, especially in clinical application. The GOER system will have wider applicability through an expanded target performance after a further gait analysis experiment. The GOER prototype with both legs will allow further functional evaluation. A new GOER system incorporating electrical stimulation will bring more training modalities and sensory feedback. With new actuation concepts and improved shoe platforms, the GOER system can eventually be developed to induce coordinated motion of both legs with adjustable stepping patterns and synchronised ground reaction forces for users in a supine position.

Due to the close research collaboration with the Queen Elizabeth National Spinal Injuries Unit, the GOER system was initially intended to be designed for patients with spinal cord injury. However, it is believed that the improved GOER system is generally applicable to patients with a range of neurological impairments who undergo therapy for rehabilitation of walking.

Appendices

Appendix 1: Model of a two-bar system

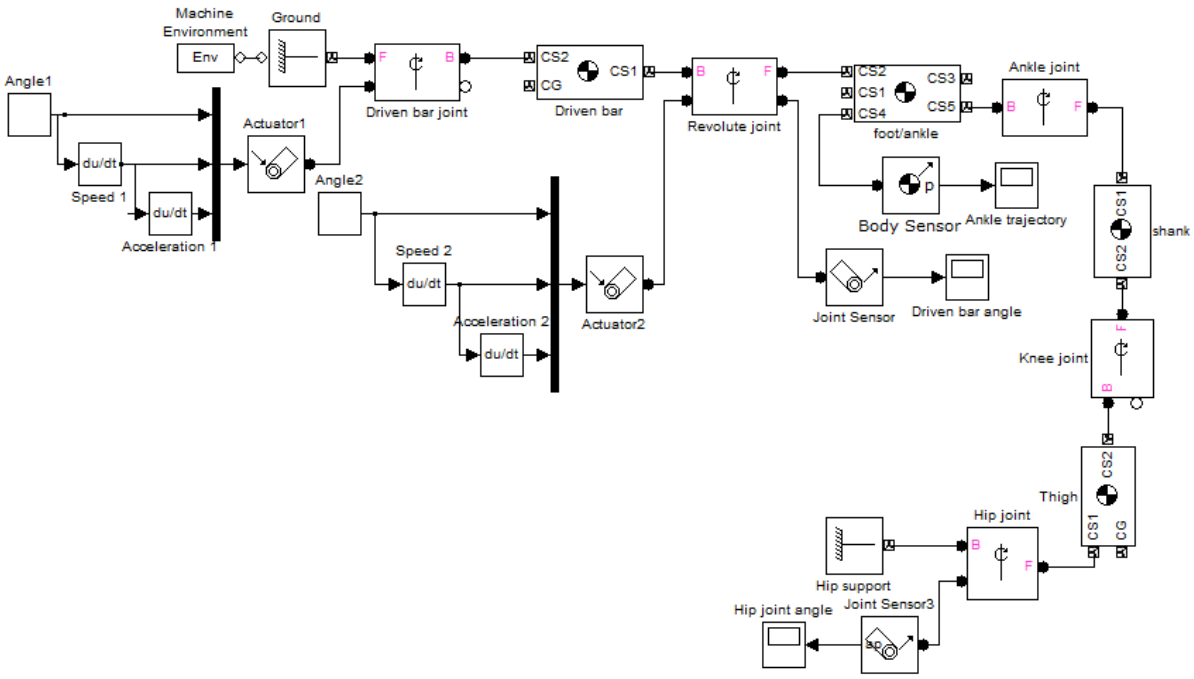

Figure A. 1: Model of a two-bar system.

All blocks use default units. The parameters of each block are as follows:

Machine Environment:

Gravity vector: [0 -9.81 0];

Ground:

Location: [0, 0.98, 0];

Driven bar:

Mass: 0.8;

Inertia: [2.7e-5 0 0; 0 0.025 0; 0 0 0.4084];

CG: [0.44 0.32 0]; world; world;

CG1: [0.44 0.32 0]; world; world;

CG2: [0 0 0]; adjoining; adjoining;

Foot:

Mass: 1.1;

Inertia: [2.69e-3 0 0;0 2.69e-3 0;0 0 2.69e-3];

CG: [0 0 0]; CS3; CS3;

CG1: [0 0 0]; CS2; CS2;

CG2: [0 0 0]; adjoining; adjoining;

CG3: [0.93 0.38 0]; world; world;

CG4: [0.97 0.35 0]; world; world;

CG5: [0.93 0.38 0]; world; world;

Shank:

Mass: 6.28;

Inertia: [0.013 0 0; 0 0.14 0; 0 0 0.14];

CG: [0 0 0]; CS3; CS3;

CG1: [0 0 0]; adjoining; adjoining;

CG2: [0 0 0]; world; world;

CG3: [0.46 0.22 0]; world; world;

Thigh:

Mass: 13.5;

Inertia: [0.052 0 0; 0 0.338 0; 0 0 0.338];

CG: [0 0 0]; CS1; CS1;

CG1: [0 0 0]; adjoining; adjoining;

CG2: [0 0 0]; adjoining; adjoining;

Hip support:

Location: [0, 0, 0];

Angle 1: the solid curve in Figure 4.10 (a).

Angle 2: the solid curve in Figure 4.10 (b).

Appendix 2: Model of a leg linkage

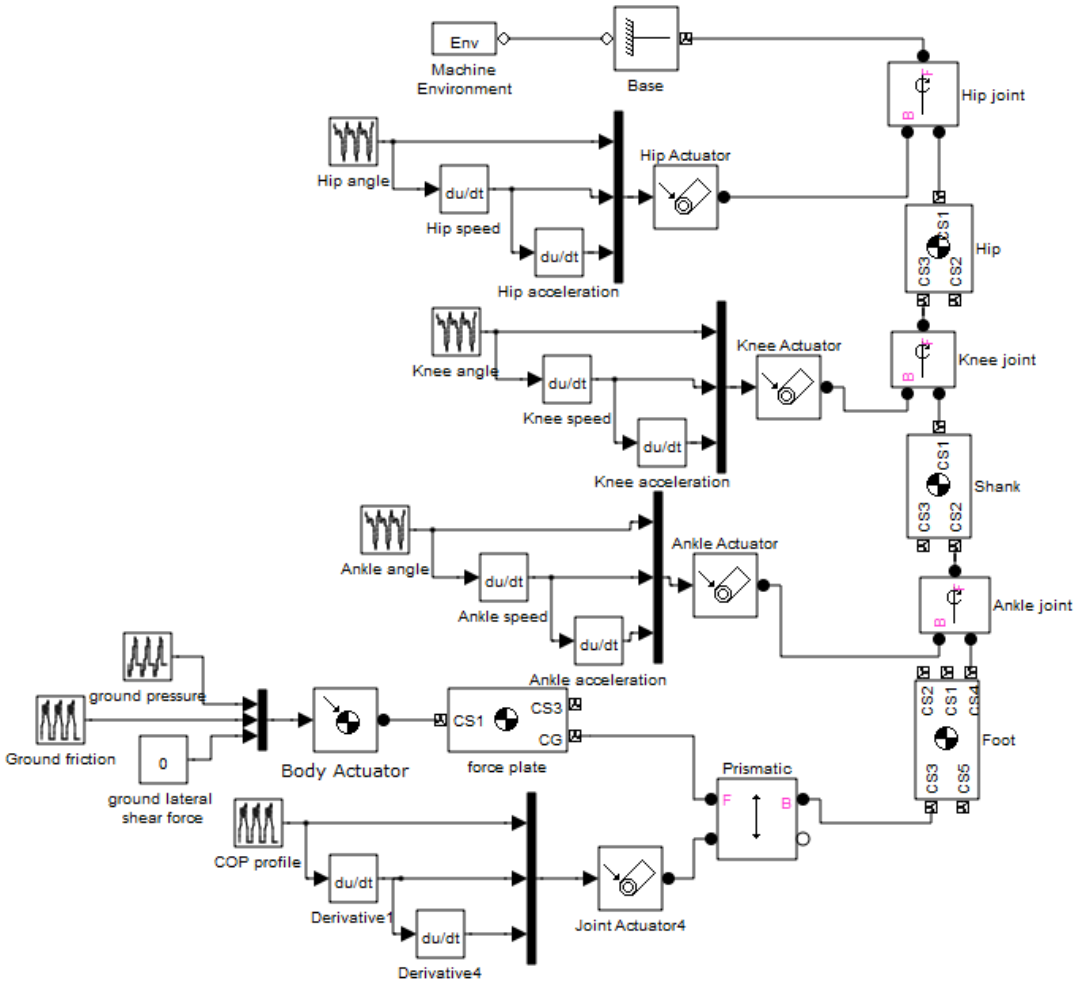

Figure A. 2: Model of a leg linkage.

All blocks use default units. The parameters of each block are as follows:

Machine Environment:

Gravity vector: [0 -9.81 0];

Ground:

Location: [0, 0, 0];

Force plate

Mass: 0.1;

Inertia: [2.69e-3 0 0; 0 2.69e-3 0; 0 0 2.69e-3];

CG: [0 0 0]; adjoining; adjoining;

CG1: [0 0 0]; CG; CG;

CG2: [0 0 0]; CG; CG;

Foot:

Mass: 1.1;

Inertia: [2.69e-3 0 0; 0 2.69e-3 0; 0 0 2.69e-3];

CG: [0 0 0]; CS3; CS3;

CG1: [0 0 0]; CS2; CS2;

CG2: [0.237 -0424 0]; world; world;

Shank:

Mass: 6.28;

Inertia: [0.013 0 0; 0 0.14 0; 0 0 0.14];

CG: [0 0 0]; CS3; CS3;

CG1: [0 0 0]; adjoining; adjoining;

CG2: [0.237 -0424 0]; world; world;

Thigh:

Mass: 13.5;

Inertia: [0.052 0 0; 0 0.338 0; 0 0 0.338];

CG: [0 0 0]; CS1; CS1;

CG1: [0 0 0]; adjoining; adjoining;

CG2: [0 0 0]; adjoining; adjoining;

Base: Location: [0, 0, 0];

Hip angle: the solid curve in the upper plot in Figure 3.4;

Knee angle: the solid curve in the middle plot in Figure 3.4;

Ankle angle: the solid curve in the bottom plot in Figure 3.4.

Appendix 3: The two-bar model for power analysis

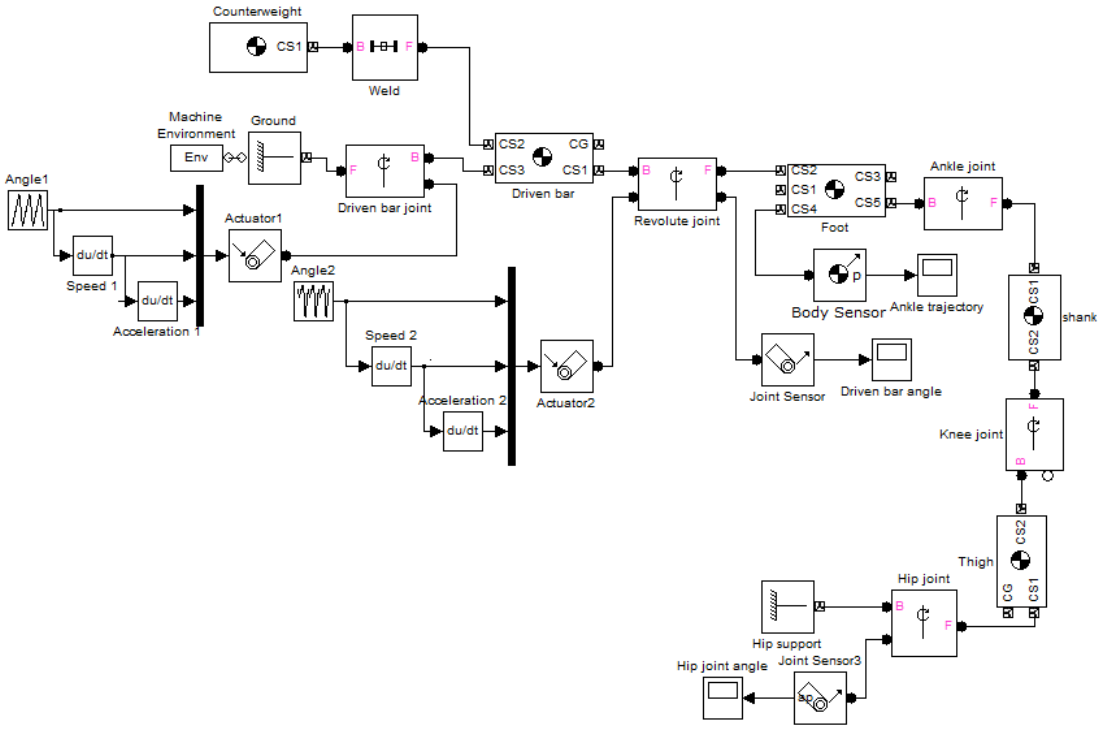

Figure A. 3: The model for torque and power simulation.

All blocks use default units. The parameters of each block are as follows:

Machine Environment:

Gravity vector: [0 -9.81 0];

Ground:

Location: [0, 0.98, 0];

Driven bar:

Mass: 2;

Inertia: [2.7e-5 0 0; 0 0.025 0; 0 0 0.4084];

CG: [0.44 0.32 0]; world; world;

CG1: [0.44 0.32 0]; world; world;

CG2: [0 0 0]; adjoining; adjoining;

Foot:

Mass: 1.1;

Inertia: [2.69e-3 0 0; 0 2.69e-3 0; 0 0 2.69e-3];

CG: [0 0 0]; CS3; CS3;

CG1: [0 0 0]; CS2; CS2;

CG2: [0 0 0]; adjoining; adjoining;

CG3: [0.93 0.38 0]; world; world;

CG4: [0.97 0.35 0]; world; world;

CG5: [0.93 0.38 0]; world; world;

Shank:

Mass: 6.28;

Inertia: [0.013 0 0; 0 0.14 0; 0 0 0.14];

CG: [0 0 0]; CS3; CS3;

CG1: [0 0 0]; adjoining; adjoining;

CG2: [0 0 0]; world; world;

CG3: [0.46 0.22 0]; world; world;

Thigh:

Mass: 13.5;

Inertia: [0.052 0 0; 0 0.338 0; 0 0 0.338];

CG: [0 0 0]; CS1; CS1;

CG1: [0 0 0]; adjoining; adjoining;

CG2: [0 0 0]; adjoining; adjoining;

Hip support: Location: [0, 0, 0];

Angle 1: the solid curve in Figure 4.9(a);

Angle 2: the solid curve in Figure 4.9(b).

Appendix 4: The cam-roller assembly

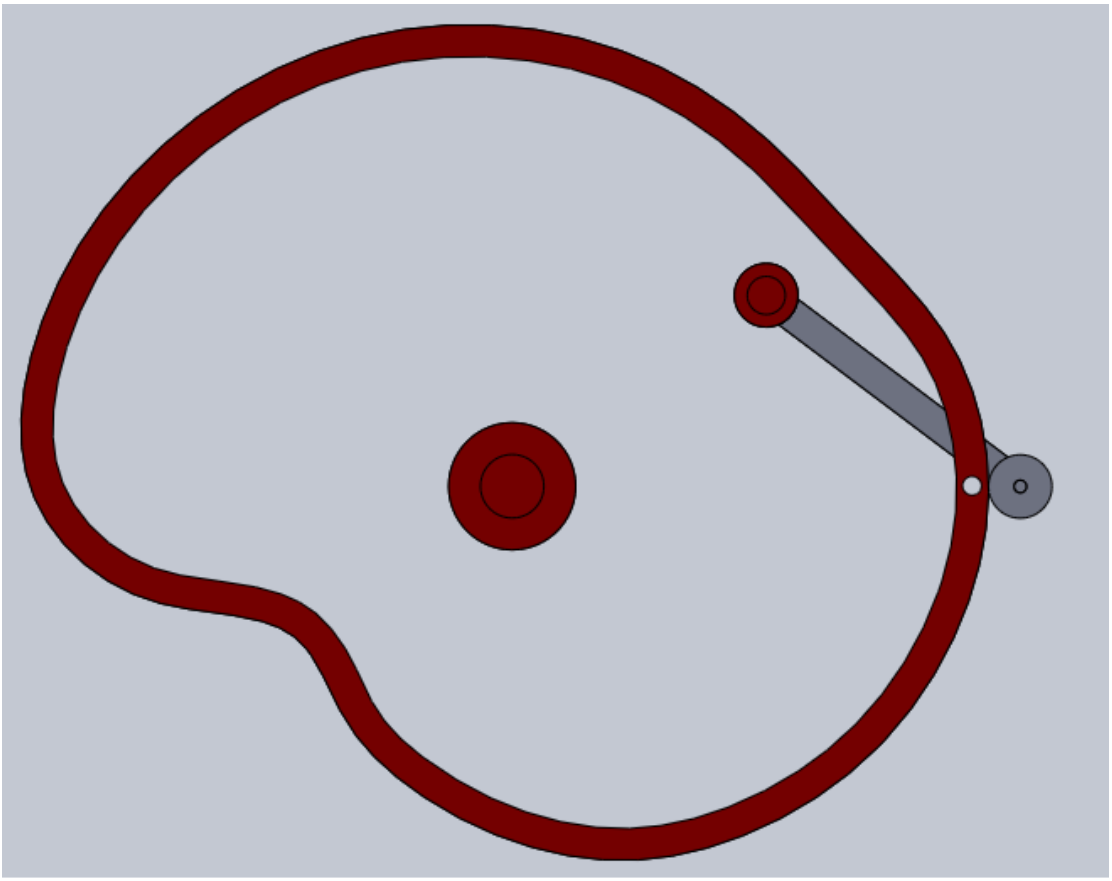

Figure A. 4: The cam-roller mechanism.

Appendix 5: The model of the bar-cam GOER system

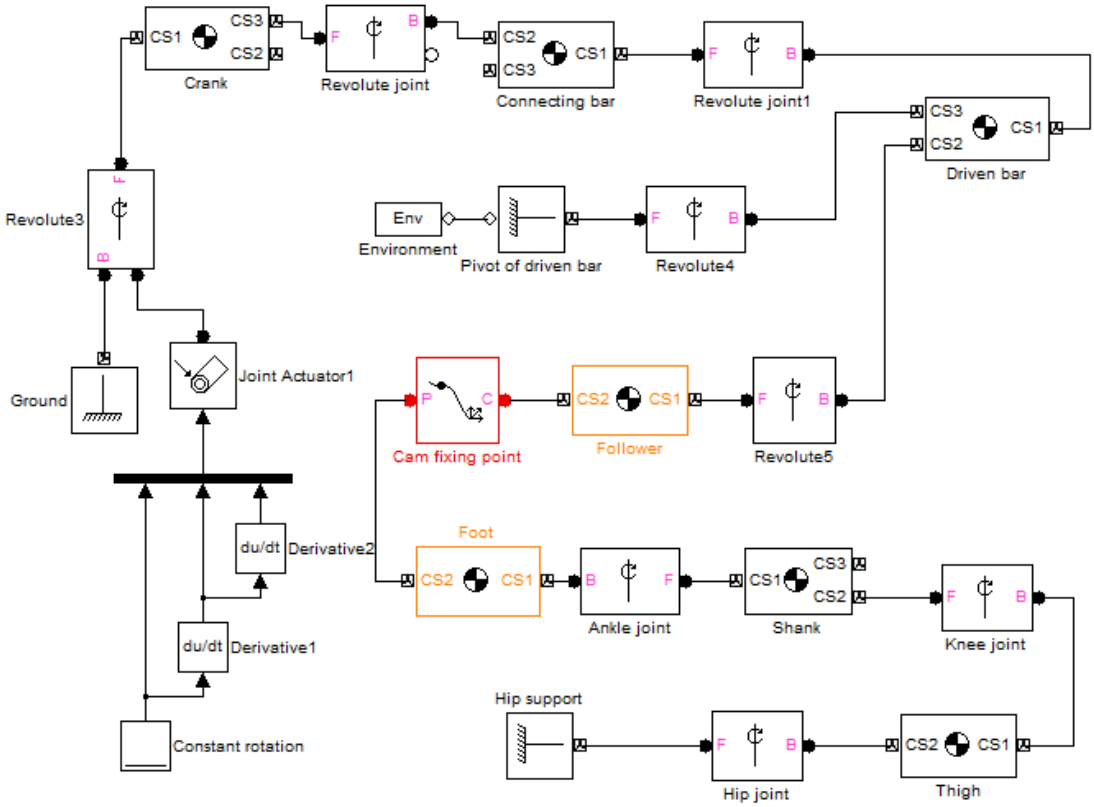

Figure A. 5: The model of the bar-cam GOER system.

All blocks use default units. The parameters of each block are as follows:

Machine Environment:

Gravity vector: [0 -9.81 0];

Position of driven bar:

Location: [0, 0, 0];

Driven bar:

Mass: 2;

Inertia: [2.7e-5 0 0; 0 0.025 0; 0 0 0.4084];

CG: [0.44 0.32 0]; world; world;

CG1: [0.44 0.32 0]; world; world;

CG2: [0 0 0]; adjoining; adjoining;

Connecting bar:

Mass: 1.6;

Inertia: [2.16e-3 0 0;0 2.16e-3 0;0 0 6.69e-4];

CG: [0 0 0]; CS3; CS3;

CG1: [0 0 0]; CS2; CS2;

CG2: [0.003 0.4 0]; world; world;

CG3: [-0.34 -0.2732 0]; world; world;

Crank:

Mass: 0.6;

Inertia: [1.96e-3 0 0; 0 1.96e-3 0; 0 0 3.07e-4];

CG: [0 0 0]; CS3; CS3;

CG1: [0 0 0]; CS2; CS2;

CG2: [0.003 0.4 0]; world; world;

CG3: [-0.926 -0.522 0]; world; world;

Ground:

Location: [0.926 -0.522 0];

Follower:

Mass: 0.7;

Inertia: [6.9e-5 0 0; 0 1.4e-3 0; 0 0 3.69e-3];

CG1: [0.06 0.18 0]; adjoining; adjoining;

CG2: [0.27 0.35 0]; CG1; CG1;

Foot:

Mass: 1.1;

Inertia: [2.69e-3 0 0; 0 2.69e-3 0; 0 0 2.69e-3];

CG: [0 0 0]; CS3; CS3;

CG1: [0 0 0]; CS2; CS2;

CG2: [0 0 0]; adjoining; adjoining;

CG3: [0.93 0.38 0]; world; world;

CG4: [0.97 0.35 0]; world; world;

CG5: [0.93 0.38 0]; world; world;

Shank:

Mass: 6.28;

Inertia: [0.013 0 0; 0 0.14 0; 0 0 0.14];

CG: [0 0 0]; CS3; CS3;

CG1: [0 0 0]; adjoining; adjoining;

CG2: [0 0 0]; world; world;

CG3: [0.46 0.22 0]; world; world;

Thigh:

Mass: 13.5;

Inertia: [0.052 0 0; 0 0.338 0; 0 0 0.338];

CG: [0 0 0]; CS1; CS1;

CG1: [0 0 0]; adjoining; adjoining;

CG2: [0 0 0]; adjoining; adjoining;

Hip support:

Location: [0, 0, 0];

Cam fixing point:

X, Y component: see Figure 5.13;

Constant rotation: 50 rpm.

Appendix 6: The CAD drawings of the driven bar and leg frame

The driven bar is designed with one tube (Figure A. 6) inside the other tube (Figure A. 7), which achieves an adjustable total length of the driven bar.

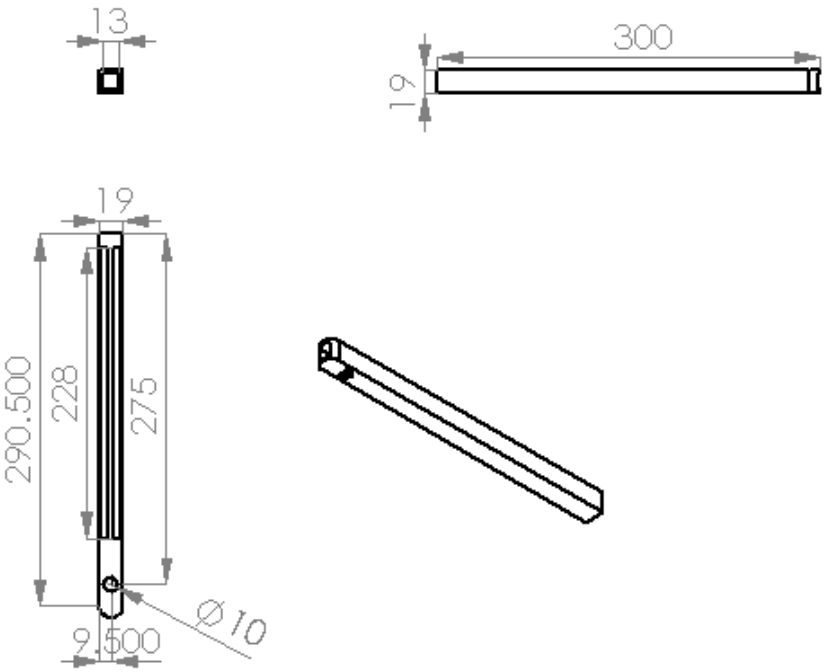

Figure A. 6: The inner tube of the driven bar.

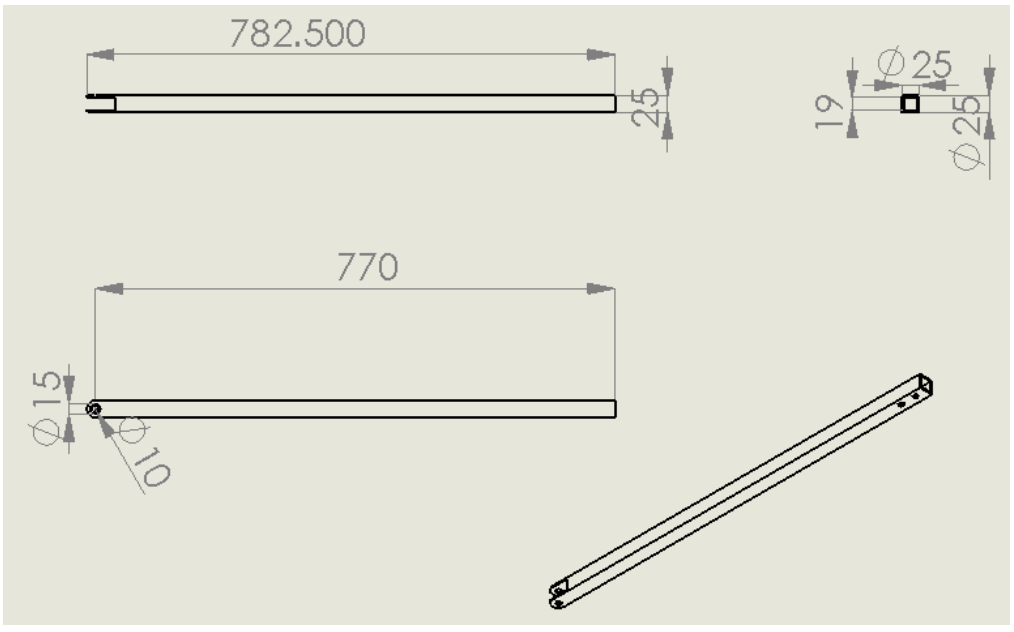

Figure A. 7: The outer tube of the driven bar.

The leg frame is made of a thigh and a shank frame. Similar to the driven bar, both the thigh and shank frames have one tube inside the other, resulting in a leg frame with an adjustable length. Furthermore, the thigh and the calf supports are designed as well.

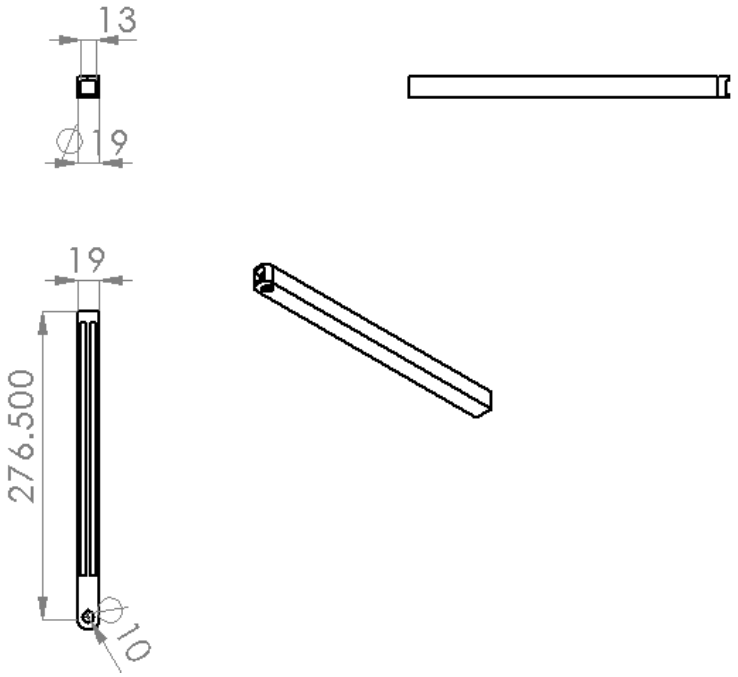

Figure A. 8: The inner tube of the thigh frame.

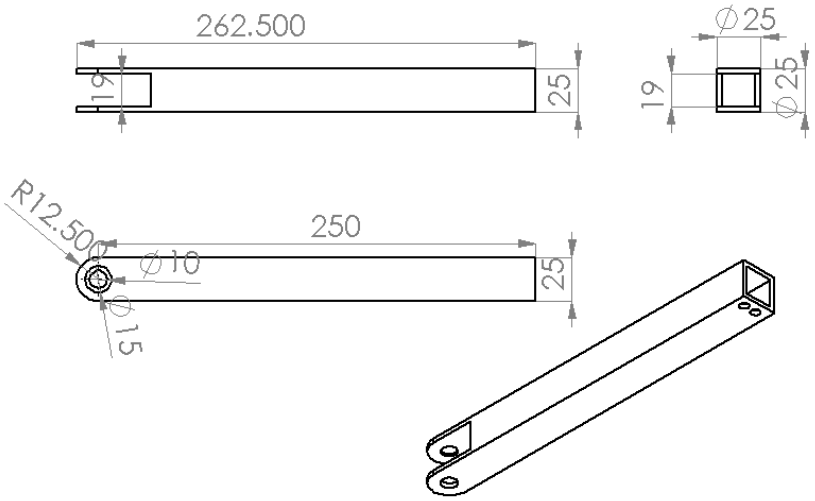

Figure A. 9: The outer tube of the thigh frame.

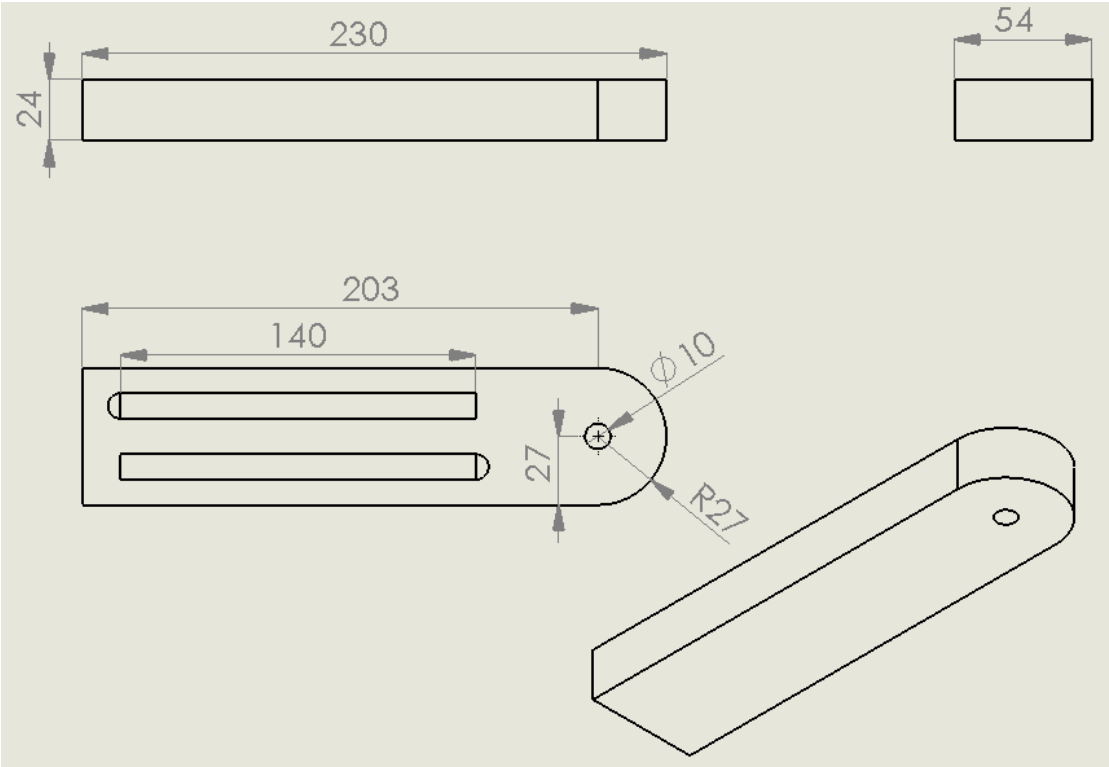

Figure A. 10: The inner tube of the shank frame.

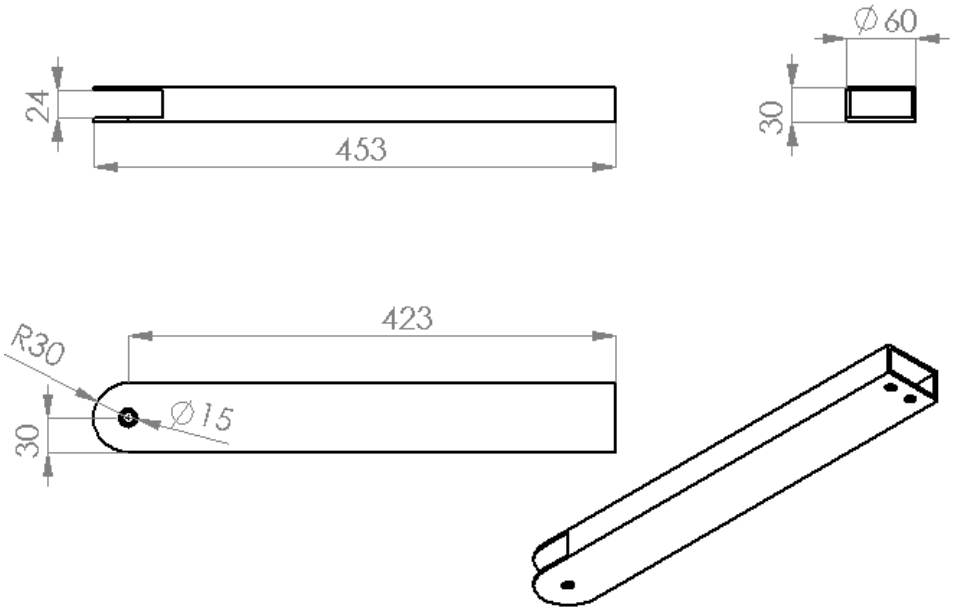

Figure A. 11: The outer tube of the shank frame.

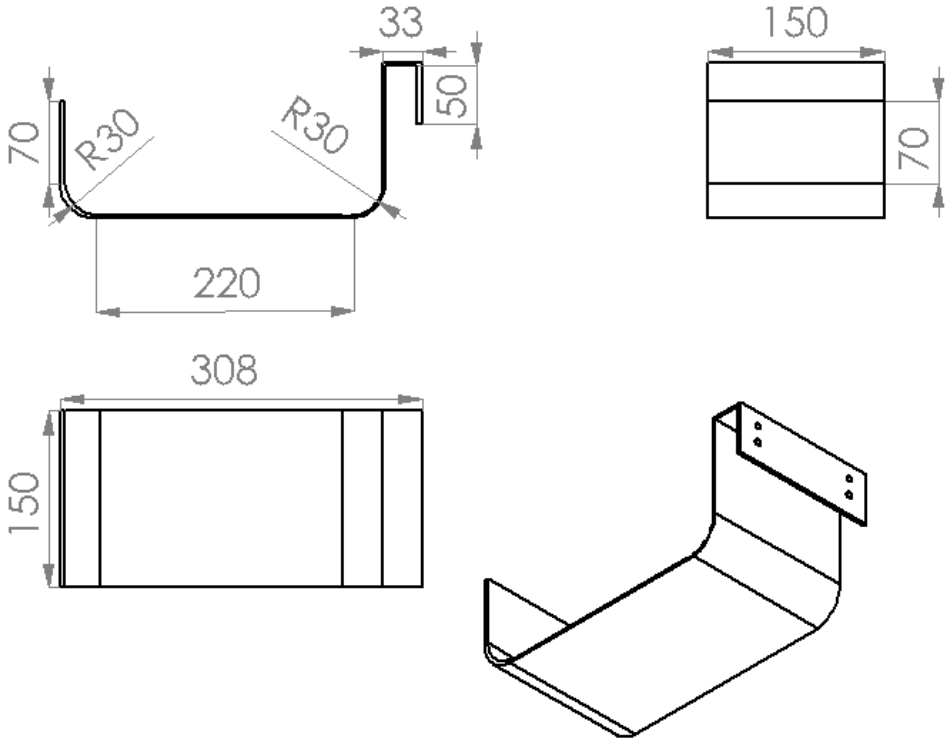

Figure A. 12: The thigh support.

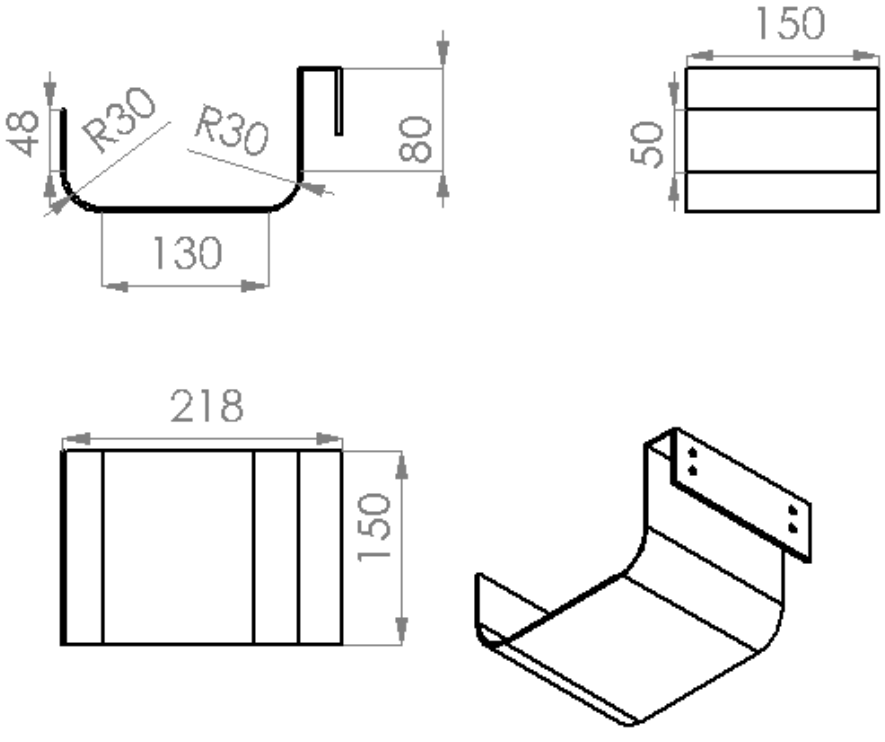

Figure A. 13: The calf support.

Appendix 7: The model of the bar-cam GOER system with a counterweight

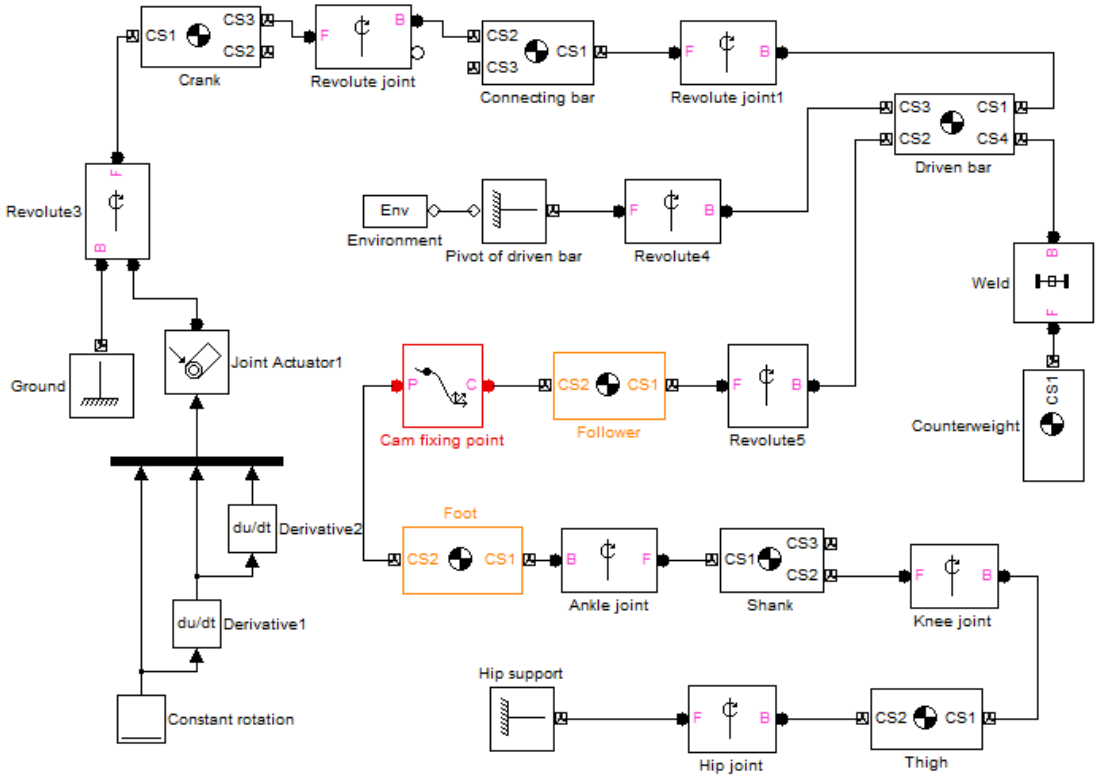

Figure A. 14: Model of the bar-cam GOER system with a counterweight.

All blocks use default units. The parameters of each block are as follows:

Machine Environment:

Gravity vector: [0 -9.81 0];

Position of driven bar:

Location: [0, 0, 0];

Driven bar:

Mass: 2;

Inertia: [2.7e-5 0 0; 0 0.025 0; 0 0 0.4084];

CG: [0.44 0.32 0]; world; world;

CG1: [0.44 0.32 0]; world; world;

CG2: [0 0 0]; adjoining; adjoining;

Counterweight:

Mass: 29.3;

Inertia: [7.2e-3 0 0; 0 7.2e-3 0; 0 0 0.4084];

CG: [0.5 0 0]; adjoining; adjoining;

CG1: [0.74 1.72 0]; world; world;

CG2: [0 0 0]; adjoining; adjoining;

Connecting bar:

Mass: 1.6;

Inertia: [2.16e-3 0 0; 0 2.16e-3 0; 0 0 6.69e-4];

CG: [0 0 0]; CS3; CS3;

CG1: [0 0 0]; CS2; CS2;

CG2: [0.003 0.4 0]; world; world;

CG3: [-0.34 -0.2732 0]; world; world;

Crank:

Mass: 0.6;

Inertia: [1.96e-3 0 0;0 1.96e-3 0;0 0 3.07e-4];

CG: [0 0 0]; CS3; CS3;

CG1: [0 0 0]; CS2; CS2;

CG2: [0.003 0.4 0]; world; world;

CG3: [-0.926 -0.522 0]; world; world;

Ground:

Location: [0.926, -0.522, 0];

Follower:

Mass: 0.7;

Inertia: [6.9e-5 0 0; 0 1.4e-3 0; 0 0 3.69e-3];

CG1: [0.06 0.18 0]; adjoining; adjoining;

CG2: [0.27 0.35 0]; CG1; CG1;

Foot:

Mass: 1.1;

Inertia: [2.69e-3 0 0;0 2.69e-3 0;0 0 2.69e-3];

CG: [0 0 0]; CS3; CS3;

CG1: [0 0 0]; CS2; CS2;

CG2: [0 0 0]; adjoining; adjoining;

CG3: [0.93 0.38 0]; world; world;

CG4: [0.97 0.35 0]; world; world;

CG5: [0.93 0.38 0]; world; world;

Shank:

Mass: 6.28;

Inertia: [0.013 0 0; 0 0.14 0; 0 0 0.14];

CG: [0 0 0]; CS3; CS3;

CG1: [0 0 0]; adjoining; adjoining;

CG2: [0 0 0]; world; world;

CG3: [0.46 0.22 0]; world; world;

Thigh:

Mass: 13.5;

Inertia: [0.052 0 0; 0 0.338 0; 0 0 0.338];

CG: [0 0 0]; CS1; CS1;

CG1: [0 0 0]; adjoining; adjoining;

CG2: [0 0 0]; adjoining; adjoining;

Hip support:

Location: [0, 0, 0];

Cam fixing point:

X, Y component: see Figure 5.13.

Constant rotation: 50 rpm.

Appendix 8: The CAD presentation of the motor and gearbox

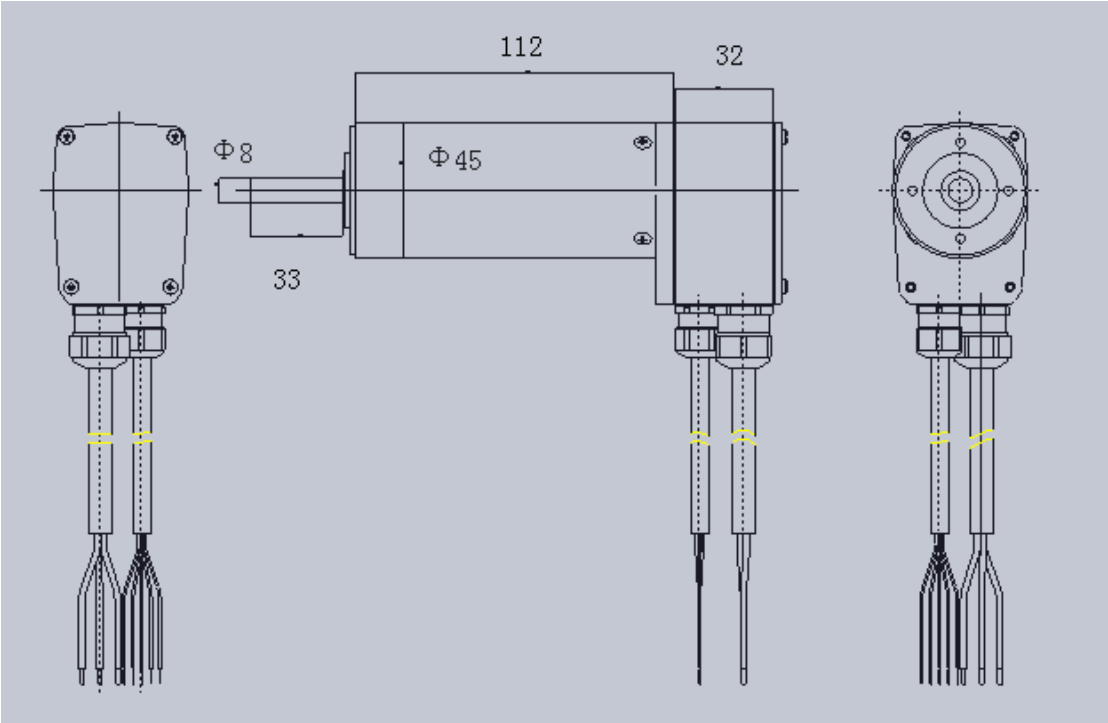

Figure A. 15: CAD presentation of the Maxon motor EC 45.

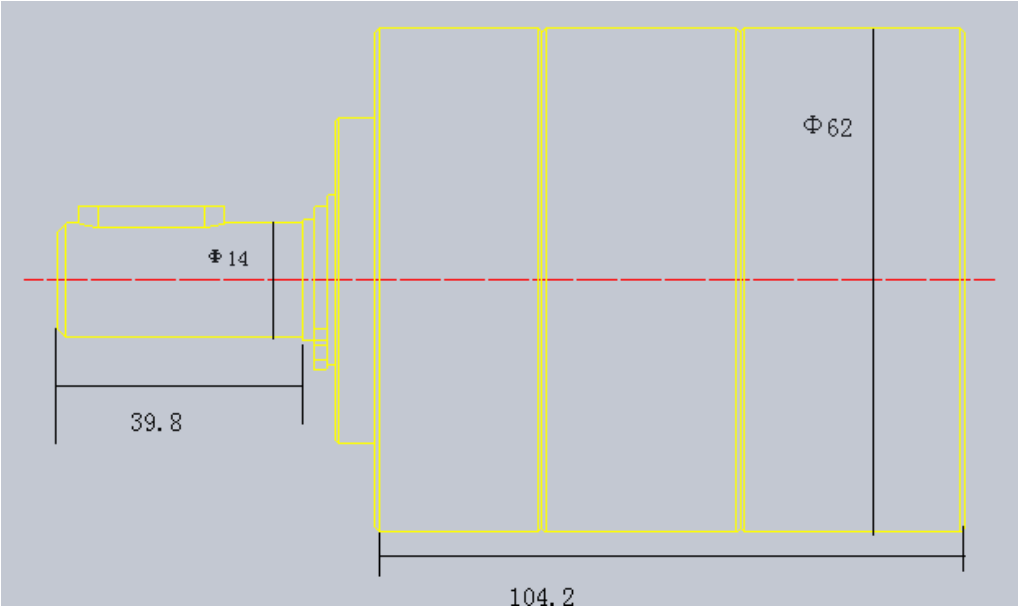

Figure A. 16: CAD presentation of the Maxon planetary gearhead GP 62.

Table. A 1: Motor specifications (Maxon EC 45).

Assigned power rating	W	250
Nominal voltage	V	48
No load speed	rpm	6500
Stall torque	mNm	3250
Max. continuous torque at 5000rpm	mNm	306
Speed / torque gradient	rpm / mNm	2.00
No load current	mA	290
Starting current	A	47.7
Terminal resistance	Ohm	1.04
Max. permissible speed	rpm	12000
Nominal current (max. continuous current)	A	4.82
Max. efficiency	%	84.9
Torque constant	mNm / A	71.0
Speed constant	rpm / V	135
Rotor inertia	gcm²	209
Motor length	mm	144
Mass	g	1150

Table. A 2: Gearbox specifications (Maxon planetary gearhead GP 62).

Reduction		236:1
No. of stages		3
Max. continuous torque	Nm	50
Intermittently permissible torque at gear output	Nm	75
Sense of rotation, drive to output		2
Maximal efficiency	%	70
Average backlash no load	degree	2
Mass inertia	gcm^2	0.09
Gearhead length L1	mm	104.2
Mass	g	1540
Max. motor shaft diameter	mm	8

Appendix 9: The CAD drawings for the shoe elements

The shoe is made of two sets of foot-pressure plates: one set for the heel (Figures A.17 and A.19) and the other set for the forefoot (Figures A.18 and A.20). The two foot plates are connected with nuts, resulting in a flexible foot length. The two pressure plates are independent of the foot plates, which allows free upward and downward movement for mechanical stimulation. As the shoe platform is designed for users in a supine position, a foot stop (Figure A. 21) is designed and mounted behind the ankle joint to prevent the foot from falling off the shoes. The shoe platform connects to the driven bar through the toe connection (Figure A. 22) and connects to the leg frame through the ankle connection (Figure A. 23).

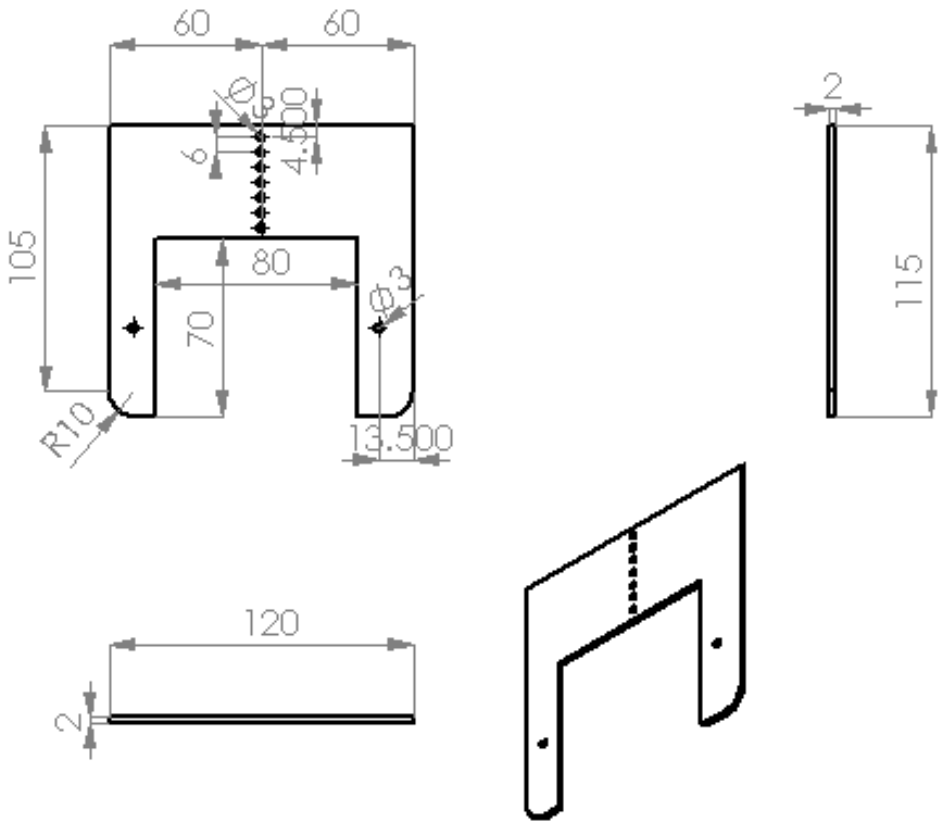

Figure A. 17: Foot plate for the heel.

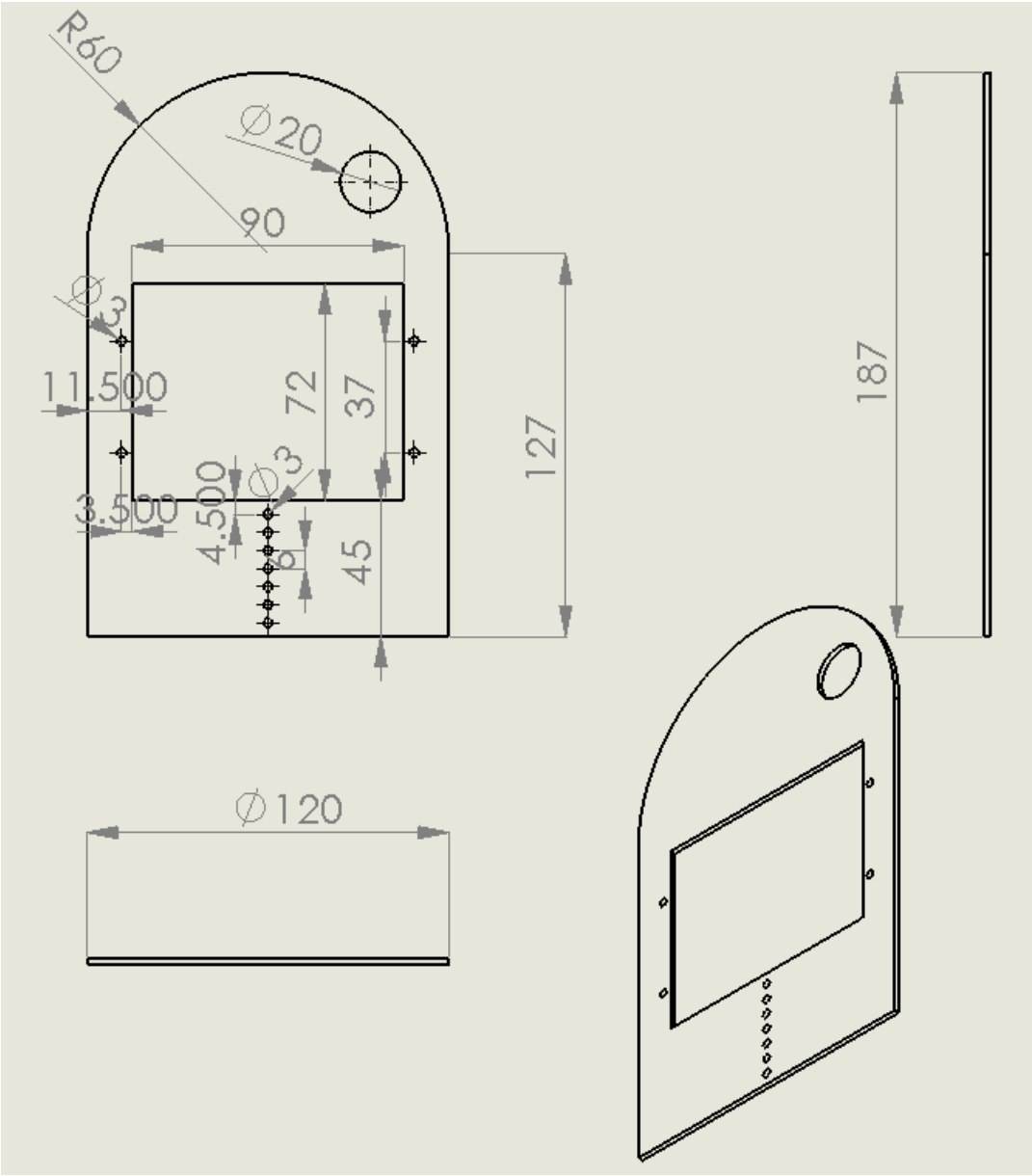

Figure A. 18: Foot plate for the forefoot.

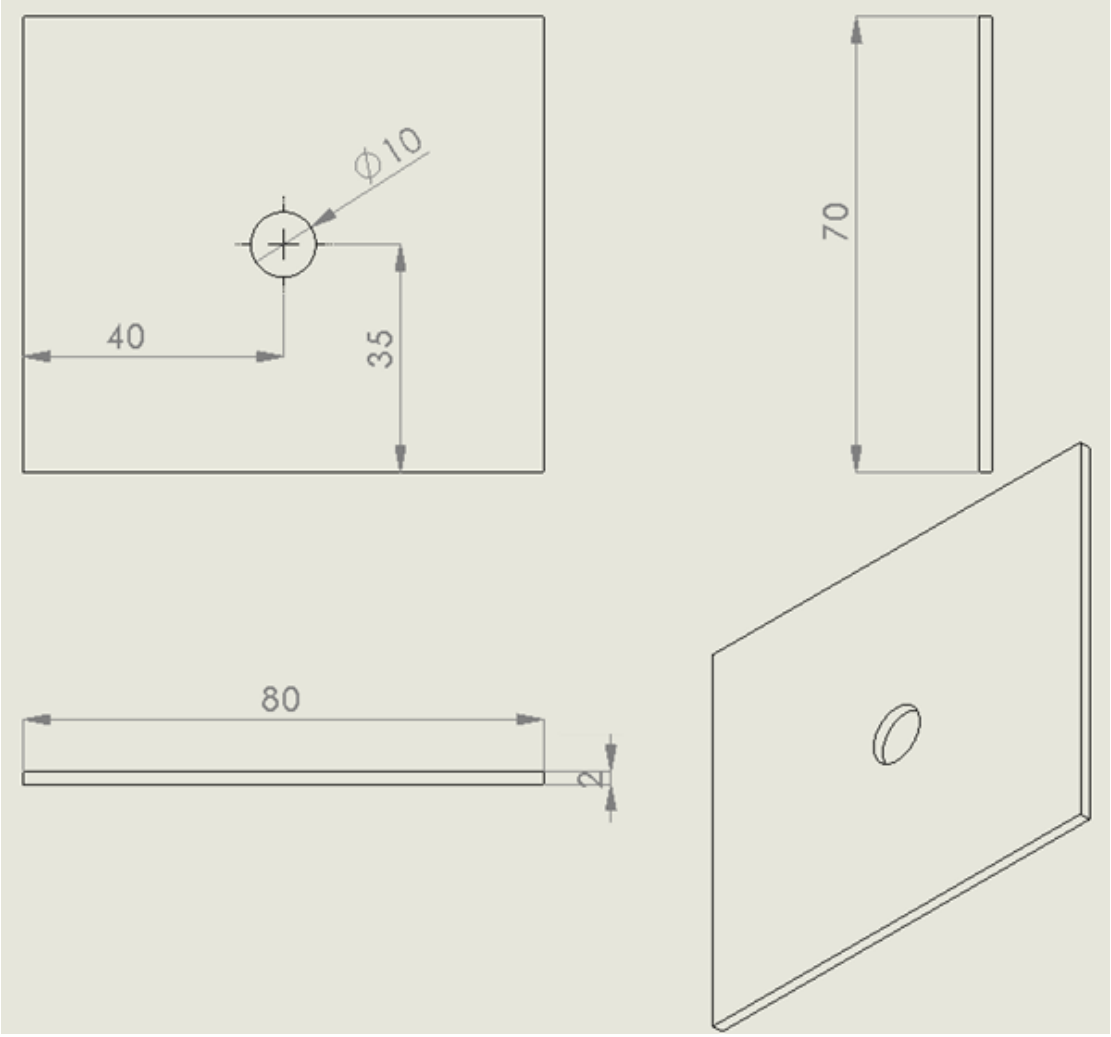

Figure A. 19: Pressure plate for the heel.

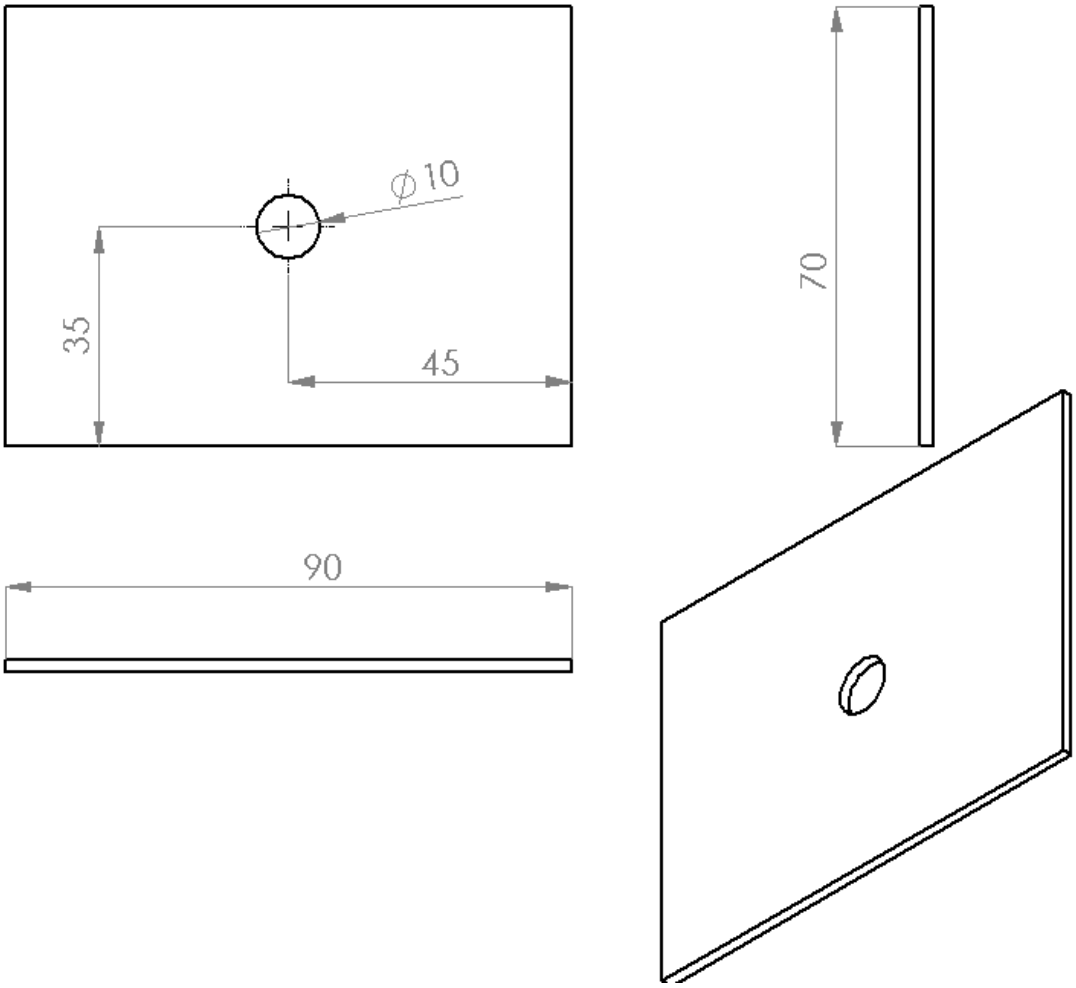

Figure A. 20: Pressure plate for the forefoot.

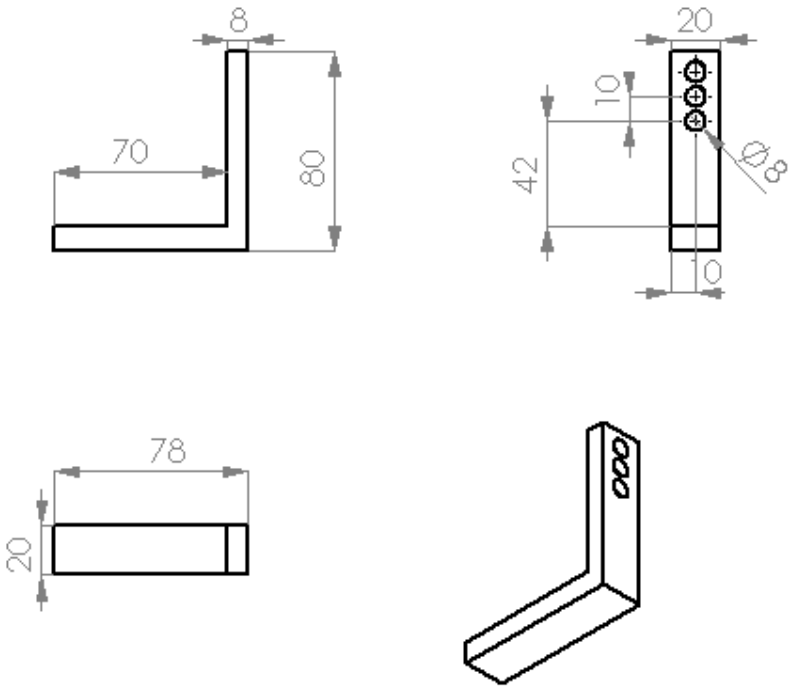

Figure A. 21: Foot stop.

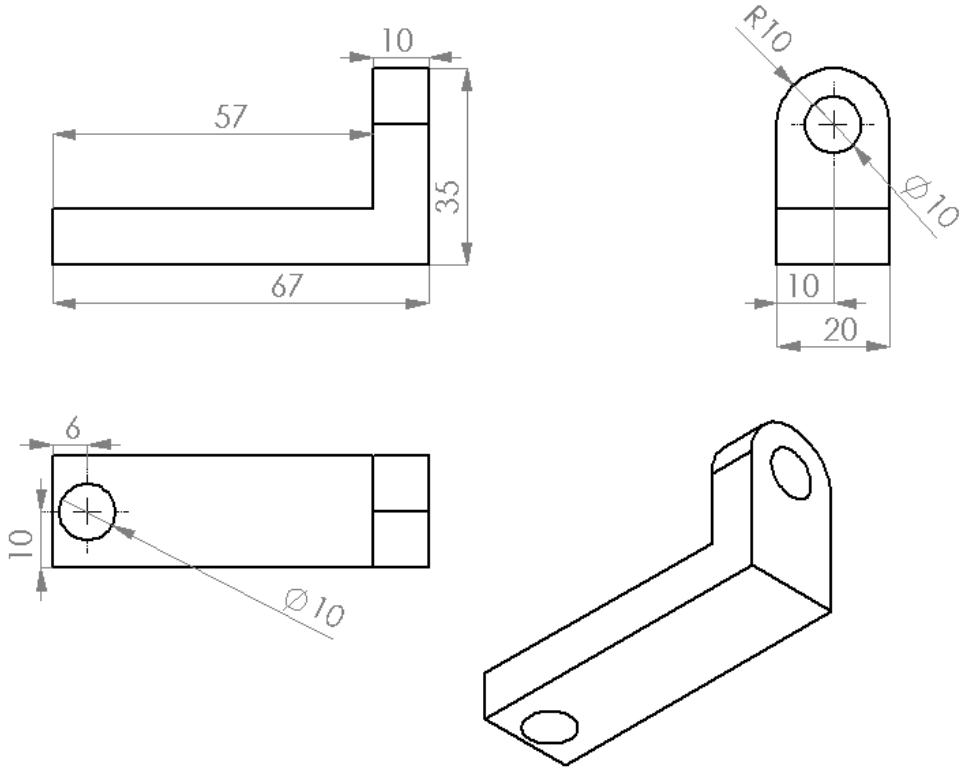

Figure A. 22: Toe connection.

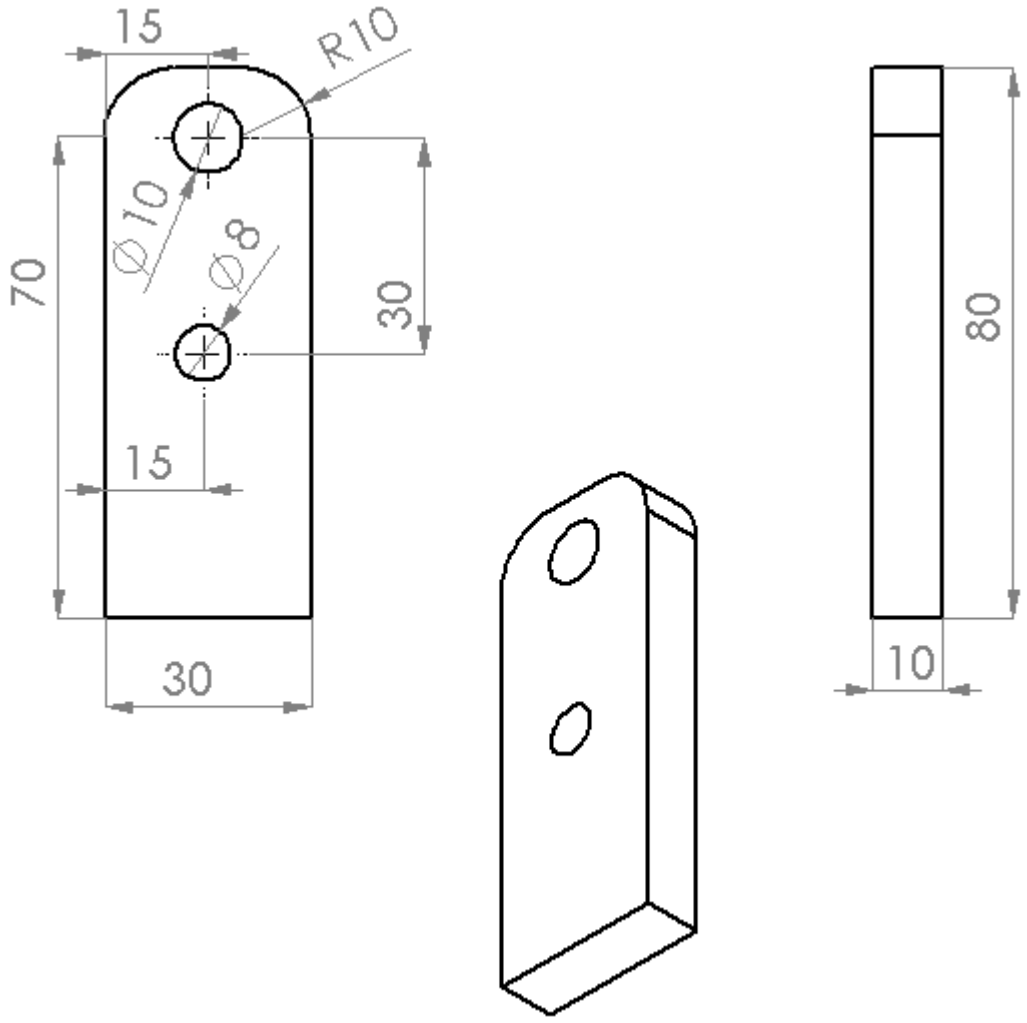

Figure A. 23: Ankle connection.

Appendix 10: The controller electronics

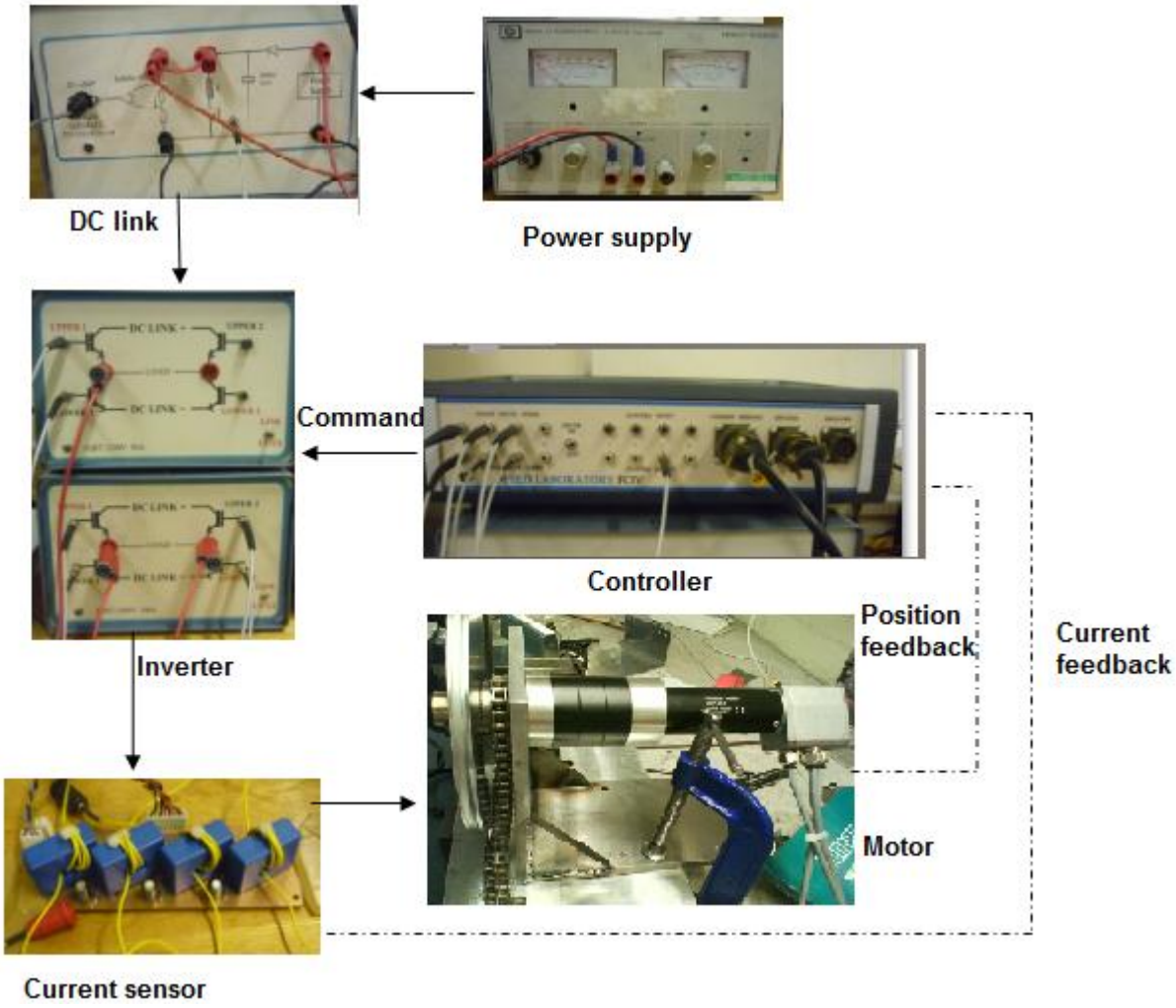

Figure A. 24: The controller electronics.

Appendix 11: Failure mode analysis

Table. A 3: Failure mode analysis.

Mode of Failure	Cause of Failure	Effect of Failure	Frequency of Occurrence (1-10)	Degree of Severity (1-10)	Detectio-n Rating (1-10)	Risk Priority (1-1000)	Recommended Actions
Mechanical failure	Bar linkage deformation	Subject's leg falling down	1	5	2	10	Manufacture a strong bar-linkage.
	Velcro becoming loose	Unnatur-al leg motion	6	1	1	6	Use several Velcro straps side by side.
	Cam deformation	Unnatur-al ankle rotation	2	4	2	16	Make the cam as strong as possible.
Electrical failure	DC motor breakdown	The whole system fails	3	9	1	27	Before any test, double check the performance of the DC motor. During the test, follow the user manuals.
	Controller breakdown	The whole system fails	2	8	1	16	Before any test, double check the performance of the DC motor. During the test, follow the user manuals.

Appendix 12: Question sheet

Question Sheet

Title of Project:
Simulation of Coordinated Movements of Lower Limbs on People in a Supine Posture with GOER system
Name of Researcher: Juan Fang
Volunteer:
Date:
Researchers will ask the questions below so as to collect feedbacks from the volunteer.

1. How much is the movement of the leg similar to walking? Please tick the scale.

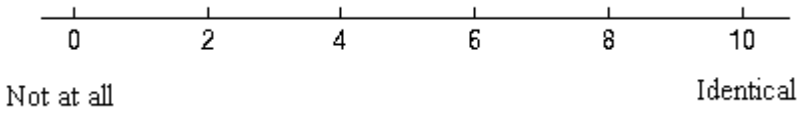

2. Please tick any part which you feel uncomfortable during the test.

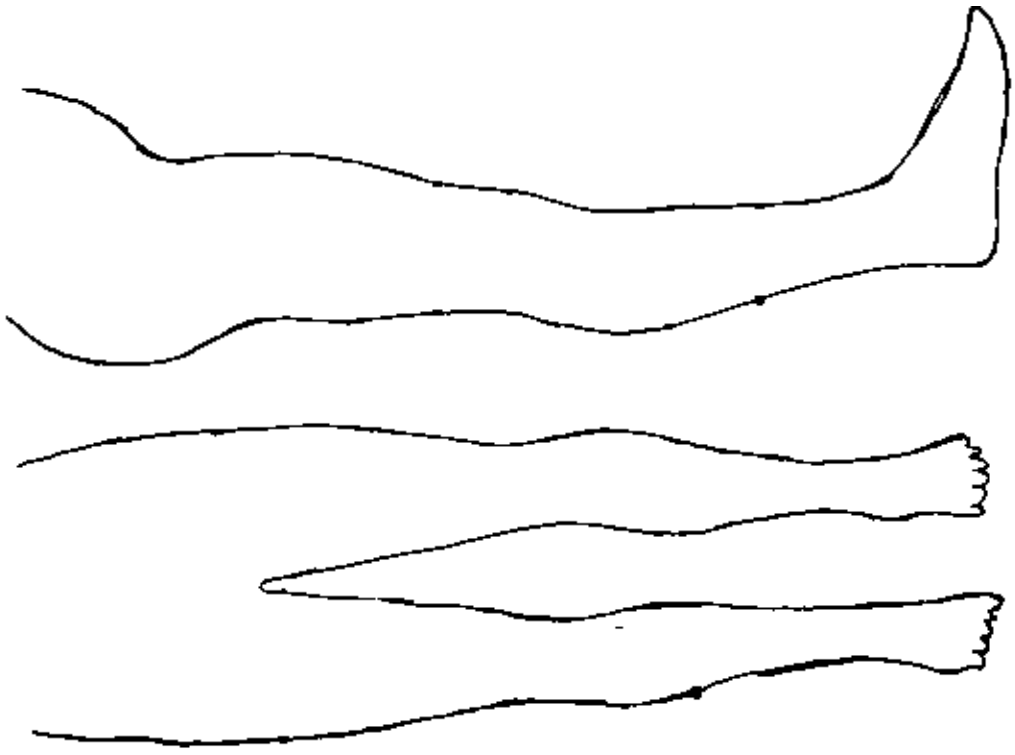

3. Please give any other comments on this device.

Appendix 13: Feedback from the subjects

13.1: Feedback from S1

University of Glasgow

Question Sheet

Title of Project:

Simulation of Coordinated Movements of Lower Limbs on People in a Supine Posture with GOER system

Name of Researcher: Juan Fang

Volunteer: [redacted] **Date:** 29/7/11

Researchers will ask the questions below so as to collect feedbacks from the volunteer.

1. How much is the movement of the leg similar to walking? Please tick the scale.

0 2 4 (6) 8 10

Not at all Identical

2. Please tick any part which you feel uncomfortable during the test.

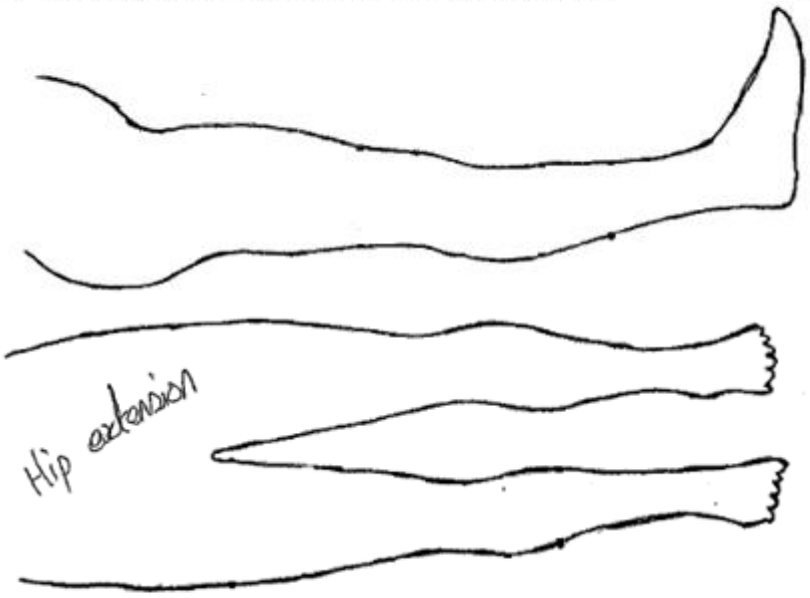

3. Please give any other comments on this device.

Motor power too small.

13.2: Feedback from S2

University of Glasgow

Question Sheet

Title of Project:

Simulation of Coordinated Movements of Lower Limbs on People in a Supine Posture with GOER system

Name of Researcher: Juan Fang

Volunteer: [redacted] **Date:** 28.07.2011

Researchers will ask the questions below so as to collect feedbacks from the volunteer.

1. How much is the movement of the leg similar to walking? Please tick the scale.

Not at all Identical

2. Please tick any part which you feel uncomfortable during the test.

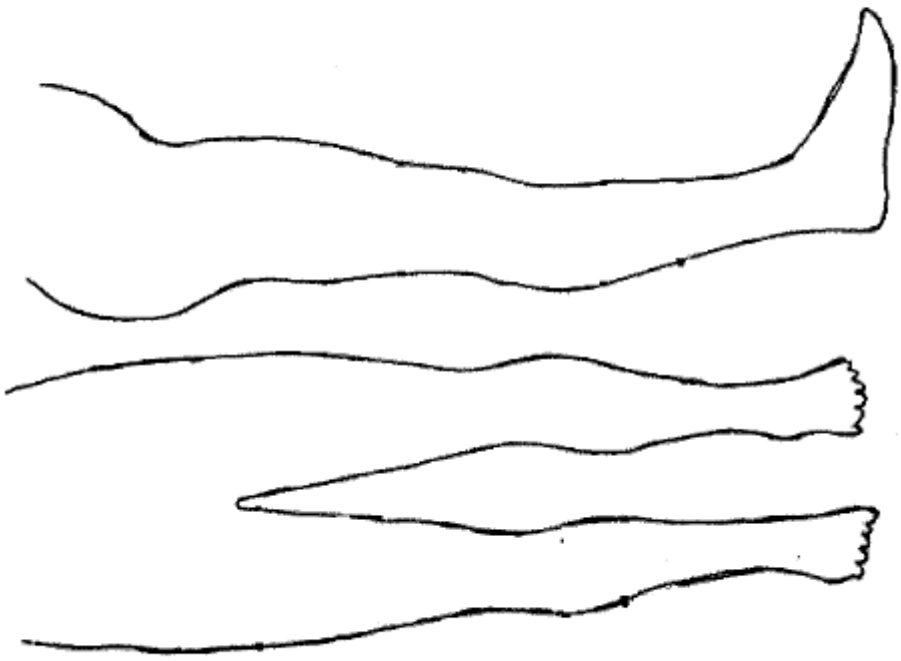

3. Please give any other comments on this device.

13.3: Feedback from S3

University of Glasgow

Question Sheet

Title of Project:

Simulation of Coordinated Movements of Lower Limbs on People in a Supine Posture with GOER system

Name of Researcher: Juan Fang

Volunteer: [redacted] **Date:** 28/7

Researchers will ask the questions below so as to collect feedbacks from the volunteer.

1. How much is the movement of the leg similar to walking? Please tick the scale.

Not at all Identical

2. Please tick any part which you feel uncomfortable during the test.

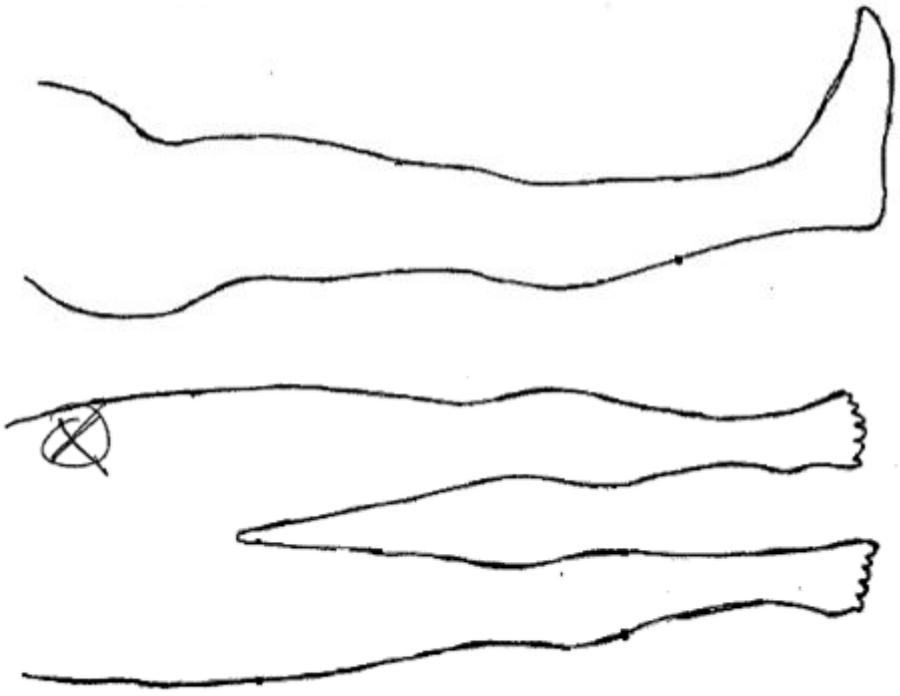

3. Please give any other comments on this device.

Appendix 14: Question sheet

Question Sheet

Title of Project:
Simulation of Ground Reaction Force and Testing of Its Biological Effects on People in a Supine Posture

Name of Researcher: Juan Fang
Subject:
Date:

Researchers will ask the questions below so as to collect feedback from the subject.

1. Are the positions of the pressure and force timing (between heel and forefoot) similar to those during overground walking?

A: both very different; B: timing is similar but not the location;

C: the location is similar but not timing; D. both very similar.

2. Is your walking-like experience (speed of force) comparable on the heel and on the foot sole?

A. comparable; B. better on heel then on the forefoot;

C. better the forefoot than on the heel; D: neither is comparable.

3. Do you feel comfortable with the dynamic force application?

A. uncomfortable; B.neutral; C. comfortable.

4. In case you didn't have a walking-like feeling on your foot sole please describe the main reason for this.

5. Choose the word that best describes your sensation during mechanical force stimulation.

A. Walking; B. Pressing; C. Punching; D. Jumping ; E. None of these.

Appendix 15: Feedback from the subjects

15.1: Feedback from S1

University of Glasgow | Faculty of Biomedical & Life Sciences

Question Sheet

Title of Project:

Simulation of Ground Reaction Force and Testing of Its Biological Effects on People in a Supine Posture

Name of Researcher: Juan Fang, Dr. Aleksandra Vuckovic

Volunteer: [redacted] **Date:** 2/5/11

Researchers will ask the questions below so as to collect feedbacks from the volunteer.

1. Are the locations of the pressure and the force timing (between heel and forefoot) similar to those during overground normal walking?
A. both are very different; B. the location is similar but not timing;
C: the timing is similar but not the location; D. both are very similar.

2. Is the walking-like simulation (speed of force) on the heel and on the forefoot comparable to daily overground walking?
A. both are comparable B. better on heel than on the forefoot
C. better on the forefoot than on the heel D. Neither is comparable.

3. Do you feel comfortable with the dynamic force application?
A. comfortable B. neutral C. uncomfortable

4. In case you don't have a walking-like feeling on your foot sole please describe the main reason for this

5. Choose the word that best describes your sensation during the mechanical force stimulation.
A. Walking B. Pressing C. Punching D. Jumping E. Neither of these

15.2: Feedback from S2

University of Glasgow | Faculty of Biomedical & Life Sciences

Question Sheet

Title of Project:

Simulation of Ground Reaction Force and Testing of Its Biological Effects on People in a Supine Posture

Name of Researcher: Juan Fang, Dr. Aleksandra Vuckovic

Volunteer: [redacted] **Date:** 01/03/2011

Researchers will ask the questions below so as to collect feedbacks from the volunteer.

1. Are the locations of the pressure and the force timing (between heel and forefoot) similar to those during overground normal walking?
A. both are very different; B. the location is similar but not timing;
C: the timing is similar but not the location; D. both are very similar. ✓

2. Is the walking-like simulation (speed of force) on the heel and on the forefoot comparable to daily overground walking?
✓A. both are comparable B. better on heel than on the forefoot
C. better on the forefoot than on the heel D. Neither is comparable.

3. Do you feel comfortable with the dynamic force application?
A. comfortable ✓B. neutral C. uncomfortable

4. In case you don't have a walking-like feeling on your foot sole please describe the main reason for this

5. Choose the word that best describes your sensation during the mechanical force stimulation.
A. Walking B. Pressing C. Punching D. Jumping E. Neither of these
4 for 2nd session 5 for 1st session

15.3: Feedback from S3

University of Glasgow | Faculty of Biomedical & Life Sciences

Question Sheet

Title of Project:

Simulation of Ground Reaction Force and Testing of Its Biological Effects on People in a Supine Posture

Name of Researcher: Juan Fang, Dr. Aleksandra Vuckovic

Volunteer: [redacted] **Date:** 02/05/2011

Researchers will ask the questions below so as to collect feedbacks from the volunteer.

1. Are the locations of the pressure and the force timing (between heel and forefoot) similar to those during overground normal walking?
A. both are very different; B. the location is similar but not timing;
C: the timing is similar but not the location; D. both are very similar.

2. Is the walking-like simulation (speed of force) on the heel and on the forefoot comparable to daily overground walking?
A. both are comparable B. better on heel than on the forefoot
C. better on the forefoot than on the heel D. Neither is comparable.

3. Do you feel comfortable with the dynamic force application?
A. comfortable B. neutral C. uncomfortable

4. In case you don't have a walking-like feeling on your foot sole please describe the main reason for this

5. Choose the word that best describes your sensation during the mechanical force stimulation.
A. Walking B. Pressing C. Punching D. Jumping E. Neither of these

15.4: Feedback from S4

University of Glasgow | Faculty of Biomedical & Life Sciences

Question Sheet

Title of Project:

Simulation of Ground Reaction Force and Testing of Its Biological Effects on People in a Supine Posture

Name of Researcher: Juan Fang, Dr. Aleksandra Vuckovic

Volunteer: [redacted] **Date:** 02/05/2011

Researchers will ask the questions below so as to collect feedbacks from the volunteer.

1. Are the locations of the pressure and the force timing (between heel and forefoot) similar to those during overground normal walking?
A. both are very different; B. the location is similar but not timing;
C: the timing is similar but not the location; D. both are very similar.

2. Is the walking-like simulation (speed of force) on the heel and on the forefoot comparable to daily overground walking?
A. both are comparable B. better on heel than on the forefoot
C. better on the forefoot than on the heel D. Neither is comparable.

3. Do you feel comfortable with the dynamic force application?
A. comfortable B. neutral C. uncomfortable

4. In case you don't have a walking-like feeling on your foot sole please describe the main reason for this

5. Choose the word that best describes your sensation during the mechanical force stimulation.
A. Walking B. Pressing C. Punching D. Jumping E. Neither of these

15.5: Feedback from S5

University of Glasgow | Faculty of Biomedical & Life Sciences

Question Sheet

Title of Project:

Simulation of Ground Reaction Force and Testing of Its Biological Effects on People in a Supine Posture

Name of Researcher: Juan Fang, Dr. Aleksandra Vuckovic

Volunteer: [redacted] **Date:** 28/04/2011

Researchers will ask the questions below so as to collect feedbacks from the volunteer.

1. Are the locations of the pressure and the force timing (between heel and forefoot) similar to those during overground normal walking?
A. both are very different; B. the location is similar but not timing;
C. the timing is similar but not the location; D. both are very similar.

2. Is the walking-like simulation (speed of force) on the heel and on the forefoot comparable to daily overground walking?
A. both are comparable B. better on heel than on the forefoot
C. better on the forefoot than on the heel D. Neither is comparable.

3. Do you feel comfortable with the dynamic force application?
A. comfortable B. neutral C. uncomfortable

4. In case you don't have a walking-like feeling on your foot sole please describe the main reason for this

5. Choose the word that best describes your sensation during the mechanical force stimulation.
A. Walking B. Pressing C. Punching D. Jumping E. None of these

15.6: Feedback from S6

University of Glasgow | Faculty of Biomedical & Life Sciences

Question Sheet

Title of Project:

Simulation of Ground Reaction Force and Testing of Its Biological Effects on People in a Supine Posture

Name of Researcher: Juan Fang, Dr. Aleksandra Vuckovic

Volunteer: [redacted] **Date:** 28/04/11

Researchers will ask the questions below so as to collect feedbacks from the volunteer.

1. Are the locations of the pressure and the force timing (between heel and forefoot) similar to those during overground normal walking?
A. both are very different; (B) the location is similar but not timing;
C: the timing is similar but not the location; D. both are very similar.

2. Is the walking-like simulation (speed of force) on the heel and on the forefoot comparable to daily overground walking?
(A) both are comparable B. better on heel than on the forefoot
C. better on the forefoot than on the heel D. Neither is comparable.

3. Do you feel comfortable with the dynamic force application?
(A) comfortable B. neutral C. uncomfortable

4. In case you don't have a walking-like feeling on your foot sole please describe the main reason for this Pressure on the top of the foot. Timing between heel and toe pressure was very long

5. Choose the word that best describes your sensation during the mechanical force stimulation.
A. Walking (B.) Pressing C. Punching D. Jumping E. None of these

15.7: Feedback from S7

University of Glasgow | Faculty of Biomedical & Life Sciences

Question Sheet

Title of Project:

Simulation of Ground Reaction Force and Testing of Its Biological Effects on People in a Supine Posture

Name of Researcher: Juan Fang, Dr. Aleksandra Vuckovic

Volunteer: [redacted] **Date:** 8/5/2011

Researchers will ask the questions below so as to collect feedbacks from the volunteer.

1. Are the locations of the pressure and the force timing (between heel and forefoot) similar to those during overground normal walking?
A. both are very different; B. the location is similar but not timing;
C: the timing is similar but not the location; (D.) both are very similar.

2. Is the walking-like simulation (speed of force) on the heel and on the forefoot comparable to daily overground walking?
A. both are comparable (B.) better on heel than on the forefoot
C. better on the forefoot than on the heel D. Neither is comparable.

3. Do you feel comfortable with the dynamic force application?
(A.) comfortable B. neutral C. uncomfortable

4. In case you don't have a walking-like feeling on your foot sole please describe the main reason for this

5. Choose the word that best describes your sensation during the mechanical force stimulation.
A. Walking (B.) Pressing C. Punching D. Jumping E. Neither of these

15.8: Feedback from S8

University of Glasgow | Faculty of Biomedical & Life Sciences

Question Sheet

Title of Project:

Simulation of Ground Reaction Force and Testing of Its Biological Effects on People in a Supine Posture

Name of Researcher: Juan Fang, Dr. Aleksandra Vuckovic

Volunteer: [redacted] **Date:** May 2nd 2011

Researchers will ask the questions below so as to collect feedbacks from the volunteer.

1. Are the locations of the pressure and the force timing (between heel and forefoot) similar to those during overground normal walking?
A. both are very different; B. the location is similar but not timing;
C: the timing is similar but not the location; D. both are very similar.

2. Is the walking-like simulation (speed of force) on the heel and on the forefoot comparable to daily overground walking?
A. both are comparable B. better on heel than on the forefoot
C. better on the forefoot than on the heel D. Neither is comparable.

3. Do you feel comfortable with the dynamic force application?
A. comfortable B. neutral C. uncomfortable

4. In case you don't have a walking-like feeling on your foot sole please describe the main reason for this

5. Choose the word that best describes your sensation during the mechanical force stimulation.
A. Walking B. Pressing C. Punching D. Jumping E. Neither of these

15.9: Feedback from S9

University of Glasgow | Faculty of Biomedical & Life Sciences

Question Sheet

Title of Project:

Simulation of Ground Reaction Force and Testing of Its Biological Effects on People in a Supine Posture

Name of Researcher: Juan Fang, Dr. Aleksandra Vuckovic

Volunteer: [redacted] **Date:** 5 May 2011

Researchers will ask the questions below so as to collect feedbacks from the volunteer.

1. Are the locations of the pressure and the force timing (between heel and forefoot) similar to those during overground normal walking?
A. both are very different; (B.) the location is similar but not timing;
C: the timing is similar but not the location; D. both are very similar.

2. Is the walking-like simulation (speed of force) on the heel and on the forefoot comparable to daily overground walking?
A. both are comparable B. better on heel than on the forefoot
(C.) better on the forefoot than on the heel D. Neither is comparable.

3. Do you feel comfortable with the dynamic force application?
A. comfortable (B.) neutral C. uncomfortable

4. In case you don't have a walking-like feeling on your foot sole please describe the main reason for this

5. Choose the word that best describes your sensation during the mechanical force stimulation.
(A) Walking B. Pressing C. Punching D. Jumping E. None of these

15.10: Feedback from S10

University of Glasgow | Faculty of Biomedical & Life Sciences

Question Sheet

Title of Project:

Simulation of Ground Reaction Force and Testing of Its Biological Effects on People in a Supine Posture

Name of Researcher: Juan Fang, Dr. Aleksandra Vuckovic

Volunteer: [redacted] **Date:** 16/3/11

Researchers will ask the questions below so as to collect feedbacks from the volunteer.

1. Are the locations of the pressure and the force timing (between heel and forefoot) similar to those during overground normal walking?
A. both are very different; (B) the location is similar but not timing;
C: the timing is similar but not the location; D. both are very similar.

2. Is the walking-like simulation (speed of force) on the heel and on the forefoot comparable to daily overground walking?
A. both are comparable (B) better on heel than on the forefoot
C. better on the forefoot than on the heel D. Neither is comparable.

3. Do you feel comfortable with the dynamic force application?
A. comfortable (B) neutral C. uncomfortable

4. In case you don't have a walking-like feeling on your foot sole please describe the main reason for this Delay between heel & toe too long

5. Choose the word that best describes your sensation during the mechanical force stimulation.
A. Walking B. Pressing (C) Punching D. Jumping E. None of these

List of References

1. Winter, D.A., *Biomechanics and Motor Control of Human Movement*. 3rd ed. 2005: John Wiley & Sons, Inc.

2. Fang, J., et al., *Kinematic modelling of a robotic gait device for early rehabilitation of walking.* Proceedings of the Institution of Mechanical Engineers, Part H: Journal of Engineering in Medicine, 2011. **225**(12): p. 1177-1187.

3. Bouri, M., et al. *The WalkTrainer: a robotic system for walking rehabilitation*. in *IEEE International Conference on Robotics and Biomimetics*. 2006.

4. Jeannerod, M., *Neural simulation of action: a unifying mechanism for motor cognition.* NeuroImage, 2001. **14**(1): p. S103-S109.

5. Bear, M.F., B.W. Connors, and M.A. Paradiso, *Chapter 7: the structure of nervous system*, in *Neuroscience: Exploring the Brain*. 2007, Lippincott Williams & Wilkins. p. 167-249.

6. DeVivo, M.J., J.S. Krause, and D.P. Lammertse, *Recent trends in mortality and causes of death among persons with spinal cord injury.* Archives of Physical Medicine and Rehabilitation, 1999. **80**(11): p. 1411-1419.

7. Dietz, V. and R. Müller, *Degradation of neuronal function following a spinal cord injury: mechanisms and countermeasures.* Brain, 2004. **127**(10): p. 2221-2231.

8. Bear, M.F., B.W. Connors, and M.A. Paradiso, *Chapter 2: neurons and glia*, in *Neuroscience: Exploring the Brain*. 2007, Lippincott Williams & Wilkins. p. 23-51.

9. Freeman, T.L., et al., *Chapter 5: electrodiagnostic medicine and clinical neuromuscular physiology*, in *Physical Medicine and Rehabilitation Board Review*, S.J. Cuccurullo, Editor. 2004, Demos Medical Publishing: New York. p. 295-408.

10. Porter, R. and R.N. Lemon, *Corticospinal Function and Voluntary Movement*. 1993, Oxford: Oxford University Press.

11. Kandel, E., J. Schwartz, and T. Jessel, *Chapter 18: the functional organization of perception and movement* in *Principles of Neuroscience*. 2000, McGraw Hill Publishers: New York. p. 337-348.

12. Kandel, E., J. Schwartz, and T. Jessel, *Chapter 1: the brain and behavior*, in *Principles of Neuroscience*. 2000, McGraw Hill Publishers: New York. p. 5-18.

13. Bear, M.F., B.W. Connors, and M.A. Paradiso, *Chapter 12: the somatic sensory system*, in *Neuroscience: Exploring the Brain*. 2007, Lippincott Williams & Wilkins. p. 387-422.

14. Maynard, F.M., et al., *International standards for neurological and functional classification of spinal cord injury.* Spinal Cord, 1997. **35**(5): p. 266-274.

15. Kirshblum, S., et al., *Chapter 7: spinal cord injuries*, in *Physical Medicine and Rehabilitation Board Review.*, S.J. Cuccurullo, Editor. 2004, Demos Medical Publishing: New York. p. 489-552.

16. Kandel, E., J. Schwartz, and T. Jessel, *Chapter 19: integration of sensory and motor function: the association areas of the cerebral cortex and the cognitive capabilities of the brain*, in *Principles of Neuroscience*. 2000, McGraw Hill Publishers: New York. p. 349-380.

17. Kandel, E., J. Schwartz, and T. Jessel, *Chapter 33: the organization of movement*, in *Principles of Neuroscience*. 2000, McGraw Hill Publishers: New York. p. 653-673.

18. Bear, M.F., B.W. Connors, and M.A. Paradiso, *Chapter 13: spinal control of movement* in *Neuroscience: Exploring the Brain*. 2007, Lippincott Williams & Wilkins. p. 423-450.

19. Marieb, E. and K. Hoehn, *Human Anatomy & Physiology* 7th ed. 2007: Pearson Benjamin Cummings.

20. Kandel, E., J. Schwartz, and T. Jessel, *Chapter 35: diseases of the motor unit*, in *Principles of Neuroscience*. 2000, McGraw Hill Publishers: New York. p. 695-712.

21. Kandel, E., J. Schwartz, and T. Jessel, *Chapter 36: spinal reflex*, in *Principles of Neuroscience*. 2000, McGraw Hill Publishers: New York. p. 713-736.

22. Walker, B., *The Anatomy of Stretching*. 2007: North Atlantic Books.

23. Grey, M.J., J. Van Doornik, and T. Sinkjær, *Plantar flexor stretch reflex responses to whole body loading/unloading during human walking.* European Journal of Neuroscience, 2002. **16**(10): p. 2001-2007.

24. Roby-Brami, A. and B. Bussel, *Long latency spinal reflex in man after flexor*

reflex afferent stimulation. Brain, 1987. **110**(3): p. 707-725.

25. Andersen, O.K., et al., *Expansion of nociceptive withdrawal reflex receptive fields in spinal cord injured humans.* Clinical Neurophysiology, 2004. **115**(12): p. 2798-2810.

26. Shahani, B.T. and R.R. Young, *Human flexor reflexes.* Journal of Neurology Neurosurgery and Psychiatry, 1971. **34**(5): p. 616-&.

27. Schillings, A.M., B.M.H. Van Wezel, and J. Duysens, *Mechanically induced stumbling during human treadmill walking.* Journal of Neuroscience Methods, 1996. **67**(1): p. 11-17.

28. Tax, A.A., B.M. Van Wezel, and V. Dietz, *Bipedal reflex coordination to tactile stimulation of the sural nerve during human running.* Journal of Neurophysiology, 1995. **73**(5): p. 1947-1964.

29. Nolte, J., *Chapter 18: overview of motor systems* in *The Human Brain. An Introduction to Its Functional Anatomy*, J. Shreiner, Editor. 2002, Mosby Inc.: Louis, Missouri. p. 457-474.

30. van Elswijk, G.A.F., *Corticospinal excitability in human voluntary movement*, in *F.C. Donders Centre for Cognitive Neuroimaging Neurology, Department of Clinical Neurophysiology* 2008, RU Radboud Universiteit Nijmegen: Enschede, Netherlands. p. 17-81.

31. Wyndaele, M. and J.J. Wyndaele, *Incidence, prevalence and epidemiology of spinal cord injury: what learns a worldwide literature survey?* Spinal Cord, 2006. **44**(9): p. 523-529.

32. *Spinal cord injury: facts and figures at a glance*. 2005, National Spinal Cord Injury Statistical Center: Birmingham.

33. Grundy, D. and A. Swain, *ABC of Spinal Cord Injury*. 4th ed. 2002: BMJ Publishing Group.

34. *Annual report 2003-2004*. 2003, Spinal Injuries Association.

35. Guttman, L., *Spinal Cord Injuries. Comprehensive Management and Research*. 1973: Blackwell, Oxford.

36. Schwab, M.E., *Bridging the gap in spinal cord regeneration.* Nature Medicine, 1996. **2**(9): p. 976-977.

37. Schwab, M.E. and D. Bartholdi, *Degeneration and regeneration of axons in the lesioned spinal cord.* Physiological Reviews, 1996. **76**(2): p. 319-370.

38. Zai, L.J., S. Yoo, and J.R. Wrathall, *Increased growth factor expression and cell proliferation after contusive spinal cord injury.* Brain Research, 2005. **1052**(2): p. 147-155.

39. Field-Fote, E., *Chapter 1: spinal cord injury: an overview*, in *Spinal Cord Injury Rehabilitation*. 2009, F.A. Davis Company. p. 3-20.

40. McKinley, W.O., R.T. Seel, and J.T. Hardman, *Nontraumatic spinal cord injury: incidence, epidemiology, and functional outcome.* Archives of Physical Medicine and Rehabilitation, 1999. **80**(6): p. 619-623.

41. Murray, P.K. and M.F. Kusior, *Epidemiology of nontraumatic and traumatic spinal cord injury.* Archives of Physical Medicine and Rehabilitation, 1984. **65**(10): p. 634.

42. Arnold, P.B., et al., *Functional electric stimulation: its efficacy and safety in improving pulmonary function and musculoskeletal fitness.* Archives of Physical Medicine and Rehabilitation, 1992. **73**(7): p. 665-668.

43. *Annual report* 2009-10, Queen Elizabeth National Spinal Injuries Unit, NHS Great Glasgow and Clyde.

44. *Guide to Physical Therapist Practice*. Revised Second edition ed. 2003, American Physical Therapy Association.

45. Jacobs, P.L., et al., *Hypokinetic circulation in persons with paraplegia.* Medicine and Science in Sports and Exercise, 2002. **34**(9): p. 1401-1407.

46. Sircar, S., *Chapter 41: neural control of the cardiovascular system*, in *Principles of Medical Physiology*. 2008, Georg Thieme Verlag: Stuttgart, Germany. p. 267-268.

47. Illman, A., K. Stiller, and M. Williams, *The prevalence of orthostatic hypotension during physiotherapy treatment in patients with an acute spinal cord injury.* Spinal Cord, 2000. **38**(12): p. 741-747.

48. Chao, C.Y. and G.L. Cheing, *The effects of lower-extremity functional electric stimulation on the orthostatic responses of people with tetraplegia.* Archives of Physical Medicine and Rehabilitation, 2005. **86**(7): p. 1427-1433.

49. Bauman, W.A. and A.M. Spungen, *Metabolic changes in persons after spinal cord injury.* Physical Medicine and Rehabilitation Clinics of North America, 2000. **11**(1): p. 109-40.

50. Shields, R.K. and S. Dudley-Javoroski, *Musculoskeletal deterioration and*

hemicorporectomy after spinal cord injury. Physical Therapy, 2003. **83**(3): p. 263-275.

51. Castro, M.J., et al., *Influence of complete spinal cord injury on skeletal muscle cross-sectional area within the first 6 months of injury.* European Journal of Applied Physiology and Occupational Physiology, 1999. **80**(4): p. 373-378.

52. Kandel, E., J. Schwartz, and T. Jessel, *Chapter 34: the motor unit and muscle action*, in *Principles of Neuroscience*. 2000, McGraw Hill Publishers: New York. p. 674-694.

53. Scelsi, R., *Skeletal muscle pathology after spinal cord injury: our 20 year experience and results on skeletal muscle changes in paraplegics, related to functional rehabilitation.* Basic and Applied Myology, 2001. **11**(2): p. 75-85.

54. Eser, P., et al., *Relationship between the duration of paralysis and bone structure: a pQCT study of spinal cord injured individuals.* Bone, 2004. **34**(5): p. 869-880.

55. Shields, R.K. and S. Dudley-Javoroski, *Musculoskeletal plasticity after acute spinal cord injury: effects of long-term neuromuscular electrical stimulation training.* Journal of Neurophysiology, 2006. **95**(4): p. 2380-2390.

56. Lanyon, L.E., *Using functional loading to influence bone mass and architecture: objectives, mechanisms, and relationship with estrogen of the mechanically adaptive process in bone.* Bone, 1996. **18**(1): p. S37-S43.

57. Keating, J.F., M. Kerr, and M. Delargy, *Minimal trauma causing fractures in patients with spinal cord injury.* Disability and Rehabilitation, 1992. **14**(2): p. 108-109.

58. Zehnder, Y., et al., *Long-term changes in bone metabolism, bone mineral density, quantitative ultrasound parameters, and fracture incidence after spinal cord injury: a cross-sectional observational study in 100 paraplegic men.* Osteoporosis International, 2004. **15**(3): p. 180-189.

59. Frey-Rindova, P., et al., *Bone mineral density in upper and lower extremities during 12 months after spinal cord injury measured by peripheral quantitative computed tomography.* Spinal Cord, 2000. **38**(1): p. 26-32.

60. Ditunno, J.F., et al., *Spinal shock revisited: a four-phase model.* Spinal Cord, 2004. **42**(7): p. 383-395.

61. Katz, R. and W.Z. Rymer, *Spastic hypertonia: mechanisms and management.* Archives of Physical Medicine and Rehabilitation, 1989. **70**: p. 144-155.

62. Little, J.W., et al., *Lower extremity manifestations of spasticity in chronic spinal cord injury.* American Journal Physical Medicine & Rehabilitation, 1989. **68**(1): p. 32-36.

63. Dietz, V. and T. Sinkjaer, *Spastic movement disorder: impaired reflex function and altered muscle mechanics.* Lancet Neurology, 2007. **6**(8): p. 725-733.

64. Hornby, T.G., et al., *Windup of flexion reflexes in chronic human spinal cord injury: a marker for neuronal plateau potentials?* Journal of Neurophysiology, 2003. **89**(1): p. 416-426.

65. van Hedel, H.J.A. and V. Dietz, *Rehabilitation of locomotion after spinal cord injury.* Restorative Neurology and Neuroscience, 2010. **28**(1): p. 119-130.

66. Dunlop, S.A., *Activity-dependent plasticity: implications for recovery after spinal cord injury.* Trends in Neurosciences, 2008. **31**(8): p. 410-418.

67. Wolpaw, J.R., *Spinal cord plasticity in acquisition and maintenance of motor skills.* Acta Physiologica, 2007. **189**(2): p. 155-169.

68. Kim, B.G., et al., *Remodeling of synaptic structures in the motor cortex following spinal cord injury.* Experimental Neurology, 2006. **198**(2): p. 401-415.

69. Schwab, M.E., *Experimental aspects of spinal cord regeneration.* Current Opinion in Neurology and Neurosurgery, 1993. **6**(4): p. 549-553.

70. Zai, L.J. and J.R. Wrathall, *Cell proliferation and replacement following contusive spinal cord injury.* Glia, 2005. **50**(3): p. 247-257.

71. Bareyre, F.M., et al., *The injured spinal cord spontaneously forms a new intraspinal circuit in adult rats.* Nature Neuroscience, 2004. **7**(3): p. 269-277.

72. Merzenich, M.M., et al., *Topographic reorganization of somatosensory cortical areas 3b and 1 in adult monkeys following restricted deafferentation.* Neuroscience, 1983. **8**(1): p. 33-55.

73. Jain, N., K.C. Catania, and J.H. Kaas, *Deactivation and reactivation of somatosensory cortex after dorsal spinal cord injury.* Nature, 1997. **386**(6624): p. 495-498.

74. Ghosh, A., et al., *Functional and anatomical reorganization of the sensory-motor cortex after incomplete spinal cord injury in adult rats.* Journal of Neuroscience, 2009. **29**(39): p. 12210-12219.

75. Huntley, G.W., *Correlation between patterns of horizontal connectivity and*

the extent of short-term representational plasticity in rat motor cortex. Cerebral Cortex, 1997. **7**(2): p. 143-156.

76. Topka, H., et al., *Reorganization of corticospinal pathways following spinal cord injury.* Neurology, 1991. **41**(8): p. 1276.

77. Streletz, L.J., et al., *Transcranial magnetic stimulation: cortical motor maps in acute spinal cord injury.* Brain Topography, 1995. **7**(3): p. 245-250.

78. Bruehlmeier, M., et al., *How does the human brain deal with a spinal cord injury?* European Journal of Neuroscience, 1998. **10**(12): p. 3918-3922.

79. Hagg, T. and M. Oudega, *Degenerative and spontaneous regenerative processes after spinal cord injury.* Journal of Neurotrauma, 2006. **23**(3-4): p. 263-280.

80. Calancie, B., et al., *Interlimb reflex activity after spinal cord injury in man: strengthening response patterns are consistent with ongoing synaptic plasticity.* Clinical Neurophysiology, 2005. **116**(1): p. 75-86.

81. Edgerton, V.R., et al., *Plasticity of the spinal neural circuitry after injury.* Annual Review of Neuroscience, 2004. **27**(1): p. 145-167.

82. Wernig, A., et al., *Laufband therapy based on 'rules of spinal locomotion' is effective in spinal cord injured persons.* European Journal of Neuroscience, 1995. **7**(4): p. 823-829.

83. Wernig, A. and S. Muller, *Laufband locomotion with body weight support improved walking in persons with severe spinal cord injuries.* Paraplegia, 1992. **30**(4): p. 229-238.

84. Harkema, S.J., *Neural plasticity after human spinal cord injury: application of locomotor training to the rehabilitation of walking.* The Neuroscientist, 2001. **7**(5): p. 455-468.

85. Wolpaw, J.R., *What can the spinal cord teach us about learning and memory?* The Neuroscientist, 2010. **16**(5): p. 532-549.

86. Beekhuizen, K.S. and E.C. Field-Fote, *Sensory stimulation augments the effects of massed practice training in persons with tetraplegia.* Archives of Physical Medicine and Rehabilitation, 2008. **89**(4): p. 602-608.

87. Harvey, L., et al., *Early intensive hand rehabilitation after spinal cord injury ("Hands On"): a protocol for a randomised controlled trial.* Trials, 2011. **14**(12).

88. Beekhuizen, K.S. and E.C. Field-Fote, *Massed practice versus massed practice with stimulation: effects on upper extremity function and cortical plasticity in individuals with incomplete cervical spinal cord injury.* Neurorehabilitation and Neural Repair, 2005. **19**(1): p. 33-45.

89. Engesser-Cesar, C., et al., *Wheel running following spinal cord injury improves locomotor recovery and stimulates serotonergic fiber growth.* European Journal of Neuroscience, 2007. **25**(7): p. 1931-1939.

90. Goldshmit, Y., et al., *Treadmill training after spinal cord hemisection in mice promotes axonal sprouting and synapse formation and improves motor recovery.* Journal of Neurotrauma, 2008. **25**(5): p. 449-465.

91. Vavrek, R., et al., *BDNF promotes connections of corticospinal neurons onto spared descending interneurons in spinal cord injured rats.* Brain, 2006. **129**(6): p. 1534-1545.

92. Wolpaw, J.R. and A.M. Tennissen, *Activity-dependent spinal cord plasticity in health and disease.* Annual Review of Neuroscience, 2001. **24**(1): p. 807-843.

93. Dimitrijevic, M.R., Y. Gerasimenko, and M.M. Pinter, *Evidence for a spinal central pattern generator in humans.* Annals of the New York Academy of Sciences, 1998. **860**: p. 360-376.

94. Harkema, S., et al., *Effect of epidural stimulation of the lumbosacral spinal cord on voluntary movement, standing, and assisted stepping after motor complete paraplegia: a case study.* The Lancet, 2011. **377**(9781): p. 1938-1947.

95. Maegele, M., et al., *Recruitment of spinal motor pools during voluntary movements versus stepping after human spinal cord injury.* Journal of Neurotrauma, 2002. **19**(10): p. 1217-1229.

96. Hiersemenzel, L.-P., A. Curt, and V. Dietz, *From spinal shock to spasticity: neuronal adaptation to spinal cord injury.* Neurology, 2000. **54**(8): p. 1574-1582.

97. Yeo, J.D., et al., *Mortality following spinal cord injury.* Spinal Cord, 1998. **36**(5): p. 329-336.

98. Hesse, S. and C. Werner, *Connecting research to the needs of patients and clinicians.* Brain Research Bulletin, 2009. **78**(1): p. 26-34.

99. Field-Fote, E.C., *Spinal cord control of movement: implications for locomotor rehabilitation following spinal cord injury.* Physical Therapy, 2000. **80**(5): p.

477-484.

100. Lovely, R.G., et al., *Effects of training on the recovery of full-weight-bearing stepping in the adult spinal cat.* Experimental Neurology, 1986. **92**(2): p. 421-435.

101. Barbeau, H. and S. Rossignol, *Recovery of locomotion after chronic spinalization in the adult cat.* Brain Research, 1987. **412**(1): p. 84-95.

102. de Leon, R.D., et al., *Locomotor capacity attributable to step training versus spontaneous recovery after spinalization in adult cats.* Journal of Neurophysiology, 1998. **79**(3): p. 1329-1340.

103. Grillner, S. and P. Wallen, *Central pattern generators for locomotion, with special reference to vertebrates.* Annual Review of Neuroscience, 1985. **8**: p. 233-261.

104. Grillner, S. and P. Zangger, *The effect of dorsal root transection on the efferent motor pattern in the cat's hindlimb during locomotion.* Acta Physiologica Scandinavica, 1984. **120**(3): p. 393-405.

105. Edgerton, V.R., et al., *Retraining the injured spinal cord.* Journal of Physiology, 2001. **533**(1): p. 15-22.

106. Brown, T.G., *The intrinsic factors in the act of progression in the mammal.* Proceedings of the Royal Society of London Series B-Containing Papers of a Biological Character, 1911. **84**(572): p. 308-319.

107. Mortin, L.I. and P.S.G. Stein, *Spinal-cord segments containing key elements of the central pattern generators for 3 forms of scratch reflex in the turtle.* Journal of Neuroscience, 1989. **9**(7): p. 2285-2296.

108. Ho, S. and M.J. Odonovan, *Regionalization and intersegmental coordination of rhythm-generating networks in the spinal cord of the chick embryo.* Journal of Neuroscience, 1993. **13**(4): p. 1354-1371.

109. Deliagina, T.G., G.N. Orlovsky, and G.A. Pavlova, *The capacity for generation of rhythmic oscillations is distributed in the lumbosacral spinal cord of the cat.* Experimental Brain Research, 1983. **53**(1): p. 81-90.

110. Kiehn, O. and S.J.B. Butt, *Physiological, anatomical and genetic identification of CPG neurons in the developing mammalian spinal cord.* Progress in Neurobiology, 2003. **70**(4): p. 347-361.

111. Forssberg, H., S. Grillner, and J. Halbertsma, *The locomotion of the low spinal*

cat. I. Coordination within a hindlimb. Acta Physiologica Scandinavica, 1980. **108**(3): p. 269-281.

112. Miller, S., J. Van Der Burg, and F.G.A. Van Der Mechéé, *Locomotion in the cat: basic programmes of movement.* Brain Research, 1975. **91**(2): p. 239-253.

113. Amemiya, M. and T. Yamaguchi, *Fictive locomotion of the forelimb evoked by stimulation of the mesencephalic locomotor region in the decerebrate cat.* Neuroscience Letters, 1984. **50**(1-3): p. 91-96.

114. Bouyer, L.J.G. and S. Rossignol, *Contribution of cutaneous inputs from the hindpaw to the control of locomotion. II. Spinal cats.* Journal of Neurophysiology, 2003. **90**(6): p. 3640-3653.

115. Forssberg, H., *Stumbling corrective reaction: a phase-dependent compensatory reaction during locomotion.* Journal of Neurophysiology, 1979. **42**(4): p. 936-953.

116. Giuliani, C. and J. Smith, *Stepping behaviors in chronic spinal cats with one hindlimb deafferented.* Journal of Neuroscience, 1987. **7**(8): p. 2537-2546.

117. Duysens, J. and K.G. Pearson, *Inhibition of flexor burst generation by loading ankle extensor muscles in walking cats.* Brain Research, 1980. **187**(2): p. 321-332.

118. Conway, B.A., H. Hultborn, and O. Kiehn, *Proprioceptive input resets central locomotor rhythm in the spinal cat.* Experimental Brain Research, 1987. **68**(3): p. 643-656.

119. Grillner, S. and P. Zangger, *On the central generation of locomotion in the low spinal cat.* Experimental Brain Research, 1979. **34**(2): p. 241-261.

120. Duysens, J. and H.W.A.A. Van de Crommert, *Neural control of locomotion; part 1: the central pattern generator from cats to humans.* Gait & Posture, 1998. **7**(2): p. 131-141.

121. Pang, M.Y.C. and J.F. Yang, *The initiation of the swing phase in human infant stepping: importance of hip position and leg loading.* Journal of Physiology, 2000. **528**(2): p. 389-404.

122. Yang, J.F., M.J. Stephens, and R. Vishram, *Infant stepping: a method to study the sensory control of human walking.* Journal of Physiology, 1998. **507**(3): p. 927-937.

123. Calancie, B., et al., *Involuntary stepping after chronic spinal cord injury.*

Evidence for a central rhythm generator for locomotion in man. Brain, 1994. **117**: p. 1143-1159.

124. Yang, J.F., et al., *Infant stepping: a window to the behaviour of the human pattern generator for walking.* Canadian Journal of Physiology and Pharmacology, 2004. **82**(8-9): p. 662-674.

125. Bussel, B., et al., *Myoclonus in a patient with a spinal cord transection. Possible involvement of the spinal stepping generator.* Brain, 1988. **111**: p. 1235-1245.

126. Dietz, V., et al., *Locomotor capacity of spinal cord in paraplegic patients.* Annals of Neurology, 1995. **37**(5): p. 574-582.

127. Dobkin, B.H., et al., *Modulation of locomotor-like EMG activity in subjects with complete and incomplete spinal cord injury.* Journal of Neurologic Rehabilitation, 1995. **9**(4): p. 183-190.

128. Harkema, S.J., et al., *Human lumbosacral spinal cord interprets loading during stepping.* Journal of Neurophysiology, 1997. **77**(2): p. 797-811.

129. Schmitz, T.J., *Chapter 14: locomotor training*, in *Physical Rehabilitation*, S.B. O'Sullivan and T.J. Schmitz, Editors. 2007, F.A. Davis Company: Philadelphia. p. 523-560.

130. Dobkin, B.H., *Chapter 6: approaches for walking*, in *The Clinical Science of Neurologic Rehabilitation* 2003, Oxford University Press. p. 250-270.

131. Yarkony, G.M., et al., *Functional skills after spinal cord injury rehabilitation: three-year longitudinal follow-up.* Archives of Physical Medicine and Rehabilitation, 1988. **69**(2): p. 111-114.

132. Dobkin, B., et al., *The evolution of walking-related outcomes over the first 12 weeks of rehabilitation for incomplete traumatic spinal cord injury: the multicenter randomized spinal cord injury locomotor trial.* Neurorehabilitation and Neural Repair, 2007. **21**(1): p. 25-35.

133. Lyles, M. and J. Munday, *Report on the evaluation of the Vannini-Rizzoli Stabilizing Limb Orthosis.* Journal of Rehabilitation Research and Development, 1992. **29**(2): p. 77-104.

134. Edelstein, J.E., *Chapter 31: orthotics*, in *Physical Rehabilitation*, S.B. O'Sullivan and T.J. Schmitz, Editors. 2007, F.A. Davis Company: Philadelphia. p. 1213-1250.

135. Wu, K.K., *Foot orthoses: principles and clincal applications*. 1990, Baltimore: Williams & Wilkins.

136. Kent, H.O., *Vannini-Rizzoli Stabilizing Orthosis (boot): preliminary report on a new ambulatory aid for spinal cord injury.* Archives of Physical Medicine and Rehabilitation, 1992. **73**(3): p. 302-307.

137. McGhee, R.B., et al., *An experimental study of a sensor-controlled external knee locking system.* IEEE Transactions on Biomedical Engineering, 1978. **BME25**(2): p. 195-199.

138. Irby, S.E., et al., *Automatic control design for a dynamic knee-brace system.* IEEE Transactions on Rehabilitation Engineering, 1999. **7**(2): p. 135-139.

139. Fatone, S., *A review of the literature pertaining to KAFOs and HKAFOs for ambulation.* Journal of Prosthetics and Orthotics, 2006. **18**(7): p. 137-168.

140. Nash, B., J.M. Roller, and M.G. Parker, *The effects of tone-reducing orthotics on walking of an individual after incomplete spinal cord injury.* Journal of Neurologic Physical Therapy, 2008. **32**(1): p. 39-47.

141. Kaufman, K.R., S.E. Irby, and J.W. Mathewson, *Energy-efficient knee-ankle-foot orthosis: a case study.* Journal of Prosthetics and Orthotics., 1996. **8**: p. 79-85.

142. Kim, C.M., J.J. Eng, and M.W. Whittaker, *Effects of a simple functional electric system and/or a hinged ankle-foot orthosis on walking in persons with incomplete spinal cord injury.* Archives of Physical Medicine and Rehabilitation, 2004. **85**(10): p. 1718-1723.

143. Roussos, N., et al., *A long-term review of severely disabled spina bifida patients using a reciprocal walking system.* Disability and Rehabilitation, 2001. **23**(6): p. 239-244.

144. Suzuki, T., et al., *Prediction of gait outcome with the knee-ankle-foot orthosis with medial hip joint in patients with spinal cord injuries: a study using recursive partitioning analysis.* Spinal Cord, 2006. **45**(1): p. 57-63.

145. Massucci, M., et al., *Walking with the advanced reciprocating gait orthosis (ARGO) in thoracic paraplegic patients: energy expenditure and cardiorespiratory performance.* Spinal Cord, 1998. **36**(4): p. 223-227.

146. Merati, G., et al., *Paraplegic adaptation to assisted-walking: energy expenditure during wheelchair versus orthosis use.* Spinal Cord, 2000. **38**(1): p. 37-44.

147. Johnson, W.B., S. Fatone, and S.A. Gard, *Walking mechanics of persons who use reciprocating gait orthoses.* Journal of Rehabilitation Research and Development, 2009. **46**(3): p. 435-446.

148. Thoumie, P., et al., *Restoration of functional gait in paraplegic patients with the RGO-II hybrid orthosis. A multicentre controlled study. I. Clinical evaluation.* Paraplegia, 1995. **33**(11): p. 647-653.

149. Thoumie, P., et al., *Restoration of functional gait in paraplegic patients with the RGO-II hybrid orthosis. A multicenter controlled study. II: Physiological evaluation.* Paraplegia, 1995. **33**(11): p. 654-659.

150. Dobkin, B.H., *An overview of treadmill locomotor training with partial body weight support: a neurophysiologically sound approach whose time has come for randomized clinical trials.* Neurorehabilitation and Neural Repair, 1999. **13**(3): p. 157-165.

151. Sousa, C.O., et al., *The use of body weight support on ground level: an alternative strategy for gait training of individuals with stroke.* Journal of NeuroEngineering and Rehabilitation, 2009. **6**.

152. Barbeau, H., et al., *Does neurorehabilitation play a role in the recovery of walking in neurological populations?*, in *Neuronal Mechanisms for Generating Locomotor Activity*, O. Kiehn, et al., Editors. 1998. p. 377-392.

153. Barbeau, H., M. Wainberg, and L. Finch, *Description and application of a system for locomotor rehabilitation.* Medical and Biological Engineering and Computing, 1987. **25**(3): p. 341-344.

154. Dobkin, B.H., et al., *Methods for a randomized trial of weight-supported treadmill training versus conventional training for walking during inpatient rehabilitation after incomplete traumatic spinal cord injury.* Neurorehabilitation and Neural Repair, 2003. **17**(3): p. 153-167.

155. Duncan, P., et al., *Protocol for the Locomotor Experience Applied Post-stroke (LEAPS) trial: a randomized controlled trial.* BMC Neurology, 2007. **7**(1): p. 39.

156. Wirz, M., G. Colombo, and V. Dietz, *Long term effects of locomotor training in spinal humans.* Journal of Neurology, Neurosurgery & Psychiatry, 2001. **71**(1): p. 93-96.

157. Grasso, R., et al., *Distributed plasticity of locomotor pattern generators in spinal cord injured patients.* Brain, 2004. **127**(5): p. 1019-1034.

158. Dietz, V., et al., *Locomotor pattern in paraplegic patients: training effects and recovery of spinal cord function.* Spinal Cord, 1998. **36**(6): p. 380-390.

159. Wernig, A., A. Nanassy, and S. Muller, *Maintenance of locomotor abilities following Laufband (treadmill) therapy in para- and tetraplegic persons: follow-up studies.* Spinal Cord, 1998. **36**(11): p. 744-749.

160. Barbeau, H., et al., *Walking after spinal cord injury: Evaluation, treatment, and functional recovery.* Archives of Physical Medicine and Rehabilitation, 1999. **80**(2): p. 225-235.

161. Visintin, M., et al., *A new approach to retrain gait in stroke patients through body weight support and treadmill stimulation.* Stroke, 1998. **29**(6): p. 1122-1128.

162. Dobkin, B., et al., *Weight-supported treadmill vs over-ground training for walking after acute incomplete SCI.* Neurology, 2006. **66**(4): p. 484-493.

163. Brown, T.H., et al., *Body weight-supported treadmill training versus conventional gait training for people with chronic traumatic brain injury.* Journal of Head Trauma Rehabilitation, 2005. **20**(5): p. 402-415.

164. Kralj, A., T. Bajd, and R. Turk, *Electrical stimulation providing functional use of paraplegic patient muscles.* Medical Progress through Technology, 1980. **7**(1): p. 3-9.

165. Graupe, D., et al., *Walking performance, medical outcomes and patient training in FES of innervated muscles for ambulation by thoracic-level complete paraplegics.* Neurological Research, 2008. **30**(2): p. 123-130.

166. O'Halloran, T., et al., *Modified implanted drop foot stimulator system with graphical user interface for customised stimulation pulse-width profiles.* Medical and Biological Engineering and Computing, 2003. **41**(6): p. 701-709.

167. Liberson, W.T., et al., *Functional electrotherapy: stimulation of the peroneal nerve synchronized with the swing phase of the gait of hemiplegic patients.* Archives of Physical Medicine and Rehabilitation, 1961. **42**: p. 101-105.

168. Kralj, A. and S. Grobelnik, *Functional electrical stimulation-A new hope for paraplegic patients?* Bulletin of Prosthetics Research, 1973. **10-20**: p. 75-102.

169. Kralj, A., T. Bajd, and R. Turk, *Enhancement of gait restoration in spinal injured patients by functional electrical stimulation.* Clinical Orthopaedics and Related Research, 1988(233): p. 34-43.

170. Kralj, A., et al., *Gait restoration in paraplegic patients: a feasibility demonstration using multichannel surface electrode FES.* Journal of Rehabilitation Research and Development, 1983. **20**(1): p. 3-20.

171. Bajd, T., et al., *Symmetry of FES responses in the lower-extremities of paraplegic patients.* Journal of Biomedical Engineering, 1990. **12**(5): p. 415-418.

172. Marsolais, E.B. and R. Kobetic, *Functional electrical stimulation for walking in paraplegia.* Journal of Bone and Joint Surgery-American Volume, 1987. **69A**(5): p. 728-733.

173. Kobetic, R., R.J. Triolo, and E.B. Marsolais, *Muscle selection and walking performance of multichannel FES systems for ambulation in paraplegia.* IEEE Transactions on Rehabilitation Engineering, 1997. **5**(1): p. 23-29.

174. Granat, M., et al., *The use of functional electrical stimulation to assist gait in patients with incomplete spinal cord injury.* Disability and Rehabilitation, 1992. **14**(2): p. 93-97.

175. Stein, R.B., et al., *Modification of reflexes in normal and abnormal movements*, in *Progress in Brain Research*, J.H.J. Allum, et al., Editors. 1993, Elsevier. p. 189-196.

176. Thrasher, T.A., H.M. Flett, and M.R. Popovic, *Gait training regimen for incomplete spinal cord injury using functional electrical stimulation.* Spinal Cord, 2005. **44**(6): p. 357-361.

177. Bütefisch, C., et al., *Repetitive training of isolated movements improves the outcome of motor rehabilitation of the centrally paretic hand.* Journal of the Neurological Sciences, 1995. **130**(1): p. 59-68.

178. de Kroon, J.R., et al., *Relation between stimulation characteristics and clinical outcome in studies using electrical stimulation to improve motor control of the upper extremity in stroke.* Journal of Rehabilitation Medicine, 2005. **37**(2): p. 65-74.

179. Granat, M.H., et al., *The role of functional electrical stimulation in the rehabilitation of patients with incomplete spinal cord injury - observed benefits during gait studies.* Paraplegia, 1993. **31**(4): p. 207-215.

180. Ladouceur, M. and H. Barbeau, *Functional electrical stimulation-assisted walking for persons with incomplete spinal injuries: changes in the kinematics and physiological cost of overground walking.* Scandinavian Journal of

Rehabilitation Medicine, 2000. **32**(2): p. 72-79.

181. Phillips, C.A., *Electrical muscle stimulation in combination with a reciprocating gait orthosis for ambulation by paraplegics.* Journal of Biomedical Engineering, 1989. **11**(4): p. 338-344.

182. Solomonow, M., et al., *Reciprocating gait orthosis powered with electrical muscle stimulation (RGO II) .1. Performance evaluation of 70 paraplegic patients.* Orthopedics, 1997. **20**(4): p. 315-324.

183. Solomonow, M., et al., *Reciprocating gait orthosis powered with electrical muscle stimulation (RGO II) .2. Medical evaluation of 70 paraplegic patients.* Orthopedics, 1997. **20**(5): p. 411-418.

184. Field-Fote, E., *Combined use of body weight support, functional electric stimulation, and treadmill training to improve walking ability in individuals with chronic incomplete spinal cord injury.* Archives of Physical Medicine and Rehabilitation, 2001. **82**(6): p. 818-824.

185. Field-Fote, E.C. and D. Tepavac, *Improved intralimb coordination in people with incomplete spinal cord injury following training with body weight support and electrical stimulation.* Physical Therapy, 2002. **82**(7): p. 707-715.

186. Postans, N.J., et al., *Functional electric stimulation to augment partial weight-bearing supported treadmill training for patients with acute incomplete spinal cord injury: a pilot study.* Archives of Physical Medicine and Rehabilitation, 2004. **85**(4): p. 604-610.

187. Wieler, M., et al., *Multicenter evaluation of electrical stimulation systems for walking.* Archives of Physical Medicine and Rehabilitation, 1999. **80**(5): p. 495-500.

188. Roy, A., et al., *Robot-aided neurorehabilitation: a novel robot for ankle rehabilitation.* IEEE Transactions on Robotics, 2009. **25**(3): p. 569-582.

189. Veneva, I., *Design and implementation of device for control of active ankle-foot orthosis,* in *National Congress on Theoretical and Applied Mechanics*. 2009: Borovets, Bulgaria.

190. Mankala, K.K., S.K. Banala, and S.K. Agrawal, *Novel swing-assist un-motorized exoskeletons for gait training.* Journal of NeuroEngineering and Rehabilitation, 2009. **6:24**.

191. Gordon, K.E., G.S. Sawicki, and D.P. Ferris, *Mechanical performance of artificial pneumatic muscles to power an ankle-foot orthosis.* Journal of

Biomechanics, 2006. **39**(10): p. 1832-1841.

192. Sawicki, G. and D. Ferris, *A pneumatically powered knee-ankle-foot orthosis (KAFO) with myoelectric activation and inhibition.* Journal of NeuroEngineering and Rehabilitation, 2009. **6**(1): p. 23.

193. Beyl, P., et al. *An exoskeleton for gait rehabilitation: prototype design and control principle*. in *IEEE International Conference on Robotics and Automation*. 2008.

194. Veneman, J.F., et al., *Design and evaluation of the LOPES exoskeleton robot for interactive gait rehabilitation.* IEEE Transactions on Neural Systems and Rehabilitation Engineering, 2007. **15**(3): p. 379-386.

195. Banala, S.K., S.K. Agrawal, and J.P. Scholz. *Active Leg Exoskeleton (ALEX) for gait rehabilitation of motor-impaired patients*. in *10th IEEE International Conference on Rehabilitation Robotics*. 2007. Noordwijk, The Netherlands.

196. Emken, J.L., et al., *A robotic device for manipulating human stepping.* IEEE Transactions on Robotics, 2006. **22**(1): p. 185-189.

197. Aoyagi, D., et al., *A robot and control algorithm that can synchronously assist in naturalistic motion during body-weight-supported gait training following neurologic injury.* IEEE Transactions on Neural Systems and Rehabilitation Engineering, 2007. **15**(3): p. 387-400.

198. Colombo, G., et al., *Treadmill training of paraplegic patients using a robotic orthosis.* Journal of Rehabilitation Research and Development, 2000. **37**(6): p. 693-700.

199. Freivogel, S., et al., *Gait training with the newly developed 'LokoHelp'-system is feasible for non-ambulatory patients after stroke, spinal cord and brain injury. A feasibility study.* Brain Injury, 2008. **22**(7-8): p. 625-632.

200. Tomelleri, C., et al. *Adaptive locomotor training on an end-effector gait robot: evaluation of the ground reaction forces in different training conditions*. in *IEEE International Conference on Rehabilitation Robotics* 2011. Zurich, Switzerland.

201. Banala, S.K., et al., *Novel gait adaptation and neuromotor training results using an active leg exoskeleton.* IEEE/ASME Transactions on Mechatronics, 2010. **15**(2): p. 216-225.

202. Banala, S.K., et al., *Robot assisted gait training with active leg exoskeleton (ALEX).* IEEE Transactions on Neural Systems and Rehabilitation Engineering,

2009. **17**(1): p. 2-8.

203. Emken, J.L., et al., *Feasibility of manual teach-and-replay and continuous impedance shaping for robotic locomotor training following spinal cord injury.* IEEE Transactions on Biomedical Engineering, 2008. **55**(1): p. 322-334.

204. Stauffer, Y., et al., *The WalkTrainer-a new generation of walking reeducation device combining orthoses and muscle stimulation.* IEEE Transactions on Neural Systems and Rehabilitation Engineering, 2009. **17**(1): p. 38-45.

205. Hidler, J., W. Wisman, and N. Neckel, *Kinematic trajectories while walking within the Lokomat robotic gait-orthosis.* Clinical Biomechanics, 2008. **23**(10): p. 1251-1259.

206. Hornby, T.G., D.H. Zemon, and D. Campbell, *Robotic-assisted, body-weight-supported treadmill training in individuals following motor incomplete spinal cord injury.* Physical Therapy, 2005. **85**(1): p. 52-66.

207. Nooijen, C., N. ter Hoeve, and E. Field-Fote, *Gait quality is improved by locomotor training in individuals with SCI regardless of training approach.* Journal of NeuroEngineering and Rehabilitation, 2009. **6**(1): p. 36.

208. Field-Fote, E.C., S.D. Lindley, and A.L. Sherman, *Locomotor training approaches for individuals with spinal cord injury: a preliminary report of walking-related outcomes.* Journal of Neurologic Physical Therapy, 2005. **29**(3): p. 127-37.

209. Mehrholz, J., J. Kugler, and M. Pohl, *Locomotor training for walking after spinal cord injury.* Spine, 2008. **33**(21): p. E768-77.

210. Freivogel, S., D. Schmalohr, and J. Mehrholz, *Improved walking ability and reduced therapeutic stress with an electromechanical gait device.* Journal of Rehabilitation Medicine, 2009. **41**(9): p. 734-739.

211. Cai, L.L., et al., *Effects of consistency vs. variability in robotically controlled training of stepping in adult spinal mice*, in *IEEE 9th International Conference on Rehabilitation Robotics*. 2005. p. 575-579.

212. Schmidt, H., et al., *Gait rehabilitation machines based on programmable footplates.* Journal of NeuroEngineering and Rehabilitation, 2007. **4**(2).

213. Hesse, S. and D. Uhlenbrock, *A mechanized gait trainer for restoration of gait.* Journal of Rehabilitation Research and Development, 2000. **37**(6): p. 701-708.

214. Pohl, M., et al., *Repetitive locomotor training and physiotherapy improve*

walking and basic activities of daily living after stroke: a single-blind, randomized multicentre trial (DEutsche GAngtrainerStudie, DEGAS). Clinical Rehabilitation, 2007. **21**(1): p. 17-27.

215. Hesse, S., C. Werner, and A. Bardeleben, *Electromechanical gait training with functional electrical stimulation: case studies in spinal cord injury.* Spinal Cord, 2004. **42**(6): p. 346-352.

216. Schmidt, H., et al. *Design of a robotic walking simulator for neurological rehabilitation*. in *IEEE/RSJ International Conference on Intelligent Robots and Systems*. 2002.

217. Schmidt, H., et al., *HapticWalker--a novel haptic foot device.* ACM Transactions on Applied Perception, 2005. **2**(2): p. 166-180.

218. Hesse, S., A. Waldner, and C. Tomelleri, *Innovative gait robot for the repetitive practice of floor walking and stair climbing up and down in stroke patients.* Journal of NeuroEngineering and Rehabilitation, 2010. **7**(1): p. 30.

219. Colombo, G., et al. *Novel tilt table with integrated robotic stepping mechanism: design principles and clinical application*. in *9th International Conference on Rehabilitation Robotics*. 2005.

220. Hunt, K.J., et al., *Control strategies for integration of electric motor assist and functional electrical stimulation in paraplegic cycling: utility for exercise testing and mobile cycling.* IEEE Transactions on Neural Systems and Rehabilitation Engineering 2004. **12**(1): p. 89-101.

221. Schmitt, C., P. Métrailler, and A. Al-Khodairy, *The Motion Maker: a rehabilitation system combining an orthosis with closed-loop electrical muscle stimulation*, in *8th Vienna International Workshop on Functional Electrical Stimulation*. 2004: Vienna, Austria. p. 117-120.

222. Rupp, R., et al. *MotionTherapy@Home - a robotic device for automated locomotion therapy at home*. in *IEEE International Conference on Rehabilitation Robotics* 2009.

223. Knestel, M., E.P. Hofer, and R. Rupp, *Model-based feedback control of a rehabilitation robot*, in *Proceedings of the 2nd International Convention on Rehabilitation Engineering & Assistive Technology*. 2008, Singapore Therapeutic, Assistive & Rehabilitative Technologies (START) Centre: Bangkok, Thailand. p. 175-178.

224. Berry, H.R., et al., *Cardiorespiratory and power adaptations to stimulated*

cycle training in paraplegia. Medicine and Science in Sports and Exercise, 2008. **40**(9): p. 1573-1580.

225. Rupp, R., et al., *MotionTherapy@Home - First results of a clinical study with a novel robotic device for automated locomotion therapy at home.* Biomedizinische Technik, 2011. **56**(1): p. 11-21.

226. Knestel, M., E.P. Hofer, and R. R. *The artificial muscle as an innovative actuator in rehabilitation robotics*. in *17th World Congress of the International Federation of Automatic Control*. 2008. Seoul.

227. Thomas, C.K. and I. Zijdewind, *Fatigue of muscles weakened by death of motoneurons.* Muscle & Nerve, 2006. **33**(1): p. 21-41.

228. Waters, R.L., et al., *Motor and sensory recovery following incomplete tetraplegia.* Archives of Physical Medicine and Rehabilitation, 1994. **75**(3): p. 306-311.

229. Waters, R.L., et al., *Motor and sensory recovery following complete tetraplegia.* Archives of Physical Medicine and Rehabilitation, 1993. **74**(3): p. 242-247.

230. Waters, R.L., et al., *Motor and sensory recovery following incomplete paraplegia.* Archives of Physical Medicine and Rehabilitation, 1994. **75**(1): p. 67-72.

231. Smith, H.C., et al., *Corticospinal function studied over time following incomplete spinal cord injury.* Spinal Cord, 2000. **38**(5): p. 292-300.

232. Bharadwaj, K., et al., *Design of a robotic gait trainer using spring over muscle actuators for ankle stroke rehabilitation.* Journal of Biomechanical Engineering, 2005. **127**(6): p. 1009-1013.

233. Murray, M.P., *Gait as a total pattern of movement.* American Journal of Physical Medicine, 1967. **46**(1): p. 290-333.

234. Whittle, M., ed. *Gait Analysis: An Introduction.* 3rd ed. 2002, Butterworth-Heinemann.

235. Rose, J. and J.G. Gamble, *Human Walking*, J. Rose and J.G. Gamble, Editors. 2006, Lippincott Williams & Wilkins.

236. Stansfield, B.W., et al., *Regression analysis of gait parameters with speed in normal children walking at self-selected speeds.* Gait & Posture, 2006. **23**(3): p. 288-294.

237. Kadaba, M.P., H.K. Ramakrishnan, and M.E. Wootten, *Measurement of lower extremity kinematics during level walking.* Journal of Orthopaedic Research, 1990. **8**(3): p. 383-392.

238. Stansfield, B.W., et al., *Sagittal joint kinematics, moments, and powers are predominantly characterized by speed of progression, not age, in normal children.* Journal of Pediatric Orthopaedics, 2001. **21**(3): p. 403-411.

239. Tudor-Locke, C. and D.A. Rowe, *Using cadence to study free-living ambulatory behaviour.* Sports Medicine, 2012. **42**(5): p. 381-398.

240. Winter, D.A., *Energy generation and absorption at the ankle and knee during fast, natural, and slow cadences.* Clinical Orthopaedics and Related Research, 1983(175): p. 147-154.

241. Roerdink, M., et al., *Walking to the beat of different drums: practical implications for the use of acoustic rhythms in gait rehabilitation.* Gait & Posture, 2011. **33**(4): p. 690-694.

242. Carty, C.P. and M.B. Bennett, *The use of dimensionless scaling strategies in gait analysis.* Human Movement Science, 2009. **28**(2): p. 218-225.

243. Winter, D.A., *Kinematic and kinetic patterns in human gait: variability and compensating effects.* Human Movement Science, 1984. **3**(1-2): p. 51-76.

244. Eng, J.J. and D.A. Winter, *Kinetic analysis of the lower limbs during walking: What information can be gained from a three-dimensional model?* Journal of Biomechanics, 1995. **28**(6): p. 753-758.

245. Cappozzo, A., et al., *The interplay of muscular and external forces in human ambulation.* Journal of Biomechanics, 1976. **9**(1): p. 35-43.

246. Alexander, R.M., *Mechanics of bipedal locomotion*, in *Perspectives in Experimental Biology*, P.S. Davies and N. Sunderland, Editors. 1976, Pergamon Press: Oxford. p. 493-504.

247. Alexander, R.M. and G. Goldspink, *Mechanics and Energetics of Animal Locomotion*. 1977, New York: Halsted Press.

248. Maillardet, F.J., *The swing phase of locomotion.* Engineering in Medicine, 1977. **6**(3): p. 67-75.

249. Marshall, E.A., *A dynamical model for the stride in human walking.* Mathematical Modelling, 1983. **4**(5): p. 391-415.

250. Maillardet, F.J., *The swing phase of locomotion.* Engineering in Medicine,

1977. **6**(4): p. 101-106.

251. Ren, L., et al., *A generic analytical foot rollover model for predicting translational ankle kinematics in gait simulation studies.* Journal of Biomechanics, 2010. **43**(2): p. 194-202.

252. McGeer, T., *Passive dynamic walking.* International Journal of Robotics Research, 1990. **9**(2): p. 62-82.

253. Perry, J., *Gait Analysis: Normal and Pathological Function*. 1992, New Jersey: SLACK Incorporated.

254. Coope, I.D., *Circle fitting by linear and nonlinear least squares.* Journal of Optimization Theory and Applications, 1993. **76**(2): p. 381-388.

255. Winter, D.A., *Foot trajectory in human gait: a precise and multifactorial motor control task.* Physical Therapy, 1992. **72**(1): p. 45-53.

256. Gard, S.A. and D.S. Childress, *What determines the vertical displacement of the body during normal walking?* Journal of Prosthetics and Orthotics, 2001. **13**(3): p. 64-67.

257. Hansen, A.H., D.S. Childress, and E.H. Knox, *Roll-over shapes of human locomotor systems: effects of walking speed.* Clinical Biomechanics, 2004. **19**(4): p. 407-414.

258. Whittlesey, S.N. and J. Hamill, *An alternative model of the lower extremity during locomotion.* Journal of Applied Biomechanics, 1996. **12**(2): p. 269-279.

259. Kwan, M. and M. Hubbard, *Optimal foot shape for a passive dynamic biped.* Journal of Theoretical Biology, 2007. **248**(2): p. 331-339.

260. Kuo, A.D., *A simple model of bipedal walking predicts the preferred speed-step length relationship.* Journal of Biomechanical Engineering, 2001. **123**(3): p. 264-269.

261. Dietz, V., R. Müller, and G. Colombo, *Locomotor activity in spinal man: significance of afferent input from joint and load receptors.* Brain, 2002. **125**(12): p. 2626-2634.

262. Harkey, H.L., et al., *A clinician's view of spinal cord injury.* The Anatomical Record Part B: The New Anatomist, 2003. **271B**(1): p. 41-48.

263. Edgerton, V.R. and R.R. Roy, *Robotic training and spinal cord plasticity.* Brain Research Bulletin, 2009. **78**(1): p. 4-12.

264. MathWorks.Inc., T., *SimMechanics User's Guide*. 2010.

265. Brenan, K.E., S.L. Campbell, and L.R. Petzold, *Numerical Solution of Initial-Value Problems in Differential-Algebraic Equations*. 1989, New York: Elsevier Science Publishing Co. .

266. Fong, A.J., et al., *Recovery of control of posture and locomotion after a spinal cord injury: solutions staring us in the face*, in *Progress in Brain Research*, J. Verhaagen, et al., Editors. 2009. p. 393-418.

267. Cappozzo, A., T. Leo, and A. Pedotti, *A general computing method for the analysis of human locomotion.* Journal of Biomechanics, 1975. **8**(5): p. 307-320.

268. Hansen, A.H., et al., *The human ankle during walking: implications for design of biomimetic ankle prostheses.* Journal of Biomechanics, 2004. **37**(10): p. 1467-1474.

269. Hsiang, S.M. and C. Chang, *The effect of gait speed and load carrying on the reliability of ground reaction forces.* Safety Science, 2002. **40**(7–8): p. 639-657.

270. Bautista, E., *Theory of Machines and Mechanisms I.* 4th ed. 2009: Nirali Prakashan.

271. Mundo, D., G. Gatti, and D.B. Dooner, *Optimized five-bar linkages with non-circular gears for exact path generation.* Mechanism and Machine Theory, 2009. **44**(4): p. 751-760.

272. Liu, J.Y., S.L. Chang, and D. Mundo, *Study on the use of a non-circular gear train for the generation of Figure-8 patterns.* Proceedings of the Institution of Mechanical Engineers Part C: Journal of Mechanical Engineering Science, 2006. **220**(8): p. 1229-1236.

273. Huey Jr, C.O. and M.W. Dixons, *The Cam-link mechanism for structural error-free path and function generation.* Mechanism and Machine Theory, 1974. **9**(3–4): p. 367-384.

274. Norton, R.L., *Cam Design and Manufacturing Handbook*. 2002, New York: Industrial Press.

275. Huston, R.L., *Principles of Biomechanics*. 2009: CRC press.

276. Beer, F.P., E.R. Johnston, and J.T. DeWolf, *Chapter 5: analysis and design of beams for bending*, in *Mechanics of Materials*. 2001, McGraw-Hill: New York.

p. 308-371.

277. Pilkey, W.D., *Analysis and Design of Elastic Beams: Computational Methods* 2002: John Wiley & Sons, Inc.

278. AISC, *AISC Manual of Steel Construction: Allowable Stress Design*. 9th ed. 1989.

279. Marghitu, D.B., *Chapter 3: mechanics of materials*, in *Mechanical Engineer's Handbook*. 2001, Academic Press. p. 119-188.

280. Knikou, M. and B.A. Conway, *Modulation of soleus H-reflex following ipsilateral mechanical loading of the sole of the foot in normal and complete spinal cord injured humans.* Neuroscience Letters, 2001. **303**(2): p. 107-110.

281. Pheasant, S., *Bodyspace: Anthropometry, Ergonomics and the Design of Work* 2003: Taylor & Francis Ltd.

282. Drury, B., *The Control Techniques Drives and Controls Handbook*. 2nd ed. 2009, London, United Kingdom: The Institution of Engineering and Technology.

283. Duysens, J., F. Clarac, and H. Cruse, *Load-regulating mechanisms in gait and posture: comparative aspects.* Physiological Reviews, 2000. **80**(1): p. 83-133.

284. Dietz, V., *Evidence for a load receptor contribution to the control of posture and locomotion.* Neuroscience & Biobehavioral Reviews, 1998. **22**(4): p. 495-499.

285. Berger, W., V. Dietz, and J. Quintern, *Corrective reactions to stumbling in man: neuronal coordination of bilateral leg muscle activity during gait.* Journal of Physiology-London, 1984. **357**(DEC): p. 109-125.

286. Van Wezel, B.M.H., F.A.M. Ottenhoff, and J. Duysens, *Dynamic control of location-specific information in tactile cutaneous reflexes from the foot during human walking.* Journal of Neuroscience, 1997. **17**(10): p. 3804-3814.

287. Konrad, P., *The ABC of EMG: A Practical Introduction to Kinesiological Electromyography*. 2005: Noraxon INC. USA.

288. Sonnenborg, F.A., O.K. Andersen, and L. Arendt-Nielsen, *Modular organization of excitatory and inhibitory reflex receptive fields elicited by electrical stimulation of the foot sole in man.* Clinical Neurophysiology, 2000. **111**(12): p. 2160-2169.

289. Hodges, P.W. and B.H. Bui, *A comparison of computer-based methods for the*

determination of onset of muscle contraction using electromyography. Electromyography and Motor Control-Electroencephalography and Clinical Neurophysiology, 1996. **101**(6): p. 511-519.

290. Lynch, S.A., et al., *Electromyographic latency changes in the ankle musculature during inversion moments.* American Journal of Sports Medicine, 1996. **24**(3): p. 362-369.

291. af Klint, R., et al., *Sudden drop in ground support produces force-related unload response in human overground walking.* Journal of Neurophysiology, 2009. **101**(4): p. 1705-1712.

292. Walter, C.B., *Temporal quantification of electromyography with reference to motor control research.* Human Movement Science, 1984. **3**(1–2): p. 155-162.

293. Jöllenbeck, T., *Chapter 18: determination of the onset of EMG and force in EMG-based motion analysis: methodological problems and limitations* in *International Research in Sports Biomechanics*, Y. Hong, Editor. 2002, Taylor & Francis. p. 148-157.

294. Brown, J.E. and J.S. Frank, *Influence of event anticipation on postural actions accompanying voluntary movement.* Experimental Brain Research, 1987. **67**(3): p. 645-650.

295. Sinkjaer, T., J.B. Andersen, and B. Larsen, *Soleus stretch reflex modulation during gait in humans.* Journal of Neurophysiology, 1996. **76**(2): p. 1112-1120.

296. Fellows, S.J. and A.F. Thilmann, *The role of joint biomechanics in determining stretch reflex latency at the normal human ankle.* Experimental Brain Research, 1989. **77**(1): p. 135-139.

297. Andersen, O.K., F.A. Sonnenborg, and L. Arendt-Nielsen, *Reflex receptive fields for human withdrawal reflexes elicited by non-painful and painful electrical stimulation of the foot sole.* Clinical Neurophysiology, 2001. **112**(4): p. 641-649.

298. Sandrini, G., et al., *The lower limb flexion reflex in humans.* Progress in Neurobiology, 2005. **77**(6): p. 353-395.

299. Grimby, L., *Normal plantar response - integration of flexor and extensor reflex components.* Journal of Neurology Neurosurgery and Psychiatry, 1963. **26**(1): p. 39-50.

300. Dietz, V., et al., *Regulation of bipedal stance: dependency on "load" receptors.*

Experimental Brain Research, 1992. **89**(1): p. 229-231.

301. Frotzler, A., et al., *High-volume FES-cycling partially reverses bone loss in people with chronic spinal cord injury.* Bone, 2008. **43**(1): p. 169-176.